



## OPEN ACCESS

## EDITED BY

Nicola Maria Pugno,  
University of Trento, Italy

## REVIEWED BY

Nilakantha Meher,  
Weizmann Institute of Science, Israel  
Aleksy E. Kuznetsov,  
Federico Santa Maria Technical University,  
Chile

## \*CORRESPONDENCE

Vincent G. Harris,  
✉ v.harris@northeastern.edu

RECEIVED 23 November 2023

ACCEPTED 26 March 2024

PUBLISHED 09 October 2024

## CITATION

Harris VG and Andalib P (2024), Modern quantum materials.  
*Front. Mater.* 11:1343005.  
doi: 10.3389/fmats.2024.1343005

## COPYRIGHT

© 2024 Harris and Andalib. This is an open-access article distributed under the terms of the [Creative Commons Attribution License \(CC BY\)](https://creativecommons.org/licenses/by/4.0/). The use, distribution or reproduction in other forums is permitted, provided the original author(s) and the copyright owner(s) are credited and that the original publication in this journal is cited, in accordance with accepted academic practice. No use, distribution or reproduction is permitted which does not comply with these terms.

# Modern quantum materials

Vincent G. Harris<sup>1,2\*</sup> and Parisa Andalib<sup>1</sup>

<sup>1</sup>Department of Electrical and Computer Engineering and Center for Microwave Magnetic Materials and Integrated Circuits, Boston, MA, United States, <sup>2</sup>Department of Chemical Engineering Northeastern University, Boston, MA, United States

Quantum phenomena, including entanglement, superposition, tunneling, and spin-orbit interactions, among others, are foundational to the development of recent innovations in quantum computing, teleportation, encryption, sensing, and new modalities of electronics, such as spintronics, spin-orbitronics, caloritronics, magnonics, twistrionics, and valleytronics. These emerging technologies provide disruptive influences to global commercial markets. These remarkable advances in quantum technologies are nearly always enabled by the discovery of materials and their quantum behaviors. Such advances are governed by quantum principles that are strongly influenced by environmental, physical, topological, and morphological conditions such as very small length scales, short time durations, ultrahigh pressures, ultralow temperatures, etc., which lead to quantum behaviors that manifest as quantum tunneling, entanglement, superpositioning, superfluidity, low-dimensional, high-temperature and high-pressure superconductivity, quantum fluctuations, Bose-Einstein condensates, topological effects, and other phenomena that are not yet fully understood nor adequately explored. Here, we provide a review of quantum materials developed up to 2023. Remarkable advances in quantum materials occur daily, and therefore, by the time of publication, new and exciting breakthroughs will have occurred that are regrettably not covered herein.

## KEYWORDS

entanglement, superposition (SP), spin-orbit coupling, qubit, quantum computing (QC), quantum annealing (QA)

## 1 Introduction

The widely venerated Richard Feynman once explained to a layperson that electrons participate in all chemical bonds, determining not only classical properties such as hardness, density, malleability, and color but also adhering to quantum principles that often give rise to rather *weird* behaviors. Some of these weird behaviors appear in common water.

For example, upon freezing, water takes on six-sided fractalized crystalline structures (Harvey, 2017; Wikipedia, 2022b) where each molecule's H<sup>+</sup> ions bond to an average of ~17.6% more partners, giving rise to an increase in volume of ~9% (Jain, 2014). This increased volume lowers the density of water and allows ice to float in water. The large expansion of freezing water exerts extreme pressures on its container walls, in some cases beyond 1 GPa, depending upon the specific phase of

ice<sup>1</sup>, leading to the commonly experienced fracturing of thick iron pipes in winter climes.

In this frozen state, ice was long thought to form a thin layer of liquid water under the application of pressure, for example, under ice skates, allowing for the astonishing exploits of Bobby Orr and others on the ponds of North America (Schwegler et al., 2008). In recent years, this description of *slippery* ice has proven incomplete, as illuminated by the work of<sup>2</sup> Canale et al. (2019) and Bonn (2020).

To this day, water continues to offer *weird quantum surprises*; for example, common water consists of two hydrogen cations and an oxygen anion that take on spin isomerisms of ortho- and para-forms. Ortho-water has both hydrogen ion magnetic spins aligning parallel ( $\uparrow\uparrow$ ), whereas para-water has hydrogen spins aligning antiparallel ( $\downarrow\uparrow$ ) (Beduz et al., 2012). However, unlike spin isomers of hydrogen gas molecules (i.e.,  $H^+$  ions in  $H_2$ ), water spin isomers experience *electric dipoles*, giving rise to properties like *ferroelectricity*. An orthorhombic, low-temperature form of hexagonal ice has been shown to be ferroelectric and described as ice XI, which is considered a stable configuration of ice  $I_h$  (Iedema et al., 1998).

We comment on *quantum water* merely to demonstrate that even materials that we consider common offer *quantum weirdness*. Other quantum behaviors discussed in this article include quantum tunneling, spin-orbit interactions, entanglement, superpositioning, and other phenomena.

In preparing this manuscript, we have noted that during the last several years, the term “quantum materials” has evolved into a universally accepted term of the quantum lexicon; however, an equally accepted *definition* of quantum materials (QMs) has remained elusive. Although many definitions have been proffered by practitioners who describe QMs within the frameworks of their own experiences, our field continues to grapple with a degree of self-identity.

We proffer a definition of QMs that we hope captures both breadth and specificity:

- 
- 1 Ice exhibits at least eighteen phases depending on temperature and pressure. When water is quenched, up to three types of amorphous ice can form depending on its history of pressure and temperature.
  - 2 In 2020, the simultaneous measurement of rheological and surface kinetical properties of the lubricating layer forming on the surface of ice revealed that its viscous and elastic behavior depends upon both its intrinsic character upon melting as well as its interaction with the incident skating blades. The findings suggest that lubrication and concomitant wear of the ice surface leads to the formation of a *third* layer that forms between the layer of ice and water. Few materials form such viscoelastic, liquid–solid layers in response to friction and wear as those observed in ice. This interpretation provides important missing pieces in the quest to better understand water and ice.

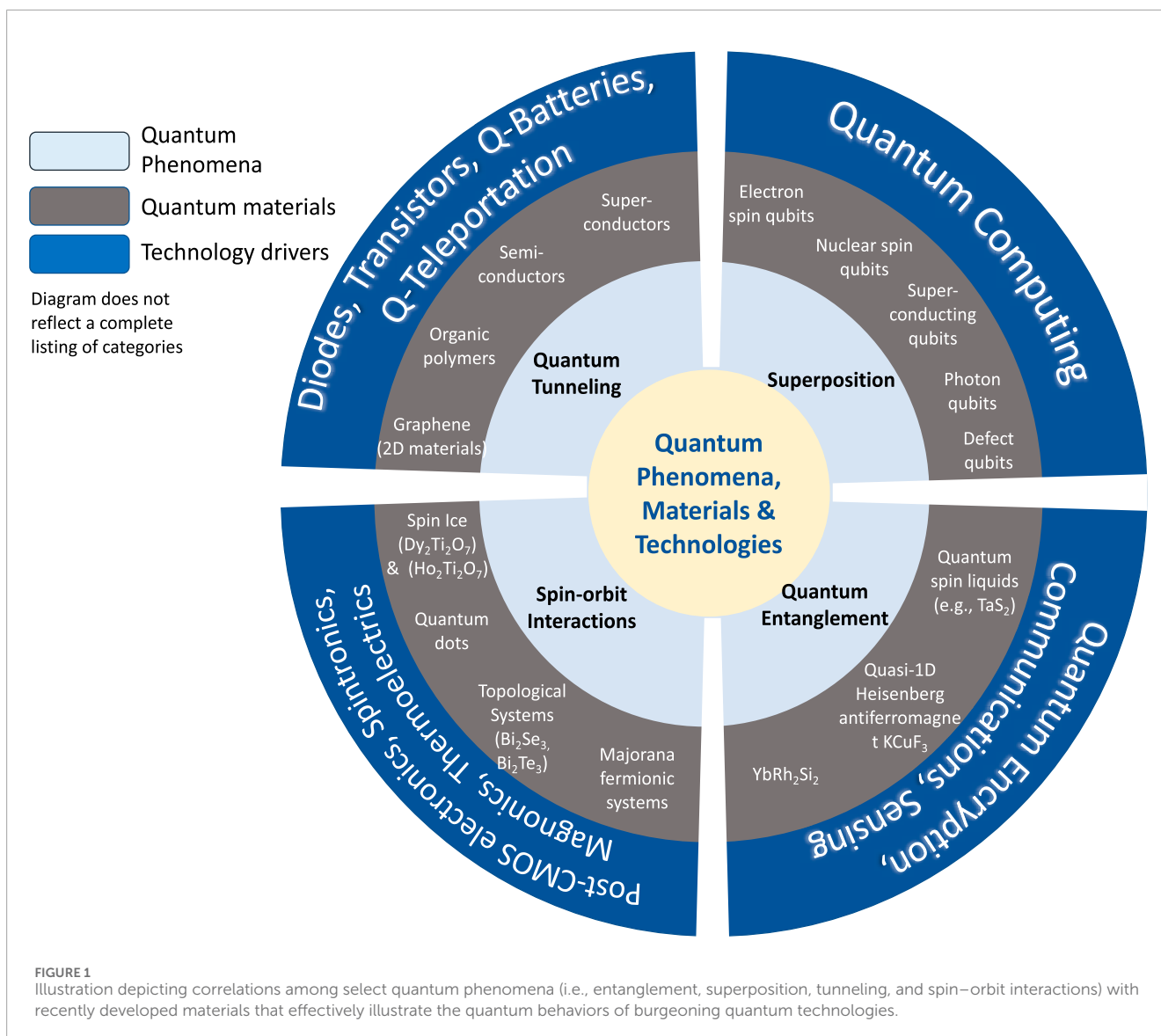
Quantum materials are those whose properties cannot be thoroughly explained within the framework of classical deterministic theories where individual particles through electron confinement, collective quasiparticle excitations, and many-body interactions, express their quantum behavior as superconductivity, quantum fluctuations, entanglement and superposition, quantum tunneling, and superfluidity, among other phenomena; these effects often occur at nanoscales, ultralow temperatures, ultrahigh pressures, or ultrashort time durations.

The broad goals of the present article are to provide insight into the complex and rich field of quantum materials, reflecting some of the recently recognized challenges and successes. This review is presented for those new to the field, for example, scholars considering quantum materials as a future research topic or perhaps as a component to their formal education or those wishing to expose themselves to new opportunities made available by our increasingly *quantum society*.

We aim to cast quantum materials in the context of phenomena that are actively explored in practical *quantum technologies*. These phenomena include coherence of qubits, fidelity of quantum states, quantum error-correction stratagems, and implementation of powerful quantum algorithms, all essential to realizing practical quantum computing, quantum information, and quantum communication technologies. Alternatively, and of equal import, is the development of long-lived superposition states that enable encryption and ultra-secure communication, quantum teleportation, sensing, and other quantum applications.

The extraordinary extension of performance of modern electronics includes the development of spintronics (Žutić et al., 2004), spin-orbitronics (Manchon et al., 2015), caloritronics (Bauer et al., 2012), magnonics (Kruglyak et al., 2010), twistronics (Hennighausen and Kar, 2021), and valleytronics (Schaibley et al., 2016), and the other “-ics” unintentionally omitted that are emerging every day. Such advances are nearly always enabled by newly discovered materials and their quantum behaviors. Such remarkable advances in technologies not only positively influence society but are also governed by quantum principles that are strongly impacted by environmental, physical, topological, and morphological conditions. For example, at very small length scales, short time durations, ultrahigh pressures, and ultralow temperatures, etc., quantum behaviors manifest as quantum tunneling, entanglement, superpositioning, superfluidity, low-dimensional, high-temperature and high-pressure superconductivity, quantum fluctuations, Bose–Einstein condensates, topological effects, and other phenomena that are not yet fully understood nor adequately explored.

Figure 1 illustrates a depiction of correlations among select quantum phenomena (i.e., entanglement, superposition, tunneling, and spin-orbit interactions) correlated with recently developed materials that effectively illustrate quantum behaviors, with technologies such as quantum computing (Nielsen and Chuang, 2000), teleportation (Bennett et al., 1993), encryption (Gisin et al., 2002; Pirandola et al., 2020), sensing (Degen et al., 2017), and new modalities of electronics that provide effective driving forces to global markets. The international business community responds to these opportunities with investments in quantum materials due to



their promise of considerable financial returns. We will address these relationships and others in greater detail in forthcoming sections.

In its entirety, this perspective on quantum materials applies to emerging quantum technologies and their societal impact.

We begin this article with a discussion of the evolution of quantum mechanics, both in the early part of the twentieth century (i.e., the first quantum revolution) and later (the second quantum revolution), with the latter being defined here in the context of influences upon quantum advances related to emerging quantum technologies depicted in Figure 1 that promise to strongly influence the global society of the twenty-first century.

## 2 The first quantum revolution

To fully understand the state of today's modern sciences and technologies, one must first understand the history of society's transition from classical to quantum science. The evolution of basic physics and chemistry, and to a lesser extent health sciences,

engineering, and mathematics, during the last century to today are presented and discussed.

Figures 2, 3 present timelines of major events of the twentieth and twenty-first centuries that have contributed to what we refer to as the quantum revolution(s).

At the time of the first quantum revolution (see Figure 2), circa 1900, experimental techniques had advanced to a degree of accuracy and precision that provoked some in the scientific community to challenge the veracity of classical theories of the age.

### 2.1 Quantization of radiation

One such phenomenon was that of black body radiation, a problem that in 1859 was described by Kirchhoff as: "...how does the intensity of the electromagnetic radiation emitted by a black body depend on the frequency of the radiation and the temperature of the body?" (Wikipedia, 2022d).

### The 1<sup>st</sup> Quantum Revolution

- 1900** Max Planck introduces his postulate that the energy of oscillators in a black body is quantized,  $E=h\nu$ , where  $h$  is Planck's constant and  $\nu$  is the frequency of light. Planck receives the 1918 Nobel prize in physics.
- 1905** Albert Einstein explains the photoelectric effect—shining light on certain materials release electrons from their surfaces. Relying on Planck's constant, he proposes that light consists of individual quanta. Einstein receives the 1921 Nobel prize in physics. Robert Millikan receives the 1923 Nobel in physics for experimentally validating Einstein's photoelectric theory and measurement of electron charge.
- 1913** Neils Bohr proposes his model of the atom that has a positively-charged centrally-located nucleus with orbiting negatively-charged electrons that are confined to discrete orbits (i.e. stationary orbits) defined by quantized energy and angular momentum predicting spectral emission lines among other properties. Bohr receives the 1922 Nobel in physics.
- 1923** Louis de Broglie puts forth his theory of *matter waves* postulating that quantum particles exhibit wave-like characteristics. He receives the 1929 Nobel prize in physics.
- 1925** Werner Heisenberg, Max Born, and Pascual Jordan formulate *matrix mechanics*, the first conceptually autonomous formulation of quantum mechanics. Heisenberg is awarded the 1934 Nobel in physics.
- 1925-** Bohr and colleagues develop the *Copenhagen Interpretation* that proposes quantum mechanics is indeterministic and obeys the principle of complementarity.
- 1926** Erwin Schrödinger, building upon the work of de Broglie, creates *wave mechanics*.
- 1927** Paul Dirac introduces relativity to the electron wavefunction as the *Dirac Equation* allowing for the prediction of electron spin and antimatter. Dirac shares the 1933 Nobel prize in physics with Schrödinger.



FIGURE 2

A brief review of the first quantum revolution defined by the seminal contributions made by principals from 1900 to c. 1927. Photographs from top to bottom: Planck, Einstein, Bohr, de Broglie, Heisenberg, Schrodinger, and Dirac.

This problem had been explored experimentally, but no theory was proffered that adequately matched the known data of the time. For example, circa 1900, Wien's law (Wien, 1897) correctly predicted behavior at low wavelengths, that is,  $\lambda < 0.1 \mu\text{m}$ , but failed at higher wavelengths, while the Rayleigh–Jeans law (Pais, 1979–10) agreed with results at higher wavelengths, that is,  $\lambda > 0.4 \mu\text{m}$ , but failed at the lower wavelengths; the later providing its  $\lambda^{-4}$  dependence based on classical physical arguments derived from the equipartition theorem. Over the ultraviolet bands, that is,  $0.1 < \lambda < 0.4 \mu\text{m}$ , no theory adequately predicted the electromagnetic radiation emitted by black bodies; this was referred to as the “ultraviolet catastrophe” (Ehrenfest, 1911).

Max Planck, having just been named Kirchhoff's successor at the Friedrich Wilhelm Universität, took up this challenge.

Employing Boltzmann's statistical interpretation of the second law of thermodynamics, he developed what is now known as *Planck's Law*. Planck's Law specifically states that electromagnetic energy can only be emitted in quantized fragments, defined as  $h\nu$ , where  $h$  is a constant of action,  $6.62607015 \times 10^{-34} \text{ m}^2 \text{ kg/s}$  or J·s, to become known as *Planck's constant*, and  $\nu$  is the frequency of the thermal radiation.

Planck empirically obtained an expression (Eq. (1)) for black body spectral radiance ( $B$ ) expressed in terms of wavelength (where  $\lambda = c/\nu$ ):

$$B_\nu(T) = \frac{2h\nu^3}{c^2} \frac{1}{e^{h\nu/kT} - 1}, \quad (1)$$

where  $B_\nu(T)$  is the spectral radiance density of frequency  $\nu$  at thermal equilibrium of temperature  $T$ ;  $h$  is Planck's constant;  $c$  is the speed of light in free space; and  $k$  is Boltzmann's constant.



### The 2<sup>nd</sup> Quantum Revolution

- 1935 Einstein, Podolsky, and Rosen put forth their *EPR criterion* challenging the counterintuitive nature of quantum mechanics claiming it provides an incomplete description of reality.
- 1935 Schrödinger, critiquing the Copenhagen Interpretation of quantum mechanics, develops a thought experiment in which a cat (forever known as Schrödinger's cat) is simultaneously dead and alive until confirmed. That year, he introduces for the first time the term *verschränkung*, translated as *entanglement*.
- 1947 In a letter to Born, Einstein refers to entanglement as "spukhafte fernwirkung", translated loosely as "spooky action at a distance."
- 1964 John Stewart Bell, ironically motivated to establish supremacy of EPR, proposes that entangled particles are correlated in quantum ways that cannot be explained by *hidden variables*. His work leads to *Bell's theorem* that states through an experimentally testable inequality (the *Bell inequality*) that statistical models of hidden variables cannot reproduce the predictions of quantum mechanics for entangled particles.
- 1976 Roman Stanisław Ingarden publishes the first attempt at creating a quantum information theory.
- 1980 Paul Benioff proffers a quantum mechanical model of a *Turing machine*; the first to demonstrate the possibility of *quantum computing*.
- 1982 Richard Feynman argues classical physics is local, causal, and deterministic so classical computer simulations typically prove to be adequate. To simulate quantum systems that are inherently nonlocal and indeterministic one requires quantum computers of similar characteristics.
- 1985 David Deutsch formulates a description for a *quantum Turing machine*.
- 1992 The Deutsch–Jozsa algorithm is one of the first examples of a quantum algorithm that is exponentially faster than deterministic classical algorithms.
- 1993 First paper describing *quantum teleportation*, i.e. the transfer of quantum information of great distances, is published by Charles Bennett.
- 1994 Peter Shor develops a quantum algorithm for factoring integers that has the potential to decrypt RSA-encrypted communications, a widely-used method for securing data transmissions.

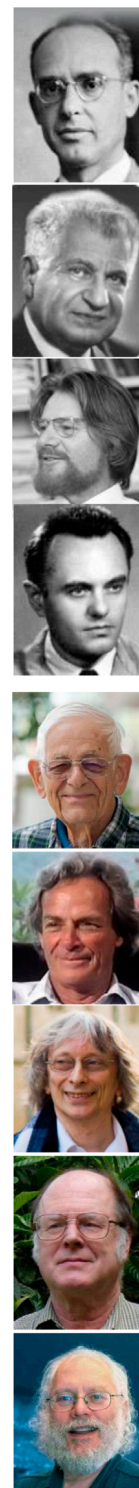


FIGURE 3  
(Continued).

At the time of his breakthrough, Planck did not believe his theory captured *physical reality* and thought that  $h$  served as nothing more than a mathematical convenience. Notwithstanding his lack of self-confidence, Planck's work grew in relevance and import, eventually being recognized as the *first pillar of quantum*

*physics*. Planck was subsequently awarded the 1918 Nobel Prize in physics.

Another who took up the mantle to challenge foundational canons of classical physics was a then largely unknown, third-class patent clerk, Albert Einstein. Armed with only thought experiments,



FIGURE 3

(Continued). (A) The second quantum revolution is defined by the seminal contributions made by principals in advancing quantum theory in entanglement and superposition over the period of 1935–1994. Photographs from top to bottom include Podolsky, Rosen, Bell, Stanislaw, Benioff, Feynman, Deutsch, Bennett, and Shor. The timeline presented defines major events in the quantum revolution influencing the future of quantum computing, teleportation, and encryption. (B) The second quantum revolution continues with seminal contributions made by principals in quantum computing, information sciences, teleportation, and quantum communication from 1995 to the present. Photographs from top to bottom include Lloyd, Grover, DiVincenzo, Nakamura, Tsai, Pan, Hanson, Awschalom, Aspect, Clauser, and Zeilinger.

that is, *gedankenexperiments*, Einstein dared to challenge some of the most established tenets of science, including those of the illustrious Sir Isaac Newton.

## 2.2 Quantization of electromagnetic energy: The photoelectric effect

In 1905, since declared Einstein's "*annus mirabilis*" or miraculous year, he published four articles that ushered in a new era of scientific enlightenment (Einstein, 1905a; Einstein, 1905b; Einstein, 1905c; Einstein, 1905d).

His first published work, "On a Heuristic Point of View about the Creation and Conversion of Light" (Einstein, 1905a), employed Planck's proposed quanta of electromagnetic energy to solve the paradox of the photoelectric effect.

The photoelectric effect, first reported in c. 1880s, refers to the emission of electrons when light is incident upon a material's surface. Electrons emitted in this manner are identified as *photoelectrons*. By proposing a theory that electrons can only escape the surface of a material when light of a *discrete energy* strikes the surface, as opposed to a flux or polychromatic intensity of light, Einstein provided a second key pillar to early quantum physics. His treatment of light as quanta would usher in the treatment of light as particles, later to be known as *photons*.

This work led to Einstein receiving the 1921 Nobel Prize in physics (delayed by WWI) and established the quantization of light, much as Planck provided the quantization of black body radiation. Robert Millikan, who experimentally confirmed Einstein's theory, as well as accurately measured the electron's mass and charge, was awarded the Nobel Prize in physics in 1923.

Einstein's second article, "Investigations on the Theory of Brownian Movement" (Einstein, 1905b), led to the confirmation of the existence of atoms and their approximate size. Some argue this work could well have earned him the Nobel because the existence of atoms at that time was not universally accepted, and this work placed both the existence and the approximate size of atoms on a firm footing.

His third article, and arguably the most bold and influential work of 1905, was his introduction of special relativity that challenged the pedagogy of Newtonian mechanics. This article, "On the Electrodynamics of Moving Bodies" (Einstein, 1905c), reconciled Maxwell's equations for electricity and magnetism with the laws of Newtonian mechanics by introducing major changes to the interpretation as relative speed approaches the speed of light. This became known as Einstein's *Special Theory of Relativity*. It is here that Einstein introduces a theory of time, distance, mass, and energy that are consistent with Maxwell's electromagnetism but omits the force of gravity, which would appear in his later opus on the *General Theory of Relativity* (Einstein, 1905e). An essential component of this third article is Einstein's proposal that the speed of light is a fundamental constant of nature for all reference frames (i.e., independent of the state of motion of the light-emitting body). Einstein's embrace of the foundational import of the speed of light as a fundamental constant will be revisited in our discussion of entanglement, which challenges this principle. As a result of this third article, the symmetries of spacetime were augmented by internal symmetries. The world view of modern theoretical physics can be traced back to the fundamental

postulate that physical phenomena do not change just because you happen to be moving instead of standing still. As reported by Jackson, "Asking about the impact of special relativity on theoretical physics, is like asking about the impact of Shakespeare on the English language" (Jackson, 1987).

In his fourth and final article of 1905, entitled "Does the Inertia of a Body Depend Upon its Energy Content?" (Einstein, 1905d), Einstein introduces his mass-energy equivalence theory, providing what is inarguably the most famous equation in human history:  $E = mc^2$  (Wikipedia, 2022c). This equation states that the energy of a body at rest equals its mass times the speed of light squared. Because the speed of light, or  $c$ , is 299,792,458 m/s, the amount of potential energy that is available is enormous. This would be confirmed in later years through the development of atomic bombs and nuclear reactors.

## 2.3 Quantization of electronic angular momentum

Circa 1911–1912, soon after earning his Ph.D. under the tutelage of Christian Christiansen at the University of Copenhagen, Niels Bohr joined the renowned experimentalist Ernest Rutherford at Victoria University of Manchester. For his first assignment, Rutherford challenged Bohr to bring stability to his (Rutherford's) planetary model of the atom that had recently eclipsed the "plum pudding" model of J.J. Thomas (the discoverer of the electron). Although popular, Rutherford's atomic model came under attack for a critical flaw, whereupon orbiting negatively charged electrons would lose energy and spiral inward, ultimately crashing into the positively charged nucleus and annihilating the atom. It is noteworthy that both Joseph Larmor and Jean Perrin had proposed planetary atomic models (DBpedia, 2023) earlier than Rutherford, but Rutherford's model was more widely accepted and attributed to him.

In a series of three articles published in 1913 (Bohr, 1913a; Bohr, 1913b; Bohr, 1913c), Bohr's proposed model of the atom ushered in another quantum milestone. Bohr's model, similar to Rutherford's (and others), had a positively charged centrally-located nucleus with orbiting negatively charged electrons. However, he confined electrons to discrete orbits defined by their quantized angular momentum and energy by applying Planck's constant.

A key attribute of the Bohr model is its ability to explain the spectral emission lines of hydrogen, that is, the Balmer series, using discrete transitions of electrons between quantized orbits. These stable orbits, labeled stationary orbits, are maintained at discrete energies from the nucleus. The electron cannot have any other orbit in between these discrete orbits; those energies are *forbidden*. Electrons only gain and lose energy by jumping from one allowed orbit to another, absorbing or emitting electromagnetic radiation with a frequency,  $\nu$ , determined by the energy difference of the orbital levels in accordance with the relation, for example,  $\Delta E = E_2 - E_1 = h\nu$ , where  $h$  is Planck's constant. The energy level of such orbits became the principal quantum number,  $n$ . This work led to Bohr receiving the 1922 Nobel Prize in physics.

The seminal works of Planck, Einstein, and Bohr provided quantization of black body radiation, light, and electron angular momentum, respectively, and allowed the photon and electron

to assume particle-like behavior in contradiction to the accepted Maxwellian doctrine.

This particle-dominated interpretation of quantum physics continued until circa 1923, whereupon Louis de Broglie, son of Victor Duc de Broglie and Pauline d'Armaillé, put forth the disruptive theory of *matter waves*, postulating that quantum particles exhibit wave-like characteristics (Broglie, 1924); a theory he derived from Einstein's *Special Theory of Relativity* and subsequently earned him the (singular) 1929 Nobel Prize in physics.

## 2.4 Equivalence of matrix and wave mechanical quantum theories: enter the Copenhagen Interpretation

During 1925–1926, quantum theory entered into a time of rapid evolution and conflict, whereupon a dual theoretic framework that included the work of Heisenberg, Born, and Jordan, championing particle-like behavior and *matrix mechanics* (Heisenberg, 1925) and Schrödinger, building upon the work of de Broglie, advocated for wave-like behavior of quantum particles described by *wave mechanics* (Schrödinger, 1926). For his contributions, Heisenberg was solely awarded the 1934 Nobel in physics, while Born was solely awarded the same prize much later in 1954 for his lifetime contributions to quantum mechanics.

In 1927, Dirac stunned the physics community by introducing relativity to Schrödinger's electron wavefunction equation. This led to what is known as the *Dirac Equation*, which provided a more accurate description of the behavior of the hydrogen atom and predicted *electron spin*, *magnetic monopoles*, and *antimatter*, among other surprises (Dirac, 1926; Dirac, 1927). Dirac shared the 1933 Nobel Prize in physics with Schrödinger.

Shortly thereafter, an important contribution was made by a young Hungarian mathematician, physicist, computer scientist pioneer, engineer, and polymath, Jancsi “Johnny” von Neuman, who was the first to prove the mathematical equivalence of Heisenberg's *matrix* and Schrödinger's *wave* mechanical quantum theories<sup>3</sup> (Maeda, 1937). During his lifetime, von Neuman made

numerous seminal contributions to quantum physics, mathematics, economics, game theory, cellular automata, early digital computer development in hardware, software, and information theory, among others (Macrae, 1992).

Finally, of relevance to this article, the concept of electron *spin*, that is, the fourth quantum number, was first proposed by Kronig in 1925 while a graduate student at Columbia University. His concept was soundly criticized by a visiting Wolfgang Pauli leading to Kronig opting not to publish. Several months later, Goudsmit and Uhlenbeck of Leiden developed a comparable theory that was also criticized by a visiting Pauli, but their advisor Ehrenfest, being favorably impressed, immediately submitted the work for publication (Uhlenbeck and Goudsmit, 1926). Goudsmit and Uhlenbeck have since been attributed as the discoverers of electron spin. Perhaps due to confusion over credit, no Nobel Prize was ever awarded for the discovery of *spin*. This is considered a considerable oversight by the physics community due to the immense significance and impact of spin (Commins, 2012).

The *Copenhagen Interpretation* dominates much of the twenty-first century's discourse on quantum mechanics.

This theory evolved to accommodate both wave and particle views of quantum systems, perhaps in response to von Neuman's rigorous proof of equivalence. Although the *Copenhagen Interpretation* is largely attributed to Niels Bohr, its most recognized champion, it represents a plurality of views attributed to Bohr, his colleagues, and students at the Institute of Theoretical Physics of the University of Copenhagen, an institute founded by Bohr in 1921 that continues to provide leadership to the quantum community. Common themes of the *Copenhagen Interpretation* include the idea that quantum mechanics is inherently *indeterministic* and obeys the principle of *complementarity*; that is, quantum particles have certain complementary properties that cannot be simultaneously observed and measured. In Bohr's view, the behavior of quantum particles cannot be separated from the influence of measurement; hence, one must consider the particle under study together with its measurement in order to obtain a comprehensive description. Either one, without the other, provides an incomplete picture of reality.

## 3 The second quantum revolution

The second quantum revolution (see Figure 3A,B), as defined here, begins with the controversial 1935 publication by Einstein, Podolsky, and Rosen (henceforth EPR). EPR challenged the completeness provided by the state of quantum mechanics at that time (Einstein et al., 1935-05).

### 3.1 The Einstein–Podolsky–Rosen (EPR) paradox

EPR specifically describes a pair of particles in an *entangled state* and asserts that if the position of the first particle is measured, the result would allow for the prediction of the second particle's position with absolute certainty. Alternatively, if the momentum of the first particle is measured, then the momentum of the second

<sup>3</sup> von Neumann was the first to establish a rigorous mathematical framework for quantum mechanics, known as Dirac–von Neumann axioms, in his 1932 text *Mathematical Foundations of Quantum Mechanics*. He realized (c. 1926) that a state of a quantum system could be represented by a point in complex Hilbert space as infinite-dimensional, even for a single particle. In this formalism, observable quantities such as position or momentum are represented as linear operators acting on the Hilbert space associated with the quantum system. Quantum mechanics was hence reduced to the mathematics of Hilbert spaces and the linear operators acting on them. This new mathematical formulation included the formulations of both Heisenberg and Schrödinger as special cases. Remarkably, in this work, von Neumann also foundationally addressed issues that would appear years later, such as determinism *versus* non-determinism, hidden-variable theory, and Bell's theorem together with the experiments of Aspect (c. 1982) that support today's interpretation of quantum physics, including the validity of nonlocality in apparent violation of special relativity.



particle could be similarly predicted with certainty. EPR argues that no action taken on the first particle could instantaneously affect the other because that would require information to be transmitted faster than the speed of light, which is forbidden by Einstein's *Special Theory of Relativity*. In short, physics is local and deterministic.

From this, they developed the EPR criterion:

“If, without in any way disturbing a system, we can predict with certainty (i.e. with probability equal to unity) the value of a physical quantity, then there exists an element of physical reality corresponding to this physical quantity.” (Commins, 2012).

However, in accordance with Heisenberg's *Uncertainty Principle*, those observables are incompatible, and therefore, quantum theory does not provide a complete description of reality.

Schrödinger first employed the word *Verschränkung*, translated from German as *entanglement*, to describe correlations between two distant particles in a letter to Einstein (c. 1935). He expanded upon this concept in a later publication (Schrödinger, 1935).

Like Einstein, Schrödinger was dissatisfied with the idea of transmission of information exceeding the speed of light. Einstein famously ridiculed entanglement as “spukhafte Fernwirkung” or “spooky action at a distance.”

## 3.2 De Broglie–Bohm theory

In 1951, 16 years after the publication of EPR, David Bohm proposed a variant to the EPR thought experiment in which the measurement of a variety of discrete possible outcomes, unlike position and momentum, were considered (Bohm and Aharonov, 1957).

The *EPR–Bohm* thought experiment employed an electron–positron pair. In that experiment, the electron is sent to destination *A*, where it is observed, somewhat famously, by Alice, and the positron is sent to destination *B*, where it is observed by her equally famous colleague Bob. According to quantum mechanics, the emitted pair contributes to a quantum state called a *spin singlet*. A spin singlet refers to a set of particles whose net angular momentum is zero; that is, its overall spin quantum number, *s*, is zero. As a result, only one spectral line is emitted from this singlet, and the particles are said to be *entangled*.

This can be viewed as a quantum *superposition* of two states. In state 1, the electron has its spin aligned upward  $\uparrow$ , and the positron has its spin aligned downward  $\downarrow$ . In state 2, the electron has spin  $\downarrow$  and the positron spin  $\uparrow$ . Because it is in a state of superposition, it is impossible without measurement to know the definite spin state of either particle. This is akin to Schrödinger's famous cat, who is both dead and alive until its box is opened to confirm its state of livelihood.

Alice now measures the spin of the electron, whereupon she obtains one of two possible outcomes  $\uparrow$  or  $\downarrow$ . If she measures  $\uparrow$ , the quantum state of the system has collapsed into state 1, and if Bob subsequently measures the spin of the positron, there is a 100% probability that he will obtain  $\downarrow$ . Similarly, if Alice measures electron spin  $\downarrow$ , Bob measures positron spin  $\uparrow$ .

The *de Broglie–Bohm* theory is an interpretation of quantum mechanics that postulates that the configuration of particles exists before measurement. Furthermore, the evolution over time of such quantum particles is governed by the time-dependent Schrödinger equation.

The theory is *deterministic* and *explicitly nonlocal* and depends on the configuration of particles under consideration. Measurements represent a particular case of quantum processes described by the theory of standard quantum predictions adherent to the *Copenhagen Interpretation*.

Physicists who support the *de Broglie–Bohm* theory maintain that the underlying probabilistic behavior of the Universe represents deterministic foundations validated by *hidden variables*.

Although the motivation for the introduction of a hidden variable stems in large part from the pursuit to validate quantum mechanics' determinism, some indeterministic theories attempt to explain the underlying reality of quantum mechanics employing hidden variables, for example, Nelson's stochastic mechanics (Nelson et al., 1986).

## 3.3 Bell's local realism

The principle of *locality* evolved out of classical field theories and proposes that an object is influenced only by its immediate surroundings and interacts with other objects directly through fields between those objects.

As such, the formalization of locality states that if there are two *observables*, each existing within two distinct but localized regions of spacetime, they must *commute*. Alternatively, a solution to field equations is considered local only if the underlying equations are *covariant* or locally *Lorentz invariant*<sup>4</sup> (Wikipedia, 2022e).

In 1964, John Stewart Bell formulated the *Bell inequality*, sometimes known as *Bell's theorem*, which, if violated, indicates that quantum mechanics violates *local realism*, which relates to the value of unmeasured quantities (Bell, 1964). Oddly, Bell's initial motivation was to establish determinism in physics, but the result has proven quite the opposite.

## 3.4 Hidden variables

The consequence of Bell's theorem is that quantum mechanics is *incompatible* with local hidden-variable theories. Hidden variables, in this context, possess properties related to quantum particles that are undetectable by measurement. They are *local* but do not agree with conventional quantum mechanics pedagogy, and if they do—then they are not local (Bell, 1987).

4 A physical quantity is said to be Lorentz covariant if it transforms under a given representation of the Lorentz group. According to the representation theory of the Lorentz group, these quantities are built out of scalars, four-vectors, four-tensors, and spinors. A Lorentz covariant scalar (e.g., the spacetime interval) remains the same under Lorentz transformations and is said to be a Lorentz invariant (i.e., they transform under the trivial representation).



Specifically, Bell deduced that if measurements were performed on entangled particles, then the assumption that outcomes would depend upon hidden variables implies mathematical constraints on how measurements correlate. Bell showed that quantum mechanics predict correlations that violate this inequality and that no local hidden-variable theories can reproduce statistical predictions of quantum mechanics.

Entering the 1970s, optical experiments had advanced to a degree that allowed robust testing of Bell's theorem. Kocher and Commins demonstrated that an atomic cascade of calcium atoms was a practical source of polarized correlated photons (Kocher and Commins, 1967). This research catalyzed the team of Freedman and Clauser to measure linearly polarized correlated photons emitted in such a cascade (Freedman and Clauser, 1972). By employing a generalization of Bell's inequality, they showed that the existence of local hidden variables imposed restrictions upon observed correlations in conflict with predictions of quantum mechanics. Their findings supported a quantum mechanical description of the Universe *violating* these restrictions to an unprecedented statistical accuracy *against* the existence of local hidden variables.

Aspect et al. followed in 1982, measuring linearly polarized entangled-photon pairs using time-varying analyzers and acousto-optical switching supporting a violation of Bell's inequality to a statistical accuracy greater than *five* standard deviations (Aspect et al., 1982).

Zeilinger's group further advanced experimental work in multiparticle violations of Bell's inequalities (Greenberger et al., 1990) and provided important foundational contributions to quantum teleportation (Bouwmeester et al., 1997a).

As a result of their seminal contributions, Aspect, Clauser, and Zeilinger shared in the 2022 Nobel Prize in physics "for experiments with entangled photons, establishing the violation of Bell inequalities and pioneering quantum information science" (Nobel Prize, 2022).

From these studies and others, it has been shown that the only manner in which hidden variables can explain predictions of quantum physics is if they are inherently *nonlocal*, or in other words, entangled particles are able to interact instantaneously across immense distances (Mermin, 1993). This profound declaration provides guardrails for much of the present and future development of modern quantum theories, models, and technologies.

## 4 Early concepts of quantum computers and information theory

Circa 1960, Feynman reasoned that because classical physics is local, causal, and deterministic, classical computers are only adequate in solving problems of similar character. However, where quantum systems are inherently nonlocal and indeterministic, he proffered one must bring to bear computers of similar nondeterministic properties, that is, quantum computers, to solve quantum problems (Feynman, 1982).

This concept was embodied in the work of Paul Benioff, who laid the foundation of quantum computing with his work (Benioff, 1980) describing a quantum mechanical model of

*Turing Machines*<sup>5</sup> (Wikipedia, 2023), based on Schrödinger's formalism that was motivated in part by the classical description of reversible Turing machines by Charles Bennett of IBM (Bennett, 1973).

However, identifying Benioff's work as the launch point of quantum computing and bestowing upon him the title "Father of quantum computing" would not be without challenge.

David Deutsch, circa 1985, described Benioff's work as "quantum kinematics and dynamics, but effectively classical..." (Deutsch, 1985). Deutsch further defined a *universal* quantum computer as being capable of "perfectly simulating every finite, realizable physical system...with high but not perfect accuracy" (Deutsch, 1985). In that same article, he introduced the first quantum algorithm designed to run on a quantum computer and proposed the use of entangled states as quantum keys. These contributions have led many to assign Deutsch the mantle of "Father of Quantum Computing" (Quantumzeitgeist, 2022).

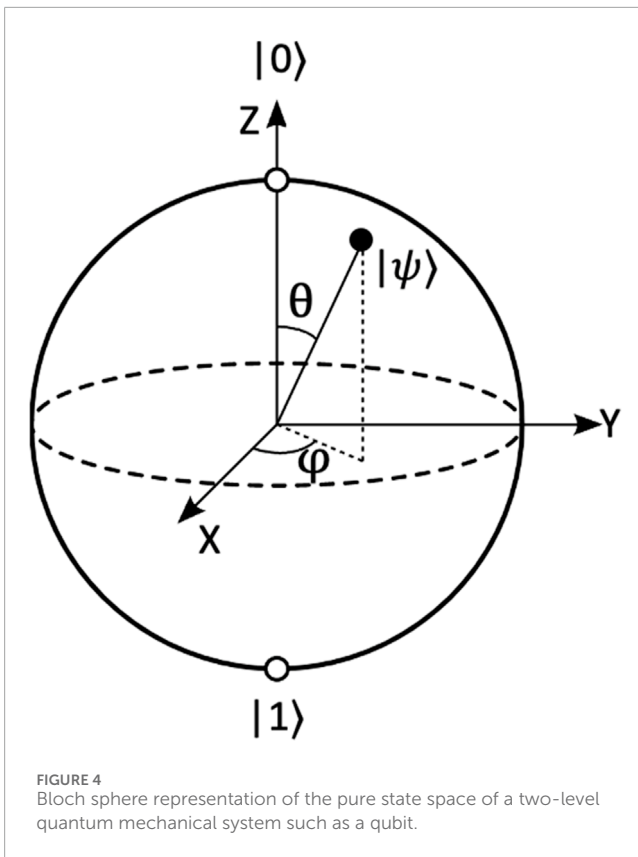
In 1988, Yamamoto and Iqeta proposed the first physical validation of a quantum computer incorporating Feynman's controlled NOT (CNOT) gate (Iqeta and Yamamoto, 1988). Their approach was the forerunner of modern quantum computers and networking protocols using photons to transmit qubits and atoms to perform two-qubit operations.

### 4.1 The DiVincenzo criteria

Moving from theoretical to experimental manifestations of quantum computers, DiVincenzo published an article in 1996 entitled: "Topics in Quantum Computing" (DiVincenzo, 2000), where he outlined five requirements for creating a tangible quantum computer. His criteria have guided much of the experimental research developing quantum computers ever since, allowing for the realization of the ambitions of many quanta computational theorists (Pérez-Delgado and Kok, 2011-01). These requirements have been canonized as the *DiVincenzo criteria* and state that a quantum computer must consist of the following:

1. A scalable physical system with well-characterized qubits,
2. The ability to initialize the state of the qubits to a simple fiducial state,
3. A universal set of quantum gates,

5 A Turing machine is an idealized model of a central processing unit (CPU) that controls all data manipulation done by a computer, with the canonical machine using sequential memory to store data. Typically, the sequential memory is represented as a tape of infinite length on which the machine can perform read and write operations. In the context of formal language theory, a Turing machine (automaton) can enumerate some arbitrary subset of valid strings of an alphabet. A set of strings that can be enumerated in this manner is called a recursively enumerable language. The Turing machine can equivalently be defined as a model that recognizes valid input strings rather than enumerating output strings.



4. Long relevant decoherence times, much longer than the gate-operation times, and
5. A qubit-specific measurement system (Bohm and Aharonov, 1957).

## 4.2 Development of qubits

In accordance with DiVincenzo's first and second criteria, qubits must be initialized to a well-defined and understood (fiducial) state.

By definition, a qubit is a basic unit of quantum information that can be any two-level, that is, two-state, system that can exist in superposition. (The name *qubit* was contrived in 1995 by Schumacher, who shares credit with his colleague Wootters (Schumacher, 1995).) Further, whereas in a classical system, a bit would exist in a well-defined state of "1" or "0," the qubit may exist as a "1" or "0" or a *superposition* of both states. This quantum mechanical property is described using a geometrical representation of the pure state space in Hilbert space, referred to as a Bloch sphere (see Figure 4).

For a two-dimensional Hilbert space, the space of all such states is the complex vector. The north and south poles of the Bloch sphere are assigned to standard quantum basis vectors,  $|0\rangle$  and  $|1\rangle$ , respectively. When applied to an electron qubit, the poles would correspond to spin-up  $\uparrow$  and spin-down  $\downarrow$  states of the electron, respectively. The points on the surface of the sphere correspond to

*pure* states of the system, whereas the interior points correspond to *mixed* states.

In further consideration of an electron as a qubit, under the application of a magnetic field, the electron spin will polarize down  $\downarrow$ , while after exposure to microwave energy, the spin aligns up  $\uparrow$ . If the microwave pulse is terminated between transitions, the spin may exist in a state of superposition (Eq. (2)), such that:

$$\sum_x \psi(x)|x\rangle \quad (2)$$

where  $\psi(x)$  represents the electron wavefunction, summing over all infinite terms. This equation completely describes the quantum state of the electron. A qubit having both position and spin would be described as Eq. (3):

$$\sum_x \psi_+(x)|x, \uparrow\rangle + \psi_-(x)|x, \downarrow\rangle \quad (3)$$

If one generalizes this term for a particle that can be in any one of infinitely many discrete positions, the superposition principle informs Eq. (4):

$$\sum_x \psi_n |n\rangle \quad (4)$$

This expression gives rise to the state vector in Hilbert space, an infinite-dimensional complex vector space. The sum of the state's *absolute squares of the amplitudes* must sum to unity (Eq. (5)) (Wikipedia, 2022g).

$$\sum \psi_n^* \psi_n = 1 \quad (5)$$

Researchers have implemented qubits as several physical manifestations, including:

- Photonic qubits,
- Spin qubits (including spin-orbit qubit),
- Superconducting qubits as charge, flux, and phase qubits,
- Vibrational qubits,
- Topological qubits, that is, anyons,
- Trapped ions,
- among other variants.

A key attribute of qubits is their *coherence*, or rather, their ability to retain quantum information. The loss of such information is referred to as *decoherence*. If qubits remain perfectly isolated from their environment, then coherence will be maintained for prolonged periods. However, as soon as a qubit is allowed to interact with its environment, quantum decoherence occurs. The rate of decoherence depends upon the degree of coupling by the qubit to its environment and its intrinsic stability to encode quantum information. As with any quantum-coupled system, entanglements are generated between the system and its environment and its measurement (i.e., in accordance with the Copenhagen Interpretation).

Guided by the *DiVincenzo criteria*, the development of modern quantum computers has been enabled by the rapid advance of qubit modalities and their coherence and subsequent computational fidelities. We delve more deeply into these concepts later in this article.

To better understand the differences between quantum annealing and gate-based adiabatic quantum computers (AQC), problems must be expressed in terms of quantum gates and associated quantum circuitry.

### 4.3 Quantum logic gates

Although this article focuses predominantly on quantum materials, a brief review of quantum logic gates and circuitry is called for to provide the reader with the necessary background in quantum information theory to appreciate the overall import and impact of QMs.

Unlike many classical logic gates, all quantum logic gates are *reversible*. It is possible to perform classical computing operations using only reversible gates. For example, the reversible Toffoli gate can implement all Boolean functions, often at the cost of having to use ancilla bits. The Toffoli gate has a direct quantum equivalent, showing that quantum circuits can perform all operations performed by classical circuits.

Quantum logic gates are represented by unitary matrices, such that a gate that acts on  $n$  is represented by the unitary matrix, and the set of all such gates with group operation of matrix multiplication represents the symmetry group  $U(2^n)$ . The quantum states that gates act upon are unit vectors in  $2^n$  complex dimensions, with complex Euclidean norm (the 2-norm) (Nielsen and Chuang, 2000; Yanofsky and Mannucci, 2013). The basis vectors, that is, eigenstates, are possible outcomes when measured, and a quantum state is a linear combination of such measurements. Although common quantum gates operate on vector spaces of one or two qubits, quantum gates are now being developed to act on three or more qubits.

Figure 5 presents a list of some common gates categorized as operating on one, two, and three (or more) qubits. Further, Table 1 provides a further subset of these gates in which details such as symbols, permutation matrices, operational descriptions, and, when appropriate, truth tables are presented. Even though quantum logic gates belong to continuous symmetry groups, their implementation as hardware is inexact and introduces errors that lead to the degradation of quantum-state fidelities. When error-correction stratagems are employed, gates are further restricted to finite sets (Bennett, 1973; Williams and Clearwater, 1998).

Progress has been made on some gate classifications (Grier and Schaeffer, 2022). For example, Bouland et al. (2016) classified all 2-qubit commuting Hamiltonians, while Childs et al. (2010) characterized all 2-qubit Hamiltonians that are restricted to circuits over two qubits. Bouland and Aaronson (2014) completed a classification for linear optics of 2-mode beam splitters, while Amy et al. (2020) provided a classification for Clifford + T circuits based on elements appearing as unitary matrices.

In Figure 5, some popular gates are presented as *Clifford* and *non-Clifford*. In quantum computing and information theory, Clifford gates are elements of the Clifford group, a set of transformations that normalize the  $n$ -qubit Pauli group. The concept was introduced by Gottesman and is named after the mathematician William Clifford (Gottesman, 1998a). Quantum circuits that consist of Clifford gates can be readily

simulated with a classical computer due to the Gottesman–Knill theorem (GKT)<sup>7</sup>.

Clifford gates are further notable in that they are pivotal to the development of a universal quantum computer. For instance, the stabilizer formalism that tracks state evolution through conjugated Pauli elements is the foundation of several quantum error-correction stratagems (Gottesman, 2010).

There have been many variants involving entangling two-qubit gates with superconducting qubits.

The gates can be classified into two classes. One class contains gates that rely on the dynamical flux-tunability of either the underlying qubits or some separate sub-circuitry. This class includes the direct-resonant iSWAP (Bialczak et al., 2010; Dewes et al., 2012) and the higher-level resonance-induced dynamical  $c$ -phase (DP) (DiCarlo et al., 2009; Barends et al., 2014a) gates.

The second class contains gates in which the qubits have fixed frequencies and microwave activation sources. The gates in this class include the resonator side-band-induced iSWAP (Leek et al., 2009), the cross-resonance (CR) gate (Chow et al., 2012), the Bell–Rabi gate (Poletto et al., 2012), the microwave activated phase gate (Chow et al., 2013), and the driven resonator induced  $c$ -phase (RIP) (Cross and Gambetta, 2015).

## 5 Quantum Annealers, Analog Quantum Simulators, and Universal Quantum Computers

There are three different types of quantum computers: quantum annealers (adiabatic quantum computers, or AQCs), analog quantum simulators (AQS; or analog quantum computers), and universal quantum computers.

*Quantum annealers* are defined as generic solvers of optimization problems such as QUBO<sup>8</sup> problems (Wikipedia, 2022f). Researchers are actively defining ways to improve design efficiencies and application value. Notwithstanding such timely advances, quantum annealing is projected to remain the least powerful and most inflexible of the present quantum computing paradigms.

In contrast, analog quantum simulators (or analog quantum computer) are asserted as powerful and flexible quantum computing platforms. They are anticipated to be employed to solve some of the most challenging problems in drug design, biochemistry, and quantum theory.

<sup>7</sup> The GKT states that quantum circuits can be simulated efficiently on classical computers using 1. Preparation of qubits in computational basis states; 2. the use of Clifford gates; and 3. measurements in the computational basis, enabling the use of standard algorithms for assessing entanglement and quantum error correction.

<sup>8</sup> Quadratic unconstrained binary optimization (QUBO) is a combinatorial optimization problem with a wide range of applications from finance and economics to artificial intelligence and machine learning.

Single-qubit gates	2-qubit gates	3-qubit gates	Clifford Gates
<ul style="list-style-type: none"> <li>• Pauli gates</li> <li>• Pauli power gates</li> <li>• Rotation gates</li> <li>• Quarter turn gates</li> <li>• Hadamard gates</li> <li>• Axis cycle gates</li> <li>• T gates</li> <li>• Global phase gates</li> </ul>	<ul style="list-style-type: none"> <li>• Identity gates</li> <li>• CN gates</li> <li>• SWAP gates</li> <li>• Ising gates</li> <li>• XY gates</li> <li>• Isotropic exchange gates</li> <li>• Parametric swap gates</li> <li>• Orthogonal gates</li> <li>• XXY gates</li> </ul>	<ul style="list-style-type: none"> <li>• Toffoli gates</li> <li>• <u>CCiX</u> gates</li> <li>• Fredkin gates</li> <li>• CCZ gates</li> <li>• Peres gates</li> <li>• Deutsch gates</li> <li>• <u>Margolus</u> gates</li> <li>• <u>CiSwap</u> gates</li> </ul>	<p><b>Clifford Gates</b></p> <ul style="list-style-type: none"> <li>• Pauli gates</li> <li>• Phase gates</li> <li>• Hadamard gates</li> <li>• Controlled-Z gates</li> <li>• Controlled-not gates</li> <li>• Swap gates</li> </ul> <p><b>Non-Clifford Gates</b></p> <ul style="list-style-type: none"> <li>• T gates</li> <li>• B gates</li> <li>• <u>Toffoli</u> gates</li> </ul>

FIGURE 5  
Some popular gates as *Clifford* and *non-Clifford* classification. The reader is directed to the text for further description.

Finally, universal quantum computing is the ultimate manifestation of analog quantum computers that will access arrays of upward of  $10^6$  entangled qubits. The principal idea behind universal computing is to vector computational power to the most thought-provoking problems of yet unimagined complexity (Essential, 2022).

## 5.1 Quantum annealers and adiabatic quantum processors

In our physical or classical experiences, we observe that time-evolving systems attempt to attain a minimum free energy. For example, in the case of metallurgy, temperature and time are used in concert to create time-varying thermal gradients to enhance atomic mobility, allowing for grain size refinement (e.g., via Ostwald ripening) and the annihilation of defects leading to desired morphologies and microstructures.

Quantum annealing originated from theoretical research performed in the 1980s and 1990s (Apolloni et al., 1988; Apolloni et al., 1989; Ray et al., 1989) and replaces time-varying thermal gradients described in our metallurgy example with quantum thermal fluctuations. Its central importance is in addressing problems of system optimization where energy minimization of a problem-specific Hamiltonian is employed. For our purposes, quantum annealing is analogous to adiabatic quantum computations (analog quantum computers) that rely on the adiabatic theorem to perform calculations (Farhi et al., 2000).

When considering the minimization of a *target variable*, the fundamental goal is to guide the system to avoid local

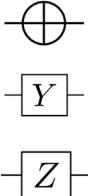
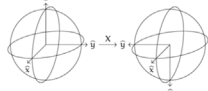
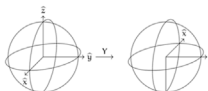

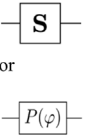
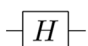
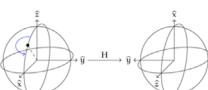
minima and attain the global minimum. D-Wave Systems of Canada has made quantum annealing computers available to commercial markets. Their platforms also run *Qbsolv*, which is open-source software that solves quadratic unconstrained binary optimization (QUBO) problems on D-Wave's quantum processors (D-Wave Initiates Open Quantum Software Environment, 2022a). D-Wave employs superconducting phase qubits for their quantum annealing computers (Harris et al., 2010a; Next Big Future, 2022). Figure 6 is a photograph of D-Wave Systems' chip designed to operate as a 128-qubit superconducting adiabatic quantum optimization processor (QCI, 2022).

In superconducting qubit modalities, electron wavefunctions allow for quantum tunneling through potential barriers instead of electrons imagined as particles jumping over such barriers governed by classical mechanics. Such quantum annealing processes take place over relatively long time durations. If a too-slow *tempering* is applied, a greater cost is incurred in terms of computing power, working memory, and processing time (Wikipedia, 2022a).

In quantum annealing, the system begins in the lowest energy eigenstate of the initial *problem-specific Hamiltonian*. Ideally, it stays in the minimum energy state throughout the quantum annealing so that by the end of the process, it is in the minimum energy state of the Hamiltonian and, therefore, has an answer to the problem at hand. For this reason, prolonged qubit coherence is required.

A classical Hamiltonian is a mathematical representation of a physical system in terms of its energies. One can input any particular state of the system, and the Hamiltonian returns the energy for that state. For most non-convex Hamiltonians, finding the minimum

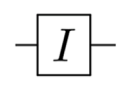
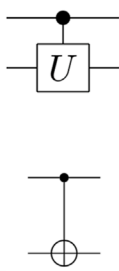
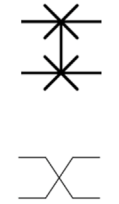
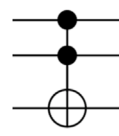
TABLE 1 Expanded properties of some common quantum gates.

Gate	Symbol <sup>vi,75</sup>	Matrix	Description	Ref.
<b>Single-qubit gates</b>				
Pauli gates (X,Y,Z)		$X = \sigma_x = \text{NOT} = \begin{bmatrix} 0 & 1 \\ 1 & 0 \end{bmatrix},$ $Y = \sigma_y = \begin{bmatrix} 0 & -i \\ i & 0 \end{bmatrix},$ $Z = \sigma_z = \begin{bmatrix} 1 & 0 \\ 0 & -1 \end{bmatrix}.$	<p>The Pauli gates (X, Y, Z) are the three Pauli matrices (<math>\sigma_x, \sigma_y, \sigma_z</math>) that act on a single qubit. The Pauli X, Y and Z equate, respectively, to a rotation around the x, y and z axes of the Bloch sphere by <math>\pi</math> radians.</p> <p>The Pauli-X gate is the quantum equivalent of the NOT gate for classical computers with respect to standard bases <math> 0\rangle</math> and <math> 1\rangle</math>, which distinguishes the z-axis on the Bloch sphere. It is sometimes called a <i>bit-flip</i> as it maps <math> 0\rangle</math> to <math> 1\rangle</math> and from <math> 1\rangle</math> to <math> 0\rangle</math>.</p>  <p>Similarly, the Pauli-Y maps <math> 0\rangle</math> to <math>i 1\rangle</math> and <math> 1\rangle</math> to <math>-i 0\rangle</math>.</p>  <p>The Pauli Y-gate can be thought of as a combination of X- and Z-gates; <math>Y=iZX</math>.</p> <p>While Pauli Z-gates leave the basis state <math> 0\rangle</math> unchanged and maps <math> 1\rangle</math> to <math>- 1\rangle</math>. Due to this, Pauli Z-gates are sometimes referred to as the phase-flip.</p> 	Nielsen and Chuang, 2000
Phase shift gate		$\begin{bmatrix} 1 & 0 \\ 0 & e^{i\varphi} \end{bmatrix}$	<p>The phase shift gates are a family of single-qubit gates that map the basis states <math> 0\rangle \rightarrow  0\rangle,  1\rangle \rightarrow e^{i\varphi} 1\rangle</math>. The probability of measuring <math> 0\rangle</math> or <math> 1\rangle</math> remains unchanged after applying this gate, however it modifies the phase of the quantum state. This is equivalent to tracing a horizontal circle about the z-axis on the Bloch sphere by radians.</p>	ibid
Hadamard gate		$\frac{1}{\sqrt{2}} \begin{bmatrix} 1 & 1 \\ 1 & -1 \end{bmatrix}$	<p>The Hadamard acts on a single qubit. It maps the basis states <math> 0\rangle \rightarrow \frac{ 0\rangle +  1\rangle}{\sqrt{2}}</math> and <math> 1\rangle \rightarrow \frac{ 0\rangle -  1\rangle}{\sqrt{2}}</math> (it creates an equal superposition state if given a computational basis state). The Hadamard gate performs a rotation of <math>\pi</math> about the axis of the Bloch sphere.</p> 	ibid

(Continued on the following page)



TABLE 1 (Continued) Expanded properties of some common quantum gates.

2-qubit gates																																																											
Identity gate		$\begin{bmatrix} 1 & 0 \\ 0 & 1 \end{bmatrix}$	The identity gate is represented by the identity matrix, usually written as I, where I is basis independent and does not modify the quantum state. The identity gate is most useful when describing mathematically the result of various gate operations or when discussing multi-qubit circuits.	Barenco et al. 1995																																																							
Controlled gates		$\begin{bmatrix} 1 & 0 & 0 & 0 \\ 0 & 1 & 0 & 0 \\ 0 & 0 & 0 & 1 \\ 0 & 0 & 1 & 0 \end{bmatrix}$	Controlled gates act on two or more qubits, where one or more qubits act as a control for an operation. For example, the controlled NOT gate (or CNOT) acts on 2 qubits and performs the NOT operation on the second qubit only when the first qubit is  1>, otherwise it leaves it unchanged.	ibid																																																							
Swap gate		$\begin{bmatrix} 1 & 0 & 0 & 0 \\ 0 & 0 & 1 & 0 \\ 0 & 1 & 0 & 0 \\ 0 & 0 & 0 & 1 \end{bmatrix}$	The swap gate swaps two qubits with respect to basis  00>,  01>,  10>,  11>. It is represented by the SWAP matrix.	ibid																																																							
3-qubit gates																																																											
Toffoli (CCNOT) gate		$\begin{bmatrix} 1 & 0 & 0 & 0 & 0 & 0 & 0 & 0 \\ 0 & 1 & 0 & 0 & 0 & 0 & 0 & 0 \\ 0 & 0 & 1 & 0 & 0 & 0 & 0 & 0 \\ 0 & 0 & 0 & 1 & 0 & 0 & 0 & 0 \\ 0 & 0 & 0 & 0 & 1 & 0 & 0 & 0 \\ 0 & 0 & 0 & 0 & 0 & 1 & 0 & 0 \\ 0 & 0 & 0 & 0 & 0 & 0 & 0 & 1 \\ 0 & 0 & 0 & 0 & 0 & 0 & 1 & 0 \end{bmatrix}$	The Toffoli gate, also called the CCNOT gate or the Deutsch gate), is a 3-bit gate that is universal for classical computation, but not for quantum computation. Since it is the quantum analog of a classical gate, it is defined by its truth table (below). The Toffoli gate is universal when combined with the single qubit Hadamard gate.	<table border="1" data-bbox="941 1467 1141 1870"> <thead> <tr> <th colspan="3">INPUT</th> <th colspan="3">OUTPUT</th> </tr> </thead> <tbody> <tr><td>0</td><td>0</td><td>0</td><td>0</td><td>0</td><td>0</td></tr> <tr><td>0</td><td>0</td><td>1</td><td>0</td><td>0</td><td>1</td></tr> <tr><td>0</td><td>1</td><td>0</td><td>0</td><td>1</td><td>0</td></tr> <tr><td>0</td><td>1</td><td>1</td><td>0</td><td>1</td><td>1</td></tr> <tr><td>1</td><td>0</td><td>0</td><td>1</td><td>0</td><td>0</td></tr> <tr><td>1</td><td>0</td><td>1</td><td>1</td><td>0</td><td>1</td></tr> <tr><td>1</td><td>1</td><td>0</td><td>1</td><td>1</td><td>1</td></tr> <tr><td>1</td><td>1</td><td>1</td><td>1</td><td>1</td><td>0</td></tr> </tbody> </table>	INPUT			OUTPUT			0	0	0	0	0	0	0	0	1	0	0	1	0	1	0	0	1	0	0	1	1	0	1	1	1	0	0	1	0	0	1	0	1	1	0	1	1	1	0	1	1	1	1	1	1	1	1	0	Toffoli 1980
INPUT			OUTPUT																																																								
0	0	0	0	0	0																																																						
0	0	1	0	0	1																																																						
0	1	0	0	1	0																																																						
0	1	1	0	1	1																																																						
1	0	0	1	0	0																																																						
1	0	1	1	0	1																																																						
1	1	0	1	1	1																																																						
1	1	1	1	1	0																																																						

(Continued on the following page)

TABLE 1 (Continued) Expanded properties of some common quantum gates.

<p>Peres</p>		$\begin{bmatrix} 1 & 0 & 0 & 0 & 0 & 0 & 0 & 0 \\ 0 & 1 & 0 & 0 & 0 & 0 & 0 & 0 \\ 0 & 0 & 1 & 0 & 0 & 0 & 0 & 0 \\ 0 & 0 & 0 & 1 & 0 & 0 & 0 & 0 \\ 0 & 0 & 0 & 0 & 0 & 0 & 0 & 1 \\ 0 & 0 & 0 & 0 & 0 & 0 & 1 & 0 \\ 0 & 0 & 0 & 0 & 0 & 1 & 0 & 0 \\ 0 & 0 & 0 & 0 & 1 & 0 & 0 & 0 \end{bmatrix}$	<p>The Peres gate is equivalent to a Toffoli gate followed by a CNOT gate and decomposes into 5 CNOTs. The Peres gate is also a reversible half-adder. If a zero bit is fed into the third position, then the output of the second bit is the sum of the first two bits, and the third bit is carries.</p>	<p>Peres, 1985</p>																																																												
<p>Fredkin</p>		$\begin{bmatrix} 1 & 0 & 0 & 0 & 0 & 0 & 0 & 0 \\ 0 & 1 & 0 & 0 & 0 & 0 & 0 & 0 \\ 0 & 0 & 1 & 0 & 0 & 0 & 0 & 0 \\ 0 & 0 & 0 & 1 & 0 & 0 & 0 & 0 \\ 0 & 0 & 0 & 0 & 1 & 0 & 0 & 0 \\ 0 & 0 & 0 & 0 & 0 & 0 & 1 & 0 \\ 0 & 0 & 0 & 0 & 0 & 1 & 0 & 0 \\ 0 & 0 & 0 & 0 & 0 & 0 & 0 & 1 \end{bmatrix}$	<p>The basic Fredkin gate is a controlled swap gate (CSWAP) that maps three inputs (C, I<sub>1</sub>, I<sub>2</sub>) onto three outputs (C, O<sub>1</sub>, O<sub>2</sub>). The C input is mapped directly to the C output. If C=0, no swap is performed; I<sub>1</sub> maps to O<sub>1</sub>, and I<sub>2</sub> maps to O<sub>2</sub>. Otherwise, the two outputs are swapped so that I<sub>1</sub> maps to O<sub>2</sub>, and I<sub>2</sub> maps to O<sub>1</sub>. This circuit is reversible and "undoes" itself when run backwards. Its truth table is presented below.</p> <table border="1" data-bbox="949 1003 1182 1391"> <thead> <tr> <th colspan="3">INPUT</th> <th colspan="3">OUTPUT</th> </tr> <tr> <th>C</th> <th>I<sub>1</sub></th> <th>I<sub>2</sub></th> <th>C</th> <th>O<sub>1</sub></th> <th>O<sub>2</sub></th> </tr> </thead> <tbody> <tr><td>0</td><td>0</td><td>0</td><td>0</td><td>0</td><td>0</td></tr> <tr><td>0</td><td>0</td><td>1</td><td>0</td><td>0</td><td>1</td></tr> <tr><td>0</td><td>1</td><td>0</td><td>0</td><td>1</td><td>0</td></tr> <tr><td>0</td><td>1</td><td>1</td><td>0</td><td>1</td><td>1</td></tr> <tr><td>1</td><td>0</td><td>0</td><td>1</td><td>0</td><td>0</td></tr> <tr><td>1</td><td>0</td><td>1</td><td>1</td><td>1</td><td>0</td></tr> <tr><td>1</td><td>1</td><td>0</td><td>1</td><td>0</td><td>1</td></tr> <tr><td>1</td><td>1</td><td>1</td><td>1</td><td>1</td><td>1</td></tr> </tbody> </table>	INPUT			OUTPUT			C	I <sub>1</sub>	I <sub>2</sub>	C	O <sub>1</sub>	O <sub>2</sub>	0	0	0	0	0	0	0	0	1	0	0	1	0	1	0	0	1	0	0	1	1	0	1	1	1	0	0	1	0	0	1	0	1	1	1	0	1	1	0	1	0	1	1	1	1	1	1	1	<p>Brown, 2000 Patel et al., 2016 Fredkin, and Toffoli, 1982</p>
INPUT			OUTPUT																																																													
C	I <sub>1</sub>	I <sub>2</sub>	C	O <sub>1</sub>	O <sub>2</sub>																																																											
0	0	0	0	0	0																																																											
0	0	1	0	0	1																																																											
0	1	0	0	1	0																																																											
0	1	1	0	1	1																																																											
1	0	0	1	0	0																																																											
1	0	1	1	1	0																																																											
1	1	0	1	0	1																																																											
1	1	1	1	1	1																																																											

energy state is an NP-hard<sup>9</sup> problem that classical computers cannot solve efficiently.

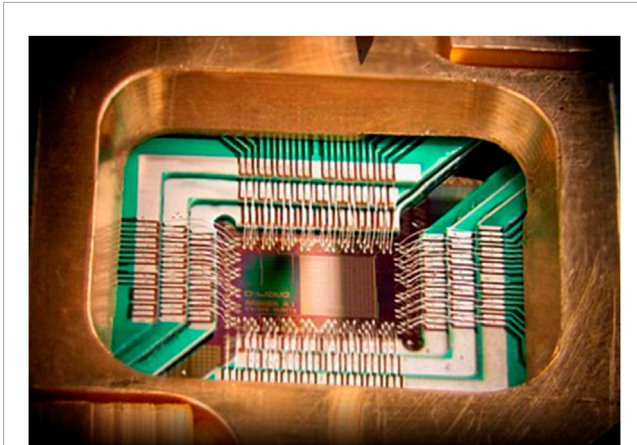
For a quantum system, the Hamiltonian maps certain states, called eigenstates, to energies. Only when the system is in an eigenstate of the Hamiltonian is its energy well defined and called an eigenenergy. The collection of eigenstates with

defined eigenenergies makes up the eigenspectrum. In quantum annealing, for every unique problem, there is a unique Hamiltonian and a unique eigenspectrum. A plot illustrating quantum annealing as eigenenergies versus time is plotted in Figure 7 (Dwavesys, 2022).

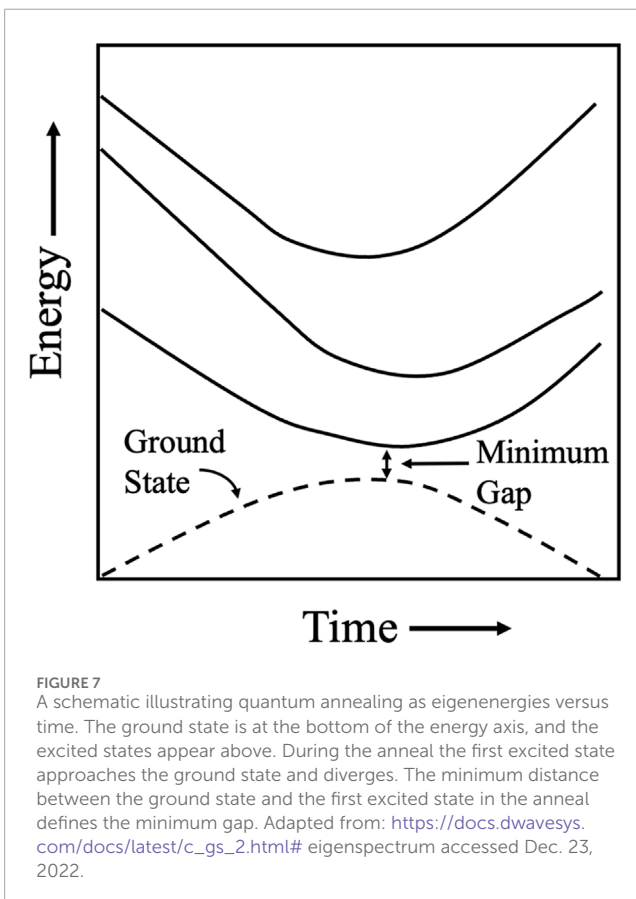
As the *problem-specific* Hamiltonian is introduced, other energy levels shift closer to the ground state, increasing the likelihood that a transition to an excited state occurs. Certain external conditions induce these transitions, including thermal fluctuations of the physical system brought on by coupling to its environment or running the annealing process too quickly. An annealing process that is isolated from external influences allows the Hamiltonian to evolve slowly; this is called an adiabatic process. Because no computation exists in perfect isolation, quantum annealing can be thought of as a close approximation of an adiabatic quantum computers (AQC). The most difficult problem in terms of quantum annealing stems from systems that possess very low *minimum gaps* where inadvertent jumps may take place.

6 The notation for quantum gates was first suggested by several leaders of the community, including Adriano Barenco, Charles Bennett, Richard Cleve, David P. DiVincenzo, Norman Margolus, Peter Shor, Tycho Sleator, John A. Smolin, and Harald Weinfurter. Their contributions built on the notations introduced by Feynman (1985).

9 In computational complexity, NP-hardness, that is, nondeterministic polynomial-time hardness, is the defining property of a class of problems solvable by a nondeterministic Turing machine (TM) in polynomial time. The proof is described, for example, in Sipser (1997).



**FIGURE 6**  
Photograph of a 128-qubit superconducting adiabatic quantum chip constructed by D-Wave Systems, Inc. (Used with permission of D-Wave Systems, Inc. under Creative Commons Attribution 4.0 International License).



**FIGURE 7**  
A schematic illustrating quantum annealing as eigenenergies versus time. The ground state is at the bottom of the energy axis, and the excited states appear above. During the anneal the first excited state approaches the ground state and diverges. The minimum distance between the ground state and the first excited state in the anneal defines the minimum gap. Adapted from: [https://docs.dwavesys.com/docs/latest/c\\_gs\\_2.html# eigenspectrum](https://docs.dwavesys.com/docs/latest/c_gs_2.html# eigenspectrum) accessed Dec. 23, 2022.

D-Wave Systems believes the combination of quantum annealing, gate-based quantum computing, and classical machines is what business users will require in the coming decades to solve mixed integer problems to enable rapid drug design

and development and chemical process optimization, logistics, scheduling, and related optimization problems.

## 5.2 Gate-based analog quantum computers

Several leading electronics companies, such as Google, IBM, and Intel, have built analog quantum computers based on gate-model designs.

These devices typically function at very low temperatures, requiring expensive and large  $\text{He}^{3+}$  dilution refrigeration instrumentation to minimize the deleterious influence of heat upon qubit coherence.

In analog quantum computers, processing power increases relative to classical computers, where  $n$  is the number of qubits. So, if the platform has three qubits, a processing power enhancement of  $2^3$ , or 8x, results relative to a classical computer. Google's *Sycamore*, with 53 qubits, or  $2^{53} \sim 9^{15}$  (Nielsen and Chuang, 2000) over classical computers. In 2019, Google claimed that the *Sycamore* would take 200 s to complete a calculation that a supercomputer of that day would take 10,000 years to complete, thus claiming to have achieved *quantum supremacy*<sup>10</sup> (Harrow and Montanaro, 2017; Kan, 2019). IBM countered that the task would have only taken a mere 2.5 days on a classical platform (On Quantum Supremacy, 2019). Since then, Google has pursued several validation experiments of *Sycamore*'s computational power and utility, including:

- In 2020, a Google research team reported the results of the application of a variational quantum eigensolver (Peruzzo et al., 2014) that approximated the binding energy of  $\text{H}^+$  ion chains in diazene by application of the Hartree–Fock formalism performed on *Sycamore*<sup>11</sup>.
- In April 2021, researchers working on *Sycamore* reported the simulation of anyon interferometry and braiding statistics of topologically ordered states demonstrating long-range entangled properties (Satzinger et al., 2021).
- In July 2021, a Google collaboration using *Sycamore* reported on the many-body localization configuration of up and down spins stimulated with a laser to achieve a periodically driven floquet system. Because no energy was absorbed from the laser, the system remained in a protracted eigenstate such that

<sup>10</sup> The goal of all international efforts in quantum computing is to demonstrate “quantum supremacy,” defined as attaining a programmable quantum device that can solve a problem that no classical computer can solve in any reasonable amount of time. Quantum supremacy involves both the engineering of a *quantum computer* and designing a theoretic task that can be solved by that quantum computer at a superpolynomial speedup over the best-known classical algorithm—“On ‘Quantum Supremacy,’” *IBM Research Blog*, 22 October 2019.

<sup>11</sup> The Hartree–Fock method is typically used to numerically solve the time-independent Schrödinger equation for multi-electron atoms (or molecules) as described by the Born–Oppenheimer approximation.

it represented a time crystal<sup>12</sup> (Zakrzewski, 2012; Wolchover, 2021; Mi et al., 2022).

- In 2022, *Sycamore* was used to simulate traversable wormhole dynamics (Jafferis et al., 2022).

All major quantum-dot cellular automata (QCA) companies are striving to scale up their quantum computational platforms with the ultimate goal of attaining a *mega-qubit computer*.

As illustrated in Figure 8, the growth of the quantum annealer product market is driven by D-Wave Systems. From 2007 to 2022, D-Wave Systems experienced near-exponential growth, with platforms boasting qubits of 128 in 2007 (*D-Wave 1*) to 5,640 in 2020 (*Advantage*). D-Wave expects to launch its next *Advantage-2* machine with over 7,000 qubits, featuring a new connectivity topology, in 2024. In 2011, D-Wave began selling its platforms to U.S. government agencies, organizations, and NGOs, including Low-Cost Mission Operations (LCMO), Google, NASA, and the Los Alamos National Lab (LANL).

Figure 8 presents the evolution of quantum computer advances as a function of the number of incorporated qubits. We note that the number of qubits does not necessarily translate to the number of active qubits in coherence or perfect fidelity. Here, advances in quantum annealing demonstrated by D-Wave Systems are presented in the top panel, whereas gate-based quantum computer advances are presented in the bottom panel for the many companies participating in this market segment. Further, the commercialization of D-Wave Systems' products is reflected beneath the top panel. We remind the reader that gate-based quantum computers are referred to here as analog quantum computers or analog quantum computers.

The first generation of analog quantum computers occurred in 1998 with the introduction of the first working 2-qubit quantum computer based on a liquid-state nuclear magnetic resonance (LS-NMR) qubit modality that employed a solution of chloroform molecules (Chuang I. L. et al., 1998). Soon afterward, circa 2000, researchers demonstrated a 5-qubit (Vandersypen et al., 2000) NMR quantum computer using perfluorobutadienyl complexes and a 7-qubit (Knill et al., 2000) NMR quantum computer using transcrotonic acid with a second 7-qubit NMR quantum computer. Vandersypen et al. (2001) demonstrated using a perfluorobutadienyl iron complex with two inner carbon ions.

The first 12-qubit quantum computer was demonstrated by researchers at the Institute for Quantum Computing and the Perimeter Institute for Theoretical Physics in Waterloo in collaboration with MIT and Cambridge University (Science Daily, 2006).

The years 2017–2019 saw a plethora of activity in large-qubit AQC platforms from Google, IBM, Intel, and IonQ. The evolution

of IBM platforms is presented in Table 2 with details of their designation, number of qubits, and other differentiators.

In late 2022, IBM released *Osprey*, a 433-transmon-based qubit analog quantum computers boasting a new ribbon wiring modality, depicted in Figure 9A, with enhanced electrical and thermal resistance at cryogenic temperatures, leading to a 77% increase in on-chip connections to replace their famous “chandelier” design as depicted in Figure 9B (SCL, 2022).

While IBM and Google invested in superconducting qubits (i.e., transmons and other forms), IonQ adopted trapped-ion technology (Maunz, 2016). Their work consisted specifically of a laser-cooled  $32 \times 1$  (Ma X. S. et al., 2012)  $\text{Yb}^+$  ion-chain trapped above a microfabricated chip. Each physical qubit was encoded in  $^2S_{1/2}$  electronic ground-state hyperfine “clock” states,  $|0\rangle \equiv |F = 0; m_F = 0\rangle$ ,  $|1\rangle \equiv |F = 1; m_F = 0\rangle$ , with a qubit frequency splitting of  $\omega_0 = 2\pi \times 12.642820424$  (4) GHz. The qubits have a measured decoherence time in excess of 2.75 s, limited by the stability of the external magnetic field, and an average single-shot detection fidelity of >99.5% (Egan et al., 2020; Wikipedia, 2022c).

Other key players in quantum computational platforms are Xanadu (photonic qubits), Rigetti (superconducting qubits), Intel (“hot” silicon spin qubits (Petit et al., 2020)), Baidu (superconducting qubits), and Google and Microsoft (topological qubit). Note: The qubit modality is presented in parentheses after each company.

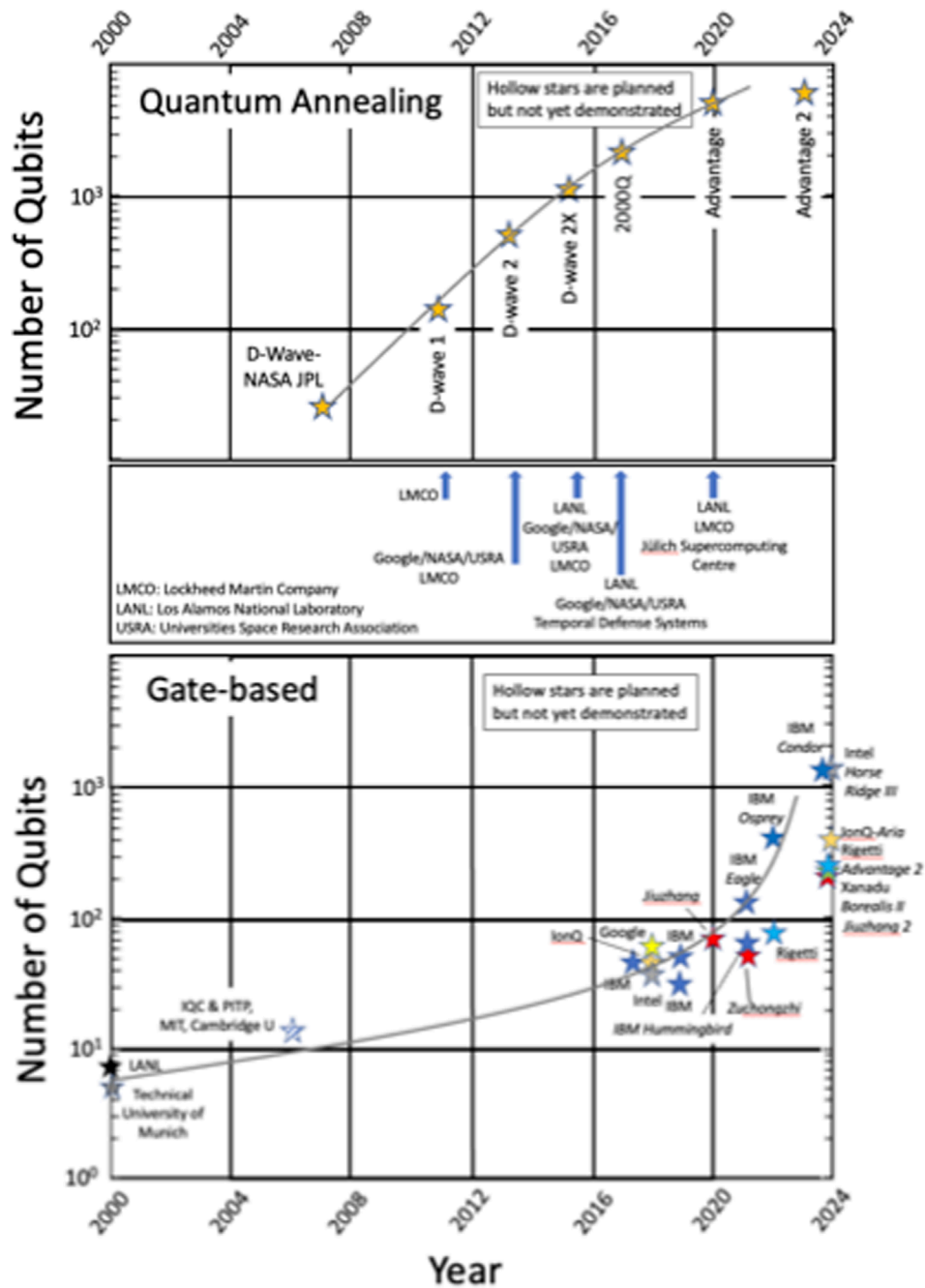
Finally, we report the demonstrations and breakthroughs by Chinese scientists in this realm of quantum physics. Competition in quantum computing between the United States and China, the two dominant global economies, and other international players has resulted in an expansion of the international market size in quantum technologies from USD 10 B in 2021 (Quantum Technology Market Size, 2022b). In addition to the investments made in the private sector, the U.S. government has invested billions in quantum projects sponsored by the Department of Energy (DOE), the Defense Advanced Research Projects Agency (DARPA), and the National Security Agency (NSA), among others.

The Chinese government has kept pace with domestic investments in quantum computing with the creation of a *National Laboratory for Quantum Information Science* (Quantumcomputing, 2022). Additionally, Alibaba has invested USD 15 B to establish the *Academy for Discovery, Adventure, Momentum, and Outlook*, which includes new research laboratories in China, the United States, Russia, Israel, and Singapore (Techniasia, 2022).

Representing China's advances, in 2019, *Jiuzhang* became the first photonic quantum computer to claim quantum supremacy. *Jiuzhang* was developed by researchers at the University of Science and Technology of China (USTC) led by Pan and Lu (Conover, 2020-12). Previously, quantum supremacy had been achieved by Google's *Sycamore* based on superconducting qubits (Kan, 2019).

In December 2020, USTC announced that *Jiuzhang* performed a Gaussian boson sampling in 200 s. The USTC group estimated that it would take 2.5 billion years for the *Sunway* to perform the same calculation (Ball, 2020-12; Letzter, 2020).

<sup>12</sup> A time crystal is a quantum system of particles whose lowest energy state is one in that the particles are in a repetitive motion that does not lose energy to the environment and come to rest because it is already in its quantum ground state. The motion of the particles does not represent kinetic energy; it has “motion without energy.” The atoms in a time crystal are arranged periodically in both space and time.



**FIGURE 8** A comprehensive illustration of the time evolution of qubit-based quantum annealing (top) and AQC's (bottom) quantum computational platforms up to 2022 (and projected beyond). Industrial sources are denoted for each, and, in some cases, industrial buyers are noted (middle).

### 5.3 Universal quantum computer (a quantum Turing machine)

A universal quantum computer, sometimes referred to as a quantum Turing machine (QTM), harnesses the power of quantum computation by implementation of quantum algorithms. QTMs relate to the classical, or probabilistic, Turing machine by application of the transition matrix. A transition matrix is a square matrix whose elements are probabilistic values of each transition in a Markov chain (Asmussen, 2003; Lawler, 2006). As shown by Fortnow (2003) in the

QTM example, a transition matrix is one in which its product with a matrix representing a classical machine delivers the probability matrix of the quantum machine. [NEW- [https://en.wikipedia.org/wiki/Quantum\\_Turing\\_machine#cite\\_ref-transition\\_3-0](https://en.wikipedia.org/wiki/Quantum_Turing_machine#cite_ref-transition_3-0)].

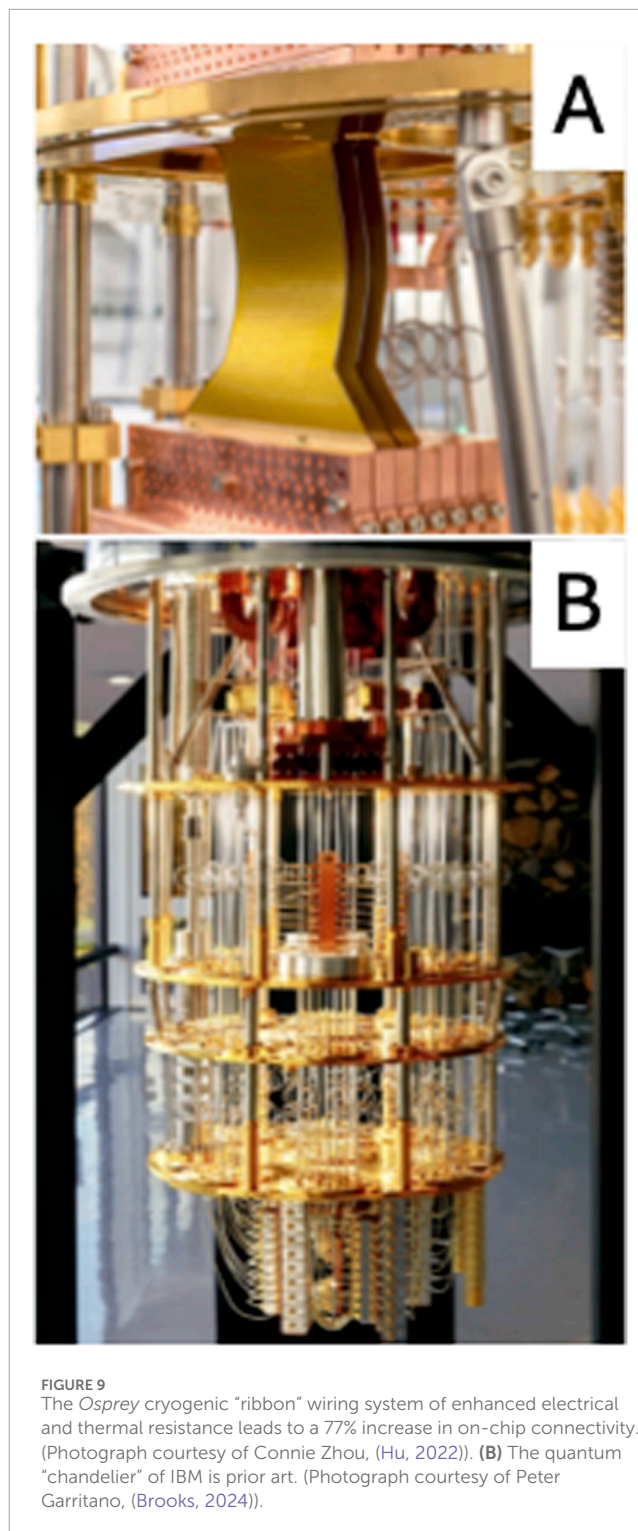
The first description of a quantum mechanical model of a Turing machine was by Benioff in a pair of papers published in 1980 and 1982 (Benioff, 1980; 1982). Deutsch (1985) further suggested that quantum gates could function in a similar fashion to traditional digital computing binary gates.



TABLE 2 Evolution of qubit technology.

Year	Name	Qubits	Differentiators
2017	5Q	5	Resonators and qubits are all on a single lithography layer.
2017	5Q	17	Continuation of 5Q technologies
2019	5Q	27	Cloud-share offering
2019–2020	Canary	16	Optimized 2D lattice: All of the qubits and readout resonators are on the same layer.
2020	Falcon	28	Flip-chip technology allows scaling to a larger number of qubits. The heavy-hex connectivity graph is employed for the first time here, optimal for our two-qubit gate of choice, S. Additionally, pace-saving “direct-couplers” are used to couple qubits.
2021	Hummingbird	65	Includes readout multiplexing, space-efficient qubit-qubit couplers, and flip-chip technology
2021	Eagle	127	More scalable packaging technologies than previous generations. In particular, signals pass through multiple chip layers so as to allow high-density I/O without sacrificing performance, with 3000 gates (2022–2023).
2022	Osprey	433	Introduction of a new ribbon wiring system with superior thermal and electrical resistance at cryogenic temperatures leads to a 77% increase in on-chip connectors.
2023	Condor	1121	IBM invests in the largest to date “dry” dilution refrigerator to manage unprecedented cooling demands to 2 milliKelvin operational temperatures.
2025	Flamingo	1386	Three “Flamingo” processors will be linked into a 1,386-qubit system with demonstrated scaling of modular connectors, with 5000 gates (2025) up to 15,000 gates (2027).
2025–2026	Kookaburra	4158	The “Kookaburra” processor will be a 1,386-qubit multichip processor with a 4,158-qubit system connected by a quantum communication link that scales with a nonlocal c-coupler(s).
2027	Cockatoo	Unk.	Tightly coupled multi-Kookaburra processors of improved quality with logical communications.

IBM'S Condor, debuted in December of 2023, sports a quantum processor with 1,121 superconducting qubits, a 50% increase in qubit density with over a mile of high-density cryogenic flex wiring within its single dilution refrigerator. The Condor is believed to



**FIGURE 9**  
The *Osprey* cryogenic “ribbon” wiring system of enhanced electrical and thermal resistance leads to a 77% increase in on-chip connectivity. (Photograph courtesy of Connie Zhou, (Hu, 2022)). (B) The quantum “chandelier” of IBM is prior art. (Photograph courtesy of Peter Garritano, (Brooks, 2024)).

be the world's first universal quantum computer [NEW- [https://en.wikipedia.org/wiki/IBM\\_Condor](https://en.wikipedia.org/wiki/IBM_Condor). Accessed July 22, 2024].

## 6 Quantum algorithms

Table 3 lists the major milestones in quantum algorithms that have occurred over the past 3 decades. Deutsch's algorithm,

TABLE 3 Evolution of popular quantum algorithms (theory and experimental validation).

Algorithm	Year (discovery)	Year (validation)	Description	Ref.
Deutsch algorithm	1985		Somewhat trivial algorithm of little practical value that addresses functions that take a 1-qubit argument and return a 1-qubit output. It demonstrates a quantum speedup arising from quantum parallelism and interference and is foundational to more sophisticated quantum algorithms to come later, such as Shor's. This work is claimed by many as the start of quantum computing.	Deutsch (1985)
Deutsch and Jozsa algorithm	1992		Deutsch and Jozsa proposed a computational problem that can be solved efficiently with the determinist Deutsch–Jozsa algorithm on a quantum computer, but for which no deterministic classical algorithm is possible.	Deutsch and Jozsa (1992)
Deutsch and Jozsa algorithm		1994	A quantum-optical experiment is proposed on a quantum computer to implement Deutsch's algorithm. Their work introduces dual-rail encoding for photonic qubits.	Chuang and Yamamoto (1995)
Deutsch and Jozsa algorithm		1998	First experimental demonstration of a quantum algorithm. Jones and Mosca use a working 2-qubit NMR quantum computer to solve Deutsch's problem at Oxford University. This demonstration is repeated shortly thereafter by Chuang at IBM's Almaden Research Center and Kubinec at the University of California, Berkeley, together with coworkers at Stanford University and MIT.	Chuang et al. (1998a)
Deutsch and Jozsa algorithm		2003	Implementation of the Deutsch–Jozsa algorithm on an ion-trap quantum computer is demonstrated by researchers at the University of Innsbruck.	Gulde et al. (2003)
Deutsch and Jozsa algorithm		2007	First use of Deutsch's algorithm in a cluster-state quantum computer.	PhysOrg.com Miranda Marquit, (2007), Tame et al. (2007)
Simon's oracle problem	1993		Simon, of the Université de Montréal, invents an oracle problem for which a quantum computer would be exponentially faster than a conventional computer. This formulism introduces the main ideas that are then developed in Shor's factorization algorithm.	Simon (1997-10)
Quantum Fourier transform	1994		In quantum computing, the quantum Fourier transform (QFT) is a linear transformation on quantum bits and is the quantum analog of the discrete Fourier transform. The quantum Fourier transform is a part of many quantum algorithms, notably Shor's algorithm for factoring and computing the discrete logarithm, the quantum phase estimation algorithm for estimating the eigenvalues of a unitary operator, and algorithms for the hidden subgroup problem. The quantum Fourier transform was discovered by Don Coppersmith.	Coppersmith, (1994), Hales and Hallgren, (2000), Nielsen and Chuang (2000)

(Continued on the following page)

TABLE 3 (Continued) Evolution of popular quantum algorithms (theory and experimental validation).

Algorithm	Year (discovery)	Year (validation)	Description	Ref.
Shor's algorithm	1994		Shor, of AT&T's Bell Labs, put forth an algorithm that allows a quantum computer to factor large integers quickly. It solves both the factoring problem and the discrete log problem.	Shor (1994)
Shor's algorithm		2001	The first execution of Shor's algorithm at IBM's Almaden Research Center and Stanford University, where the number 15 was factored using 1,018 identical molecules, each containing seven active nuclear spins.	Vandersypen et al. (2001)
Shor's algorithm		2009	Researchers at the University of Bristol demonstrated Shor's algorithm on a silicon photonic chip.	Politi et al. (2009)
Shor's algorithm		2016	Scientists at the Universitat Innsbruck, MIT, and Akademie der Wissenschaften (Innsbruck) efficiently implemented Shor's algorithm in an ion-trap-based quantum computer.	Monz et al. (2016)
Grover's algorithm	1996		Lov Grover, at Bell Labs, invented the quantum database search algorithm. The quadratic speedup is not as dramatic as that demonstrated for factoring, logs, or physics simulations. The Grover algorithm can be applied to a wide variety of problems that are typically solved by exhaustive means.	Grover (1996-07), Grover (1996-07)
Grover's algorithm		1998	First execution of Grover's algorithm on an NMR quantum computer.	Chuang et al. (1998b)
HHL algorithm	2008		The quantum algorithm for linear systems of equations, also known as the HHL algorithm, designed by Aram Harrow, Avinatan Hassidim, and Seth Lloyd, is a quantum algorithm for solving linear systems. The algorithm estimates the result of a scalar measurement on the solution vector to a given linear system of equations. The algorithm is one of the main fundamental algorithms expected to provide a speedup over classical counterparts, along with Shor's factoring algorithm, Grover's search algorithm, and the quantum Fourier transform.	Harrow et al. (2008)

reported in 1985, has been labeled by some as the start of quantum computing. However, this algorithm is overly simplistic, addressing functions of 1-qubit arguments and returning 1-qubit outputs; it finds little practical utility. As an extension of this work, in 1992, Deutsch and co-author Jozsa produced the landmark Deutsch–Jozsa algorithm (Deutsch and Jozsa, 1992), which is the first example of a quantum algorithm that is exponentially faster than any deterministic classical algorithm. In 1998, 2003, and 2007, teams of researchers validated the Deutsch–Jozsa algorithm in the laboratory using NMR, ion traps, and entangled-photon clusters, respectively (Kan, 2019; Ball, 2020-12; Letzter, 2020; Deutsch and Jozsa, 1992; Chuang and Yamamoto, 1995; Gulde et al., 2003).

In 1994, Peter Shor of MIT, employing Coppersmith's recently developed quantum Fourier transform, conceived a quantum algorithm that calculates prime factors of large numbers vastly more efficiently than classical computers (Simon, 1997-10). Researchers have since experimentally validated Shor's algorithm. Specifically, validation was provided by a team featuring researchers

from IBM and Stanford University employing spin-1/2 nuclei in a perfluorobutadienyl iron complex using room temperature liquid-state nuclear magnetic resonance; a team from the Centre for Quantum Photonics (Bristol, United Kingdom) carried out an elegant experiment on an integrated silica-on-silicon waveguide that guided four single-photon qubits; and a team of scientists at the Universitat Innsbruck, MIT, and the Akademie der Wissenschaften (Innsbruck) efficiently implemented Shor's algorithm using an ion-trap-based quantum computer by effectively controlling seven qubits and four cache-qubits, together with implementation of generalized arithmetic operations, known as modular multipliers (Coppersmith, 1994; Shor, 1994; Hales and Hallgren, 2000).

In 1996, Lov Grover of AT&T Bell Labs conceived a quantum database search algorithm that presents a quadratic "speedup" for a variety of problems that are typically performed by brute force (Grover, 1996-07). In 1998, the first quantum computer, that is, a 2-qubit LS-NMR machine, demonstrated the Grover algorithm. Unlike other quantum algorithms, which may provide exponential

speedup over classical machines, Grover's algorithm provides only a quadratic speedup. However, even a quadratic speedup can be applied to increase the speed of broad classes of searches (Nielsen and Chuang, 2000).

## 7 Select quantum phenomena and technologies

In this section, we return to Figure 1 and more deeply examine select quantum phenomena related to emerging quantum technologies; these include entanglement and superposition, cavity- and circuit-based quantum electrodynamics, teleportation, tunneling, and spin-orbit interactions.

### 7.1 Entanglement and superposition

*Quantum entanglement* describes the state of two or more particles connected even when separated by vast distances. In principle, under these conditions, if one changes the properties of one particle, typically by measurement of one of its intrinsic properties such as spin or polarization, the properties of the entangled partner(s) change *instantly*. In theory, this would be the case even if the entangled particles are on opposite sides of the Universe—some ninety-two billion light years apart (Bars and Terning, 2018).

Entangled qubits become a system with a single quantum state. If you measure one qubit (i.e., collapse its *superposition* to a single state), you will have the same impact on other entangled qubits in the system.

Einstein rejected this phenomenon because such transmission of information, being spontaneous across vast distances, violates his prized fundamental constant—the speed of light ( $c$ ), a concept he introduced in 1905 as a fundamental constraint upon all physical systems.

However, entanglement has since been extensively studied, and findings have brought into question the speed of light as a fundamental constant. Recently, Yin et al. investigated the continuous violation of the Bell inequality and concluded that the lower bound of the speed of light was as much as four orders of magnitude ( $\times 10,000$ ) its value if Earth's speed in an inertial reference frame is less than  $10^{-3}$  times the speed of light (Yin et al., 2013).

Because the speed of light, as a constraint on physical systems, has been a pillar of physics since 1905 (Einstein, 1905f), any rigorous theory proposing a change  $c$ , supported by careful experimentation and withstanding rigorous peer review, would indeed be widely heralded.

Notwithstanding debates challenging the speed of light, entanglement continues to create opportunities in applied physics and engineering, specifically, for example, in enhancing the security of communications through quantum encryption. In this example, one considers a particle of an entangled pair to be sent as an *encryption key*. If a malign actor intercepts the transmission, this triggers an *instant* change in the remote quantum state of an entangled particle's quantum state, resulting in the detection of the eavesdropping attempt (Ekert et al., 1994).

The state of superposition just introduced will next be discussed in greater detail. The state of *superposition* creates a near-infinite range of possibilities, a *smearing of classical determinism*. Quantum superposition is a theory that quantum particles simultaneously exist in a multiplicity of quantum states. This phenomenon is responsible for numerous properties that are key features of quantum theory, including quantum interference (Anderson and Kasevich, 1998), entanglement, and teleportation (Pirandola et al., 2015).

The in-phase summation of delocalized wavefunctions is responsible for quantum coherence, a feature of quantum states (Baumgratz et al., 2014), as well as providing the underlying foundations for ultrafast quantum algorithms such as the Deutsch–Jozsa algorithm (Deutsch and Jozsa, 1992), the Shor algorithm (Shor, 1997), the Grover algorithm (Grover, 1996), quantum cryptography (Gisin N. et al., 2002), and quantum metrology (Giovannetti et al., 2011), among others.

### 7.2 Quantum teleportation

*Quantum teleportation* describes the communication of quantum information from source to target locations without this information being classically transferred between sites. It is noteworthy that matter and energy cannot be teleported without passing through an intermediate location. However, teleportation of quantum states is indeed possible: only quantum states are teleported—physical matter remains at the source and must be already present at the target location.

In this context, classical communications include, for example, conventional radio frequency (RF) wireless systems. The quantum state in classical communication is irrelevant because the information transfer is intrinsically *decoherent*.

However, in 1993, Bennett et al. (1993) proposed that a quantum state of a particle could be transferred to a distant particle without physical displacement of either particle or the classical communication of information by electromagnetic signals or other means. This has become the basis of quantum teleportation that has since been explored theoretically and experimentally (Bouwmeester et al., 1997b; Werner, 2001).

Specifically, quantum teleportation has been verified in laboratories using a wide variety of qubit modalities including photonic qubits (Bouwmeester et al., 1997c; Boschi et al., 1998; Kim et al., 2001; Ursin et al., 2004; Jin et al., 2010; Ma X. S. et al., 2012; Yin et al., 2012) (as single rail (Giacomini et al., 2002; Lombardi et al., 2002) and dual rail (Fattal et al., 2004; Metcalf et al., 2014) as well as time-bin (Marcikic et al., 2003; de Riedmatten et al., 2004; Landry et al., 2007)), spin-orbital (Wang et al., 2015), nuclear magnetic resonance (Nielsen et al., 1998), optical modes (Furusawa et al., 1998; Bowen et al., 2003; Zhang et al., 2003; Takei et al., 2005a; Takei et al., 2005b; Yonezawa et al., 2007; Yukawa et al., 2008; Lee et al., 2011; Takeda et al., 2013), atomic ensembles (Sherson et al., 2006; Chen et al., 2008; Bao et al., 2012; Krauter et al., 2013), trapped atoms (Barrett et al., 2004; Riebe et al., 2004; Riebe et al., 2007; Olmschenk et al., 2009; Nölleke et al., 2013), and various other *solid-state* systems (Gao et al., 2013; Steffen et al., 2013; Bussières et al., 2014a; Pfaff et al., 2014).

Due to the successes of quantum teleportation experiments, it has rapidly become a keystone to quantum information



networks. It contributes meaningfully to a variety of quantum information protocols, including quantum repeaters (Briegel et al., 1998), quantum teleportation networks (Xu et al., 2016), quantum gate teleportation (Pan et al., 1998; Gottesman and Chuang, 1999; Raussendorf and Briegel, 2001; Makino et al., 2016; Su et al., 2016; Bouchard et al., 2017), and quantum computation and communication systems (Pan et al., 2012; Pirandola et al., 2015; Xia et al., 2017).

However, the further realization of a global quantum network, the ultimate prize of this community, will require demonstrated high-fidelity quantum teleportation over great distances. Teleportation employing optical fibers in tandem with free-space channels (Bouwmeester et al., 1997d; Landry et al., 2007; Ma et al., 2012; Yin et al., 2012; Sun Q.-C. et al., 2016; Valivarthi et al., 2016) is typically limited to 100 s of kilometers due to degradation of signal fidelity by environmentally induced interference or loss of photons within the optical fibers (Ursin et al., 2007). Next, we delve deeper into advances in optical-fiber- and free-space-based quantum teleportation efforts.

Proposed in 1984, quantum key distribution (QKD) allows two users to exchange provably secure keys via a potentially insecure quantum channel (Bennett and Brassard, 1984). On the application front, however, the operating distance of practical fiber-based QKD systems is limited to about 150 km (Lo et al., 2014), mainly due to the high background noise of practical single-photon detectors (Hadfield, 2009; Eisaman et al., 2011) and inefficient finite-key security analysis (Scarani and Renner, 2008; Tomamichel et al., 2012; Lim et al., 2014).

## 7.2.1 Optical-fiber-based quantum teleportation

Figure 4 presents the major demonstrations of fiber optic- and free space-based quantum teleportation. Presented are the distance traveled prior to qubit decoherence with measured fidelities together with commentary providing key insights to details of the experiments. Quantum key distribution (QKD) offers an unconditionally secure means of communication based on the laws of quantum mechanics. A major challenge in realizing a practical QKD system is to attain a 40 dB channel loss: This is required for global scale QKD networks using communication satellites.

As early as 2003, Marcikic et al. (2003) reported on a demonstration of probabilistic quantum teleportation of photonic time-bin qubits of 1.3  $\mu\text{m}$  wavelength generated by a femtosecond laser whose beam is split into two entangled beams by a variable beam-splitter. The 1.3  $\mu\text{m}$  photons were teleported onto photons of 1.55  $\mu\text{m}$  wavelength from one location to another, separated by 55 m but connected by 2 km of standard optical telecommunications fiber. The overall mean fidelity was  $81.2\% \pm 2.5\%$ , a value six standard deviations greater than the maximum fidelity of 66.7% achievable using the best protocols using classical decoherent photon transmissions.

In 2004, Gobby et al. demonstrated a QKD over standard telecom fiber exceeding 100 km (Gobby et al., 2004). By peering an interferometer and single-photon detector, key formation rates of up to 1.9 kbit/s with a quantum bit error ratio of 8.9% for a 122 km link were achieved.

In 2007, Landry et al. realized a quantum relay configuration using existing Swisscom telecommunication networks that allowed the Bell-state measurement of entangled photons with a fidelity

of  $93\% \pm 4\%$ : Qubits were generated from a single-photon source (Landry et al., 2007).

Further advances were introduced by Takesue et al. in 2007, who reported the first QKD experiment in which secure keys were distributed at a 12.1 bit/s secure key rate with a 42 dB channel loss over 200 km of optical fiber. These authors employed a differential phase shift quantum key distribution protocol implemented with a 10 GHz clock frequency and superconducting single-photon detectors based on NbN nanowires (Takesue et al., 2007).

In 2008, Honjo et al. reported the entanglement-based QKD experiment over a 100-km optical fiber. They employed superconducting single-photon detectors based on NbN nanowires that provided high-speed single-photon detection for the 1.5- $\mu\text{m}$  telecom band, an efficient entangled-photon pair source that consists of a fiber-coupled periodically poled lithium niobate waveguide and ultralow loss filters, and planar light wave circuit Mach-Zehnder interferometers (MZIs) with ultra-stable operation. Experiments verified a 16-kbit sifted key with a quantum bit error rate of 6.9% at a rate of 0.59 bits per second, from which a distilled 3.9-kbit secure key was extracted (Honjo et al., 2008).

Long-distance transmission of quantum information using quantum repeaters (Briegel et al., 1998; Sangouard et al., 2011) requires the efficient distribution of entanglement between remote nodes of a network (Kimble, 2008). In 2014, Bussi eres et al. (2014b) demonstrated quantum teleportation of the polarization state of a telecom-wavelength photon onto the state of a solid-state quantum memory. Entanglement was established between a rare-earth-ion-doped crystal storing a single photon that was polarization-entangled with a flying telecom-wavelength photon (Clausen et al., 2011; Saglamyurek et al., 2011). The latter was jointly measured with another flying polarization qubit to be teleported, which heralds the teleportation. The fidelity of the qubit retrieved from the memory was shown to be greater than the maximum fidelity achievable without entanglement, even when the combined distances traveled by the two flying qubits was 25 km along standard optical fiber.

In 2015, Korzh et al., for the first time, presented a compact and autonomous QKD system that was capable of distributing provably secure cryptographic keys over 307 km of optical fiber. This was achieved by using semiconductor single-photon detectors with record low background noise (Korzh et al., 2014) and a novel finite-key security analysis, which is efficient even for short key lengths. This demonstrates the feasibility of practical long-distance QKD based on standard fiber-optic telecom components.

Quantum teleportation over optical fibers remains challenging due to the very poor efficiencies of telecom-band single-photon detectors. Motivated to overcome this impediment, Takesue et al. (2015) reported the successful quantum teleportation over optical fiber using four high-detection-efficiency superconducting nanowire single-photon detectors that made it possible to perform highly efficient multifold photon measurements, allowing confirmation of successful teleportation over 100 km of fiber with an average fidelity of  $83.7\% \pm 2.0\%$ .

By 2016, Sun et al. reported the construction of a 30 km optical-fiber-based quantum network distributed over a 12.5 km<sup>2</sup> area. This network with active stabilization displayed a unique robustness against environmental noise. Both quantum-state and process-tomography measurements and independent statistical testing



confirmed the quantum nature of quantum teleportation over this network (Sun QC. et al., 2016).

Soon after, Huo et al. experimentally demonstrated deterministic quantum teleportation of an optical coherent state through fiber channels (Huo et al., 2018), whereupon two sub-modes of an entangled state were transmitted from sender to receiver through a 3 km fiber. The deterministic teleportation of optical modes over the fiber channel of 6 km was realized with a fidelity of  $62\% \pm 3\%$  for the retrieved quantum state, which surpassed the classical limit of 50%.

## 7.2.2 Free-space-based quantum teleportation

Although quantum teleportation (Marcikic et al., 2003; Ursin et al., 2004) and entanglement distribution (Zhang et al., 2008; Dynes et al., 2009; Lambert H. N. J. et al., 2020) over moderate distances have been realized using optical fibers, decoherence inherent to optical fibers necessitates the use of quantum repeaters<sup>203–brieg</sup> in order to realize teleportation over larger distances. However, the practical utilization of quantum repeaters remains experimentally challenging (Yuan et al., 2008).

Free-space channels, first used for quantum key demonstrations (Kurtsiefer et al., 2002), offer a promising approach because degradation of fidelity is much less through the high orbit atmosphere. Further, ultra-long-distance quantum communication can be achieved on a global scale with the use of satellites.

Previous long-distance demonstrations (see Table 4) include using free-space distribution of entangled-photon qubits over distances of 600 m (Aspelmeyer et al., 2003), 1,300 m (Peng et al., 2005), 16,000 m (Jin et al., 2010), 23,400 m (Kurtsiefer et al., 2002), and 97,000 m (Fedrizzi et al., 2009).

Quantum teleportation of entangled multiphoton qubits was demonstrated over 101.8 km via a two-link free-space channel with an average fidelity of  $80.4 \pm 0.9\%$  (Yin et al., 2012).

A key experimental demonstration of entangled-photon quantum key distribution over 144 km was carried out by the Zeilinger group of the University of Vienna, where the local state was at the Canary Island of La Palma, and the receiver was located at the Tenerife Ground Station of the European Space Agency. Photons were sent over an optical free-space link (Ursin et al., 2007; Ma et al., 2012).

In 2017, Ren et al. of the University of Science and Technology of China reported the quantum teleportation of single-photon qubits from a ground observatory to a low-Earth-orbit satellite through an uplink channel over distances of up to 1,400 km (Ren et al., 2017). Successful quantum teleportation of six input states in mutually unbiased bases with an average fidelity of  $80 \pm 1\%$  was demonstrated. Quantum teleportation through space is particularly attractive because degradation from the molecular scattering of entangled particles is lessened. Such a demonstration of reliable and ultra-long-distance quantum teleportation from ground-to-satellite uplink marks an essential step in realizing a global quantum internet.

### 7.2.2.1 Time-bin qubits

Qubits encoded by the time of arrival of individual photons are referred to as time-bin qubits (TBQ) (Brendel et al., 1999). TBQs are useful for fiber networks due to their simplicity of generation, interfacing with quantum devices, and independence of dynamic

polarization transformations experienced in the use of standard optical fibers. Individual telecom-band photons with a  $\sim 1.5 \mu\text{m}$  wavelength are ideal qubits due to their ability to travel over long optical fibers or free space.

Valivarthi et al. (2020) reported on the utility of time-bin qubits and their freedom from polarization transformations typically unique to standard optical fibers. The growing availability of sources and detectors of individual telecom-bands has further accelerated progress toward quantum networks and associated technologies, such as quantum memories (Lvovsky et al., 2009), quantum transducers (Lambert N. J. et al., 2020), or quantum nondestructive measurement devices (Braginsky and Khalili, 1996).

Quantum teleportation has been advanced via various photon teleportation modalities. In recent years, such advancement has manifested as *bidirectional quantum teleportation (BQT)* that has attracted much attention from the scientific community, where it finds utility in quantum-secure direct communication (QSDC) (Li et al., 2013), quantum remote control (Huelga et al., 2002), and cryptographic switching (Srinatha et al., 2014).

Whereas standard quantum teleportation modalities, that is, unidirectional teleportation, realize quantum communication from one party to another, BQT provides an exchange of quantum information between two or more sites. In an ideal version of BQT, parties share maximally entangled qubits and teleport from source to target(s), employing standard quantum teleportation two or more times through redundant or multiple channels (Siddiqui and Wilde, 2022).

### 7.2.2.2 BQT protocols

Several protocols now exist for BQT involving two participants (Hassanpour and Houshmand, 2016; Sang, 2016; Sadeghi Zadeh et al., 2017; Zhou R. G. et al., 2019; Zhou et al., 2020) and three participants (Yan, 2013; Duan Y. J. et al., 2014; Choudhury and Dhara, 2016; Hong, 2016; Li and Jin, 2016; Yang et al., 2016) using various types of entangled states as quantum channels, including EPR states (Rigolin, 2005), GHZ states (Dong and Teng, 2008; Espoukeh and Pedram, 2014), GHZ-like states (Nandi and Mazumdar, 2014; Yuan, 2015; Zhang et al., 2016), W states (Cao and Song, 2007; Zuo et al., 2009), W-like states (Man et al., 2007), and cluster states (Liu and Zhou, 2014; Li et al., 2016; Sisodia and Pathak, 2018).

In 2013, Yan (Yan, 2013) proposed a protocol for BQT using a six-qubit cluster state as the quantum channel to realize deterministic bidirectional quantum-controlled teleportation of an arbitrary single-qubit state where a source A transmits an arbitrary single-qubit state to a receiver B, while simultaneously the receiver transmits an arbitrary single B qubit state to the original source A mediated by a controller C.

Duan et al. (Duan et al., 2014a) proposed another protocol for BQT in which two participants, A and B, share two three-qubit GHZ (Karlsson and Bourennane, 1998) (Greenberger–Horne–Zeilinger) states as the quantum channel where they mutually transmit two-qubit entangled states to one another. This is believed to be the first protocol for BQT of arbitrary two-qubit states.

An improved BQT protocol, based on a quantum channel of a six-qubit cluster state, was proposed by Zhou R. G. et al. (2019). In their protocol, source A transmits an unknown three-qubit entangled state to receiver B and, at the same time, B transmits an arbitrary

TABLE 4 Major demonstrations in quantum teleportation.

Qubit QT modality	Distance (km)	Fidelity (%)	Comment	Ref.
<i>Optical-fiber-based Quantum Teleportation</i>				
Fiber optic	2	81.2 ± 2.5	Photonic time-bin qubits of 1.3 μm wavelength were generated by a femtosecond laser whose beam is split into two entangled beams by a variable beam-splitter.	Marcikic et al. (2003)
Fiber optic	122	88.4	By peering an interferometer and single photon detector, key formation rates of up to 1.9 kbit/s with a quantum bit error ratio of 8.9% for a 122 km link were achieved.	Gobby et al. (2004)
Fiber optic	0.550	93 ± 4	Landry et al. realized a quantum relay configuration using existing Swisscom telecommunication networks that allowed the Bell-state measurement of entangled photons with qubits generated from a single-photon source.	Landry et al. (2007)
Fiber optic	200	Unk	These authors employed a differential phase shift quantum key distribution protocol implemented with a 10 GHz clock frequency and superconducting single-photon detectors based on NbN nanowire.	Takesue et al. (2007)
Fiber optic	100	93.1	A 16-kbit sifted key with a quantum bit error rate of 6.9% was transmitted at a rate of 0.59 bits per second, and a distilled 3.9-kbit secure key was extracted.	Honjo et al. (2008)
Fiber optic	100	83.7 ± 2.0	The use of four high-detection-efficiency superconducting nanowire single-photon detectors made it possible to perform highly efficient multifold photon measurements.	Takesue et al. (2015)
Fiber optic	307	Unk	Employed semiconductor single-photon detectors with record low background noise and a novel finite-key security analysis, which is efficient even for short key lengths.	Korzh et al. (2014)
Fiber optic	30	Unk	A 30 km optical-fiber-based quantum network distributed over a 12.5 km <sup>2</sup> area.	Sun et al. (2016b)
Fiber optic	6	62 ± 3	The BQT of two sub-modes of an entangled state was transmitted from sender to receiver through a 3 km standard optical fiber for a total path of 6 km.	Huo et al. (2018)
<i>Free-space-based Quantum Teleportation</i>				
Free space	Unk	96.7	Six states of polarization were teleported sequentially across an air–water interface, implementing active feed-forward operation with an average fidelity of 96.7%.	Spierings and Steinberg (2021)
Free space	0.6	87 ± 3	The experiment included independent receivers separated by 600 m with no line of sight between each other. A Bell inequality between those receivers violated by more than four standard deviations.	Aspelmeyer et al. (2003)
Free space	1.3	Unk	Entanglement survived a noisy ground environment with a distance greater than the effective thickness of the atmosphere, confirmed by observing a separated violation of Bell inequality of $2.45 \pm 0.09$ in accordance with the Bennett–Brassard (1984) quantum cryptography scheme.	Peng et al. (2005)
Free space	16	89	The Rome scheme was employed to achieve quantum teleportation in free space over a distance of 16 km. Various techniques have been developed for accomplishing this goal, including real-time feedback control of the high-stability interferometer for a single-photon Bell-state measurement (BSM), active feed-forward manipulation of the single-photon state for reconstruction of the initial teleported qubit, novel design of telescopes tailored for teleportation experiments, and so on. The excellent quality of the recovered state with an average fidelity better than 89% is thereby obtained.	Jin et al. (2010)

(Continued on the following page)

TABLE 4 (Continued) Major demonstrations in quantum teleportation.

Qubit QT modality	Distance (km)	Fidelity (%)	Comment	Ref.
Free space	144	Unk	Transmission of an entangled-photon pair over a 144 km free-space link. The received entangled states were shown to have excellent, noise-limited fidelity, even though they were exposed to extreme attenuation dominated by turbulent atmospheric effects. A total channel loss of 64 dB corresponds to the estimated attenuation regime for a two-photon satellite communication scenario. The received two-photon states were still highly entangled by violating the Clauser–Horne–Shimony–Holt inequality by more than five standard deviations. Results show that photons are subject to virtually no decoherence during their 0.5-ms-long flight through air, which is encouraging for future worldwide quantum communication scenarios.	Ursin et al. (2007), Ma et al. (2012)
Fiber/free space	8.2	Unk	A fiber network was employed through the Calgary metropolitan area demonstrating quantum teleportation. Specifically, a telecom photon of a 1.532 $\mu\text{m}$ wavelength, interacted with another telecom photon after both traveled several kilometers over a combined line-of-sight distance of 8.2 km with a photon at 0.795 $\mu\text{m}$ wavelength. This was shown to increase the effective quantum teleportation distance to 6.2 km, establishing an important threshold for quantum repeater-based communications.	Valivarthi et al. (2016)
Free space	23.4	Unk	Lumped optical losses of about 18–20 dB were measured, and using faint pulses containing 0.1 photons per bit, the detected bit rate at Bob was 1.5–2 kilobits per second.	Kurtsiefer et al. (2002)
Free space	101.8	80.4 $\pm$ 0.9	Long-distance quantum teleportation over a 35–53 dB loss one-link channel and entanglement distribution over a 66–85 dB high-loss two-link channel. The authors achieved an average fidelity of 80.4 (9)% for teleporting six distinct initial states and observed the violation of the Clauser–Horne–Shimony–Holt inequality after distributing entanglement.	Yin et al. (2012)
Low Earth orbit (free space)	1,400	80 $\pm$ 1	Quantum teleportation of single-photon qubits from a ground observatory to a low-Earth-orbit satellite.	Ren et al. (2017)

single-qubit state to A by utilizing GHZ-state measurement, Bell-state measurement, single-qubit von Neumann measurement, and unitary operations. These authors argue that their approach has advantages in higher intrinsic efficiency than other protocols.

Verma has proposed an improved protocol for asymmetric bidirectional quantum teleportation by using a quantum channel composed of two three-qubit GHZ states based on local CNOT gate operations, Bell-state measurements, GHZ-state measurements, and unitary operations (Verma, 2020). He claims, compared with previous BQT protocols, such as Zhou et al. (Zhou R. G. et al., 2019), that this protocol reduces operational complexity, requires less consumption of quantum and classical resources, and possesses a higher intrinsic efficiency.

### 7.2.2.3 BQT under water and during inclement weather

Mastriani et al., among others, have explored BQT, and other quantum tunneling (QT) demonstrations, in theory and practical experiments, under water and during inclement weather (Arnon and Kedar, 2009; Bouchard et al., 2018; Iyengar et al.,

2020; Sitharama Iyengar et al., 2020; Tarantino et al., 2020; Mastriani et al., 2021a; Mastriani et al., 2021b). These authors recently evaluated the performance of a bidirectional teleportation protocol (Cong et al., 2017; Yang et al., 2017; Zhou R.-G. et al., 2019; Chen et al., 2020) employing six or more qubits (using the *IBM Q Experience* quantum processor) where they explored the viability of BQT in a specific scenario in which two submerged submarines, on opposite sides of the ocean, serve as source and target with an optical geostationary satellite generating and distributing optical qubits. As such, optical qubits are transmitted to buoys located on the sea surface and linked to the submerged submarines. Results demonstrated a low margin of error, implying a high presence of decoherence and sensitivity to *flip* errors even in quantum circuits consisting of a few-gates.

Because quantum technologies based on superconducting qubits lose quantum information at environmental temperatures due to decoherence in a non-adiabatic situation, practical underwater quantum communications are exclusively reserved for optical circuit-based entangled photons (Mastriani et al., 20215).

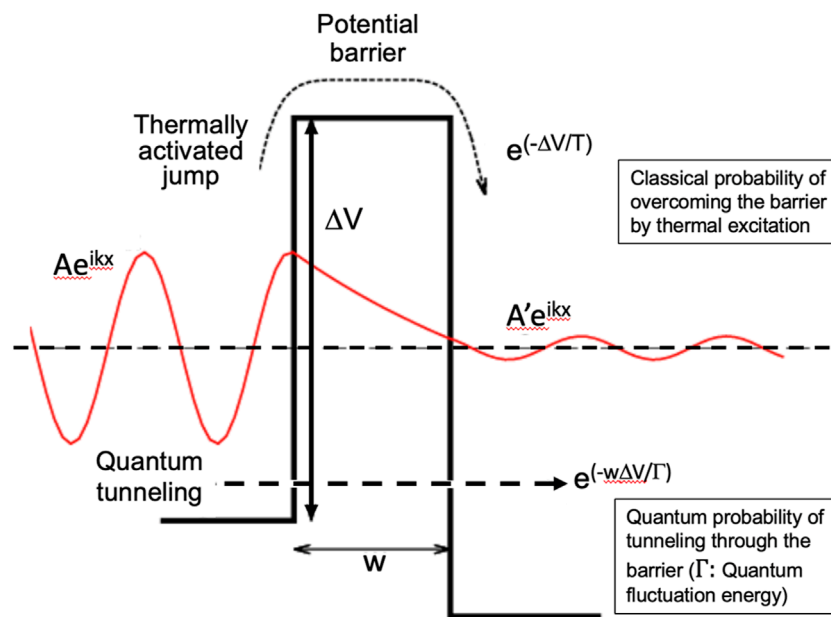


FIGURE 10

A schematic of an electronic barrier (center, solid line) with an electron approaching from the left (depicted by a sine wave,  $Ae^{ikx}$ ). The probabilities of transitioning over (classically by thermal activation,  $e^{-\frac{\Delta V}{T}}$ ) or tunneling through (quantum mechanically,  $e^{-\frac{w\Delta V}{\Gamma}}$ ) are provided.

Mastriani et al. also provided seminal contributions to understanding the role of quantum Fourier transforms in entanglement and quantum Fourier transform (QFT) (Nielsen and Chuang, 2000; Weinstein et al., 2001) by spectral analysis, whereas traditional approaches adhere to temporal approaches. Mastriani et al. conjecture that this approach will advance fault-tolerant protocols for use in quantum computing and quantum communication technologies (Mastriani et al., 2021a; Mastriani et al., 2021b).

Chakravartula et al. demonstrated in simulation the quantum teleportation of entangled pairs of photons generated from a mode-locked laser source through spontaneous four-wave mixing across an air–water interface. One of the pair was sent wirelessly to an underwater receiver. Six states of polarization were teleported sequentially, implementing active feed-forward operation with an average fidelity of 96.7% (Chakravartula et al., 2020).

### 7.3 Quantum tunneling

*Quantum tunneling* is a phenomenon in which quantum particles, such as electrons, pass through a barrier, such as an electric potential. The *strangeness* of this phenomenon is that it occurs when the particle does not possess sufficient energy to overcome the barrier according to the laws of classical mechanics. Tunneling is exclusively a consequence of the quantum wave nature of matter, whereupon the wave function describing the state of a particle, in accordance with Schrödinger's wave equation, has a *non-zero* probability of transitioning through a barrier that decreases exponentially with the barrier's height and width as well as the particle's mass. Tunneling is most prominently observed in particles of low mass, such as electrons or protons, in situations where barrier thicknesses are  $\sim 3$  nm for electrons and  $\sim 0.1$  nm for

protons (Wikipedia, 2022). A schematic illustration that captures the underlying physics is presented in Figure 10.

While the laws of quantum mechanics allow for tunneling, researchers cannot exactly explain what happens while the particle *experiences* tunneling. A topic of continued debate is the speed of the particle during tunneling. Some argue it is instantaneous, while others contend it is finite but may exceed the speed of light. The articles by Spierings and Steinberg (2020); Spierings and Steinberg (2021), Kuzmanović et al. (2022), Sainadh et al. (2020), and Pollak (2017a), Pollak (2017b), and Dumont et al. (2020), among others, are enlightening in this respect.

Quantum tunneling is integral to understanding many modern technologies, including (i) nuclear fusion (Balantekin and Takigawa, 1998), where quantum tunneling increases the probability of atomic nuclei overcoming Coulombic forces to achieve thermonuclear fusion; (ii) solid-state electronics, such as tunnel diodes, where a tunneling-induced “negative” differential resistance allows the function of oscillators, amplifiers, switches, frequency converters, and detectors at microwave frequencies (Fink, 1975); and, (iii) radioactive decay of atomic nuclei. In the latter, the nuclei experience the formation of a potential barrier originating from the equilibrium condition created by the balance of short-range nuclear forces (attraction) and Coulombic forces (repulsion). Alpha particles, emitted during tunneling from unstable nuclei, produce stable atoms. The first interpretation of alpha decay employing quantum tunneling was proffered by Gamow (1928) and independently by Gurney and Condon (1928).

The quantum tunneling effect was first proposed in theory by Hund while calculating the ground state of the double-well potential (Hund, 1927; Merzbacher, 2002). And, from the work of Gamow, Born realized the enormous potential for tunneling to be applied to many physical systems (Razavy, 2003; Wikipedia et al., 2023).



Tunneling further influenced many applications, ranging from the advent of the scanning tunneling microscope to quantum computing. The first experimental suggestion of tunneling-related anomalies was from Earhart (c. 1901), who discovered an unexpected conduction regime while investigating the conduction of gases between closely spaced electrodes, later known as the space charge regime. Circa 1911, Rother refined Earhart's experiments, allowing for the measurement of field emission currents (Cuff, 1993). Quantum tunneling, within the framework of Fowler–Nordheim tunneling (Fowler and Nordheim, 1928–05), is now the understood mechanism for electrons transitioning through a space charge barrier. Millikan and Lauritsen (1928) and Oppenheimer (1928) contributed to the understanding of this and related phenomena.

Table 5 presents a listing of technologies in which quantum tunneling plays an enabling role. The table is segmented into categories of quantum tunneling (QT) and superconducting tunneling junctions (SQT). Here, one sees the important role of QT in electronics (diodes, transistors, flash memory), nuclear reactions (alpha decay, nuclear fusion), biology, and microscopy. Magnetic tunnel junctions (MTJs) find utility in specialized applications such as magnetic field sensors, magnetic memory, memristors, spin valves, and other spintronic components. Superconducting tunnel junctions (STJs) are used in highly sensitive magnetometers, single-photon detectors, astronomical imaging, quantum computers, and fast logic elements.

## 7.4 Spin–orbit coupling (SOC)

Spin–orbit coupling (SOC), sometimes referred to more generally as spin–orbit interactions, is a relativistic interaction of a particle's spin angular momentum with its orbital angular momentum (see Figure 11A,B) or its spin with its electrostatic and/or its electrodynamic environment(s) (see Figure 11C,D). It can manifest as one of several effects that occur on electronic (<0.01 nm), atomic (0.01 < d < 0.1 nm), or multi-ionic (i.e., the atomic lattice, 0.1 nm < d ~1 nm) length scale. For this reason, SOC often brings about some confusion among novices and even expert practitioners (Scitechdaily, 2022).

In one case, considering the electron's atomic energy levels, due to electromagnetic interaction between the electron's magnetic dipole, its orbital motion, and electrostatic fields induced by the positively charged nucleus, the atom's spectral lines split. Such behavior has also become known as the Balmer series, the same Balmer series that Niels Bohr brought clarity to in his seminal articles of 1913, whereupon he introduced the concept of stationary orbits and the principle of quantized orbital energy (i.e., the principal quantum number,  $n$ ).

Another SOC effect derives from the interplay between angular momentum and the strong nuclear force within the nucleus that leads to a shift in energy levels observed in the nucleus shell model (Haxel et al., 1949; Mayer, 1949). SOC is also responsible for the origin of magnetocrystalline anisotropy that gives rise to the spin-Hall effect, which is of value to spintronics and a plethora of other magnetic phenomena.

Here, we restrict our discussions to SOC phenomena involving electronic and ionic systems that impact many of the quantum

technologies discussed in this review (Spavieri and Mansuripur, 2015; Wikipedia, 2022). As previously mentioned, SOC-induced electron energy splitting, that is,  $\Delta\mathcal{E}$ , and its influence upon the Balmer series first addressed by Bohr, was later advanced by Thomas using Bohr's atomic model in conjunction with

Schrödinger's wave mechanics and relativistic kinematics (Thomas, 1926; Thomas, 1927). This result agreed with later predictions by Dirac's relativistic quantum field theory (c. 1928) (Mansuripur, 2015). These foundational contributions were used in practical technologies such as spin-orbitronics (bib\_wikipedia\_2022j).

## 7.5 Spin-orbit technologies

Spin-orbitronic devices are relatively new to the quantum electronic lexicon, encapsulating the influence of SOC in determining the performance of some modern electronic components. Table 6 provides a listing of spin orbitronic technologies, including: embedded magnetoresistive random-access memory (eMRAM), spin–orbit torque MRAM (SOT-MRAM), resistive switching RAM (RRAM), spin-torque nanooscillators, and STT-based synapses, neurons, and the neuromorphic computing.

We next examine spin-transfer torque (STT), an effect where the orientation of a free magnetic layer in a magnetic tunnel junction is manipulated using spin-polarized currents (SPC). When an SPC is injected into this magnetic free layer, the angular momentum is transferred to the layer thus reversing its orientation, providing a bistable state useful for memory and logic devices.

Spin-transfer torque magnetic random-access memory, that is, STT-MRAM, is a nonvolatile memory that operates under sub-nanosecond and sub-picojoule conditions and provides major advantages over charge-based memories such as SRAM and DRAM (Krizakova et al., 2022a; Wikipedia, 2022). Industrial production of this memory technology was first demonstrated by Hitachi, which produced a 32-Mbit STT-RAM in 2009 (Session 8-4, 2023). The commercialization of these technologies will be addressed in Section 9.

Spin-transfer torque arises from the transfer of electron spin angular momentum to the orbital angular momentum of the lattice (see Figure 11B). When the current density is sufficiently high, the magnetization rotates. This has been experimentally demonstrated in cases when the thickness of the magnetic material is of the order of hundreds of nanometers or less. Such nanoscale devices, known as spin-torque nanooscillators (STNOs), generate high-frequency voltage signals in the GHz range. STNOs have abundant potential as RF signal generators, modulators, and RF detectors.

Recently, spin–orbit torque (SOT) has been proposed to switch the magnetization of the free magnetic layer in MTJs at lower power and faster speeds (Miron et al., 2011; Liu et al., 2012a; Liu et al., 2012b; Cai et al., 2017; Li et al., 2019). SOT provides versatility in the manipulation of magnetization using electric currents, leading to novel spintronic performance and devices. It is based on spin-transfer effects, like STT-MRAM; however, the source of spins is the lattice of the SOT layer via intrinsic SOC, and, therefore, there is no need for SPCs (Antaios, 2023).

SOT can be generated from several sources, including the use of heavy metal (large  $Z$  and hence large orbital momentum) layers

TABLE 5 Applications of quantum tunneling and superconducting tunnel junctions.

Component type	Description	Ref.
<i>Quantum Tunneling</i>		
Very-large-scale integration (VLSI)	Tunneling is a source of current leakage in very large-scale integration (VLSI) electronics and results in a substantial power drain that plagues such devices. It is considered the lower limit on how microelectronic device elements can be fabricated.	Jain (2009)
Flash memory	Tunneling is an essential phenomenon in a program of floating gates in flash memory.	Bez and Pirovano (2019)
Cold emission	Cold emission of electrons is relevant to semiconductor and superconductor physics. Like thermionic emission, a sufficiently high bias voltage, electrons overcome the material's work function and escape the crystal's surface. When the electric field is sufficiently large, the space charge barrier becomes thin enough for electrons to tunnel through, leading to a current that varies exponentially with electric field strength.	Fowler and Nordheim (1928-05)
Tunnel junctions and magnetic tunnel junctions (MTJ)	A simple barrier can be created by separating two conductors with a very thin insulator. These are tunnel junctions, the study of which requires understanding quantum tunneling. Josephson junctions take advantage of quantum tunneling and superconductivity to create the Josephson effect. This has applications in precision measurements of voltages and magnetic fields, as well as the multijunction solar cell. Alternatively, an MTJ, or magnetic tunnel junction, consists of two magnetic layers separated by a thin insulating layer. For magnetic layers that have large spin polarizations, large resistance changes occur through the junction when the moments of the magnetic layers switch from parallel to antiparallel alignments. MTJs can be used as magnetic field sensors, magnetic memory, memristors, nano spin valves, and resistance generators.	Zhang et al. (2021)
Quantum-dot cellular automata (QCA)	QCA is a molecular binary logic synthesis technology that operates in the inter-island electron tunneling mode. This is a very low-power and fast device that can operate at extraordinarily high frequencies of up to 15 pHz (petaHertz).	Feynman (1982), Tougaw and Lent (1994)
Tunnel diodes	The resonant tunneling diode makes use of quantum tunneling by placing two thin layers with high energy conductance bands near each other to create a quantum potential well that has an intrinsic lowest energy level. When this energy level is higher than that of the electrons, no tunneling occurs, and the diode operates in reverse bias. Reverse-biased tunnel diodes act as fast rectifiers with zero offset voltage and excellent linearity. Once the two voltage energies reach equivalency, electrons flow as if in an open circuit. As the voltage increases above the intrinsic energy, tunneling becomes suppressed, and the diode acts like a conventional diode.	Logansen (1964)
Tunnel field-effect transistors	In a field-effect transistor, the channel is controlled via quantum tunneling rather than by thermally induced injection, reducing gate voltage from $\approx 1$ V to $\approx 0.2$ V, thus reducing power consumption by as much as two orders of magnitude.	Lilienfeld (1930), Lee (2003)
Nuclear fusion	Quantum tunneling is an essential mechanism of nuclear fusion. The temperature of stellar cores is insufficient to allow atomic nuclei to overcome the Coulomb barrier and achieve thermonuclear fusion. Quantum tunneling increases the probability of transitioning this barrier and maintaining a steady fusion reaction.	Balantekin and Takigawa (1998)
Radioactive Decay	In radioactive decay, the nucleus experiences a potential barrier forming from the short-range nuclear force (attraction), and Coulombic force (repulsion) requires emission particles to tunnel from within the unstable nucleus in order to stabilize the atom.	Gamow (1928)
Astrochemistry in interstellar clouds	Quantum tunneling provides astrochemical syntheses of various molecules in interstellar clouds, allowing for the synthesis of molecular hydrogen, water/ice, formaldehyde, etc.	Trixler (2013)
Quantum biology	Electron tunneling is a key factor in many biochemical redox reactions (e.g., photosynthesis, cellular respiration, etc.), as well as enzymatic catalysis. Proton tunneling is a key factor in spontaneous DNA mutation.	Page et al. (1999)

(Continued on the following page)

TABLE 5 (Continued) Applications of quantum tunneling and superconducting tunnel junctions.

Component type	Description	Ref.
Quantum conductivity	The Drude–Lorentz model of electrical conductivity accurately predicts the nature of conduction in metals. Improvements can be experienced by incorporating quantum tunneling to explain the nature of electron collisions.	Taylor (2004)
Scanning tunneling microscope (STM)	The STM allows imaging of individual atoms on the surface of a material by taking advantage of the relationship between quantum tunneling and distance. When the tip of the STM's stylus is brought close to a conducting surface that is electrically biased, measurement of the current tunneling between the stylus and the surface translates to a displacement with a vertical accuracy of 0.001 nm, or about 1% of an atomic diameter.	Binnig and Rohrer (1986)
Kinetic isotope effect	In chemical kinetics, the substitution of a heavy isotope for a lighter one typically reduces the reaction rate. This is attributed to differences in the zero-point vibrational energies for chemical bonds containing the lighter and heavier isotopes. However, in rare cases, large isotope effects are observed that cannot be explained using a semi-classical treatment. Quantum tunneling is introduced with Arrhenius kinetics to accurately model this phenomenon. Bell recognized the need to introduce quantum theory, including tunneling.	Bell (1959), Bell (1980)
<b>Superconducting Tunnel Junctions (STJs)</b>		
Radio astronomy	STJs are the most sensitive heterodyne receivers in the 100 GHz–1,000 GHz frequency range and are used at these frequencies for radio astronomy. In practice, a high-frequency signal from an astronomical object is focused onto the STJ, where photons are absorbed by the STJ, allowing quasiparticles to experience photon-assisted tunneling, causing nonlinearity in the current–voltage curve. This has the effect of creating an output at the differential frequency of the astronomical signal and the local oscillator. The output is a frequency down-converted version of the astronomical signal. These receivers are sufficiently sensitive that quantum noise must be accounted for.	Tucker, (1979), Zmuidzinas and Richards (2004)
Single-photon detection	STJs can be used as <i>direct</i> detectors where a photon is absorbed in the superconductor, breaks Cooper pairs, and creates quasiparticles that tunnel across the junction in the direction of the applied voltage. The resulting tunneling current is proportional to the photon energy. STJ devices have been employed as single-photon detectors for photon frequencies ranging from X-rays to the infrared.	SCI (2023)
Superconducting quantum interference device (SQUID)	The superconducting quantum interference device or SQUID is based on a superconducting loop containing Josephson junctions. SQUIDs are the most sensitive magnetometers, capable of measuring a single magnetic flux quantum.	Jaklevic et al. (1964)
Quantum computing	Superconducting quantum computers often utilize STJ-based circuits as charge qubits, flux qubits, and phase qubits (see Table 5. Applications of quantum tunneling and superconducting tunnel junctions, and Section 6.2 Superconducting qubits).	See Figure 14 and related discussion.
Rapid single flux quantum (RSFQ)	The STJ is the primary active element in rapid single flux quantum or RSFQ fast logic circuits.	Likharev and Semenov (1991)
Josephson voltage standard	When a high-frequency current is applied to a Josephson junction, the AC Josephson current synchronizes with the applied frequency, giving rise to regions of constant voltage in the I–V curve of the device called Shapiro steps. These provide an exact conversion from frequency to voltage. Because frequency can be measured with very high precision, this effect is used as the basis of the Josephson voltage standard, which is used as the international definition of the “conventional” volt.	Hamilton et al. (1985)

TABLE 6 Applications of spin-orbitronic devices.

Technology	Description	Ref.
Embedded magnetoresistive random-access memory (eMRAM)	Embedded magnetoresistive random-access memory (eMRAM) differs from conventional embedded memories, that is, SRAM and Flash, where information is stored as floating electrostatic charge, whereas eMRAM uses magnetic spin to store information. eMRAMs are made of many ferromagnetic and nonmagnetic materials called magnetic tunnel junctions (MTJs). MTJs can hold spin polarization virtually forever without external power, making eMRAM a type of nonvolatile memory.	Synopsys (2023)
Spin-orbit torque MRAM (SOT-MRAM)	Spin-orbit torque MRAM (SOT-MRAM) is a type of nonvolatile magnetoresistive RAM that can execute write and read operations. SOT-MRAM devices are comprised of MTJs that have thin dielectric layers between magnetic fixed layers and a magnetic layer free to rotate in response to an applied or induced magnetic field.	Prenat et al. (2015)
Resistive switching RAM (RRAM)	RRAM is an emerging memory technology providing high speed, low cost, enhanced storage density, and excellent scalability. A resistive random-access memory (RRAM) cell has a metal-insulator-metal structure (MIM) that consists of an insulating layer (I) sandwiched between two metal (M) electrodes. Depending upon the polarity of applied voltage, the RRAM cell can transition from a high resistance state, or OFF state, with logic value "0," to a low resistance state, or ON state, with logic value "1."	Lee et al. (2008)
Spin-torque nanooscillators	Spin-torque nanooscillators (STNOs) and spin-Hall nanooscillators (SHNOs) are devices with the potential to redefine microwave technologies, including wireless communication, such as radio frequency (RF) signal generators, modulators, and RF detectors.  STNOs are ultrabroadband nanoscopic microwave oscillators compatible with RF CMOS that demonstrate ultrahigh modulation rates. STNOs consist of a relatively thick "fixed" magnetic layer (remains fixed in response to magnetic stimulation), which serves as a polarizer, a nonmagnetic spacer, and a relatively thin magnetic "free" layer that can rotate in response to magnetic stimulation. A DC, spin-polarized current from the polarizer, when large enough to transfer sufficient STT to cancel out the intrinsic damping losses of the free layer, leads to useful magnetization dynamics.  Recent advances in three-terminal magnetic tunnel-junction-based SHNOs provide the possibility to develop more reliable and well-controlled oscillators, thanks to individual spin-Hall-driven precession excitation and readout paths.  SHNOs are CMOS-compatible spintronic devices for microwave signal generation and oscillator-based neuromorphic applications that combine a nanoscale footprint, fast and ultra-wide microwave frequency tunability, and strong nonlinear properties that provide robust large-scale mutual synchronization in chains and two-dimensional arrays.	Zeng et al. (2013), Fulara et al. (2020a)
STT-based synapses, neurons, and the neuromorphic computing	Spin-torque nanooscillators possess several distinctive features that are appealing for neuromorphic computing. The oscillation amplitudes have memory due to finite magnetization relaxation, which can imitate the leaky integration of neurons. They are stable and persistent, with limited drift in the behavior of precession. The frequency and amplitude of voltage oscillations are highly nonlinear as a function of current or applied field, allowing direct implementation of nonlinear activation. Additionally, their high tunability facilitates synchronization with other oscillators. It is possible to couple many devices together through these interactions to emulate the synchronization of neurons and collections of neurons in the brain.	Slavin and Tiberkevich (2009), Fell and Axmacher (2011), Pufall et al. (2015), Sengupta et al. (2016), Yogendra et al. (2016), Tsunegi et al. (2018), Locatelli et al. (2022)

such as Pt<sup>368-liu</sup> or Ta<sup>370-liu</sup> or by means of the Rashba effect<sup>13</sup> stemming from the breaking of crystal inversion symmetry. Several

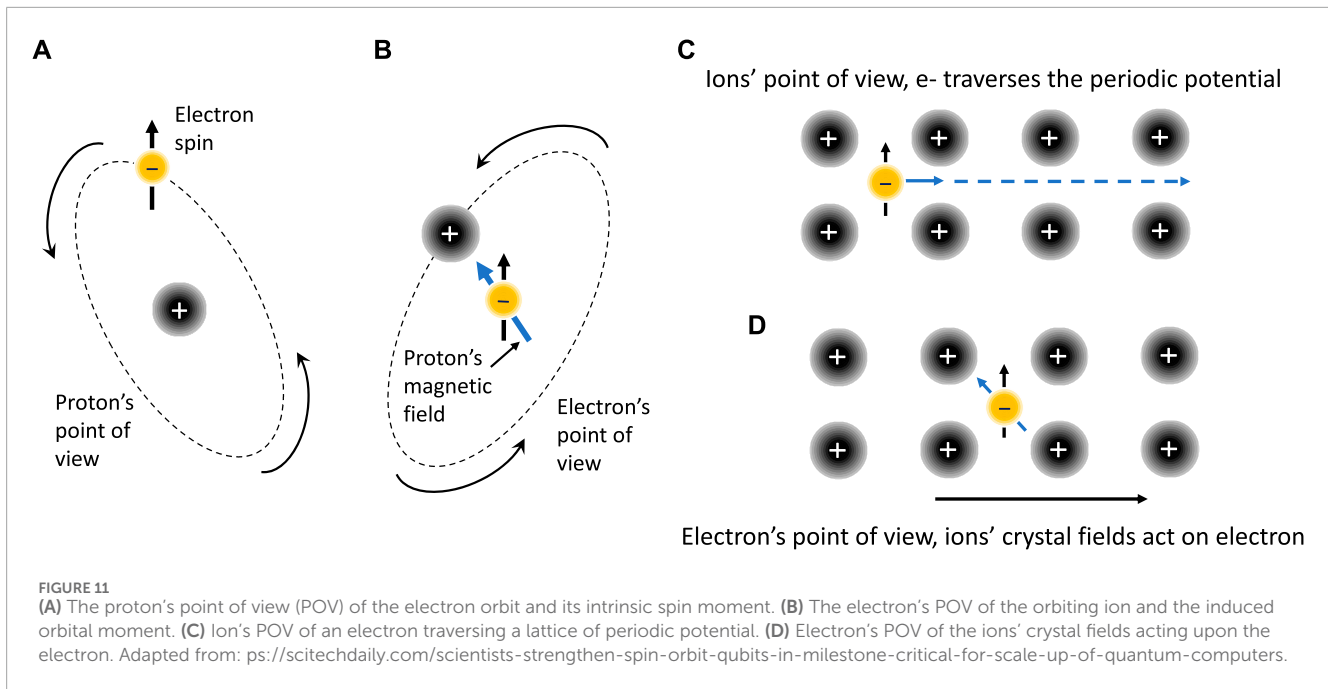
13 The Rashba effect, also called the Bychkov–Rashba effect, is a momentum-dependent splitting of spin bands in bulk crystals and low-dimensional condensed-matter systems. The splitting results from the combined effect of spin-orbit interaction and asymmetry of the crystal potential, in the direction perpendicular to the two-dimensional plane. This effect can drive a wide variety of novel physical phenomena, especially manipulating electron spins by electric fields. An example of a physical phenomenon that can be explained by the Rashba effect is the anisotropic magnetoresistance (AMR), Majorana fermions, and topological p-wave superconductors. (Adapted from: [https://en.wikipedia.org/wiki/Rashba\\_effect](https://en.wikipedia.org/wiki/Rashba_effect) accessed 7/1/2023).

investigators have shown SOT efficiency can be further improved by engineering interface structure and chemistry (Fan et al., 2013; Fan et al., 2014; Nan et al., 2015), electric field tuning (Yan Y. et al., 2016; Fan et al., 2016), ferroelectric polarization (Lin et al., 2018), or by the introduction of materials possessing higher SOT efficiencies (Valenzuela and Tinkham, 2006; Ando and Saitoh, 2010; Pai et al., 2012; Jamali et al., 2015; Akyol et al., 2016).

### 7.5.1 Spin-torque nanooscillators

Spin-torque nanooscillators (STNOs) are highly tunable by both currents and magnetic fields and, as such, have advantages over standard voltage-controlled oscillators (VCOs). While the frequency variation in VCOs is only ~20% of the carrier frequency (i.e., 1–3 GHz), STNOs can be tuned by current over several GHz and magnetic fields up to 40 GHz (Zeng et al., 2013).





STNOs are also among the smallest of microwave oscillators, operating over broad temperatures while biased using low voltages. Additionally, STNOs can be readily integrated using complementary metal-oxide semiconductor (CMOS) protocols for on-wafer systems. All these advantages make STNOs promising for microwireless communications, array transmitters, microwave sources, on-chip clocks, and massively-parallel microwave signal processors (Albertsson et al., 2019).

After the initial seminal works by Slonczewski (1996) and Berger (1996), Kiselev et al. performed systematic experiments on microwave emissions from magnetic nanostructures (Kiselev et al., 2003). Since then, many different STNO configurations have been studied that are distinguished principally by device topology, including spacer layers, patterning geometries, and magnetic configurations.

A unique type of STNO was developed, whereupon magnetic precession is caused by spin currents generated by the spin-Hall effect (Hirsch, 1999; Sinova et al., 2015). This device is called the spin-Hall nano-oscillator (SHNO). SHNOs (Liu et al., 2013; Duan Z. et al., 2014; Demidov et al., 2014; Dürrenfeld et al., 2017; Demidov et al., 2022) have advantages over STNOs in that multiple SHNOs can be integrated into a common spin-Hall material and controlled simultaneously by a single in-plane current allowing long-range synchronization (Awad et al., 2017; Zahedinejad et al., 2020; Zahedinejad et al., 2022). Additionally, a gated structure is readily incorporated in a three-terminal SHNO topology (Liu et al., 2012c; Albertsson et al., 2019; Tarequzzaman et al., 2019), allowing for an individual oscillator to be independently controlled by a common gate voltage (Liu et al., 2017; Fulara et al., 2020b; Choi et al., 2022).

As the spin-orbitronic version of STNOs, SHNOs have been developed for neuromorphic computing (Zahedinejad et al., 2020). However, the relationship between damping and SOT-induced in-plane torque in perpendicular magnetic anisotropy (PMA) systems

is asymmetrical, and challenges exist in artificial neuron-based PMA-based SHNOs (Fulara et al., 2019).

STT-based spintronic devices have demonstrated commercial success as mass-produced eMRAM (e = embedded) alternatives to existing Flash-embedded memories (Sato et al., 2018a). Due to superior performance, SOT-based spin-orbitronic devices are expected to extend nonvolatile memory technologies. Additionally, as artificial intelligence, quantum computing, and "big data" evolve to play ever greater roles in daily life, new opportunities will exist for nonvolatile spin-orbitronic devices.

## 7.5.2 STT-based neuromorphic technologies

Neuromorphic computing embraces aspects of biological processes, including brain communication and computation, by employing electronic circuits as analogs to biologic neural networks. Neuromorphic computing offers advantages over conventional von Neumann systems in energy efficiency, processing speed, and the ability to learn. Neuromorphic computing is particularly well suited to solving problems in artificial intelligence. The creation and integration of artificial synapses and neurons are required in order to realize the goal of a neuromorphic computer. Artificial synapses require multilevel differentiated nonvolatile states. One modality that allows the storage of such synaptic weights is the memristor. Any effective memristor-based technology must contain a high density of devices assembled using standard complementary metal-oxide semiconductor (CMOS) protocols employing compatible materials and back-end processes. Neuromemristive systems<sup>14</sup>

<sup>14</sup> Neuromemristive systems (NMSs) are brain-inspired, adaptive computer architectures based on emerging resistive memory technologies (i.e., memristors).

TABLE 7 Evolution of neuromorphic computing.

Year	Team	Activity	Ref.
2006	Georgia Tech	GT researchers developed a field programmable neural array of floating gate transistors that allow programmability of charge on the gates of metal-oxide-semiconductor field-effect transistors (MOSFETs) to model the channel-ion characteristics of neurons in the brain. It is one of the first cases of a silicon programmable array of neurons.	Farquhar and Hasler (2006)
2011	MIT	Poon and Zhou of MIT created a computer chip that mimics the analog, ion-based communication in synapses between neurons using 400 transistors and standard CMOS fabrication techniques.	Poon and Zhou (2011)
2012	Purdue University	Researchers at Purdue University designed a neuromorphic chip using lateral spin valves and memristors. They conjectured that the architecture works similarly to neurons and can, therefore, be used to test methods of reproducing the brain's processing. Additionally, these chips are significantly more energy-efficient than conventional technologies.	Sharad et al. (2012)
2012	HP Labs	Researchers at HP Labs report on Mott memristors that show the volatile behavior exhibited at temperatures below the phase transition temperature can be employed to fabricate a neuristor, a biologically inspired device that mimics behavior found in neurons.	Pickett et al. (2012)
2013	Human Brain Project <sup>420</sup>	A group of researchers, including experts in neuroscience, medicine, and computing, aimed to better understand how regions of the brain work cooperatively to understand how to objectively diagnose and treat brain diseases and to use the understanding of the human brain to develop neuromorphic computers. The simulation of a complete human brain will require supercomputers that are many thousands of times more powerful than today's platforms.	Amunts (2016)
2014	Stanford University	Neurogrid, built by researchers at Stanford University, is an example of hardware designed using neuromorphic engineering principles. The circuit board is composed of 16 custom-designed chips, referred to as NeuroCores. Each NeuroCore's analog circuitry is designed to emulate neural elements for 65,536 neurons, maximizing energy efficiency. The emulated neurons are connected using digital circuitry designed to maximize spiking throughput.	Waldrop (2013), Benjamin et al. (2014), Boahen et al. (2014)
2014, 2022	IBM	Research with implications for neuromorphic engineering involves the BRAIN Initiative and the TrueNorth chip from IBM. Neuromorphic devices have also been demonstrated using nanocrystals, nanowires, and conducting polymers. There is also development of a memristive device for quantum neuromorphic architectures.	Modha et al. (2014), Spagnolo et al. (2022)

Advances in time-bin qubits.

(Wikipedia, 2022) facilitate *neuroplasticity*<sup>15</sup>. i.e., the brain's ability to alter its structure and function in response to stimuli, while neuromorphic engineering centers on mimicking the brain's behavior. For example, a neuromemristive system may replace details of a cortical microcircuit with an abstract neural network (Merkel and Kudithipudi, 2014).

<sup>15</sup> Neuroplasticity is the ability of the nervous system to change its activity in response to intrinsic or extrinsic stimuli by reorganizing its structure, functions, or connections upon injury.

Alternative paths have been proffered. For example, in 2022, MIT researchers developed an integration-friendly technology using inorganic materials compatible with conventional silicon processing (Onen et al., 2022). Those CMOS-friendly materials included WO<sub>3</sub> as the channel material, nanoporous proton-conducting phosphosilicate glass (PSG) as the protonic solid electrolyte (SE), and Pd as the hydrogen reservoir and controlling gate. The basic operating principles of the device rely on the modulation of the channel conductance via electrochemically controlled intercalation of protons within the WO<sub>3</sub> channel (Yao et al., 2020; Onen et al., 2021).

Three-terminal protonic programmable resistors, having self-aligned gate structures with Pd layers, use PSG layers as etch masks. The geometry of the Au channel electrodes and the Pd layer are tailored to avoid charging and minimize deleterious capacitance, thus maximizing device energy efficiency. As a result, devices show excellent energy efficiency under ultrafast operation. Energy consumption during transients was measured to be  $\sim 2.5$  fJ per pulse. Under intense electric fields, ultrafast modulation of nanoscale protonic programmable resistors has shown exceptional energy efficiency. SOT-induced multilevel magnetization switching, as well as the conventional synaptic function of spike-timing-dependent plasticity (STDP), was experimentally demonstrated by Cao et al. in 2019 (Cao et al., 2019). Other effective strategies include fine-magnetic domain wall switching in antiferromagnetic (AFM) (Wadley et al., 2016; Olejnik et al., 2017; Shi et al., 2020) or AFM/FM (Liu et al., 2020; Yun et al., 2020) heterostructures, where many 100-nm-sized binary domains are affixed to AFM layers that are reversed independently under application of applied currents (Fukami et al., 2016; Kurenkov et al., 2017; Yan et al., 2021).

### 7.5.2.1 Advances in neuromorphic computing

Neuromorphic computing uses hardware based on artificial neurons and synapses. Table 7 provides an evolutionary history of neuromorphic computing over the last 2 decades, tracking the major advances in these areas by major universities and organizations. The most common neuromorphic hardware is spiking neural networks (SNN). Artificial synaptic devices connect SNNs with analog circuitry to transfer signals that mimic brain functions. Instead of encoding data through binary systems of 0–1 s, SNNs encode analog signals (Techtarget, 2022). Neuromorphic computers are non-von Neumann systems<sup>16</sup> inspired by principles that mimic biological neural activity and are particularly well suited for solving problems related to artificial intelligence, among others. Artificial neurons and synapses have been demonstrated using memristors (Maan et al., 2016), spintronic memories, threshold switches, transistors (Zhou and Ramanathan, 2015), and other electronic components. In particular, artificial synapses require multilevel, nonvolatile states to store information. Although spin-orbitronic devices show superior performance over proposed systems such as memristors, the characteristic bistable nature of MTJs makes them difficult to employ as multilevel synapses.

Memristive devices rely on electronic spin and polarization. These memristor devices can be categorized further as spintronic memristors and spin-transfer torque (STT) memristors. In spintronic memristors, the path of the spin of electrons alters the magnetization state of the device, which consequently changes its resistance. Meanwhile, in STT memristors, the comparative magnetization of the two electrodes affects the magnetic state of the tunnel junction, which, in turn, changes its resistance. Because these devices operate under differing

physical principles, their memristive behavior is markedly different (Maan et al., 2016).

## 8 Qubit modalities

As previously stated, a qubit represents quantum information as a 0 or 1, or both. It is difficult to envision the simultaneous existence of a 0 and 1, a phenomenon called *superposition*. A superposition of 0 and 1 means the quantum state is made up of part 0 and part 1. The superposition state can be expressed as  $|0\rangle|0\rangle$  and  $|1\rangle|1\rangle$  or  $|0\rangle+|1\rangle|0\rangle+|1\rangle$ . A qubit can be established using any two-level quantum system. There are many ways to establish qubits. Some are presented in Table 8 and are described below.

Before we progress further in describing qubits, we introduce key terms, such as relaxation time  $T_1$  and dephasing time  $T_2$ . Both  $T_1$  and  $T_2$  are together referred to as decoherence times.  $T_1$  describes how long the phase of a qubit remains intact. For example, it is the transition time between state  $|+\rangle$  and state  $|-\rangle$ , that is (Eqs. 6 and 7):

$$|+\rangle = \frac{1}{\sqrt{2}}(|0\rangle + |1\rangle) \quad (6)$$

$$|-\rangle = \frac{1}{\sqrt{2}}(|0\rangle - |1\rangle). \quad (7)$$


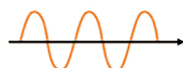
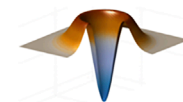
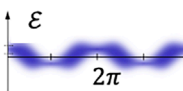
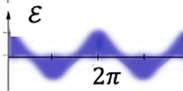
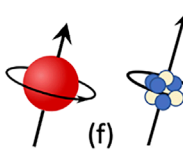
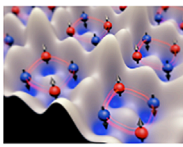
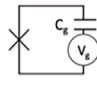
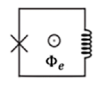
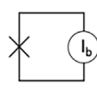
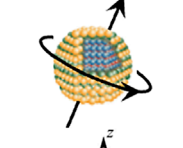
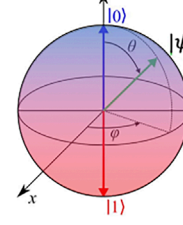
Similarly,  $T_2$  is not the time after which an initial state  $|+\rangle$  switches to state  $|-\rangle$  but rather the time after which these states effectively disentangle. Figure 12A depicts the exponential decay typical of relaxation time  $T_1$ , while oscillations defining a Gaussian decay envelope allow the determination of the dephasing time  $T_2^*$ . Figure 21, introduced and discussed later in the text, provides a compilation of coherence times of charge qubits according to material system and coherence type.

The inhomogeneous dephasing time  $T_2^*$  implies a Ramsey experiment<sup>17</sup>. A  $T_2^*$  Ramsey experiment measures the dephasing time,  $T_2^*$ , of a qubit and the qubit's detuning, which is a measure of the difference between the qubit's resonant frequency and the frequency of the rotation pulses being used to perform

<sup>16</sup> A non-von Neumann architecture attempts to eliminate redundant load-and-store operations by performing numerical and logical operations on memory elements for the calculation of nondeterministic polynomial time (i.e., NP-Hard) problems.

<sup>17</sup> A  $T_2^*$  Ramsey experiment consists of an  $\frac{\pi}{2}$  pulse, bringing the qubit to the equator on the Bloch sphere, followed by a delay of variable duration, during which the qubit precesses about the Z-axis on the equator. A Z rotation is then applied through  $2\pi \cdot t$  detuning. Finally, another  $\frac{\pi}{2}$  pulse is applied, which, if the precession from the delay and the manual Z rotation offset each other perfectly, should land the qubit in the excited state. When the precession from the delay and the Z rotation do not offset each other perfectly, the qubit does not land perfectly in the excited state, and the state visibility oscillates, creating fringes. While this is happening, dephasing also causes the state to contract toward the center of the Bloch sphere, away from its surface. This causes the amplitude of the fringes to decay in time, so we expect an exponentially decaying sinusoidal waveform as a function of the delay time. The time decay constant is calculated from these fringes ([https://forest-benchmarking.readthedocs.io/en/latest/examples/qubit\\_spectroscopy\\_t2.html](https://forest-benchmarking.readthedocs.io/en/latest/examples/qubit_spectroscopy_t2.html) accessed 7/1/23).

TABLE 8 Types and properties of popular qubit systems.

Physical qubit	Property	Information	Differentiators		
			$ 0\rangle$	$ 1\rangle$	
Photon	Polarization encoding	Polarization of light	Horizontal polarization: (a)	Vertical polarization: (b)	 (a)
	Number of photons	Fock state	Vacuum	Single photon state: (c)	 (b)
	Time-bin encoding	Time of arrival	Early	Late	 (c)
Coherent state of light (QED)	Squeezed light	Quadrature: Operators obey Heisenberg's Uncertainty Principle	Amplitude-squeezed state: (d)	Phase-squeezed state: (e)	 (d)
Quantum dot	Electronic spin	Spin	Up (f)	Down (f)	 (e)
	Electron number	Charge	No electron	One electron	
LS-NMR	Nuclear spin	Spin	Up (g)	Down (g)	 (f) (g)
SS-NMR	Nuclear spin	Spin	Up (g)	Down (g)	
Optical lattices	Atomic spin	Spin	Up (h)	Down (h)	 (h)
Josephson junction	Superconducting charge qubit	Charge 	Charge-neutral superconducting island ( $Q=0$ )	Charged superconducting island ( $Q=2e^-$ , extra Cooper pair)	
	Superconducting flux qubit	Current 	CW current	CCW current	
	Superconducting phase qubit	Energy 	Ground state	First excited state	
Singly charged quantum dot pair	Electron localization	Charge	Depends on specific electron localization		 (i)
Quantum dot	Dot spin	Spin	Up (i)	Down (i)	
Gapped topological system	Non-abelian anyons (a)	Braiding of Excitations(b)	Depends on specific topological system		 (j)
Vibrational qubit	Vibrational states	Phonon	$ 0\rangle$ superposition (j)	$ 1\rangle$ superposition (j)	
van der Waals heterostructure	Electron localization	Charge	Depends on specific electron localization		

the Ramsey experiment. Ideally, this detuning would be 0, meaning pulses are perfectly tailored to address each qubit without enacting any unintended interactions with neighboring qubits. In practice, qubits drift, and the pulse parameters must be adjusted. Retuning qubits and pulses requires the running of a  $T^*_2$  Ramsey experiment to measure the size of the qubit detuning.

### 8.1 Photon (boson) qubits

One of the most effective means of transmitting quantum information is the encoding of photon polarization (see Table 8).

Such encoding requires two distinct optical modes. This is referred to as *dual-rail encoding*<sup>18</sup>. The photon state is an eigenstate, that is, a single *Fock state*<sup>19</sup>; dual-rail qubits are states that do not evolve under

18 A qubit can be encoded in terms of probability amplitudes corresponding to the photon occupation of two modes of some degree of freedom of the optical field. This is referred to as dual-rail encoding.

19 A Fock state is an element of Fock space with a well-defined number of particles. The Fock states of bosons and fermions obey relations with respect to the Fock space creation and annihilation operators. When the number of particles is variable, one constructs the Fock space as the direct sum of the tensor product Hilbert spaces for each particle number.



propagation. Alternatively, if one considers the electromagnetic field as encoded as two distinct Fock states, then this entails the use of a single optical mode and is referred to as *single rail encoding* (Lund and Ralph, 2002)<sup>18</sup>. In these cases, optical modes are a superposition of eigenstates and experience phase evolution under propagation.

### 8.1.1 Time bin qubits

Time-bin qubits, originally developed in 1999 by Brendel et al. (1999) propagate over long distances along optical fibers with unusually robust fidelity. In 2013, Humphreys et al. developed a technique for optical quantum computing using time-bin qubits (Humphreys et al., 2013). This concept allows photonic quantum computing using a single optical path and greatly reduces system complexity. In that same year, Donohue et al. demonstrated an ultrafast measurement technique for time-bin qubits that enables high data rates with minimal errors (Donohue et al., 2013). Humphreys et al. also showed the use of time-bin qubits enabling linear optic quantum computing (LOQC) (Knill et al., 2001) in a single spatial mode, further minimizing complexity. Together, these developments are foundational in realizing practical quantum information systems using photonic qubits.

Additionally, the photonic temporal degree of freedom is one of the most promising quantum communication modalities over fiber and free-space channel networks. Bouchard et al. demonstrated the feasibility of picosecond time-bin states of light for applications in quantum communications. With the ability to measure time-bin superpositions with superb phase stability, they helped realize efficient quantum key distribution protocols such as BB84 (Bouchard et al., 2022).

Gündoğan et al. demonstrated the first solid-state spin-wave optical quantum memory with on-demand readout using a full atomic frequency comb in a  $\text{Pr}^{3+}:\text{Y}_2\text{SiO}_5$  crystal. These authors stored weak coherent pulses with a signal-to-noise ratio greater than 10:1. Narrow-band spectral filtering based on spectral hole burning in a second  $\text{Pr}^{3+}:\text{Y}_2\text{SiO}_5$  crystal was shown effective in filtering out excess noise to a level of  $2.0 \pm 0.3 \times 10^{-3}$  photons per pulse. These authors also reported spin-wave storage of photonic time-bin qubits, demonstrating that spin-wave memory operates in the quantum regime (Gündoğan et al., 2015).

### 8.1.2 Advances in squeezed light

Shahmoon et al. calculated the entanglement between a short pulse of resonant squeezed light (SL) and a two-level atom in free space. They found that the squeezing phase, that is, the phase of the EM field and the atomic superposition phase, determine the performance of atom-pulse mode entanglement and gate errors (Shahmoon et al., 2009).

Callus and Kok (2021) demonstrated how to create maximal entanglement between two qubits encoded in two spectrally distinct solid-state quantum emitters embedded in a waveguide interferometer. Their method does not require identical emitters, accommodates a degree of spectral variation arising from slight deviations introduced during fabrication, and creates entanglement

with a concurrence<sup>21</sup> above 99% in the event of scattering losses and detector inefficiencies.

Ortu et al. demonstrated long-duration quantum memories for photonic qubits and achieved long-distance quantum networks by mapping optical states onto coherent spin-waves (Ortu et al., 2022). However, this approach suffers from readout noise caused by spin-wave manipulation. A dynamical decoupling technique and small magnetic fields were employed to achieve storage of six temporal modes for 20 ms, 50 ms, and 100 ms in a  $\text{Eu}^{3+}:\text{Y}_2\text{SiO}_5$  crystal based on an atomic frequency comb-type memory (Grover, 1996-07c). The quantum coherence of this memory was verified by storing two time-bin qubits for 20 ms with an average memory output fidelity of  $85\% \pm 2\%$ .

## 8.2 Superconductor qubits

Superconducting qubits are characterized as employing Josephson junctions (JJs). A JJ is an electrical component that exists as a weak-link circuit between two superconductive leads on either side of a thin layer of insulator material a few atoms in thickness (see Figure 13). The resulting JJ device exhibits the *Josephson Effect*<sup>22</sup>, producing a supercurrent. The condensate wave function on either side of the junction is weakly correlated, having different superconducting phases. Current through the JJ occurs by quantum tunneling (discussed earlier), creating a nonlinear inductance that allows for a qubit design that behaves as an anharmonic oscillator of quantized energy levels (Strogatz, 2004).

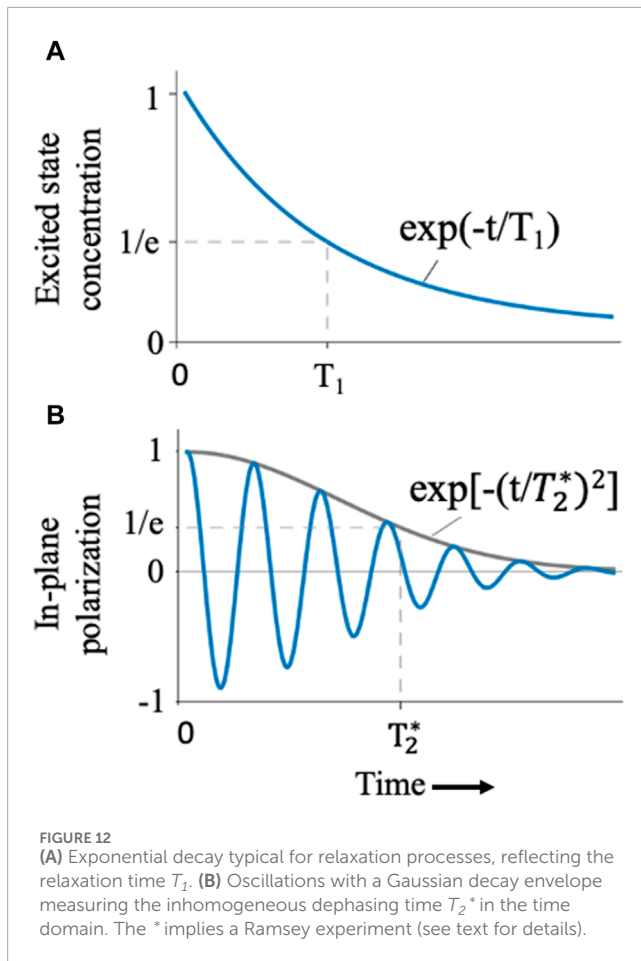
### 8.2.1 Charge qubits

The simplest superconducting qubit is the “Cooper-pair box,” more generally referred to as the superconducting “charge” qubit (see Figure 14A). The charge qubit, first described in theory by Büttiker (1987), was demonstrated experimentally a decade later by Bouchiat et al. (1998). Its time-domain quantum dynamic behavior was described by Nakamura et al. (1999) (Martinis, 2009; Siddiqi, 2021).

In superconducting quantum computing, a charge qubit is formed by an infinitesimal superconducting island (denoted in its circuit diagram of Figure 14A as the dashed box) coupled by a JJ to a superconducting reservoir (Makhlin et al., 2001). The charge qubit's basis states are charge states, that is, states that represent the presence or absence of excess Cooper pairs in the islands. The state of the qubit is determined by the number of Cooper pairs that have

21 Concurrence is a scalar function defining an entanglement monotone, i.e. that is, a way of measuring entanglement, for bipartite density matrices describing the mixed states of a two-qubit system.

22 The Josephson effect is an example of a macroscopic quantum phenomenon that occurs when two superconducting materials are separated by a small distance or across a thin layer, whereupon a current is produced that flows continuously without voltage bias (known as a Josephson junction). Josephson junctions play important roles in SQUIDs, qubits, and RSFQ (rapid single flux quantum (RSFQ) electronics, among other technologies.



tunneled across the junction. The quantum superposition of charge states can be achieved by tuning the gate voltage that controls the chemical potential of the island. The qubit is typically read out by electrostatically coupling the island to a sensitive RF single-electron transistor.

Charge qubits are fabricated using techniques like those used in microelectronics. The devices are usually made on silicon wafers employing electron beam lithography and physical vapor deposition. Typical coherence times for a charge qubit are on the order of a few microseconds (Houck et al., 2009-02). However, recent works using transmons<sup>23</sup> have demonstrated dramatic enhancements in coherence times.

The transmon's enhanced coherence derives from a reduced sensitivity to charge noise originating from an increase in the ratio of Josephson energy to charging energy using a shunting capacitor. Planar on-chip transmon qubits have coherence times

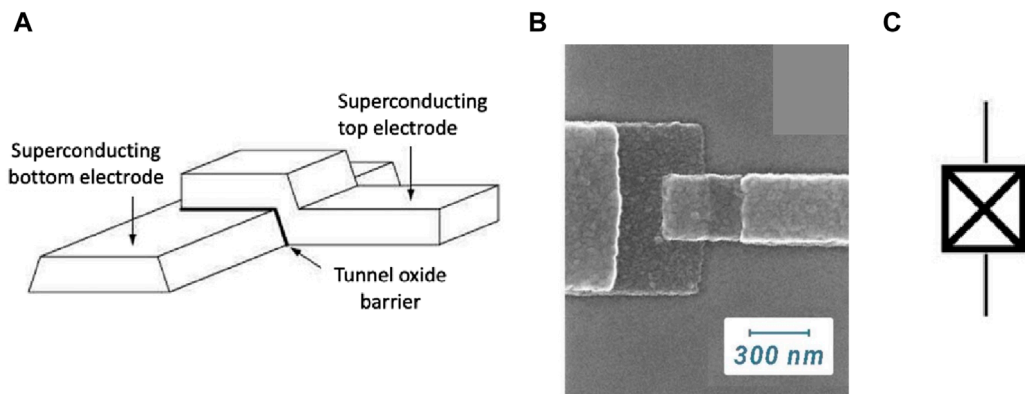
<sup>23</sup> A transmon is a type of superconducting charge qubit that was designed to have reduced sensitivity to charge noise. Its name is an abbreviation of the "transmission line shunted plasma oscillation qubit". This consists of a Cooper-pair box where two superconductors are capacitively shunted in order to decrease the sensitivity to charge noise, while maintaining a sufficient anharmonicity for selective qubit control. It was first developed by Robert J. Schoelkopf, Michel Devoret, and Steven M. Girvin.

of approximately 30  $\mu\text{s}$ –40  $\mu\text{s}$  (Barends et al., 2013-08), with recent work approaching  $\sim 100 \mu\text{s}$  attained by replacing the superconducting transmission line cavity with a three-dimensional superconducting cavity (Paik et al., 2011-12; Rigetti et al., 2012-09). Replacement of niobium with tantalum in the transmon device leads to coherence times as high as 300  $\mu\text{s}$  (Place et al., 2021-03; Wikipedia, 2022).

Chow et al. describe a route toward a logical memory with superconducting transmons employing a rotated surface code (RSC). Quantum error correction, necessary to realize scalable quantum computers, is theoretically possible with an error rate below the threshold. Two-dimensional surface coding permits relatively high fault-tolerant thresholds at the  $\sim 1\%$  level and only requires a latticed network of qubits with nearest-neighbor interactions. These authors describe single- and two-qubit gate tune-up procedures simultaneously benchmarking pairs of two-qubit gates (Chow et al., 2015). While there are many approaches to achieving quantum fault tolerance, one of the most promising is the two-dimensional (2D) surface code (Bravyi and Kitaev, 1998; Kitaev, 2003; Raussendorf and Harrington, 2007; Fowler A. G. et al., 2012). This code has a high tolerance to errors, or threshold (approximately  $6.7 \times 10^{-3}$ ), requires only nearest-neighbor qubit interactions, and has simple error syndrome extraction circuits (Dennis et al., 2002) and a suite of fault-tolerant logic based on transversal gates, code deformation (Raussendorf et al., 2007), or lattice surgery (Horsman et al., 2012). To realize this code, coupling between data qubits and the syndromes was induced by using a quantum bus (Majer et al., 2007; Sillanpaa et al., 2007) where each bus couples to four data qubits and each qubit couples to two buses, allowing a tiling that achieves the connectivity required for the RSC (Chow et al., 2014). IBM uses coplanar waveguide microwave resonators for buses. An example of a connected multi-qubit device consisting of eight transmon qubits, four quantum buses, and eight readout resonators allowing for studying both Z and X parity checks is presented as the optical micrograph of Figure 15 (Gambetta et al., 2017-01).

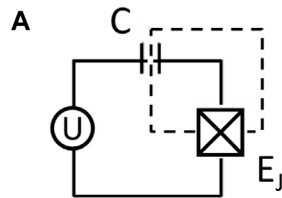
Figure 14A The circuit schematic of the superconducting charge qubit is also known as the "Cooper-pair box." The dashed square denotes the superconducting island. Beneath is its Hamiltonian, where  $E_C$  is the charging energy, the JJ capacitance is  $C_J$ , and the gate capacitor is  $C_g$ .  $N$  is the number of Cooper pairs to tunnel through the junction. The quantum superposition of charge states is achieved by tuning the gate voltage that controls the chemical potential of the island. (b) The circuit schematic of the flux qubit is also known as the RF-superconducting quantum interference device (SQUID) qubit. Its Hamiltonian is presented below the image with key parameters defined. (c) The circuit schematic of the phase qubit is also known as the current-biased qubit. Its Hamiltonian is presented below the image, where the gauge invariant phase difference operator is equivalent to the flux across the JJ.

Wang et al. of the Beijing Academy of Quantum Information Sciences produced a transmon chip that contained five independent transmons, four independent quarter-wave resonators for measuring the intrinsic  $Q$  factor of the resonator, and three



**FIGURE 13** (A) Schematic of a Josephson junction (JJ), (B) scanning electron microscopy image of a JJ (used with permission of Angstrom Engineering), and (C) circuit element representation.

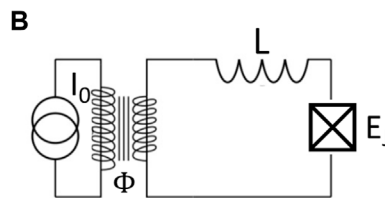
“Cooper pair box” (charge) qubit



$$H = E_C (N - N_g)^2 - E_J \cos \theta$$

where  $E_C = (2e)^2 / (2(C_J + C_g))$  is the charging energy of the island of the box and  $N_g = Q_r + C_g U / 2e$ .

RF-SQUID (flux) qubit



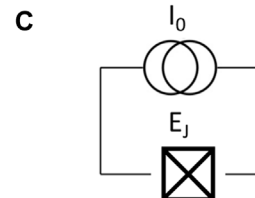
**Hamiltonians**

$$H = \frac{q^2}{2C_J} + \frac{\phi^2}{2L} - E_J \cos \left[ \frac{2e}{\hbar} (\phi - \Phi_{\text{ext}}) \right]$$

where the dynamical variables are the node fluxes and node charges:

$$\phi_n = \int_{-\infty}^t v(t_1) dt_1; \quad q_n = \int_{-\infty}^t i(t_1) dt_1$$

Current-biased (phase) qubit



$$H = E_C J p^2 - I \varphi_0 \delta - I_0 \varphi_0 \cos \delta$$

where the gauge invariant phase difference operator  $\delta$  is, apart from the scale factor  $\varphi_0$ , precisely the branch flux across  $C_J$ .

**FIGURE 14** A simple circuit diagram of each superconducting qubit with their Hamiltonian and other key parameters. This figure was constructed in part from data presented in Wikipedia (2022m) and Devoret et al. (2004).

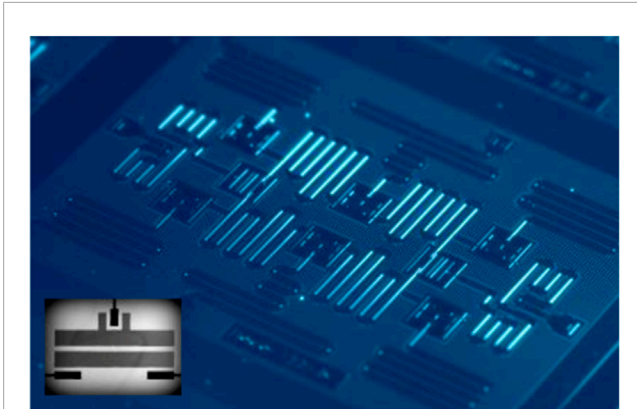
additional transmons for testing resistance. The Purcell effect<sup>24</sup> limited transmon temporal decoherence to over 2 milliseconds. The coupling strength between the readout resonator and transmons was  $50 \text{ MHz} \times 2\pi$ . The measured  $T_1$  and  $T_2^*$  were  $50 \mu\text{s}$  and  $75 \mu\text{s}$ , respectively (Wang C. et al., 2022).

### 8.2.2 Flux qubits

Flux qubits, also known as persistent-current qubits or SQUID qubits, are micron-sized loops of superconducting material that are spatially divided by JJs (see Figure 14B). The flux qubit was first proposed by Orlando et al. (1999) and fabricated shortly thereafter. In fabrication, the JJ parameters are engineered so that a persistent current flows continuously when an external magnetic flux is applied. Only an integer number of flux quanta are allowed to penetrate the superconducting ring, resulting in clockwise or counterclockwise supercurrents in the loop to compensate a non-integer external flux bias. When the applied flux through the loop is close to a half-integer number of flux quanta, the two lowest energy eigenstates of the loop will be a quantum superposition of the clockwise and counterclockwise currents (Wikipedia, 2022).

The two lowest energy eigenstates differ only by the relative quantum phase between the composing current-direction states. Higher energy eigenstates correspond to much larger (macroscopic) persistent currents that induce an additional flux quantum to the

24 The Purcell effect is the enhancement of a quantum system's spontaneous emission rate by its environment. Edward Mills Purcell (c. 1940s) discovered the enhancement of spontaneous emission rates of atoms when they are incorporated into a resonant cavity. The magnitude of the enhancement is given by the Purcell factor is:  $F_p = \frac{3}{4\pi^2} \left( \frac{\lambda_{\text{free}}}{n} \right)^3 \frac{Q}{V}$ , where  $\lambda_{\text{free}}$  is the vacuum wavelength,  $n$  is the refractive index of the cavity material (so  $\lambda_{\text{free}}/n$  is the wavelength inside the cavity), and  $Q$  and  $V$  are the cavity quality factor and mode volume, respectively. (see: "Purcell Factor - Qwiki". Retrieved 2023-04-16.)



**FIGURE 15**  
A device consisting of eight transmon qubits, four quantum busses, and eight readout resonators (i.e., 8Q/4B/8) fabricated at IBM (Gambetta et al., 2017). Inset shows an optical micrograph of an individual transmon qubit. Used with permission of IBM under Creative Commons Attribution 4.0 International License.

qubit loop, which is well separated energetically from the lowest two eigenstates. This separation, known as the *qubit nonlinearity*, allows operations with the two lowest eigenstates, thus effectively creating the necessary two-level system for qubit operation.

Computational operations are performed by pulsing the qubit with microwave radiation that has an energy comparable to that of the gap between the energy of the two basis states. Properly selected pulse durations and amplitudes can put the qubit into a quantum superposition of the two basis states, while subsequent pulses can manipulate the probability weighting that the qubit will be measured in either of the two basis states, thus performing a computational operation (Paladino et al., 2014).

### 8.2.3 Phase qubits

The phase qubit is also a superconducting device based on a superconductor–insulator–superconductor JJ (Nielsen and Chuang, 2000) closely related to the previously mentioned flux qubit and charge qubit. The major distinction among the three is the ratio of Josephson energy to charging energy, that is, the required energy for one Cooper pair to charge the total capacitance of the circuit (see Figure 14C) (You and Nori, 2007-01).

For a phase qubit, this ratio is on the order of  $10^6$ , which allows for macroscopic bias currents through the JJ. For flux qubits, it is on the order of  $10^1$ , which allows for mesoscopic supercurrents on the order of 300 nA. For charge qubits, it is on the order of  $< 10^0$ , whereupon only a few Cooper pairs tunnel through and charge the Cooper-pair box. However, transmons (Koch et al., 2007-10; Fink, 2010; Schreier et al., 2008-05b) can have very low charging energy due to the circuit's large shunt capacitance and, therefore, have a ratio on the order of 10–100 (Eng et al., 2015).

## 8.3 Electron spin qubits

Spin is an effective and popular way of encoding quantum information, is a common qubit modality, and manifests in several systems.

### 8.3.1 Quantum-dot spin qubits

An electrostatic quantum dot typically consists of a stacked heterostructure that is designed to create quantum confinement in three dimensions by combining electric fields and topological constraints. Stano and Loss provide an excellent review of the performance metrics of spin qubits in gated semiconducting quantum-dot nanostructures (Stano and Loss, 2022).

The electron is quantum-confined at the interface between the active materials. For these spins to be considered as potential qubits, it is necessary to be able to isolate a single spin, establish entanglement between pairs, and ultimately read the quantum-encoded information. Moreover, all these tasks must be performed with sufficient spatiotemporal precision to avoid degradation to quantum fidelity from environmental influence (Escalera-Moreno et al., 2018).

As previously discussed, the strength of spin–orbit interactions is an important factor influencing the coherence of select qubit modalities and is key in the development of quantum-dot spin qubits. In one such case, researchers have found larger than expected spin–orbit interactions at the surface of silicon where electrons are confined as if they existed within quantum dots (Q-dots) (Osika et al., 2022).

An interesting and potentially valuable finding was the manipulation of electron spin bound to a single phosphorus (P) donor ion in silicon that was measured with fidelities greater than 99% (Muhonen J. T. et al., 2014; Watson et al., 2015), which is above the threshold for coded quantum error correction (Raussendorf et al., 2007; Wang D. S. et al., 2011). One of the main sources of error during single-shot spin readout is the relaxation of spins prior to measurement (Baart et al., 2016). The spin relaxation time,  $T_1$ , also represents an upper bound to the spin coherence time,  $T_2$ , where  $T_2 < 2T_1$  (Tyryshkin et al., 2012). Watson et al. (2017) showed that electrons bound to 2P and 3P donor dots can have spin relaxation times up to 16 times greater than those of 1P donors because of higher confinement potential. This agrees with the theoretical work of Hsueh et al. (2014). Enhanced spin relaxation times, combined with high signal-to-noise single-electron transistor charge sensors, allow for a fidelity of 99.8% in the sequential readout of two donor-bound electron spin qubits.

The isolation of qubits from noise sources, such as surrounding nuclear spins and spin–electric susceptibility (Balasubramanian et al., 2009; Kuhlmann et al., 2013; Muhonen J. T. et al., 2014; Reed et al., 2016), has enabled extensions of quantum coherence times. The possibility of achieving enhanced quantum coherence was doubted due to background charge fluctuations (Paladino et al., 2014; Bermeister et al., 2014; Huang and Hu, 2014). Still, a sizeable spin–electric coupling will be needed in multiple-qubit systems to support single-spin and spin–spin interactions (Tokura et al., 2006; Trif et al., 2008; Hu et al., 2012).

Yoneda et al., and references contained therein, reported on single-electron spin qubits with an isotopically enriched phase coherence time of 20  $\mu$ s (Veldhorst et al., 2014; Eng et al., 2015) and fast electrical control speed of up to 30 MHz mediated by extrinsic spin–electric coupling. Using rapid spin rotation, they revealed that the free-evolution dephasing is caused by charge noise—rather than conventional magnetic noise—as highlighted by a  $1/f$  spectrum extending over 7 decades of frequency. The qubit exhibits superior performance with single-qubit gate fidelities exceeding 99.9% on



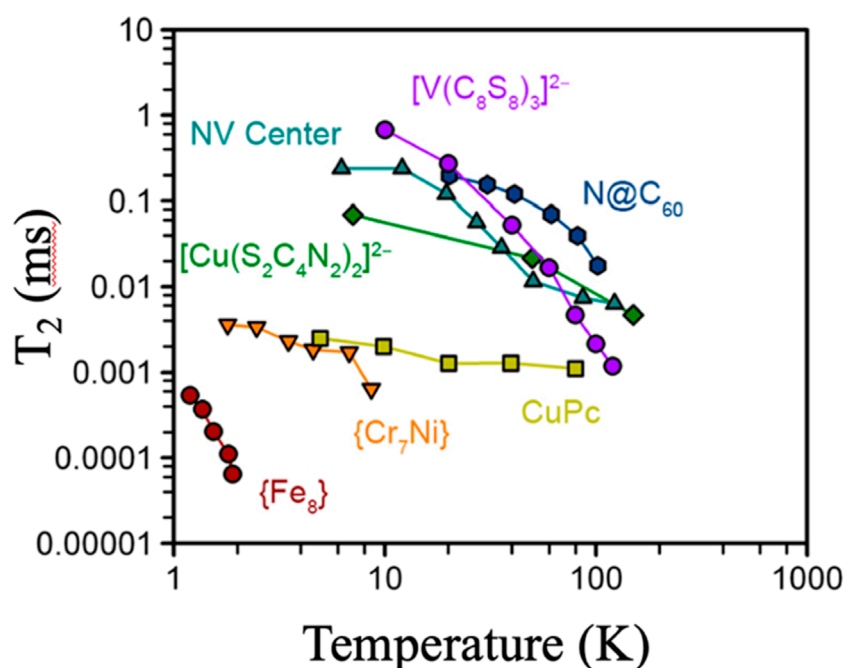


FIGURE 16

Comparison of  $T_2$  values of  $[V(C_8S_8)_3]^{2-}$  with other molecular and solid-state electronic spin-qubit systems. Data listed are referenced by Zadrozny et al. (2015). This figure is modified and reproduced with permission of the American Chemical Society under Creative Commons Attribution 4.0 International License.

average, offering a path to large-scale spin-qubit systems with controllable fault tolerance (Yoneda et al., 2018).

### 8.3.2 Molecular spin qubits

Molecular nanomagnets have many intrinsic low-energy states that can be used to define qubits and allow quantum computation with embedded quantum error correction (Chiesa et al., 2020). The magnetic materials community has witnessed a dramatic increase in molecular magnetism research activity, including advances in phase coherence of spin qubits from a few microseconds to a few milliseconds.

The method of Chiesa et al. (2020), using a sequence of RF pulses to actuate error corrections, has been applied to a simple  $s = 3/2$  molecule and scaling to larger spin systems.

Transition-metal complexes offer a unique potential as tunable qubits, in some cases, challenge solid-state systems. Zadrozny et al. harnessed molecular design to create a series of qubits, for example,  $(Ph_4P)_2 [V(C_8S_8)_3]$ , with  $T_2$  values of 1–4  $\mu$ s at 80 K in protiated and deuterated environments (Zadrozny et al., 2015). Through chemical tuning of nuclear spins in the vanadium environment, these authors realized a  $T_2$  of  $\sim 1$  ms for the species  $(d_{20}-Ph_4P)_2 [V(C_8S_8)_3]$ . This  $T_2$  value surpasses the performance of other coordination complexes by more than an order of magnitude.

Einstein–Podolsky–Rosen (EPR) data reveal the electronic role of ligands in interacting with cations. However, pulsed EPR measurements specifically reveal decoherence is strongly influenced by nuclear spins in protiated and deuterated solvents.

The results illustrated in Figure 16 and presented in Table 9 show improvements in transition-metal complexes with coherence times appropriate for more advanced quantum interactive polynomial

(QIP) applications, including creating hybrid electronuclear quantum memory (Morton et al., 2008) with  $^{51}V$  nuclear spin.

### 8.3.3 2-Dimensional spin qubits systems

Trauzettel et al. proposed a route to form spin qubits as graphene quantum dots, allowing for the lifting of the well-known valley degeneracy experienced in graphene (Trauzettel et al., 2007). These authors showed that this problem can be avoided in quantum dots based on ribbons of graphene with armchair boundaries. A new feature of these proposed spin qubits is that an array formed of such qubits allows the coupling of any two via Heisenberg exchange if others are decoupled by detuning.

Wang et al. integrated hexagonal boron nitride (hBN) capacitors with aluminum JJs to realize transmon qubits with coherence times reaching 25  $\mu$ s, consistent with the hBN loss tangent inferred from resonator measurements. The hBN PPC (polypropylene carbonate) reduces the qubit feature size by approximately two orders of magnitude compared to conventional all-aluminum coplanar transmons. These results establish hBN as a promising dielectric for building high-coherence quantum circuits with substantially reduced form factor and a reduction in deleterious qubit crosstalk (Wang J. I. et al., 2022).

The discovery of *atom-like spin emitters* associated with defects in wide bandgap semiconductors presents further opportunities for versatile qubits. Research activities in this area have focused on defects in hBN because hBN contains a high density of nuclear spins that are expected to create a strong, incoherent spin bath, resulting in poor coherence of spins. New 2D-WBG materials as qubit candidates are the subject of ongoing research.

TABLE 9 Examples of molecular qubits.

Qubit complexes	Preparation	Irradiation	References
<b>[V(C<sub>8</sub>S<sub>8</sub>)<sub>3</sub>]<sup>2-</sup></b>			
(Ph <sub>4</sub> P) <sub>2</sub> [V(C <sub>8</sub> S <sub>8</sub> ) <sub>3</sub> ] Note: Sample preparation is contained in the published supplemental materials section of this reference at DOI: 10.1021/acscentsci.5b00338	Protiated and deuterated solvents	X-band	Zadrozny et al. (2015)
<b>{Fe8}</b>			
[(C <sub>6</sub> H <sub>15</sub> N <sub>3</sub> ) <sub>6</sub> Fe <sub>8</sub> (μ <sub>3</sub> -O) <sub>2</sub> (μ <sub>2</sub> -OH) <sub>12</sub> ]Br <sub>7</sub> · 8H <sub>2</sub> O Note: Wieghardt et al. (1984) contains processing conditions	Single crystal	240 GHz	Wieghardt et al. (1984), Takahashi et al. (2011)
<b>{Cr<sub>7</sub>Ni}</b>			
[nPr <sub>2</sub> NH <sub>2</sub> ][Cr <sub>7</sub> NiF <sub>8</sub> Ac <sub>16</sub> ] Note: Molecular nanomagnet ground state (S = 1/2)	0.1 mM d8-Tol solution	X-band	Wedge et al. (2012)
<b>{CuPc}</b>			
CuPc: copper phthalocyanine (C <sub>32</sub> H <sub>16</sub> CuN <sub>8</sub> ); H <sub>2</sub> Pc: phthalocyanine ((C <sub>8</sub> H <sub>4</sub> N <sub>2</sub> ) <sub>4</sub> H <sub>2</sub> ) Note: CuPc:H <sub>2</sub> Pc was grown via organic molecular beam deposition on a layer of perylene-3,4,9,20-tetracarboxylic dianhydride coated Kapton™	0.1% cocrystallization with unmetallated ligand	X-band	Warner et al. (2013)
<b>(Ph<sub>4</sub>P)<sub>2</sub>[Cu(S<sub>2</sub>C<sub>4</sub>N<sub>2</sub>)<sub>2</sub>]</b>			
Note: (PPh <sub>4</sub> ) <sub>2</sub> [Cu(mnt) <sub>2</sub> ] (1Cu, mnt <sub>2</sub> = maleonitriledithiolate or 1,2-dicyanoethylene-1,2-dithiolate) doped into diamagnetic isostructural host (PPh <sub>4</sub> ) <sub>2</sub> [Ni(mnt) <sub>2</sub> ] (1Ni)	1:500 Cu:Ni cocrystallization with deuterated PPh <sup>4+</sup> counter ion	X-band	Bader et al. (2014)
<b>NV center</b>			
Note: Single crystal of high-temperature, high-pressure type-Ib diamond (Sumitomo Electric Industries, Ltd.). The density of N impurities is 1,019–1,020 cm <sup>-3</sup> . The sample was irradiated with 1.7 MeV electrons with a dose of 5 × 1,017 cm <sup>-3</sup> and subsequently annealed at 900°C for 2 h to increase the N-V concentration. (Epstein et al., 2005)	Defects in diamond	240 GHz	Takahashi et al. (2008)
<b>N@C60</b>			
Note: N@C60 and N@C70 comprise atomic nitrogen trapped within a carbon cage in a liquid CS <sub>2</sub> solution	<0.8 mM in 3:1 CS <sub>2</sub> :S <sub>2</sub> Cl <sub>2</sub>	X-band	Morton et al. (2006), Morton et al. (2007)

Defo et al. present a method for rapid estimation of the zero-phonon line (ZPL), a key property of atomic qubits in WBG materials (Kuate Defo et al., 2021). Their approach to calculating ZPL employs Janak's theorem<sup>25</sup> and converges more rapidly than the standard method ( $\Delta$ SCF)<sup>26</sup>. They apply this and related theoretical techniques to the case of singly charged calcium vacancies in SiS<sub>2</sub>, which they propose as a qubit material. This work could assist

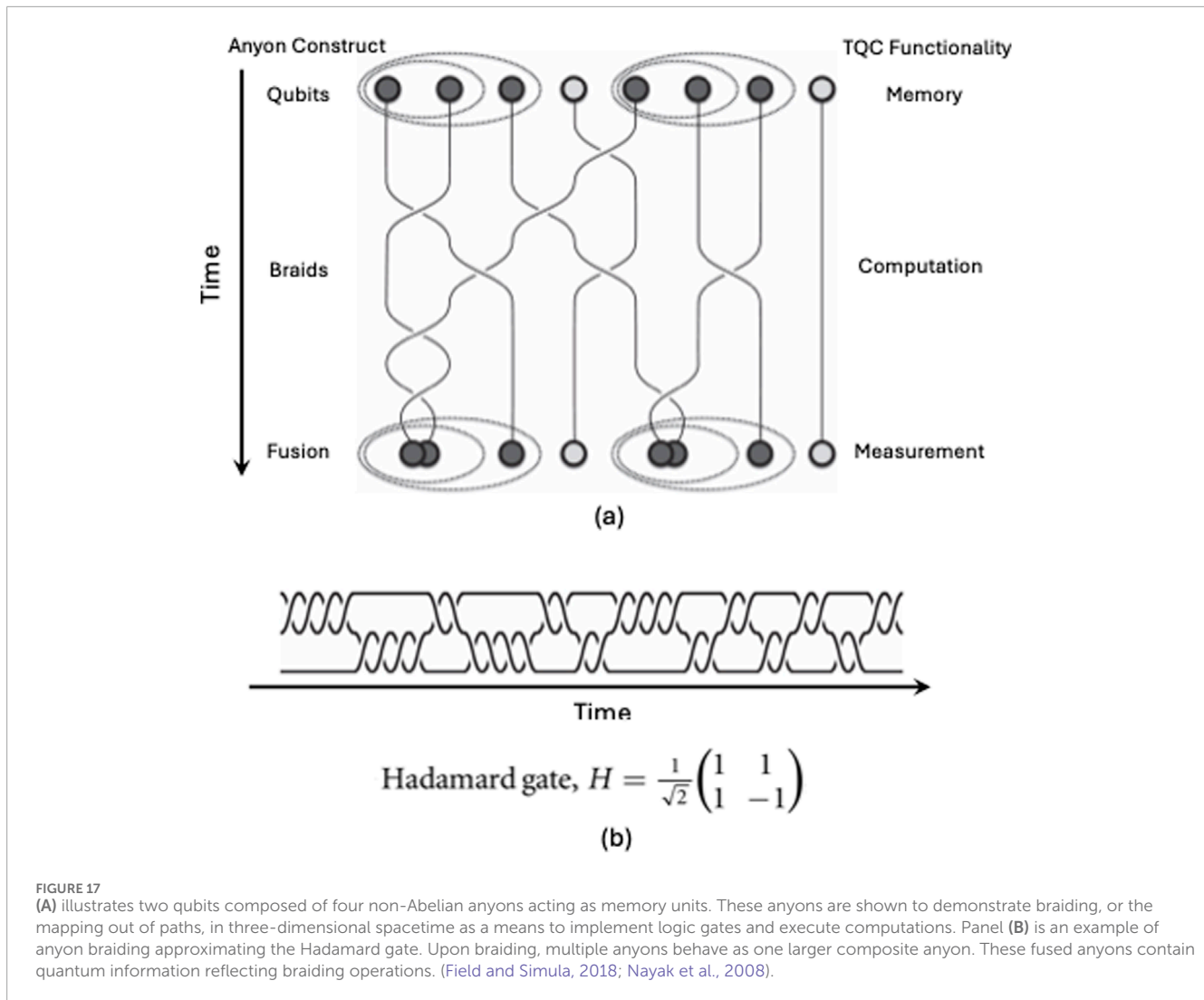
25 Janak's theorem allows a calculation of charge transition levels by analyzing the Kohn–Sham eigenvalues of density-functional theory without needing to explicitly compare differently charged systems. Specifically, the eigenvalue is the derivative of the total energy with respect to the occupation of a state.

26 The  $\Delta$ SCF approximation is a density-functional method closely resembling standard density-functional theory (DFT), the only difference being that in  $\Delta$ SCF, one or more electrons are placed in higher-lying Kohn–Sham orbitals instead of placing all electrons in the lowest possible orbitals as one does when calculating the ground-state energy within standard DFT.

in accelerating high-throughput searches for 2D materials with unique potential for quantum sensing and quantum computing applications.

Point defects and defect complexes in AlN have been studied by Varley et al. for potential as single-spin centers and solid-state qubits similar to those observed in diamond and SiC, finding that isolated anion vacancies ( $V_N$ ) meet many of the criteria for an individually addressable quantum system (Varley et al., 2016). However, since these states reside near the conduction-band, studies have focused on how properties can be tuned by complexing vacancies with near-neighbor substitutional impurities. Transition-metal dopants Ti and Zr favorably substitute on the Al site, form complexes with  $V_N$ , and possess the desired electronic and optical properties, such as charge and spin states, binding energies, and optical excitation energies, making this material a practical individually addressable solid-state qubits host.

Koehl et al. have endeavored to identify and develop robust quantum systems (Koehl et al., 2011) that can be readily manipulated for use in advanced information and communication technologies (Awschalom and Flatte, 2007) by building upon recent



results of nitrogen-vacancy (NV) centers in diamond that have attracted interest based on atomic-scale electronic spin states that can be used as individual addressable, solid-state qubits, even under ambient conditions (Jelezko et al., 2004). These attractive quantum properties have motivated others to identify similar defects in other 2D semiconductor systems, as they may offer an expanded functionality not available to NV-diamond (Weber et al., 2010).

Notably, defects in silicon carbide (SiC) have been suggested as a potential qubit candidate owing to a combination of theoretical predictions and experimental magnetic resonance studies (Baranov et al., 2005; Son et al., 2006; Baranov et al., 2011; Gali, 2011; Ruskov and Tahan, 2012; Mizuochi et al., 2022; Son et al., 2022). Koehl et al. demonstrated several defect spin states in 4H-SiC that can be optically addressed and coherently controlled in the time domain at temperatures that approached ambient (~300 K). Using conventional optical and microwave techniques, they studied the spin-1 ground state of each of four inequivalent forms of neutral carbon-silicon divacancies, as well as a pair of defect spin states of unidentified origin. These defects are optically active near telecommunication bands (Saleh and Teich, 1991) and are found in a host material for which industrial-scale crystal growth capacity already exists (Powell et al., 2006) and has undergone

advanced microfabrication process refinement (Zetterling, 2002). Additionally, they possess desirable spin coherence properties that are comparable to those of NV-diamond systems, making them promising candidates for various photonic, spintronic, and quantum information applications that merge quantum degrees of freedom with classical electronic and optical technologies.

## 8.4 Nuclear spin qubits

### 8.4.1 Nuclear spin-enabled NMR quantum computers

The spin states of nuclei within molecules were suggested as qubits and probed through nuclear magnetic resonances as early as 1993 (Lloyd, 1993; DiVincenzo, 1995a; DiVincenzo, 1995b).

Manipulation of nuclear spins as qubits using liquid state NMR was introduced independently circa 1996–1997 by Cory, Fahmy and Havel (Cory et al., 1996; Cory et al., 1997) and Gershenfeld and Chuang (1997; 1998).

Initial NMR approaches employed spins of a collective of atoms or molecules in the liquid state known as liquid state NMR or LSNMR. Menicucci and Caves (2002) proffer that all

experiments to date involving LSNMR ensemble quantum computing have not demonstrated quantum entanglement, a requirement for quantum computation. Research has since evolved towards solid state NMR (SSNMR) as a more viable method for quantum computation. SSNMR allows the precise localization and measurement of qubits thus alleviating the requirement of measuring an ensemble. IBM researchers reported in 2001 the first implementation of Shor's algorithm in a 7-qubit NMR quantum computer (Vandersypen, 2001).

## 8.4.2 Nitrogen-vacancy (NV) centers

Single defects in diamond, especially negatively charged NV centers, have shown unusual potential as qubit systems. It has been shown that their coherence properties are strongly improved by growing ultrapure diamond with low concentrations of parasitic spins. Wood et al. demonstrated quantum control of a single NV center within diamond at 200,000 rpm, a rotational period comparable to NV spin coherence times of  $T_2^{HFE} = 177 \pm 24 \mu\text{s}$ , ( $T_2^{XY8-1} = 323 \pm 21 \mu\text{s}$ , and  $T_2^{XY8-4} = 462 \pm 130 \mu\text{s}$  for the Hahn echo, XY8-1, and XY8-4 pulse sequences, respectively) (Wood et al., 2022). Stroboscopic imaging of individual NV centers shows rapid circular motion in addition to rotation with demonstrated control and readout of qubit quantum states under microwave excitation. Using spin-echo interferometry of such qubits, these authors were able to detect modulation of the NV Zeeman shift arising from the rotating NV axis under DC magnetic fields. These authors and others established single NV qubits in the physically rotating frame as a path forward for Jakobi et al. to demonstrate single-qubit diamond-based rotational sensors (Jakobi et al., 2016).

Coherently coupled pairs of NV defect electron spins in diamond promise further advances. Scalable registers of spin qubits are essential to advancing quantum interactive polynomials (QIPs). Ion implantation is a plausible technique to produce defect pairs in close enough proximity to allow spin coupling via dipolar interaction. Residual radiation-induced defects, resulting in degraded qubit performance, is a principal hindrance.

Alternatively, Dréau et al. used the electronic spin of a single NV defect in diamond to observe the real-time evolution of neighboring single nuclear spins under ambient conditions (Dréau et al., 2013). Using a diamond sample with a natural abundance of C, these authors demonstrated high-fidelity initialization and single-shot readout of an individual C nuclear spin (Hennighausen and Kar, 2021). By including the intrinsic N nuclear spin of the NV defect in the quantum register (Schaibley et al., 2016), they reported the simultaneous observation of quantum jumps linked to both nuclear-spin species, providing an efficient initialization of two qubits. These results provide a viable path forward for diamond-based quantum information processing that includes active feedback in quantum error correction and tests of quantum correlations with solid-state single spins at room temperature.

Jahnke et al. reported a high-quality  $^{12}\text{C}$ -enriched polycrystalline chemical vapor-deposited diamond with properties comparable to single crystals. Single NVs in the grains of this material show extremely long electron spin coherence times of greater than 2 ms (Jahnke et al., 2012).

Coherent manipulation of an individual electron spin and nearby individual nuclear spins create a controllable quantum register. Using optical and microwave excitations to control electron

spin associated with NV color centers in diamond, Dutt et al. demonstrated robust initialization of electron and nuclear-spin qubits and transfer of arbitrary quantum states between them at room temperature. Nuclear-spin qubits were isolated from the electron spin even during optical polarization and measurement of their electronic state (Dutt et al., 2007).

## 8.5 Topological qubits

### 8.5.1 Non-Abelian anyons

A topological quantum computer (TQC) was proposed by Kitaev in 1997 that employs anyons<sup>27</sup> as qubits (Kitaev, 1997), which are quasiparticles in two-dimensional systems whose world lines wrap around one another to form braids in three-dimensional spacetime (i.e., one temporal plus two spatial dimensions). Figures 17A–C depict topological qubits (i.e., anyons) and their functions, including braiding (i.e., computation) and fusion (i.e., measurement). Braids form logic gates that are largely impervious to small perturbations that normally would compromise coherence in other qubit modalities, leading to computational errors (Pachos, 2012; Topological Quantum Computer, 2023). Anyons appear as quasiparticles in fractional quantum Hall states and as excitations in some frustrated quantum magnetic systems (Wilczek, 2006).

The exchange statistics of quantum Hall states are typically Abelian. However, Moore et al. proposed that anyons can be realized in fractional quantum Hall states (Moore and Read, 1991; Wen and Xiao-Gang, 1991) that are described by non-Abelian statistics<sup>28</sup>; these are Ising anyons<sup>29</sup> and Fibonacci anyons<sup>30</sup>.

27 An anyon is a type of quasiparticle that occurs in two-dimensional systems that are classified as Abelian or non-Abelian. Abelian anyons play a major role in explaining the fractional quantum Hall effect.

28 Non-Abelian anyonic statistics are higher-dimensional representations of the braid group. Anyonic statistics are not to be confused with parastatistics, which describe the statistics of particles whose wave functions are higher-dimensional representations of the permutation group.

29 The Ising anyon model is a model of non-Abelian anyons that represent a path to experimental verification that arises by Majorana zero modes (MZM) and consists of three types of particles including vacuum ( $1$ ), anyon and ( $\sigma$ ), and fermion ( $\psi$ ), that obey the fusion rules:  $\sigma \times \sigma = 1 + \psi$ ;  $\sigma \times \psi = \sigma$  and  $\psi \times \psi = 1$ , respectively.

30 The Fibonacci model for topological quantum computing is based on the fusion rules for a Majorana fermion as described above. The particles described as Fibonacci anyons correspond, in theory, to collectivities of electrons, as in the quantum Hall effect. Fusion rules for such quasiparticles were conjectured by Moore and Read [see G. Moore and N. Read, Nucl. Phys. B 360, 362 (1991).] as part of a larger conjecture that links the fractional quantum Hall effect with braiding associated via conformal field theory with Chern–Simons theory. (Note: The Chern–Simons theory is a 3-dimensional topological quantum field theory first proffered by mathematical physicist Albert Schwarz and further developed by Edward Witten. In condensed-matter physics, Chern–Simons theory describes the topological order in fractional quantum Hall effect states).



While early on, non-Abelian anyons were considered a mathematical conception, Alexei Kitaev showed in 2003 that non-Abelian anyons could be used to construct a topological quantum computer (Kitaev, 2003). It was 10 years before Willett et al. presented the first experimental evidence of non-Abelian anyons (Willett et al., 2013).

As a rule, in a system with non-Abelian anyons, there are composite particles whose statistics are not uniquely determined by the statistics of their components but rather as quantum superposition. If the overall statistics of the fusion of several anyons are known, there remains ambiguity in the fusion of the subsets of these anyons, and each possibility is a unique quantum state. These multiple states provide a Hilbert space on which quantum computations can be performed (Nayak et al., 2008; Wikipedia, 2022).

### 8.5.2 Quasiparticle braiding

An example of an anyon derives from the fractional quantum Hall state at  $1/3$  filling. One can envision these quasiparticles as one-third of a composite boson, consisting of an electron with three bound flux quanta. Therefore, they have an effective fractional charge of  $e/3$ , and the phase addition that one expects to result from braiding two of them is  $2\pi/3$  (Arovas et al., 1984). While the  $e/3$  charge has been firmly established for more than 20 years, the experimental detection of anyonic statistics—the fractional phase—has been somewhat elusive.

### 8.5.3 Majorana zero modes

Majorana zero modes are fermionic operators ( $\gamma$ ). It is important that MZMs be spatially localized for Majorana fermions to be interpreted as Ising anyons and acquire particle-like behavior. Such MZMs are decoupled from local fluctuations and are predicted to obey non-Abelian exchange statistics. Therefore, qubits encoded by such MZMs would not only have decoherence that is exponentially suppressed by the physical separation between MZMs but would also allow topologically protected gate operations through braiding. The built-in topological qubit protection is unique; however, clear experimental evidence for the existence of non-Abelian low-energy modes in solid-state devices has proven elusive (Microsoft, 2022; Wikipedia, 2022).

## 8.6 Vibrational qubits

In an ideal three-dimensional crystal, phonons play a role analogous to photons but propagate at much lower velocities. In fact, the phonon-photon analogy is also supported in semiconductor crystal systems where conduction and valence bands play a role, like the *quantum electrodynamic* (QED) vacuum, where quasi-free electrons and holes propagate according to quadratic dispersion, scattering off acoustic phonons that possess linear dispersion. Thus, the behavior of QED repeats itself in the behavior of electronic and hole quasiparticles in solid and phonon vibrations within crystals (Ruskov and Tahan, 2012).

Mortezapour et al. investigated the dynamics of coherence and entanglement of vibrating qubits of a single trapped-ion qubit inside

a perfect cavity and used it to construct bipartite systems made of two such subsystems, taken as identical and noninteracting (Mortezapour et al., 2018). These authors found that qubit phonons led to the prolonging of initial coherence in both single-qubit and two-qubit systems. They showed how photon–phonon correlations between cavity and vibrational modes stored in single-qubit systems are strongly affected by the initial state of the qubit. Such results provide insights into how phonon qubit systems maintain quantum information compared to systems of stationary qubits.

Specifically, the evolution of two-qubit coherence for various intensities of the cavity and vibrational modes for stationary qubits (column I) and vibrating qubits (column II) are shown to evolve in time in Figure 18. As can be seen in column I, an increase in the intensity of the cavity mode suppresses the decay of coherence during time evolution. Alternatively, column II displays the vibration of qubits inducing rapid oscillations and prolonging coherence compared to stationary qubits. The more intense the qubit vibrational mode, the slower the decay of two-qubit coherence, a behavior resembling that of single-qubit coherence. These results provide evidence that coherence and entanglement are, in general, quantum effects of a different nature when seen within the same composite system (Hanson et al., 2007).

Theoretical predictions support the need for quantum gate fidelities of 99.99% in order for error-correction codes to be effective. In 2012, Berrios et al. tested fidelities for a CNOT gate executed by ultrafast laser pulses interacting with vibrational modes of  $\text{SCCl}_2$  (i.e., the molecule  $\text{SCCl}_2$ : thiophosgene thiocarbonyl chloride) to be effective. These authors included all vibrational states, even those that did not encode desired qubits but were close enough in energy to interfere with a population transferred by laser pulses. They pursued two approaches: (1) optimal control theory that determined the *best possible* pulse and (2) a constrained physical model that calculated the *most likely pulse*. Optimal control theory found pulses with fidelities  $>99.99\%$ , more than the quantum error-correction threshold for  $8 \times 10^4$  iterations, and 99.92% after the  $8 \times 10^4$  iterations for most likely pulses. Both calculations converged as an inverse power law toward a fidelity of 100%. The principal finding was that fidelities necessary for quantum error correction are certainly *attainable with qubit-encoded molecular vibrations* (Berrios et al., 2012).

Ruskov and Tahan explored the possibility of strongly coupling semiconductor qubit states to *Si-etched nanomechanical resonators*. These systems are relevant to qubit transduction, as an auxiliary technology for quantum information processing, for qubit characterization, and for quantum-enabled devices. Specifically, these authors considered systems where cavity phonons interacted with qubit states over a frequency band of 1–10 GHz (Ruskov and Tahan, 2012).

Gollub et al. analyzed the effects of molecular properties on the structure of quantum gates and the complexity of the resulting mechanisms with the goal of rating a molecule's suitability for molecular quantum computing (Gollub et al., 2006).



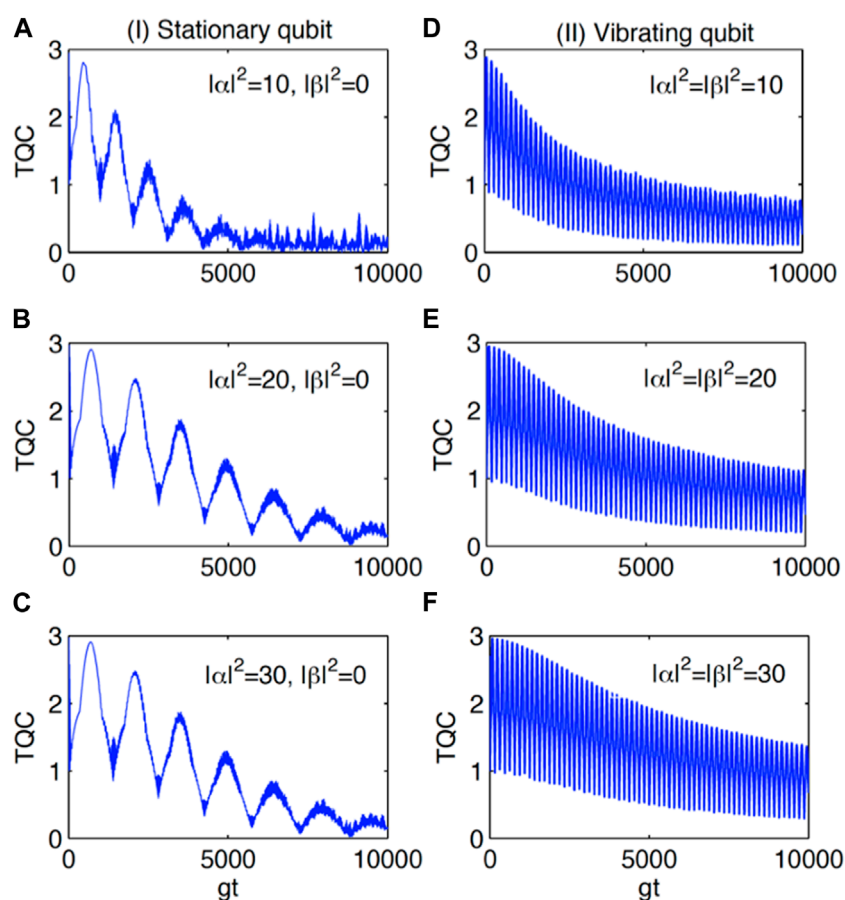


FIGURE 18

The dynamic behavior of two-qubit coherence (TQC) for different intensities of cavity and vibrational modes. Column (I) for stationary qubits and column (II) for vibrating qubits. Symbols depicted within each panel are defined and discussed in Mortezaipour et al. (2018).

A primary property of molecular vibration is its anharmonicity<sup>31</sup> and its extension to multimode systems, whereupon the mode coupling must also be accounted for. Characteristic properties are tuned in a parametrized two-dimensional model system, and their effects upon quantum gates are explored. These authors found that the interplay of anharmonicity

and coupling is of prime importance to basic control of all systems.

Key findings included the complexity of the optimized quantum gate laser fields that depended on gate length, among other parameters. For converged runs with equal gate lengths, very similar or even identical laser fields are found suitable. Calculations demonstrated that it was possible to implement highly efficient elementary global quantum gates, that is, CNOT, NOT, and Hadamard gates, for all symmetric, asymmetric, anharmonic, and coupled 2D systems (Gollub et al., 2006).

Recently, Troppmann et al. explored the possibility of quantum computing with molecular vibrations in a 2D model of acetylene, finding that specifically shaped femtosecond-laser pulses in the IR represented global quantum gates and could be acquired by optimal control theory. Leakage from the qubit basis used for quantum computation and the influence of dark, non-IR-active modes coupled via anharmonic resonances was proven to be an essential variable. In a 3D-model, it was further demonstrated that selective preparation of a vibrational eigenstate in near anharmonic resonance was essential. A Hadamard gate was realized

<sup>31</sup> Anharmonicity derives from atoms in molecules that vibrate about their equilibrium positions and plays a role in lattice and molecular vibrations in quantum oscillations, as in quantum computers. When these vibrations have small amplitudes, they can accurately be described as harmonic oscillators. However, when vibrational amplitudes become large, for example, at high temperatures, anharmonicity becomes nonnegligible. Under such circumstances, anharmonicity not only makes the potential experienced by each oscillator more complex but also introduces meaningful coupling between oscillators. Accurate anharmonic vibrational energies can then be obtained by solving anharmonic vibrational equations for atoms within mean-field theory, possibly using Møller–Plesset perturbation theory.

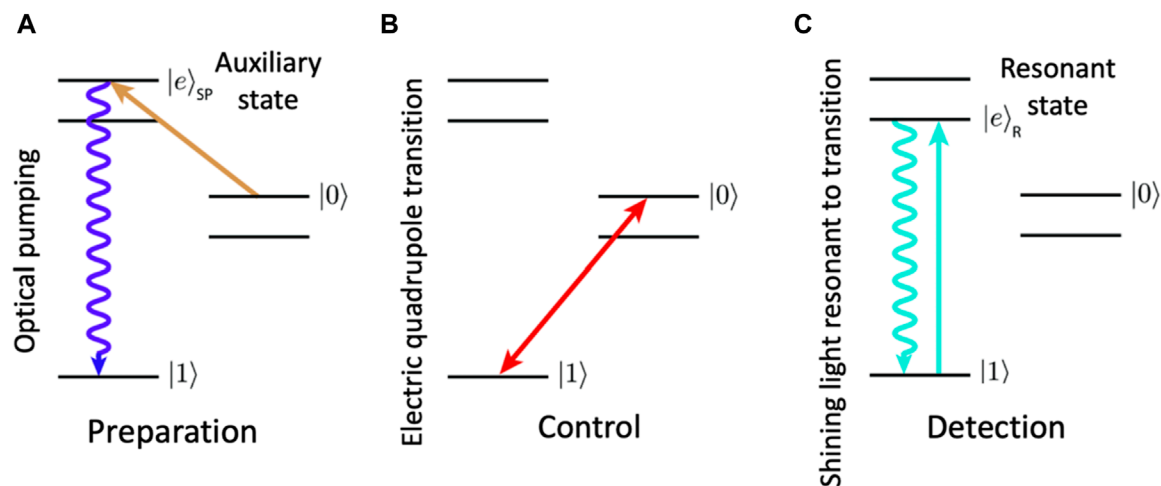


FIGURE 19

Depiction of state preparation, control, and detection in trapped-ion optical qubits as discussed by Bruzewicz et al. (2019). (A) The ion is initially pumped to the  $|1\rangle$  state by coupling the long-lived  $|0\rangle$  state to an auxiliary state  $|e\rangle_{SP}$  that rapidly decays. (B) Qubit control is achieved by directly coupling the  $|0\rangle$  and  $|1\rangle$  states using a narrow electric quadrupole transition. (C) Detection is achieved by shining light resonant on the broad transition  $|1\rangle \rightarrow |e\rangle_R$  and collecting the resulting scattered fluorescence photons. There is no similar transition  $|0\rangle \rightarrow |e\rangle_R$ , so the  $|0\rangle$  state appears dark in contrast. Rights to reproduce strictly adhere to those granted by arXiv.org as agreed upon by the original authors. Simplified depiction of state preparation, control, and detection in trapped-ion optical qubits. (A) (Initiation) The ion can be quickly optically pumped to the  $|1\rangle$  state by coupling the long-lived  $|0\rangle$  state to an auxiliary state  $|e\rangle_{SP}$  that rapidly decays. (B) Qubit control is achieved by directly coupling the  $|0\rangle$  and  $|1\rangle$  states using a narrow electric quadrupole transition. (C) Detection is achieved by shining light resonant on the broad transition  $|1\rangle \rightarrow |e\rangle_R$  and collecting the resulting scattered fluorescence photons. There is no similar transition  $|0\rangle \rightarrow |e\rangle_R$ , so the  $|0\rangle$  state appears dark.

in that work; this is the first step in the preparation of a Bell state<sup>32</sup>.

## 8.7 Trapped-ion qubits

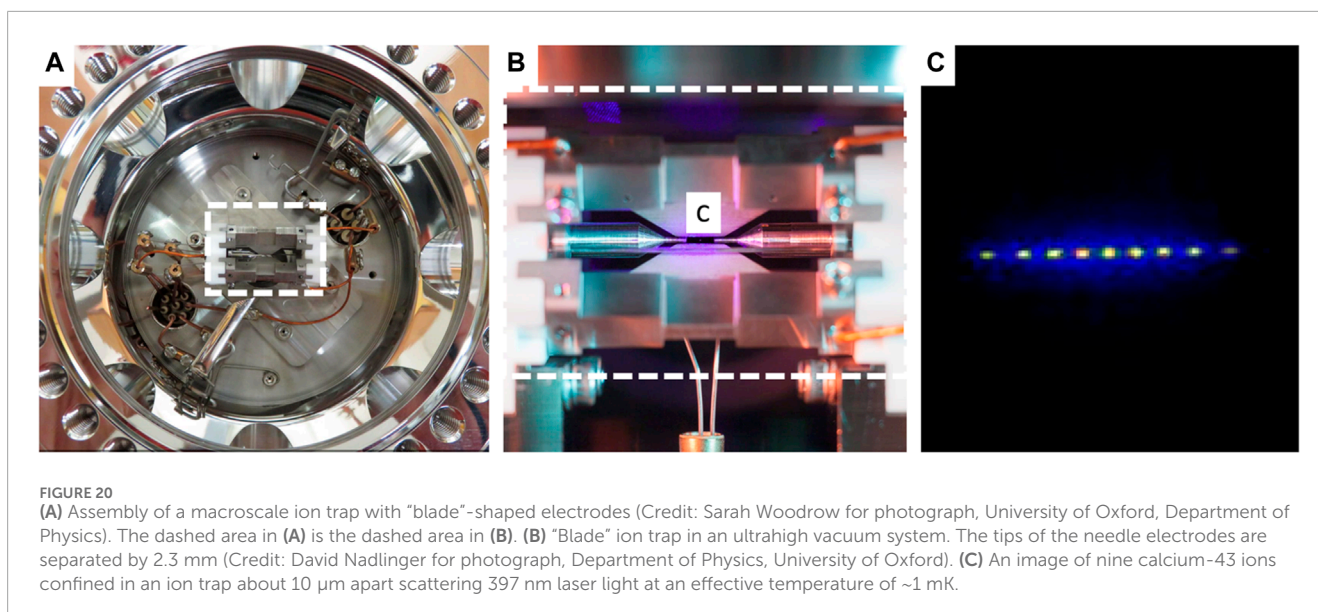
Ions can be confined and suspended in a vacuum using electromagnetic fields. Under such circumstances, qubits are stored as stable electronic states, and quantum information is transferred through a collective of quantized motion of ions in a trap interacting via Coulombic forces. Lasers are useful in inducing coupling between such qubits for single-qubit systems or coupling between internal qubits and external motional states for entangled qubits (Nielsen and Chuang, 2000).

<sup>32</sup> A Bell state is an entangled and normalized basis vector of two qubits. Their normalization implies that the overall probability is in one of the mentioned states is:  $\langle\Phi|\Phi\rangle=1$ . Because of entanglement, the measurement of one qubit will “collapse” the other qubit to a state whose measurement will yield one of two possible values, where the value depends on which Bell states the two qubits were in initially. Bell states can be generalized to certain quantum states of multi-qubit systems, such as the GHZ state for three or more subsystems. Understanding Bell states is useful in the analysis of quantum communication, among other quantum technologies, such as superdense coding and quantum teleportation.

Trapped ions are one of the most promising qubit modalities for realizing useful quantum computers. They exhibit properties necessary for building such systems that have very few fundamental limitations to achieve sufficiently high gate fidelities. The single- and two-qubit gate fidelities demonstrated in small-scale systems, combined with the ion’s long coherence times, exceed the capabilities of many other proposed modalities. However, to build a useful quantum simulator that outperforms current classical machines and therefore achieves “quantum advantage,” the system size must be scaled to at least a few tens of qubits without compromising the precision of operation (Bruzewicz et al., 2019a).

The fundamental operations in quantum computing have been demonstrated with very high accuracy in trapped-ion systems. Promising schemes to scale the system to necessarily larger numbers of qubits include transporting ions to spatially distinct locations in an array of ion traps and building larger, entangled states via photonically connected networks of remotely entangled ion chains. This makes the trapped-ion quantum computer modality one of the most promising for a scalable universal quantum computer (Friis et al., 2018-04; Monz et al., 2011; Paul, 1990).

Ionic qubit states can be prepared using a process called optical pumping. In such a process, a laser couples the ion to excited states that eventually decay to one state that is not coupled to the laser. Once the ion reaches that state, it has no excited levels to couple in the presence of the laser and, therefore, remains in that particular state. If the ion decays



to one of the other states, the laser will continue to excite the ion until it decays to a state that does not interact with the laser. This initialization process is standard in many experiments and can be performed with exceptionally high fidelity (>99.9%) (Schindler et al., 2013).

Figures 19A–C depict states of preparation, control, and detection of trapped-ion optical qubits. Here, the ion is seen to be quickly optically pumped to the  $|1\rangle$  state by coupling the long-lived  $|0\rangle$  state to an auxiliary state  $|e\rangle_{SP}$  that rapidly decays. The qubit is further controlled by directly coupling the  $|0\rangle$  and  $|1\rangle$  states using a narrow electric quadrupole transition, while readout is achieved by photo-transitioning  $|1\rangle \rightarrow |e\rangle_R$  and collecting scattered fluorescence (Bruzewicz et al., 2019).

Figures 20A–C depict an assembly of a macroscale ion trap with “blade”-shaped electrodes wherein the dashed area in (a) translates to the dashed area in (b). The blade ion trap in the ultrahigh vacuum reveals needle-type electrodes separated by mere millimeters. Finally, nine calcium-43 ions confined in an ion trap appear to be approximately 10 μm apart, scattering 397 nm laser light at an effective temperature of ~1 mK (Ion Trap Quantum Computing, 2023).

## 9 Qubit and gate coherence and fidelity

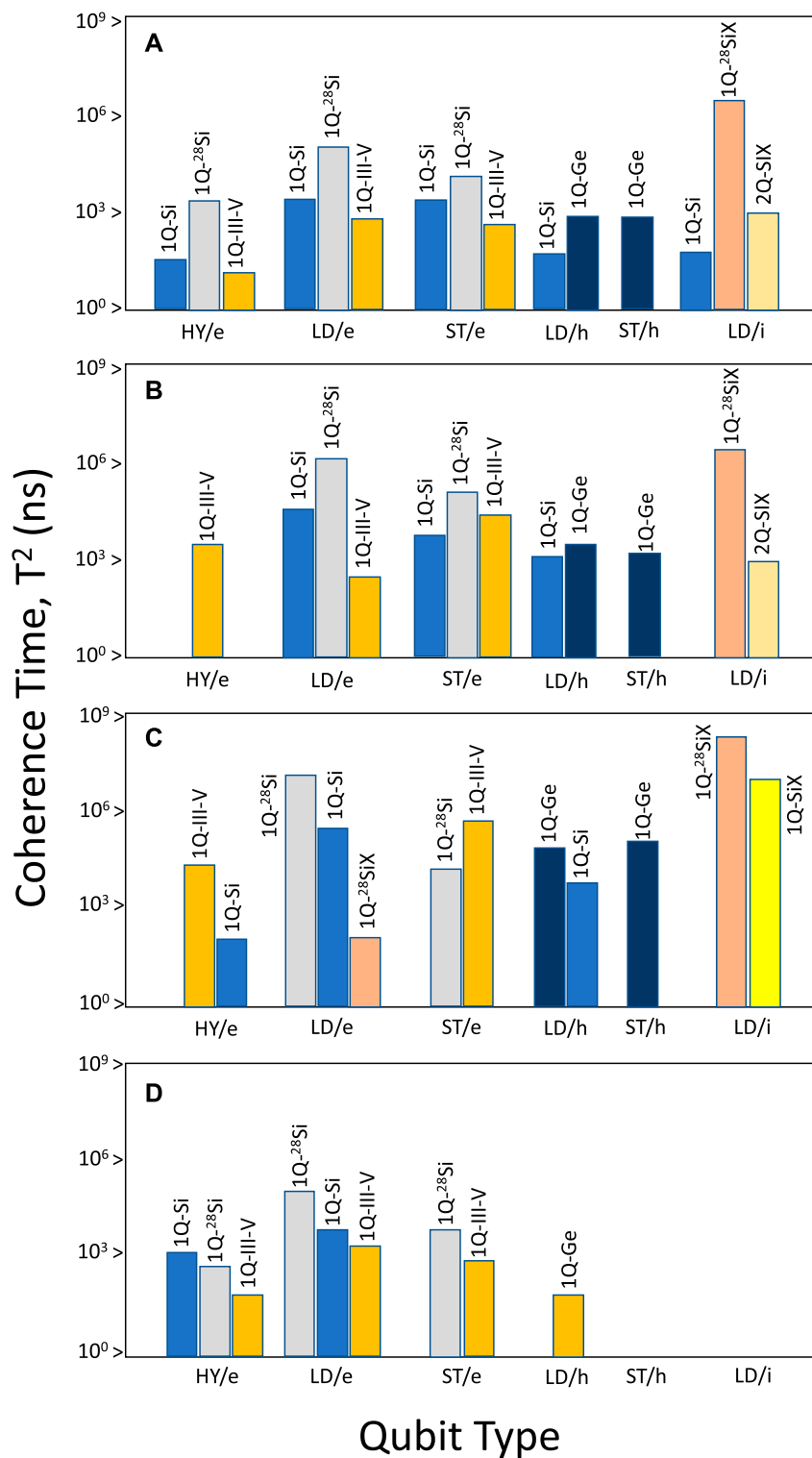
An expansive and informative review of superconducting qubits and their properties has been published by Siddiqi (2021); from this, we learn much.

Contemporary superconducting qubits combine one or a few Al/AlO<sub>x</sub>/Al Josephson junctions (JJs), which function as a nonlinear inductance (Tinkham, 2004), with other reactive elements—comprising thin-film Al, Nb, NbN, NbTiN, Ta, or TiN, for example—to form a circuit where the potential energy surface has at least two bound states. The minimalist realization of such

an anharmonic oscillator is a single Josephson tunnel junction formed by two planar superconducting electrodes separated by an insulating layer.

The geometric self-capacitance shunts the kinetic inductance associated with Cooper pairs tunneling across the barrier to yield a resonance frequency typically in the microwave frequency range, and individual quantum levels can be readily detected using microwave spectroscopy (Martinis et al., 1985; Martinis et al., 2020). Coupling the JJ circuit to a microwave resonator for control and readout robustly yields long-lived charge-based and flux-based qubits in which the lowest two energy levels form the “0” and “1” states of a physical qubit (Koch et al., 2007–10; You et al., 2007). In these circuits, the junction provides the anharmonicity needed to selectively address the 0–1 transition. JJs can be constructed by sandwiching two superconducting reservoirs around any structure that allows the condensate wavefunction to deviate from its surrounding bulk value, but the tunnel-junction geometry with an insulating barrier has thus far been the most widely used (Van Duzer and Turner, 1998) in electronic circuits, given the attractive features of a robust sinusoidal dependence of the supercurrent on the junction phase difference (Golubov et al., 2004) and the absence of electronic states below the superconducting energy gap. To tune the qubit parameters and drive quantum-state transitions, JJs can be readily integrated into superconducting loops or can be contacted with isolated submicron superconducting islands, enabling control via an external magnetic or electric field, respectively (Makhlin et al., 2001; Wendin and Shumeiko, 2007; Krantz et al., 2019; Kjaergaard et al., 2020). The values begin around 10 ns of inhomogeneous dephasing time in early experiments with qubits in GaAs. Echo techniques extend the coherence by orders of magnitude, as can different material choices. The coherence times published during 2021 span six orders of magnitude, depending on the qubit type, material, and protection measures.

The relaxation times are often comparable to coherence times, unlike spin qubits, where they can be advanced to far longer






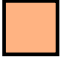
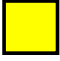




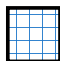


**FIGURE 21** (A)  $T_2^*$ , inhomogeneous dephasing time, also called free induction decay (FID) time. (B)  $T_2^{Echo}$ , coherence time measured under a Hahn echo. (C)  $T_2^{DyD}$ , coherence time measured under dynamical decoupling. (D)  $T_2^{Rabi}$ , decay of coherent Rabi oscillations. In each panel, the horizontal axis uses the qubit type as a discrete category. All data colors reflect the qubit material and are defined in Table 10.

amplitudes. Therefore, relaxation is a bigger issue for charge qubits, even in single-qubit experiments. Second, unlike spin qubits, the echo techniques do not prolong coherence. Third, there is much

less variation among the published data despite an upward trend in  $T_2^*$ . As the charge-qubit dephasing time,  $T_2^*$ , is related to charge noise, a clear trend would indicate an improvement

TABLE 10 Identifiers and descriptions employed in Figure 21 and Figure 24.

Symbol	Identifier	Description
	1Q-Si	1 qubit gate in silicon systems
	1Q-III-V	1 qubit gate in III-V semiconductor systems
	1Q- <sup>28</sup> Si	1 qubit gate in the isotope silicon-28, which makes up 92.21 percent of the element in nature
	1Q-Ge	1 qubit gate in germanium systems
	2Q-SiX	2 qubit gate in silicon systems where X signals impurity atom
	1Q- <sup>28</sup> SiX	1 qubit gate in the isotope silicon-28 where X signals impurity atom
	1Q-SiX	1 qubit gate in silicon systems where X signals impurity atom
	2Q- <sup>28</sup> Si	2 qubit gate in the isotope silicon-28
	2Q-III-V	2 qubit gate in III-V semiconductor systems
	3Q-Si	3 qubit gate in silicon systems
	2Q-Si	2 qubit gate in silicon systems
	1Q-C	1 qubit gate in carbon systems

in the available samples and devices concerning charge noise. Finally, one would expect no apparent difference between devices made in Si and III-V materials concerning charge-qubit coherence.

In Figure 21A–D, different coherence times,  $T_2$ , measured using different measurement techniques, are presented for various qubit systems being of discrete category on the horizontal axis. These figures depict data extracted from Stano and Loss (2022) and presented in a different format for ease of identifying trends in the format of this review. The keys that define these data are presented in Tables 10, 11. Table 12 presents a

summary of key decoherence mechanisms, their origins, and viable mitigation strategies summarized from the work of Siddiqi (2021) including: two-level system defects, quasiparticles and phonons, and  $1/f$  magnetic flux noise. The next several sections present discussion of coherence mechanisms of different qubit modalities.

## 9.1 Coherence of charge qubits

We end the overview of coherence times by examining charge qubits. As already mentioned, we include them even though they



TABLE 11 Symbol key to Figure 21 and Figure 24.

Symbol	Definition	
Charge	The qubit basis is represented by two different orbitals of a confined particle. The orbitals differ in their positions; for example, a pair of states localized each in one minimum of a double-well potential of a double dot. Unlike for spin-related qubits, we do not discriminate the carrier, be it electron, hole, or im-purity. However, most charge-qubit experiments use electrons.	Agarwal et al. (2013), Nigg et al. (2014)
HY/e	The qubit basis is represented by electron states having a hybrid character, most often differing in both the spin and charge degrees of freedom.	Agarwal et al. (2013), Nigg et al. (2014)
ST/e	The qubit basis is represented by the spin-singlet and spin-triplet states of a confined conduction-band electron pair.	Levy (2002)
ST/h	The same as “ST/e” but using valence-band holes instead of conduction-band electrons.	Campagne-Ibarcq et al. (2020)
LD/e	The qubit basis is represented by the spin-up and spin-down state of a confined conduction-band electron (or many-electron) state. The acronym stands for the names of Daniel Loss and David DiVincenzo, who established the field of spin qubits.	Loss and DiVincenzo (1998)
LD/h	The same as “LD/e” but using valence-band holes instead of conduction-band electrons.	Bell et al. (2014b)
LD/i	The same as “LD/e” but using impurity-bound electrons instead of conduction-band electrons confined by gates.	Kane (1998)
$T_{\text{Echo}}$	Dephasing under a Hahn echo reveals in measured data the decay of the qubit phase.	Agarwal et al. (2013), Nigg et al. (2014)
$T_{\text{DynD}}$	Dephasing under a dynamical decoupling protocol. The experiment measured the decay of the phase of a qubit by applying more than one echo pulse. While there are several families of pulse sequences, we do not discriminate among them.	Agarwal et al. (2013), Nigg et al. (2014)
$T_{\text{Rabi}}$	Dephasing of a driven qubit. Strictly speaking, this time should describe the decay of the relative phase of the two quasi-energy states in the rotating frame of reference. Usually, it is extracted as the observed decay time of Rabi oscillations.	Agarwal et al. (2013), Nigg et al. (2014)

implement qubits that do not rely on spin. The reason is a close relationship between the devices in which the two types of experiment are typically done and the techniques used: for example, the measurement of spin is done indirectly, converting different spin states to different charge states, which are then detected.

All types of coherence times of charge qubits, including the relaxation time, are gathered in Figure 21. In the three panels of the figure, the same data are shown according to the publication date, the device material, and the coherence type. One can see several differences compared with spin qubits. First, the relaxation times are often comparable to coherence times, unlike for most spin qubits, where they can be pushed to the longest scale by far. Therefore, relaxation is a bigger issue for charge qubits, even in single-qubit experiments. Second, unlike for spin qubits, the echo techniques do not prolong coherence substantially. Third, there is much less variation among the data: despite an upward trend in  $T_2^*$  over time, the increase is not marked. As the charge-qubit dephasing time  $T_2^*$  is directly related to charge noise, a clear trend would indicate an overall improvement of the available samples and devices concerning the level of charge noise. Finally, as one would expect based on the nuclear-spin noise being irrelevant for charge qubits, there is no apparent difference between devices made in Si and III-V materials concerning charge-qubit coherence.

The increased capacitance influences the anharmonicity and the difference in energy between successive excitations

and charge dispersion. The advantage of transmons derives from predicting that as  $E_J/E_C$  increases, the charge dispersion decreases exponentially, while anharmonicity decreases as a power law.

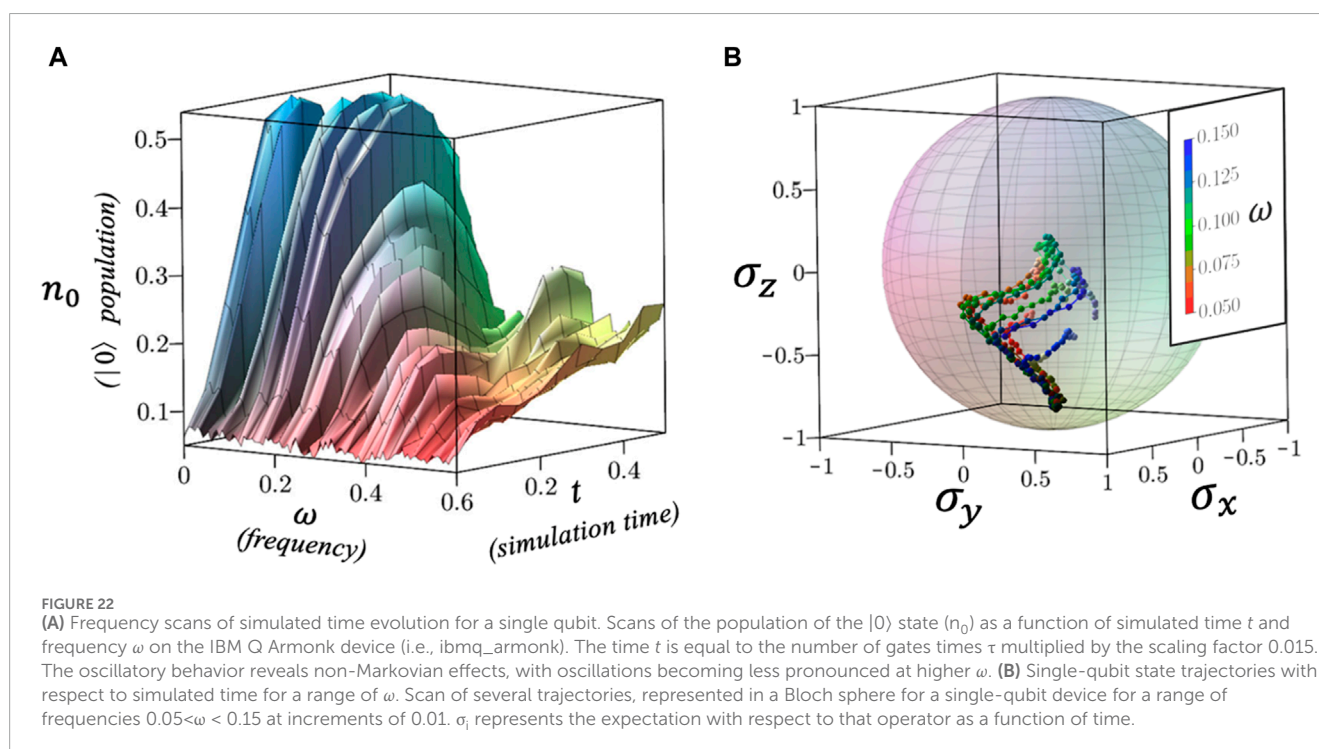
## 9.2 Coherence of semiconducting qubits

Gate-controlled semiconductor spin qubits are considered an attractive platform for massively-scalable quantum information systems due to their relatively small form factor and fast processing times (Chatterjee et al., 2021). A primary source of decoherence for spin qubits is the hyperfine interaction between electron spins and randomly fluctuating nuclear spins of their semiconductor lattice, leading to magnetic noise that causes unwanted qubit rotation (Hanson et al., 2007). A proven effective mitigation strategy for this noise source has been the use of group-IV semiconductors as opposed to group III-V semiconductor compounds. This allows for the development of nuclear-spin-free hosts that have been shown to extend coherence times by more than four orders of magnitude (Stano and Loss, 2022).

Reaching two-qubit gate fidelities greater than 99% has been a long-standing goal for semiconductors and other *spin-qubit modalities*. Such qubits are promising for scaling as they leverage mature semiconductor processing technologies (Zwerver et al., 2022). A spin-based quantum processor in silicon with single-qubit

TABLE 12 Summary of key decoherence mechanisms, their origins, and viable mitigation strategies (Siddiqi, 2021).

Decoherence description	Origin	Decoherence channel	Mitigation strategy
Two-level system (TLS) defects	Lack of crystalline order in amorphous films that creates a glass-like system characterized by quantum tunneling between two energy minima, possibly representing similar configurations of individual atoms, atomic clusters, and electronic states.	Individual TLS defects with long-lived coherence and resonant with a qubit cause energy relaxation. Ensembles of fluctuating TLS defects contribute to dephasing, and TLS–TLS interactions can result in slow drifts of qubit coherence times.	Etching and passivation to remove amorphous layers; use of crystalline dielectrics and ordered Josephson-junction barriers.
Quasiparticles and phonons	Incident ionizing radiation that breaks Cooper pairs, generating highly excited quasiparticles and phonons that scatter away energy in a multistep cascade with a complex noise spectrum.	Dissipation at microwave frequencies and dispersive shifts and/or fluctuations of the qubit frequency, which result in dephasing.	Normal metal/low-gap superconducting traps to remove quasiparticles from the qubit area; acoustic absorbers and frequency-tailored structures to suppress phonon propagation and secondary pair breaking.
$1/f$ magnetic flux noise	Spins or clusters of spins on metallic surfaces, potentially resulting from magnetic defects, electrons trapped in disorder potentials, or paramagnetic films that condense at low temperatures.	A broad $1/f$ -type noise spectrum contributes to dephasing in circuits with a superconducting loop and operates away from flux degeneracy.	Initial work indicates noise reduction with capping layers. Need to precisely identify the microscopic origin to develop robust, tailored elimination strategies.



and two-qubit gate fidelities, all of which are  $>99.5\%$  extracted from gate-set tomography, is an important step in the evolution of this technology (McArdle et al., 2020).

Electron spin qubits in silicon (Veldhorst et al., 2014; Veldhorst et al., 2015; Zajac et al., 2016; Vandersypen et al., 2017; Yoneda et al., 2018; Jones et al., 2018; Li et al., 2018; Petit et al., 2020; Yang et al., 2020) are particularly promising for a large-scale

quantum computer owing to their nanofabrication capability, but the two-qubit gate fidelity has been limited to 98% owing to the slow operation (Huang et al., 2019).

Noiri et al. employed a micromagnet-induced gradient field applied to silicon spin qubits creating fast electrical control of tuning two-qubit coupling. This allowed a demonstration of a two-qubit gate fidelity of 99.5% with single-qubit gate fidelities of 99.8%.

These authors realized Deutsch–Jozsa and Grover search algorithms with high success rates using a universal gate set. These results demonstrated universal gate fidelity beyond the fault-tolerance threshold and may enable scalable silicon quantum computers (Noiri et al., 2022).

Universal quantum logic operations were demonstrated using a pair of ion-implanted  $^{31}\text{P}$  donor nuclei in a silicon nanoelectronic device. A nuclear two-qubit controlled-Z gate was obtained by imparting a geometric phase to a shared electron spin and used to prepare entangled Bell states with fidelities up to  $94.2 \pm 2.7\%$ . The quantum operations were precisely characterized using gate-set tomography (GST) (Nielsen et al., 2021), yielding one-qubit average gate fidelities up to  $99.95 \pm 2.0\%$ , two-qubit average gate fidelity of  $99.37 \pm 11.0\%$  and two-qubit preparation/measurement fidelities of  $98.95 \pm 4.0\%$ . These three metrics indicated that nuclear spins in silicon are approaching the performance demanded in fault-tolerant quantum processors (Fowler A. G. et al., 2012). Entanglement between the two nuclei and the shared electron was demonstrated by producing a Greenberger–Horne–Zeilinger three-qubit state with  $92.5 \pm 1.0\%$  fidelity.

Because electron spin qubits in semiconductors can be further coupled to other electrons (Harvey-Collard et al., 2017; He et al., 2019; Madzik et al., 2021) or physically shuttled across different locations (Hensen et al., 2020; Yoneda et al., 2021), these results establish a viable route for scalable quantum information processing using donor nuclear and electron spins (Mądzik et al., 2022).

The use of *couplers* to control two-qubit interactions has also improved operational fidelity in many-qubit systems by reducing parasitic overcrowding (Yan et al., 2018). Nonetheless, two-qubit gate errors continue to limit the capability of near-term quantum applications. This limitation derives from dispersive approximations that do not fully incorporate three-body dynamics. Using an approach that systematically extends dispersive approximations to exploit couplers was recently employed by Sung et al. and demonstrated CZ and ZZ-free iSWAP gates with two-qubit fidelities of  $99.76 \pm 0.07\%$  and  $99.87 \pm 0.23\%$ , respectively (Sung et al., 2021).

One attractive feature of spin qubits is their compact size. Protection schemes based on local encodings in decoherence-free subspaces are particularly interesting because such encodings do not require a qualitative scale-up in qubit size, as opposed to global, for example, topological, encodings.

### 9.3 Coherence of topological qubits

Hybrid semiconductor–superconductor devices, based on novel materials (and/or processing technologies), can be engineered into topological phases that, in turn, can be used as protected qubit encodings (Sato et al., 2009; Alicea, 2010; Sau et al., 2010). For example, a quasi-one-dimensional semiconductor with strong spin–orbit coupling and large Lande  $g$ -factor can, when in proximity to an S-wave superconductor, become a topological superconductor

with localized Majorana zero modes (MZMs)<sup>33</sup> at its terminations (Lutchyn et al., 2010; Oreg et al., 2010; Hell et al., 2017). MZMs are decoupled from local fluctuations and obey non-Abelian anyonic exchange statistics. Hence, qubits encoded as MZMs experience exponentially reduced decoherence in the physical space between MZMs but would allow topologically protected gate operations through braiding (Stanescu, 2016).

Recent experiments have focused on 1D-systems (e.g., nanowires) with strong spin–orbit interaction, proximity-coupled to an S-wave superconductor, taking the form of heavy-element semiconductors such as InAs and InSb, coupled to Al and NbTiN as superconductors. However, disorder at the semiconductor–superconductor interface remains a source of subgap states that yield subgap conductance and degrade the hard superconducting gap that serves to protect against thermal quasiparticle excitation (Takei et al., 2013). Hence, the engineering of interface chemistry and structure remains a principal challenge in eliminating scattering and disorder that leads to topological qubit decoherence and less-than-ideal gate fidelity (Akhmerov et al., 2011; Krogstrup et al., 2015). Figure 22A illustrates frequency scans of simulated time evolution for a single qubit. The figure shows scans of the population of the  $|0\rangle$  state (as  $n_0$ ) as a function of simulated time  $t$  and frequency  $\omega$  on the “ibmq\_armonk device” (Team, 2020; Das et al., 2021). The time  $t$  is equal to the number of gates times  $\tau$  multiplied by the scaling factor 0.015. The oscillatory behavior reveals non-Markovian effects, with the oscillations becoming less pronounced at higher frequencies. We begin with a single-qubit system with the Hamiltonian matrix  $H(\omega) = \omega\sigma_z$ , where we use atomic units with  $\hbar = 1$ , and  $\sigma_z$  is the Pauli-Z matrix. If one allows the system to relax without applying any gates, this becomes a  $T_1$  experiment, measuring the relaxation time for an excited state. However, the noise sources here, represented by the non-vanishing memory kernel, generate non-Markovian behavior.

In Figure 22, the non-Markovian behavior is evident from the oscillations in the population of the ground state, which reveal a memory dependence beyond the pure decay of Markovian dynamics. Furthermore, the oscillations are more pronounced at lower frequencies, indicating a bath with colored noise (Smart et al., 2022). Scans of several trajectories represented in the Bloch sphere for a single-qubit device for a range of frequencies represent the expectation with respect to that operator ( $\sigma_x, \sigma_y, \sigma_z$ ) as a function of time (Figure 22B). Each simulation has an equal number of gate applications and changes only the frequency  $\omega$  in the propagation with time step  $\tau$ . We can also observe how the quantum-state vector moves within the Bloch sphere at different frequencies. A slow precession around the axis corresponding to  $H$  is observed for frequencies in the high region of the spectral density and does not allow for coupling between the bath and the system. However,

<sup>33</sup> Majorana zero modes (MZM) are a mathematical construct that allows electrons to be described as composed of two halves. From a quantum computing perspective, if an electron can be split into two parts, then the information it encodes as a qubit will be protected from local perturbations. Furthermore, MZMs realize a representation of non-Abelian braid groups that enable topological quantum computation, wherein the storage and manipulation of information occur in decoherence-free degrees of freedom.

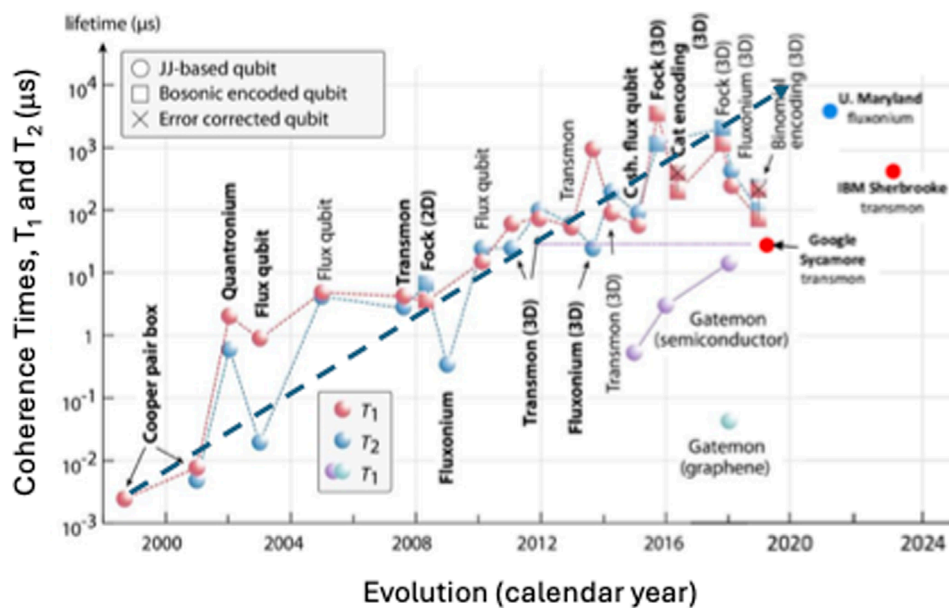


FIGURE 23

Superconducting qubit relaxation and coherence times (bold font indicates first demonstration of modality) are shown to increase logarithmically over time. Improvements are attributed to both innovations in materials science as well as device topologies (Kjaergaard et al., 2020). Reproduced with permission of the Annual Review with proper attribution.

the system can be strongly pulled around the Bloch sphere for frequencies that couple to the bath, resulting in various trajectories through the state space (Scholarpedia, 2022).

Figure 23 depicts advances in qubit coherence times for various qubit modalities from ~2000 to ~2015, including charge (McDermott, 2009; Siddiqi, 2021), quantonium (Metcalf et al., 2007), flux (Yan F. et al., 2016), 2D transmon and fluxonium (Manucharyan et al., 2009), and 3D transmon qubits (Oliver and Welander, 2013). The transmon, developed by Schoelkopf and coworkers, significantly reduced the charge sensitivity of the Cooper-pair box by adding a shunt capacitor that later advanced microsecond times to the cavity-QED architecture (Koch et al., 2007–10; Houck et al., 2008). Bylander et al. increased  $T^2$  above 20  $\mu\text{s}$  with a persistent-current flux qubit in a 2D geometry using dynamical decoupling (Bylander et al., 2011), and a 3D-cavity approach developed by Paik et al. (2011) was employed by Rigetti et al. (2012–09) to further increase  $T^2$  to ~100  $\mu\text{s}$ . A five-orders-of-magnitude increase in coherence time has defined a “Moore’s Law” equivalence for quantum coherence (Steffen, 2011), approaching levels required for a class of fault-tolerant quantum error-correction codes (DiVincenzo, 2009; Fowler et al., 2009; Fowler A. G. et al., 2012).

Fault-tolerant quantum computers that can solve hard problems rely on quantum error correction (Nielsen and Chuang, 2000). One of the most promising error-correction codes is the surface code (Fowler A. G. et al., 2012), which requires universal gate fidelities exceeding an error-correction threshold of 99% (Wang D. S. et al., 2011). Among the many qubit platforms, only superconducting circuits (Barends et al., 2014b), trapped ions (Ballance et al., 2016),

and NV centers in diamond (Rong et al., 2015) have met this high standard at the time of this publication.

## 9.4 The role of SOC in coherence

In spin-orbit qubits, information is stored between orbital and spin degrees of freedom. It is the strength of the coupling between the spin and orbital electronic and magnetic states that keeps the qubit stable and less prone to decoherence brought on by noise. Kobayashi et al. substantially lengthened the length of time that a spin-orbit qubit<sup>34</sup> in silicon can retain quantum information (van Der Heijden et al., 2018; Kobayashi et al., 2021; Scitechdaily, 2022). Although spin-orbit qubits have been investigated for over a decade, recent studies have demonstrated coherence times 10,000 times longer than previously recorded, making them an ideal candidate for scaling up silicon quantum computers. Van der Heijden et al. investigated the spin-orbit coupling of a boron atom in silicon focused on applying fast readout of the spin state of two boron atoms in a compact circuit hosted in a transistor, enabling rapid qubit manipulation

<sup>34</sup> Spin-orbit qubits are a class of spin qubits characterized by strong large spin-orbit coupling. In spin-orbit qubits, information is stored on both the spin of the electron as well as its orbit. The strength of the coupling between spin and orbital moments maintains the qubit stability and makes it less prone to being compromised by electrical noise and environmental factors.



and coupling over large distances (Van der Heijden et al., 2014; Zwerver et al., 2022).

Weber et al. also highlighted the role of spin-orbit coupling in qubits in silicon, focusing on phosphorus atom qubits (Weber et al., 2018). Their research revealed that spin-orbit coupling of the phosphorus electron spin to the induced electric fields extended spin lifetimes to minutes. The SOC interaction also allows coupling to other quantum systems, making the prospects for hybrid quantum systems possible.

Bommer et al. recently carried out a study investigating spin-orbit interaction in Majorana nanowires. By encoding quantum information into the topological property of Majorana zero modes, the decoherence error can be resolved from a fundamental device level. However, the creation of Majoranas relies on magnetic fields, which are typically incompatible with superconductivity. To overcome this limitation is to leverage the presence of spin-orbit interactions. Spin-orbit interaction materials experience weak magnetic fields required for Majoranas, thus allowing for superconductivity.

The study carried out by Bommer and his colleagues shows that superconductivity and spin-orbit interaction can exist simultaneously, unveiling that spin-orbit interaction protects superconductivity in Majorana nanowires (Bommer et al., 2019).

## 9.5 Control of qubit fidelity

High-fidelity control of qubits is of paramount importance to achieving robust fault tolerance and reliable quantum computation. This central tenet is required for effective fault tolerance and is expressed in terms of an error threshold; a common target is <1% error threshold of the surface code (Raussendorf and Harrington, 2007; Fowler A. G. et al., 2012). Reaching two-qubit gate fidelities greater than 99% has been a long-standing goal for semiconductors and the greater realm of spin-qubit modalities. Such qubits are promising for scaling as they leverage the mature semiconductor processing technologies developed over the last several decades (Zwerver et al., 2022).

The use of couplers to control two-qubit interactions has improved operational fidelity in many-qubit systems by reducing parasitic and frequency overcrowding. Nonetheless, two-qubit gate errors continue to limit the capability of near-term quantum applications. This limitation, in part, derives from the existing tunable coupler topologies that are based on dispersive approximations that do not fully incorporate three-body dynamics. Using an approach that systematically extends dispersive approximations to exploit engineered coupler structures, Sung et al. have demonstrated CZ and ZZ-free iSWAP gates with two-qubit interaction fidelities of  $99.76 \pm 0.07\%$  and  $99.87 \pm 0.23\%$ , respectively (Sung et al., 2021).

## 9.6 Superconducting qubit fidelity

The number of nodes in a quantum circuit determines the dimension of the quantum system, the size of inductors and JJs fixes the potential, and the capacitance values define the kinetic energy of the quantum state. The ability to independently control these three

aspects of quantum states allows one to construct superconducting circuits that satisfy these requirements for intrinsic noise protection and, ultimately, coherence and fidelity.

The development and design of protected superconducting qubits now evolve along three main paths: (i) Josephson-junction arrays based on multimode circuits (Gyenis et al., 2021), (ii) compact few-mode circuits (Kringhøj et al., 2018), and (iii) driven systems (Chow et al., 2010; Wu et al., 2021a). These efforts can be further categorized as presented in Table 13.

Operation fidelity is a dimensionless figure of merit, allowing the comparison of diverse qubits. Using randomized benchmarking (Epstein et al., 2014), one can extract the gate errors independently of the measurement errors, even if the former are orders of magnitude smaller than the latter. Although it is not strictly correct, the fidelity is used to judge the progress toward error-correction thresholds required for fault-tolerant quantum computing. The problem is that the fidelity, as defined below, is not the error parameter entering the threshold theorem. The two parameters can differ by orders of magnitude in the unfavorable way: whereas the fidelity extracted by the randomized benchmarking can be low, the error rate can remain much larger (Sanders et al., 2015; Blume-Kohout et al., 2017). For all these reasons, evaluating the gate fidelities is popular, and impressive values have been reached.

Figure 24 shows the published fidelities of the gates, measurements, and initializations, respectively. For gates (Figure 24A), electron spin- $\frac{1}{2}$  qubits previously reached fidelities well above 99.9%. The use of both natural and isotopically purified silicon was essential for this achievement. Recently, a new record of 99.99% was set by hole-doped germanium (Lawrie et al., 2021a). There is notable progress in almost every qubit category, and increasing the fidelity of single-qubit gates is one of the most impressive achievements within the spin-qubit field.

Figure 24 also shows measurement fidelities. Until recently, the infidelities remained above a few percent. Relying on a “latched” readout in the Pauli spin blockade (Broome et al., 2017a; Nakajima et al., 2017), the fidelities above 99% were achieved with a singlet-triplet algorithm: for example, initializing all individual qubits into single-qubit fiducial states, and then entangling them with gates into the desired entangled multi-qubit state, such as one of the two-qubit Bell states or the three-qubit Greenberger-Horne-Zeilinger (GHZ) state.

Shunting the circuit with a large capacitance leads to an electrostatic energy that is significantly reduced relative to the JJ ( $E_j/E_c \gg 1$ ). The sensitivity of the qubit frequency to the charge noise is suppressed. In this regime, the qubit is called a transmon.

Stano and Loss published an excellent review of performance metrics for qubit/gate fidelities and coherence times, among other properties (Stano and Loss, 2022). Of the plethora of data presented by these authors, we reproduce a subset here as Figures 21, 24.

## 9.7 Qubit, gate, and system fidelities

Figures 24A–C show published fidelities of gates, measurements, and initializations, respectively. For the gates shown in Figure 20A, electron spin- $\frac{1}{2}$  qubits reached fidelities above 99.9%. Using

TABLE 13 Strategies for enhancing qubit coherence.

Strategy for enhancing qubit coherence	Description	Ref.
Noise filtering	The strategy for protecting a qubit is to identify the dominating source of noise contributing to decoherence and tailoring the design and the environment of the qubit to reduce environmental noise before the noise reaches the qubit.	Green et al. (2012), Green et al. (2013), Soare et al. (2014a), CT (2022a)
Encoding qubits globally	Because environmental fluctuations are local, qubits that are insensitive to local sources of noise can be encoded globally.	Didier et al. (2019a)
Encoding in decoherence-free subspaces	Qubits can be encoded into local degrees of freedom using a subspace of the Hilbert space that couples to the fluctuations of concern such that the environment cannot distinguish the different qubit states. These subspaces are commonly referred to as decoherence-free subspaces. This works best for long-wavelength noise, where fluctuations are uniform on the scale corresponding to the subspace used for encoding.	Nakajima et al. (2017), Lawrie et al. (2021b)
Encoding in time-dependent states	Encoding qubits into time-dependent states is another emergent approach toward increasing coherence. In this approach, the qubits are subject to strong external driving fields that can compete with the noise and stabilize the qubit states, for example, through autonomous error correction or by creating dynamical sweet spots.	Metcalfe et al. (2007), McDermott (2009), Yan et al. (2016b), Smart et al. (2022)

natural and isotopically purified forms of Si was required for this achievement. These values were further enhanced using a hole in Ge (Lawrie et al., 2021b), leading to fidelities of 99.99%. Figure 24B shows measurement fidelities. Until recently, infidelities remained above a few percent. Relying on a latched readout in the Pauli spin blockade (Broome et al., 2017b; Nakajima et al., 2017b), fidelities above 99% were achieved for singlet–triplet qubits. Higher fidelities for impurity spins require exceptionally long lifetimes. In all fidelity categories presented in Figure 24, that is, gates, measurements, and initializations, infidelities remain one to two orders of magnitude above single-qubit systems. Concerning initializations, the more-qubit infidelities are initializations into a nontrivial state achieved through the application of a simple quantum algorithm. For example, initializing all individual qubits into a single-qubit state and then entangling them with gates into the desired entangled multi-qubit state, such as one of the two-qubit Bell states or the three-qubit Greenberger–Horne–Zeilinger (GHZ) state. Figure 25A is a schematic of a harmonic oscillator, where energy levels are equally spaced and un-addressable. When a JJ is added to the circuit (b), a nonlinear component is introduced in the form of a non-dissipative, nonlinear inductance. A two-level system (TLS) of eigenfunctions in a double-well potential is characterized by the strain-dependent asymmetry energy  $\epsilon$  and the tunnel coupling  $\Delta$  (see Figure 25C). The image in (c) depicts a material schematic of the JJ where superconducting electrodes sandwich an insulator. A classic example is Al/Al<sub>2</sub>O<sub>3</sub>/Al. The tunneling of individual atoms between two configurations (Phillips, 1987; Agarwal et al., 2013), displacements of dangling bonds, and hydrogen defects (Holder et al., 2013) are depicted

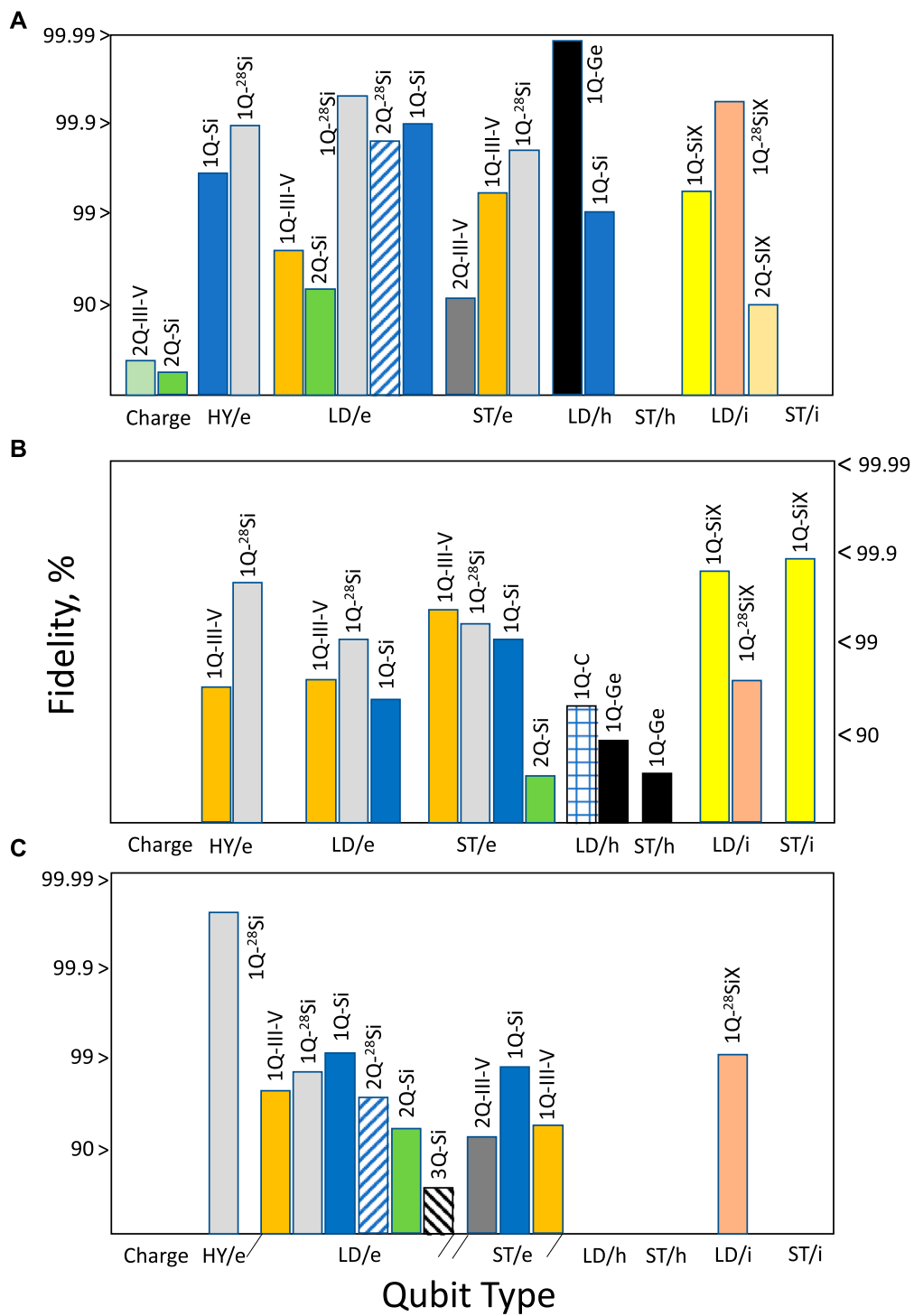
in the image. Near the interface of the superconducting electrodes, TLSs may also arise from bound electron/hole Andreev states (Faoro et al., 2005) or Kondo-fluctuators (Faoro and Ioffe, 2007).

We next turn to qubit energy relaxation. For spin qubits, for example, in considering two-electron singlet and triplet states, relaxation times are the main limitation to spin fidelity (Barthel et al., 2009; IBM, 2016; IMEC, 2023). Because of this, there are numerous values of relaxation time for singlet–triplet qubits, either explicitly reported or implicitly inferred by many experiments, for example, using Pauli spin blockade for determining spin characteristics. The use of impurities focused on isolating qubits from such reservoirs that electrons do not escape hence conserving dipole momentum. As such, qubits couple weakly to phonons, and decrease transition energies, typically using lower magnetic fields and thus setting fundamental limitations upon quantum computations (Shrivastava, 1983; Khaetskii and Nazarov, 2001).

## 10 Sources, impact, and mitigation of noise

### 10.1 Two-level system defects

Consider first the case where a TLS is coupled to a qubit with strength  $g$ , such that  $g$  is larger than the decoherence rate of both the TLS and the qubit. In this regime, the TLS acts as a random qubit that can swap information with the quantum circuit (see Figure 25).



**FIGURE 24**  
 Fidelities are shown for (A) gates, (B) measurements, and (C) initializations. In all panels, the horizontal axis shows the qubit type. The vertical axis shows the fidelity in percent. The data color indicates the material defined in the supplemental documents in Stano and Loss (2022). LD/e, ST/e, LD/h, LD/i, and ST/i qubit types are defined in Table 11. 1Q, one-qubit gate; 2Q, two-qubit gate; 3Q, three-qubit gate.

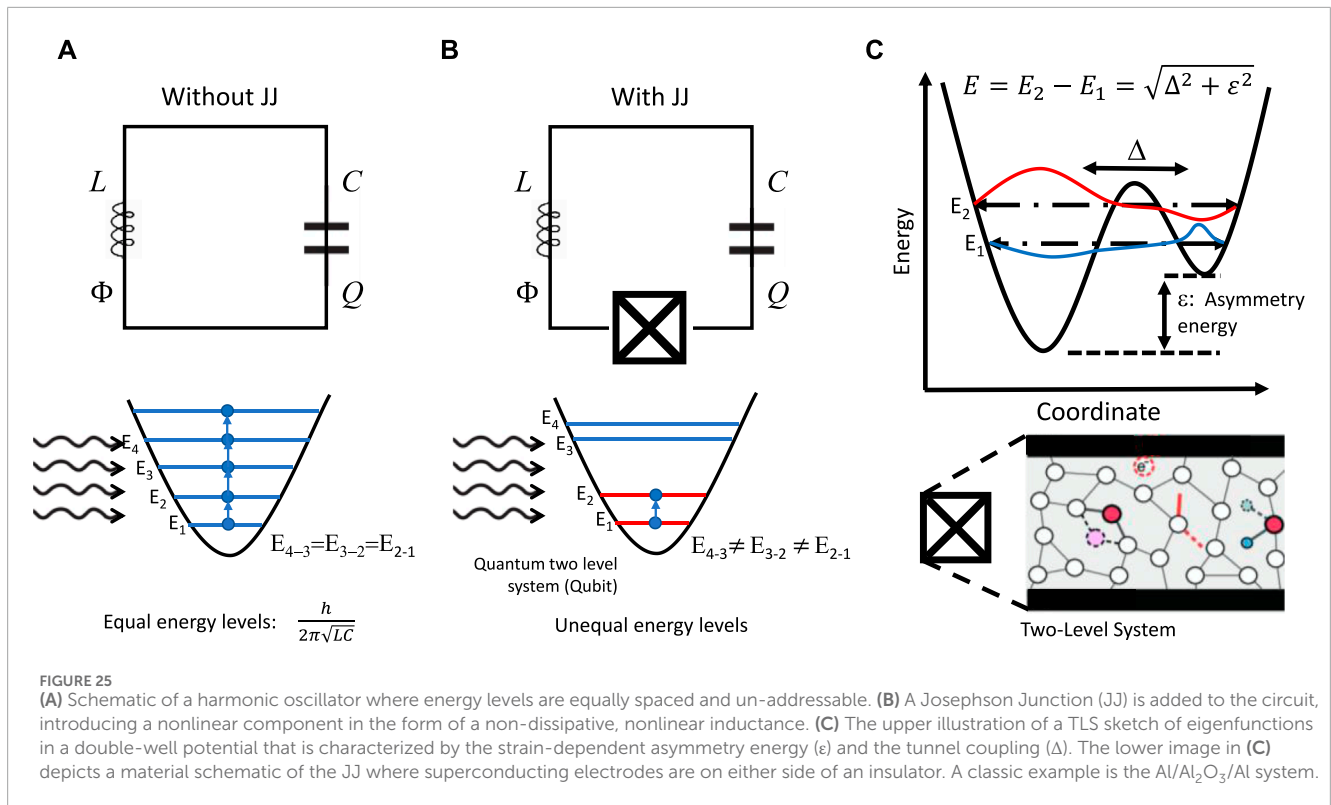


FIGURE 25

(A) Schematic of a harmonic oscillator where energy levels are equally spaced and un-addressable. (B) A Josephson Junction (JJ) is added to the circuit, introducing a nonlinear component in the form of a non-dissipative, nonlinear inductance. (C) The upper illustration of a TLS sketch of eigenfunctions in a double-well potential that is characterized by the strain-dependent asymmetry energy ( $\epsilon$ ) and the tunnel coupling ( $\Delta$ ). The lower image in (C) depicts a material schematic of the JJ where superconducting electrodes are on either side of an insulator. A classic example is the Al/Al<sub>2</sub>O<sub>3</sub>/Al system.

Phase qubits consist of a JJ and a shunt capacitor, both with lateral dimensions on the order of microns, and therefore have large areas of amorphous regions with many TLS defects. Naturally, smaller junctions have fewer defects. When such defects are exposed to intense electric fields, they give rise to classic TLS physics, including strong electromagnetic coupling among distinct TLS defects (Simmonds et al., 2004; Martinis et al., 2005). The signatures of strong EM coupling can be observed in the time domain, where beating is seen when driving coherent Rabi oscillations as a significant source of decoherence.

Best practices to improve coherence include improved shielding, which involves effective cryosinking and the use of nested radiation shields at infrared frequencies. Further, traps for both quasiparticles and phonons at the quantum-chip level must be developed. Such structures can be based on either microscopic defects or lithographically defined structures (Levenson-Falk et al., 2014; Wang et al., 2014; Taupin et al., 2016).

Engineered structures can incorporate a normal metal (Riwar et al., 2016) or lower-gap superconductor regions (Aumentado et al., 2004; Riwar and Catelani, 2019; Martinis, 2021) to trap quasiparticles, as well as circuits for active pumping using pulses (Gustavsson et al., 2016) or voltage-biased tunnel junctions (Marín-Suárez et al., 2020). Traps for phonons can be constructed using absorptive materials (Henriques et al., 2019) or by harnessing phonon bandgap and band-stop structures designed to stop phonon recombination (Rostem et al., 2018). The main intrinsic source of decoherence in superconducting qubits is  $1/f$  noise (Paladino et al., 2002).

## 10.2 $1/f$ noise

Types of  $1/f^{35}$  noise typically found in quantum circuits include charge fluctuations (Christensen et al., 2019), magnetic flux noise (Anton et al., 2012; Kumar et al., 2016), and fluctuations of the supercurrent in Josephson junctions (Constantin and Yu, 2007; Schreier et al., 2008). Background charge noise severely limits coherence in conventional Cooper-pair box-type qubits. The transmon qubit was designed to mitigate this noise source (Stanescu, 2016).

Flux qubits operate with a large shunting capacitor or in a regime where a charge is highly delocalized, rendering phase a good quantum number and obtaining immunity to charge

<sup>35</sup>  $1/f$  noise refers to the phenomenon of the spectral density,  $S(f)$ , of a stochastic process, having the form  $S(f) = \frac{C}{f^\alpha}$ , where  $f$  is the frequency on an interval bounded away from both zero and infinity, with  $1 \leq \alpha \leq 1.5$ , and  $C$  is a constant.  $1/f$  noise is an intermediate between the well-understood white noise with no correlation in time and Brownian motion noise. Brownian motion is the integral of white noise, and integration of a signal increases the exponent  $\alpha$  by 2, whereas the inverse operation of differentiation decreases it by 2.  $1/f$  noise cannot be obtained by simple integration or differentiation of signals. Also, there are no simple linear stochastic differential equations generating signals with  $1/f$  noise.  $1/f$  fluctuations are widely found in nature and have been observed and reported for more than 8 decades ([http://www.scholarpedia.org/article/1/f\\_noise](http://www.scholarpedia.org/article/1/f_noise)).



fluctuations. Operating in this regime leads to a sensitivity to magnetic fluctuations. Flux noise is common to all qubits that use a loop for magnetic bias and limit coherence. One typically operates at a point of degeneracy where the energy is insensitive to flux for fixed-frequency qubits. This noise spans DC to 10 GHz, including operations at low temperatures.

Critical current noise is currently the least deleterious of noise sources, especially for submicron junctions, and limits dephasing times when the coherence time exceeds milliseconds (Anton et al., 2012). The precise mechanism of  $1/f$  noise remains elusive. A theoretic explanation that produces  $1/f$  noise (Van Harlingen et al., 2004) is obtained by hopping between two wells in a double-well potential. Assuming a distribution of barrier heights for the hopping process yields  $1/f$ -type behavior. For charge noise and critical current noise, most models include some type of electronic traps that arise from structural disorder. In the case of critical current noise, one imagines that tunneling electrons become trapped at varying times.

Generalized filter-transfer functions as noise spectral filters (Lutchyn et al., 2010; Oreg et al., 2010) are particularly effective. Compact-protected circuits have only a few degrees of freedom and are examples of *local decoherence-free subspaces*. Protection of these qubits arises because the low-energy performance of the circuit is approximated as an effective Hamiltonian with parity symmetry, such as Cooper-pair or *fluxon*<sup>36</sup> symmetry.

Finally, systems experiencing continuous high-intensity drive conditions have also demonstrated protection against various noise sources where the interaction of the driving field and the qubit leads to beneficial properties.

QP tunneling across a JJ can cause qubit excitation (or relaxation) and result in bit flip even while driving  $E_J/E_C \gg 1$ , exponentially suppressing qubit sensitivity to charge parity and background charge fluctuations. For superconducting order fluctuations to efficiently trap quasiparticles, it is necessary to enhance frequency to increase the probability of shallow trap QP recombination.

The total number of nodes in a quantum circuit determines the dimensionality of the quantum system, while its inductance determines its kinetic energy, and its capacitance determines its potential energy.

The ability to independently control dimensionality and kinetic and potential energies allows one to create superconducting circuits that satisfy requirements for intrinsic noise protection and conditions that provide acceptable coherence and fidelity.

It has been shown that some qubit modalities allow for protected gate operations (Brooks et al., 2013a; Klots and Ioffe, 2021), which are crucial for fault-tolerant quantum computations.

The development and design of protected superconducting qubits has evolved along three main paths: JJ arrays based on

multimode circuits (Kitaev, 2003; Ioffe et al., 2002; Ioffe and Feigel'man, 2002; Douçot and Vidal, 2002; Gladchenko et al., 2009; Douçot and Ioffe, 2012; Bell et al., 2014a), compact few-mode circuits (Brooks et al., 2013b; Kalashnikov et al., 2020; Smith et al., 2020), and driven systems (Bell et al., 2014b; Mirrahimi et al., 2014; Ofek et al., 2016; Puri et al., 2017; Didier et al., 2019b; Mundada et al., 2020; Campagne-Ibarcq et al., 2020; Grimm et al., 2020; Wu et al., 2021b; Huang et al., 2021). These efforts are further categorized as presented in Table 14.

A logical qubit may be constructed by assembling a set of noisy cells to reduce the total effect of local errors along the chain, a type of global encoding. This approach to noise protection is based upon the concept of topological ground-state degeneracy<sup>37</sup>.

Alternatively, compact-protected circuits are individual qubits with degrees of freedom in local decoherence-free subspaces (DFS)<sup>38</sup>. These circuits require extreme conditions, such as large inductances and minimal parasitic capacitance. Protection in such compact qubits arises from the low-energy behavior of the circuit that is approximated by a Hamiltonian with parity symmetry, such as Cooper pair or fluxon (i.e., a quasiparticle of electric or magnetic flux) symmetry (Hsieh et al., 2019). Finally, systems under continuous driving fields can also show protection against noise sources (Vool and Devoret, 2017; Indico, 2022).

## 11 Quantum technology drivers, key players, and markets

Quantum technologies driving the development of QMs are rich and diverse and include quantum computers, cybersecurity, transportation, finance, navigation, materials discovery (biology, drug discovery, electronic materials, etc.), communication, and novel electronics, among others. Some of these will be reviewed briefly here in the context of private sector players and market dynamics. More detailed technical descriptions have appeared elsewhere in this perspective.

### 11.1 Quantum technology drivers

Quantum computers, due to their immense potential to impact international science and technology markets, have been a key focus of this review. Quantum computing is currently a topic of

<sup>36</sup> A fluxon (i.e., Josephson vortex) is made of circulating supercurrents and has no normal core in the tunneling barrier. Supercurrents circulate around the center of a fluxon, which is situated within the Josephson barrier.

<sup>37</sup> Topological degeneracy is an effect that occurs when the ground state of a gapped many-body Hamiltonian becomes degenerate in the limit of large systems such that degeneracy cannot be lifted by local perturbations.

<sup>38</sup> A decoherence-free subspace (DFS) is a subspace of a Hilbert space that is invariant to non-unitary dynamics. DFSs can also be characterized as a special class of quantum error-correcting codes. In the latter, they are passive error-preventing codes because these subspaces are encoded with information that will not require active stabilization. These subspaces prevent destructive environmental interactions by isolating quantum information.

TABLE 14 Noise mechanisms in superconducting qubits.

Noise mechanisms	Description	Ref.
<i>Noise Sources</i>		
Transmons	If one shunts the circuit described above (see Figure 25 and associated TLS discussion), which has an energy $E_j$ stored in the JJ, with a large enough capacitance such that its electrostatic energy $E_c$ is significantly reduced (i.e., $E_j/E_c \gg 1$ ), leading to a reduction in sensitivity of qubit frequency to charge noise. Under these conditions, qubits are called transmons, and their advantage derives from an increase in $E_j/E_c$ , as the charge dispersion decreases exponentially, while anharmonicity decreases with only a power law dependence. Altogether, this leads to enhanced qubit coherence.	Geerlings (2013), Indico (2022)
Quasiparticles (QP)	QP tunneling across a JJ can cause qubit excitation (or relaxation) and result in bit flip even while driving $E_j/E_c \gg 1$ , thus exponentially suppressing sensitivity on the qubit to charge parity and background charge fluctuations. Recent theory nonetheless predicts QP tunneling will remain an important source of relaxation and dephasing.	Catelani et al. (2011), Catelani et al. (2012)
Ramsey interferometry evidence of charge parity switches	Ramsey interferometry is a method that can be used to evaluate $T_2$ and the resonant frequency of a qubit—the frequency needed to drive the qubit from $ 0\rangle$ to $ 1\rangle$ . The sequence consists of two $\frac{\pi}{2}$ pulses separated by an intentional and variable delay followed by a measurement of the qubit in the basis. Introducing a known detuning frequency to the qubit pulses results in a precession around the Z-axis of the Bloch sphere at a constant rate, manifesting a sinusoidal oscillation in the output qubit basis state in measurement. Because the sinusoid decays proportional to $e^{-t/T_2}$ , $T_2$ can be determined from modeling. If there is a change in parity during these measurements, then the output will show two decaying sinusoids instead of one, with each parity having a unique frequency.	Ristè et al. (2013)
Charge parity	Mapping quasiparticle charge parity onto qubit basis states ( $ 0\rangle$ to $ 1\rangle$ ), one can modify the Ramsey sequence as follows: (i) initialize the qubit in $ 0\rangle$ through repeated quantum non-demolition measurements; (ii) apply a $\frac{\pi}{2}$ pulse around the Bloch sphere Y-axis that creates an equal superposition state; (iii) allow the system to evolve for a duration of $\Delta t$ where $\Delta t = \frac{\Delta f}{4}$ with $\Delta f$ being the frequency difference between the even and odd charge (QP) parity states. Finally, a last $\frac{\pi}{2}$ pulse around the Bloch sphere X-axis is performed. Using this protocol, charge parity maps into the qubit basis state as $ 0\rangle \rightarrow \text{even}$ and $ 1\rangle \rightarrow \text{odd}$ . By applying this method, Ristè et al. determined a tunneling time of 0.79 ms, realizing an order of magnitude increase in decoherence time, $T_1$ .	Ristè et al. (2013)
TLS and qTLS	Noise originates in the dielectric component of materials, known as two-level system (TLS) noise—surface defects with two states that have different energies close to resonance with the qubit excitation energy. TLSs act as two minima in a double-well potential separated by a barrier (see Figure 25). Recent studies by de Graaf et al. (2018) have identified a subgroup of TLS that possesses unique properties not accounted for by the Standard Tunneling Model: they are highly coherent with a low reconfiguration temperature of $\sim 300$ mK and a non-uniform density of states. The energy scaling of these TLS is similar to the expected energy scaling of the superconducting order parameter ( $\Delta$ ), which gives reason to believe fluctuations in $\Delta$ are responsible for this noise. Moreover, de Graaf suggests that the unique properties of these TLS can be explained if they were formed by QPs that became trapped in local $\Delta$ minima. Because of this, they are referred to as qTLS for quasiparticle TLS.	Müller et al. (2019)

(Continued on the following page)

TABLE 14 (Continued) Noise mechanisms in superconducting qubits.

Noise mechanisms	Description	Ref.
<i>Mitigation Strategies</i>		
Noise filtering	This approach to protecting a qubit is to identify the dominant source of noise contributing to decoherence and tailor the design and the environment of the qubit to reduce this noise source prior to it reaching the qubit.	Green et al. (2012), Green et al. (2013), Soare et al. (2014), CT (2022b)
Encoding qubits globally	Because environmental fluctuations are local, one can globally encode qubits that are insensitive to local sources of noise.	Stanescu (2016)
Encoding in decoherence-free subspaces	One can encode qubits into local degrees of freedom but employ a subspace of Hilbert space that couples to the fluctuations of concern such that the environment cannot distinguish different qubit states. These subspaces, known as decoherence-free subspaces, work best for long-wavelength noise sources, where fluctuations are uniform on the scale corresponding to the subspace used for encoding.	Lidar et al. (1998)
Encoding in time-dependent states	Encoding qubits into time-dependent states is another emergent approach toward increasing coherence. In this approach, the qubits are subject to strong external driving fields that can compete with the noise and stabilize the qubit states, for example, through autonomous error correction or by creating dynamical sweet spots.	Didier et al. (2019c), Mundada et al. (2020), Gertler et al. (2021), Huang et al. (2021)

intense interest among scientific, communication, and business communities because of its potential to disrupt existing classical performance standards and metrics.

Quantum computers exist as variants of simulators, quantum annealers, and analog quantum computers. We will consider each of these in turn and by global region.

### 11.1.1 North American region

#### 11.1.1.1 Quantum annealing.

Quantum annealing is generally used to solve combinatorial optimization problems such as machine learning, portfolio optimization, route optimization, etc. D-Wave Systems, a Canadian company founded in 1999, was the first to introduce a quantum annealing approach as a quantum solver. In 2011, the world's first commercial quantum annealing machine, operating with 128 qubits, was developed by D-Wave with a price tag of approximately USD 10,000,000. In 2019, D-Wave announced the release of *Pegasus*, which was a quantum processor chip consisting of 5,000 low-noise qubits. D-Wave Systems has since been a major player in quantum computing markets, providing quantum annealing platforms to commercial customers. Their platforms operate using *Qbsolv*, which is open-source software that solves QUBO problems on D-Wave's quantum processors (D-Wave Initiates Open Quantum Software Environment, 2022b). D-Wave exclusively employs superconducting phase qubits for their quantum annealers (Harris et al., 2010b). As illustrated in Figure 8, the growth of the quantum annealer product market is dominated by D-Wave Systems' products. D-Wave launched its Advantage-2 machine in 2024, which has more than 1,200 qubits and 10,000 couplers. D-Wave began selling its platforms to U.S. government agencies, organizations,

and NGOs, including LCMO, Google, NASA, and LANL, as early as 2011.

#### 11.1.1.2 Gate-based analog quantum computers.

Research in *superconducting* quantum computing is conducted by companies such as Google (Globe News Wire, 2023), IBM (Globe News Wire, 2023), IMEC (Castelvecchi, 2017), BBN Technologies (IBM, 2016), Rigetti (IMEC, 2023), and Intel (Ryan et al., 2017). Many recently developed quantum processing units, or quantum chips (QPUs), utilize superconducting architectures. These devices function at very low temperatures and require expensive and large He<sup>3+</sup> dilution refrigeration to minimize the deleterious influence of environmental heat upon qubit coherence.

The years 2017–2019 saw a plethora of activity in large-qubit AQC platforms from industrial leaders Google, IBM, Intel, and IonQ, among others. Other key players in quantum computational platform development employ different qubit modalities, for example: Xanadu, photonic qubits; Rigetti, superconducting qubits (Rigetti Launches Quantum Cloud Services, 2018); Intel, “hot” silicon spin qubits; Baidu, superconducting qubits; and Google and Microsoft, topological qubits.

All major AQC companies are striving to scale up their quantum computational platforms with the goal of attaining a *mega-qubit computer*.

In addition to the investments made by private sector players, the U.S. government has invested billions in quantum technologies sponsored by the Department of Energy (DOE), the Defense Advanced Research Projects Agency (DARPA), and the National Security Agency (NSA), among others.

## 11.1.2 Asia–Pacific Region

### 11.1.2.1 Quantum annealing.

Although D-Wave dominates the North American region, it is not alone in the market space of quantum annealers.

In 2018, NEC Corporation introduced the world's first LHZ<sup>39</sup> unit cell machine, facilitating scaling to a fully connectorized architecture using superconducting parametron<sup>40</sup> qubits. NEC demonstrated a quantum annealer using a four-qubit Lechner, Hauke, and Zoller (LHZ) scheme with circuit coupling technology. NEC has achieved a first-time demonstration by successfully solving small-scale combinatorial optimization problems via quantum annealing using their LHZ approach. NEC's LHZ-based machine is resistant to noise and remains capable of scaling up to a fully connectorized quantum annealing architectures while maintaining prolonged quantum superposition states.

In another first-time demonstration, NEC developed a three-dimensional topology that efficiently connects several LHZ unit cells arranged in a tile pattern with external devices. NEC is currently working to develop a quantum annealing machine using superconducting parametrons in a project commissioned by the New Energy and Industrial Technology Development Organization with the target of realizing quantum annealing machines by the end of 2023 (*Intel Invests US\$50 Million to Advance Quantum Computing, 2022*).

Tohoku University and NEC have started joint research on computer systems using an 8-qubit quantum annealing machine developed by NEC and sponsored by Japan's National Institute of Advanced Industrial Science and Technology (*Petit et al., 2020*).

Also, in the Asia–Pacific Region, an Australian quantum computing company, Silicon Quantum Computing Pty Limited (SQC), in 2017 embarked to create and commercialize a quantum computer in conjunction with the Australian Centre of Excellence for Quantum Computation and Communication Technology. Their goal is to produce a silicon-based 10-qubit prototype device. As well as developing its own proprietary technology and intellectual property, SQC continues to lead efforts to build and develop a silicon quantum computing industry to influence global markets.

### 11.1.2.2 Gate-based analog quantum computers.

In the Asia-Pacific Region, demonstrations and breakthroughs by Chinese scientists in quantum physics have been impressive. Competition in quantum computing between the U.S. and China, the two dominant global economies, and other international players has resulted in the expansion of the

international market size from USD 10 B in 2021 to a projected USD 44 B by 2028, growing at a compounded annual growth rate (CAGR) of 30.2% over this forecasted period (see *Table 15*) (*HPC, 2022*).

The Chinese government has kept pace, making domestic investments in quantum research and advanced technologies in defense, security, and artificial intelligence of around \$15 billion. (Note, this figure is disputed as high by many international experts). Notwithstanding the disagreement, it is widely believed that Chinese state funding in quantum S&T exceeds the combined investments of the total of EU and US commitments. Amongst the various projects and initiatives is the National Laboratory for Quantum Science in Hefei; the largest quantum research facility in the world, at thirty-seven hectares (370,000 m<sup>2</sup> or ~4 million sq. ft.) (*Davey, 2023*). Additionally, Alibaba has invested USD 15 B in the establishment of DAMO (i.e., the Academy for Discovery, Adventure, Momentum, and Outlook) that includes seven new research laboratories in China, the United States, Russia, Israel, and Singapore (*Quantum Technology Market Size, 2022a*).

China's advances include *Jiuzhang*, the first photonic quantum computer to claim quantum supremacy (2019). Previously, quantum supremacy had been achieved by Google's *Sycamore* based on superconducting qubits (*Quantum Computing, 2022*). *Jiuzhang* is reported to have a Hilbert space that is 10 billion times greater than that of the superconductor-based *Sycamore* processor and, as such, is harder to simulate classically (*Techinasia, 2022*). The Asia–Pacific quantum technology market is expected to experience significant growth, with a CAGR of 26.1% from 2022 to 2031. The total addressable market for this period is projected to reach USD 86.1 B. This growth is driven by the increasing demand for reliable network and computing solutions, the growing government and private funding for quantum technologies, rising investments in research and development, and the expanding applications of quantum technology across market sectors (see *Table 16*). Recent breakthroughs by Chinese scientists have identified the path forward for space-based quantum communication and teleportation, necessary developments for the creation of a quantum internet. Although the Asia–Pacific Region only accounts for 12% of the total market share of the quantum computer market in 2020, it increased dramatically to 27% in 2023 while North American and European Regions shares reduce commensurately.

## 11.1.3 European region

### 11.1.3.1 EuroQCI

Since 2019, all 27 EU member States signed the EuroQCI (QCI-Quantum Communication Infrastructure) Declaration, agreeing to work collectively with the European Commission and the European Space Agency toward the development of a quantum communication infrastructure covering the entire EU (*Kan, 2019*). The EuroQCI is planned as a secure quantum communication infrastructure composed of a terrestrial segment relying on fiber communications networks linking strategic sites at national and cross-border levels and a space segment based on satellites. It will be an integral part of the new EU space-based secure communication system spanning the whole EU, including its overseas territories.

The EuroQCI will safeguard sensitive data and critical infrastructures by integrating quantum-based systems into

<sup>39</sup> LHZ is an abbreviation for a technique proposed by Lechner, Hauke, and Zoller. As the number of qubits increases, it becomes difficult to directly connect each qubit to each other qubit with hardware. To solve this problem, the software company ParityQC and LHZ proposed a transformation that enables fully connected qubits to be obtained using qubits that are physically connected to only their nearest neighbors.

<sup>40</sup> A superconducting parametron is a superconducting resonant circuit composed of Josephson junctions and capacitors that oscillate with different phases; it is used as a qubit. The lifetime of the qubit is an order of magnitude longer than that of flux qubits.

TABLE 15 Global regions of quantum computing market share, commercial players, and market dynamics.

Private sector players by global region	2020 share of quantum markets (%) (±2%)	2023 share of quantum markets (%) (±2%)	Size/Year	CAGR (forecast period, %)
<b>North America</b>				
Rigetti Computing, Inc. (Berkeley, CA, United States) IBM Corp (Armonk, NY, United States) Zapata Computing, Inc (Boston, MA, United States) Microsoft Corp (Seattle, WA, United States) IonQ Inc (College Park, MD, United States) Intel (Santa Clara, CA, United States) Google (Mountain View, CA, United States) QC Ware (Palo Alto, CA, United States) Quantinuum Ltd (2021 Honeywell spin-out) Hewlett Packard Enterprise (Spring, TX) Aliro Quantum (Boston, MA) Alphabet, Inc (2015 Google spin-out) Gem Systems (Markham, ON, Canada) Quantum Computing, Inc. (Leesburg, VA, United States) Qubitekk (Vista, CA, United States) D-Wave Systems Inc (Burnaby, Canada)	45	33	USD 308.2 M/2022 (GREYB, 2022)	Unk
<b>Asia Pacific</b>				
Huawei Technologies Co., Ltd (Shenzhen, China) Baidu (Beijing, China) Tencent Quantum Lab (Shenzhen, China) ZTE Corporation (Shenzhen, China) Silicon Quantum Computing (Sydney, Australia) Quantum Brilliance (Sydney, NSW, Australia) Telstra Computing Inc (Melbourne, Australia) NEC Corporation (Tokyo, Japan) QD Laser Co. Inc. (Kanagawa, Japan) Fujitsu Global (Tokyo, Japan) Toshiba Corporation (Tokyo, Japan)	12	27	USD 86.1 B/2031	26.1/2023–2031

(Continued on the following page)



TABLE 15 (Continued) Global regions of quantum computing market share, commercial players, and market dynamics.

Private sector players by global region	2020 share of quantum markets (%) ( $\pm 2\%$ )	2023 share of quantum markets (%) ( $\pm 2\%$ )	Size/Year	CAGR (forecast period, %)
<b>Europe</b>				
T-Systems International GmbH (Frankfurt, Germany) Robert Bosch GmbH Riverlane (Cambridge, United Kingdom) KETS Quantum Security (Bristol United Kingdom) M-Squared Lasers Limited (Glasgow, United Kingdom)	38	20	Unk	Unk
<b>ROW</b>	5	20	Unk	Unk

TABLE 16 State of quantum markets and projections.

Market segment	Size (B USD)/Year	Forecast size (B USD)/Year	CAGR (forecast period, %)
Quantum computing (Estimates, 2022)	0.929/2023	6.529/2030	32.1
Quantum cryptography (Fortunebusinessinsights, 2022)	0.102/2021	0.477/2030	18.7
Quantum-secure communication <sup>740</sup>	0.420/2022	1.17/2031	12.3
Quantum electronics; STT-RAM (Google, 2022)	unk/2020	7.2/2027 (United States only)	32.7
	unk/2020	2.2/2027 (China only)	42.4

existing communication infrastructures, providing an additional security layer based on quantum physics. It will reinforce the protection of Europe's governmental institutions, their data centers, hospitals, energy grids, etc., becoming one of the integral pillars of the EU's Cybersecurity Strategy for the coming decades.

The EuroQCI was initially launched in 2019, and work has continued under the supervision of the European Commission. The *terrestrial segment* is implemented by the Member States, and the *space segment* is implemented by the ESA.

For the terrestrial segment, the EuroQCI's first implementation phase started in January 2023 with the support of the Commission's Digital Europe Program, with a focus on:

- A set of industrial projects with the aim of developing Europe's quantum communication ecosystem and industry.
- National projects allowing Member States to design and build the national quantum communication networks that will form the basis of the terrestrial segment.
- Establishing coordination and support action to act as a link between all projects, facilitate collaboration, and identify standardization protocols.

These first projects will make it possible to take steps toward services establishing a highly secure way of delivering encryption key material.

Alongside this, the Connecting Europe Facility (CEF) will provide funding for projects developing cross-border links between national networks and interconnections with the EuroQCI's space component.

#### 11.1.3.2 EuroQCI satellite constellation

For the space segment, the EU Commission is currently working with ESA on the specifications of a first-generation constellation of EuroQCI satellites. This will build on the first prototype satellite, Eagle1, developed by ESA and an industrial consortium, and due to be launched in late 2024. More recently, several European countries have joined to form the European High Performance Computing Joint Undertaking (EuroHPC JU) to build state-of-the-art quantum computers by circa 2023 as accelerators interconnected with the Joint Undertaking's supercomputers, forming "hybrid" machines that blend the best of quantum and classical computing technologies (Letzter, 2020). In 2022, the EuroHPC JU announced six sites across the EU will be home to the first European quantum computers, which will be integrated into EuroHPC supercomputers. These newly acquired quantum computers will be located at sites in Czechia, Germany, Spain, France, Italy, and Poland. In total,

€100 million, with 50% coming from the EU and 50% from 17 of the EuroHPC JU-participating countries, has been invested. Its substantial computing capacity will address complex simulation and optimization problems, especially in materials development, drug discovery, weather forecasting, transportation, and other real-world problems of import to industry and society. A specific aim is to deliver the first computer with quantum acceleration by 2025. Table 15 also lists individual companies that have been notably active in promoting meaningful investments in quantum technologies. Further, this table provides a listing of the top seven countries leading investments in quantum technologies. Here, we list only publicized investments made by government agencies and institutions and not those made by private companies. The latter are difficult to quantify as many companies do not make public such data, while in other countries, such as China, commercial industry is heavily subsidized by the central government, making it difficult to parse such investments. These investments also do not include the collective investments by the EU and other collaborative Member States. Nonetheless, Table 17 reflects the major investments and the seriousness of high-income countries toward quantum technology and its potential. Noteworthy investments include the timely multibillion-dollar investments by the United States, China, Germany, the United Kingdom, and France.

## 11.2 Market size and dynamics

Table 15 presents the 2020 market share for quantum computing revenues for major global regions. One sees that among these, North America maintains a dominant market position with 45%, followed by Europe at 38% and Asia Pacific at 12%. Noteworthy, the 2023 forecast reveals a dramatic increase in the Asia-Pacific share to 27%, with North America at 33% and Europe falling to 20%.

Table 16 provides a breakdown of market segments by other quantum technologies.

In 2021, the global quantum computing market was valued at USD 472 million. The market was anticipated to expand at a 30.2% CAGR from USD 472 million in 2021 to USD 1,765 million by 2026. The early utilization of quantum computing was in the medical and defense section, trailed by finance and banking, which are projected to drive the market's worldwide expansion. Geographically, North America held the highest market share, that is, approximately 45% of the global quantum computing market. Whereas the Europe and Asia-Pacific regions held approximately 38% and 12%, respectively (see Table 15) (Innovationcloud, 2022). We next examine other important quantum technologies, beginning with cybersecurity.

### 11.2.1 Cybersecurity

Security in communications touches many aspects of society, including financial and banking services. For example, price derivatives employ a highly computation-intensive calculation scheme known as Monte Carlo. This simulation model found its inception during World War II's Manhattan Project where it played an essential role in accurately accounting for neutron scattering and absorption during nuclear fission. Because computational speed is often a limiting factor in the efficiency and timeliness of financial transactions,

quantum computing schemes and algorithms enhance trading efficiency.

In *cybersecurity*, the generation of random numbers is of great value. These are generated by quantum calculations and are integral to cryptography. Quantum-secure communications enable an entirely secure exchange of quantum encryption keys. The quantum key distribution (QKD) allows someone to securely distribute encryption keys. QKDs will remain secure even from future code-breaking quantum efforts.

Quantum communications are of great interest to commercial, military, and intelligence communities. Many other quantum applications that have been proposed but not yet matured will be enabled by future entangled quantum networks (Digital Strategy, 2022b).

According to verified market research, the quantum cryptography market size was valued in 2021 at USD 102.34 M and is projected to reach USD 476.83 M by 2030, growing at a CAGR of 18.7% from 2022 to 2030 (GREYB, 2022).

### 11.2.2 Quantum teleportation

Quantum teleportation is defined as the transfer of information from one particle (source) to its entangled partner (target). The connection between entangled pairs of particles has a minimum amount of entanglement needed to successfully perform quantum teleportation. Researchers have performed many demonstrations of this type over the past decade. Famously, a research group from China teleported a photon from Earth to a satellite orbiting 1,400 km (defined as "low Earth orbit"). Quantum Experiments at Space Scale (i.e., QUESS) is a Chinese research project in the field of quantum teleportation. *Tiangong-2*, China's second Space Laboratory module, was launched in 2016. *Tiangong-2* carries out Space-Earth quantum key distribution and laser communications experiments (Science the Wire, 2022). A satellite, nicknamed *Mozi*, is operated by the Chinese Academy of Sciences, as well as ground stations in China (Google, 2022; *Tiangong-2 takes China one step closer to space station*, 2018). Quantum teleportation is the lynchpin on the path towards a quantum internet. The quantum communication market size was estimated at 570 M\$ in 2022 and projected to grow to 8.3 B\$ by 2032 with a compound annual growth rate (CAGR) of 29.3% during the forecast period of 2023–2032. Security issues, increasing cyber threats, government initiatives, and quantum technology advances are key market drivers. [NEW-<https://www.marketresearchfuture.com/reports/quantum-communication-market-12240>. Accessed 7/23/2024].

### 11.2.3 Transportation and logistics

Transportation and logistics pose optimization challenges in identifying the most efficient routes by considering variables such as route conditions, vehicle performance, driver capabilities, etc. Multiple constraints increase the computational complexity of the calculations that are well-managed by quantum computers and, in particular, quantum annealers.

TABLE 17 Countries making major investments in quantum technologies (industrial contributions omitted) (Digital Strategy, 2022a).

Country	Program (or sponsoring agency)	Foci/goals	Size
United States	U.S. government, National Quantum Initiative	Advancing quantum communications, quantum computing, and quantum cryptography	USD 1.28 B 2019–2024
	U.S. government, White House Office of Science and Technology Policy, the National Science Foundation, and the Department of Energy	Create 12 AI and quantum information science research institutes	USD 1 B 2020
China	Chinese government, Micius; also known as QUESS (Quantum Experiments at Space Scale)	Quantum experiments at space scale	Est. USD 100 M 2016
	Chinese government, creation of the National Laboratory for Quantum Information Sciences	Conduct a variety of ground-to-space quantum communication experiments	USD 10 B 2017 +
Canada	Canadian government	Delivered to D-Wave Systems for the development of quantum computing	USD 40 M 2020
	Canadian government	Broad investments in quantum technology	USD 100 M 2020
	Canadian government, National Quantum Strategy	Broad investments in quantum research	USD 360 M 2021
Germany	German government	Quantum computing investment	€650 M 2018–2022
	German government	Innovation for quantum technology (involves the creation of two quantum computers)	€2 B 2021–2025
United Kingdom	Government of the United Kingdom, national quantum plan	Broad investments in quantum research and technology	€370 M 2013–2018
	Government of the United Kingdom, establishment of National Quantum Computing Center	Design, development, and construction of a quantum computer	Unknown 2018
	Government of the United Kingdom	Quantum technology development	153 M £ 2019
	Government of the United Kingdom, National Quantum Technologies Program	Broad investments in quantum research and technology	1 B £ 2014–present
	Government of the United Kingdom	Broad investments in quantum research and development	2.4% of GDP Future
France	French government-sponsored “Quantonation” investment fund	Focuses on funding quantum start-ups	Unknown 2018
	French government	Strengthens research in quantum technologies, particularly quantum computers, increasing public investment from €60 M to €200 M per year	€1.8 B 2021–2026
Russia	Russian government	For the development of practical quantum computing technologies	USD 790 M 2020
	Russian government, Rosatom–Russia’s National Nuclear Enterprise	Established the National Quantum Laboratory aimed at developing a quantum computer by the end of 2024	Unknown 2020–2024

### 11.2.4 Molecular simulation and drug design

Physicists, chemists, and materials scientists endeavor to solve problems that often involve molecular simulations, including machine learning-based refinements. As molecules become increasingly large and more complex, the number of possible configurations grows exponentially, necessitating quantum computers. Examples of such problems include drug design, materials discovery, and optimized manufacturing processes involving thousands of individual steps to identify which complex processes play the most important roles in determining performance and the most affordable and efficient processes (First Quantum Satellite Successfully Launched, 2016).

### 11.2.5 Ultra-precise quantum clocks

Atomic clocks are the bedrock of GPS<sup>41</sup> (or GNSS<sup>42</sup>) systems that allow for highly accurate operations affecting commerce (e.g., trucking, trains, airfreight, shipping containers in the management/telematics of just-in-time supply chain management); maritime industries navigation (e.g., automatic identification system); mobile telecommunication networks (4G, 5G, and 6G); agricultural management in planting, watering, and fertilizing of crops; commercial air travel (e.g., air traffic management systems); building and construction industries, and banks and financial institutions that rely on global positioning system (GPS) for precise time-stamping of transactions, etc. The atomic clock market is estimated at 509 M\$ in 2024 and projected to reach 782 M\$ by 2031, growing at a compound annual growth rate (CAGR) of 6.3% over this period.

Quantum-based atomic clocks, whose origins date to the 1950s, are now routinely integrated into satellites providing GPS functions. In an atomic clock, a large group of atoms, often cesium or rubidium atoms, is excited by sequential microwave pulses. These EM waves trigger atoms to oscillate, whereupon these atomic oscillations are used to define a highly precise time interval; that is, a second is defined as a finite number of atomic oscillations. It is noteworthy that the second has been defined by NIST as “the duration of 9,192,631,770 periods of transitions between two hyperfine levels of the caesium-133 isotope” (Wall, 2016). However, recent demonstrations of atomic clock functions exploit the principles of quantum entanglement to greatly reduce sources of noise and produce much more accurate clocks. A perfect, noiseless comparison is impossible to achieve as the probabilistic nature of quantum mechanics allows for some intrinsic noise associated with any experiment (Innovationcloud, 2022). Work aggressively continues along these lines.

### 11.2.6 Ergotropy and Quantum Batteries

Puliyil et al. provided connections between the laws of thermodynamics and quantum information theory to propose a

concept called *ergotropy* that represents the amount of work one can extract from a system while maintaining constant entropy (Puliyil et al., 2022). This requires a phenomenon called *genuine multipartite entanglement*, where a collective of particles behaves as a single unit. The difference between work extraction from individual parts and work extraction from a collective is an *ergotropic gap*.

Ergotropy is foundational to new quantum batteries (QB). In one manifestation, QBs are microcavities where the active material consists of organic molecules dispersed in a matrix where each molecule exists in a quantum superposition. If they collectively maintain coherence, the total system behaves cooperatively, giving rise to ultrafast charging that is proportional to the number of molecular units. This, in turn, gives rise to a counterintuitive behavior where the recharging time is inversely related to the battery capacity, leading to the charging power being both sizeable and increasing with battery mass (Malia et al., 2022). In the future, this type of device may prove disruptive to wireless charging, solar cells, and electric vehicle markets.

### 11.2.7 Quantum materials institutes (QMIs)

To meet quantum technology demands, QMIs have formed all over the world, and top-tier research institutes and universities lead such efforts. To manage the potential runaway expenses and bring to bear the necessary diversity in human talent and tools, QMIs tend to exist as large consortia, combining universities, national laboratories, and large and small businesses, often funded, in part or in whole, by local and/or national governments.

It is only because industry and governments are confident of substantial return on investments that we move forward aggressively as a society in pursuit of quantum materials, science, and technologies.

The study of QMs is a nontrivial exercise and requires concerted and coordinated efforts in theory, simulation, materials processing in 0-D, 1-D, 2-D, and 3-D, and the employment of powerful characterization tools such as electron microscopy, neutron scattering, synchrotron spectroscopies, and x-ray scattering techniques, in addition to sophisticated low-temperature transport measurements and high-pressure studies (among other highly specialized techniques). Taken together, these efforts can quickly escalate to tens or even hundreds of millions of dollars (euros, yen, pounds, yuan, krona...etc.) of investment in the necessary tools, staffing, and infrastructure.

Although universities and national laboratories account for many of the fundamental breakthroughs in QMs, such technological centers often find it challenging to translate such innovations to industrial companies, which are better prepared to create products and technologies to address real-world problems.

The need for partnerships between university hubs, national laboratories, and companies that focus on QM business-oriented opportunities has become undeniably important.

41 The global positioning system (GPS), originally Navstar GPS, is a satellite-based radio navigation system owned by the United States government and operated by the United States Space Force.

42 Global navigation satellite system (GNSS) is a general term describing any satellite constellation that provides positioning, navigation, and timing (PNT) services on a global or regional basis.

## Market Demands

- **Early Adoption by Finance and Banking Sectors**
- **Increase in Strategic Alliances**
- **Continued Adoption by Medical and Defense Industries**
- **Rise in Commercial Investment in Quantum Technologies**

## Challenges to Insertion

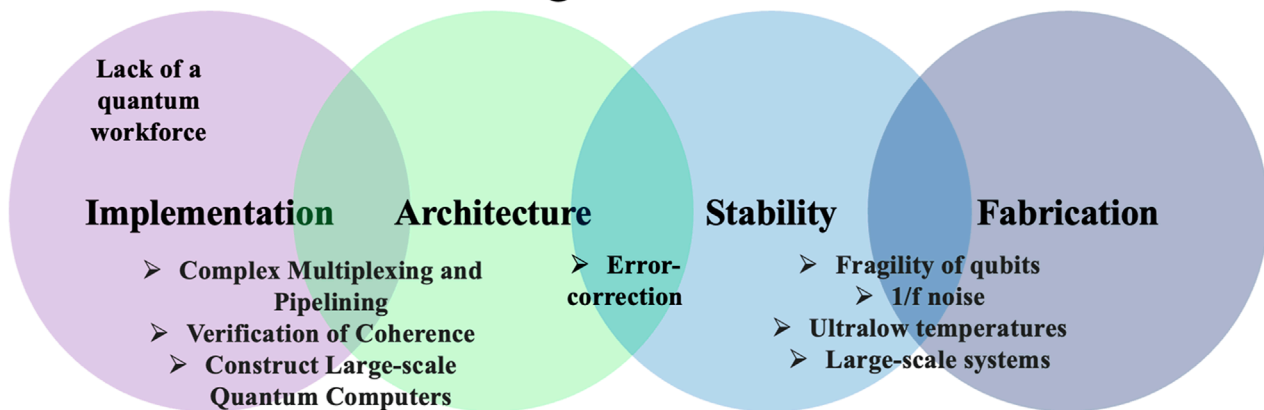


FIGURE 26

Illustrative depiction of market demands and challenges to insertion for quantum computing and related technologies. Information was accrued from <https://www.greyb.com/blog/quantum-computing-market-research>.

### 11.2.8 Quantum-based electronics

In earlier sections, we covered several subfields of electronics and devices that rely on novel quantum materials in great detail. Here, we very briefly cover a subset of these materials and devices where market information is available.

To this end, we examine spin-transfer torque magnetic random-access memory, that is, STT-MRAM. STT-MRAM is a nonvolatile memory that operates under sub-nanosecond and sub-picojoule conditions, providing major advantages over charge-based memories such as SRAM and DRAM (Puliyil et al., 2022; Quach et al., 2022). STT-RAM is a type of magnetoresistance RAM or MRAM.

This technology was first demonstrated as a viable commercial product by Hitachi, which produced a 32-Mbit STT-RAM in 2009 (Krizakova et al., 2022). By 2011, Qualcomm presented a 1 Mbit embedded STT-MRAM that was manufactured in TSMC's 45 nm LP technology (Wikipedia, 2022). In 2012, Everspin released the first commercially available DDR3 dual in-line memory module, which had a capacity of 64 Mb (Takemura et al., 2009). In 2019, Everspin started production for 28 nm 1 Gb STT-MRAM chips (Kim et al., 2011). Also in 2019, Intel demonstrated an STT-MRAM for L4-cache (Likharev and Semenov, 1991; Everspin, 2012). STT-MRAM continues to demonstrate more competitive operation speed, resistance consistency, and energy efficiency with excellent endurance (Everspin, 2019).

The MRAM market is projected to reach USD 7.2 B by 2027, growing at a CAGR of 32.7% over the analysis period of 2020–2027. China, the world's second-largest economy, is forecasted to reach a projected market size of USD 2.2 B by 2027 at a CAGR of 42.4% over the same analysis period (Tomshardware, 2022).

## 12 Challenges and outlook

The ultimate success of quantum technologies will rely on several concomitant achievements. Let us focus merely on quantum computing because many of the challenges that exist for market adoption by QC are faced by other quantum technologies.

First, all quantum technologies are based on quantum mechanics that we know to be inherently indeterministic in nature, and, therefore, problems are merely presented with degrees of probability as opposed to classical computers that deliver unambiguous solutions. As a result, quantum computers are highly specialized instruments that offer advantages for application to certain specialized problems.

Also, as we have described, QCs employ fragile qubits that are highly susceptible to decoherence from environmental factors, such as electrical, mechanical, and thermal noise, among other factors (e.g.,  $1/f$  noise) that can cause the collapse of the state function and create errors (Cao et al., 2020).



Because of these errors, it is estimated that 1,000 physical qubits are needed to make a single logical error-free qubit, a goal that has yet to be achieved. Hence, a commercially viable quantum computer is projected to require 200 logical qubits or some 200,000 physical qubits (Globe News Wire, 2023).

Figure 26 depicts market demands and challenges to market insertion. Market demands have been discussed obliquely thus far and include the need for early adoption by the finance and banking sectors with the continued adoption by medical, biomedical, and defense sectors. These can be enhanced by the formation of strategic alliances and the continued rise in commercial investment.

Challenges to insertion are more difficult to articulate because they expand over broad technical categories that include system architecture and topologies such as multiplexing and pipelining and the integration of quantum and classical components and subsystems, some of which require ultralow temperatures and others are ill-suited for such environs.

Physical challenges relate to the fragility of qubits, noise mitigation, and environmental controls. All play into error-correction stratagems and algorithms. Such constraints require innovative developments in fabrication processes, new materials, and software. Even the ability to measure a qubit's state accurately and reliably is a nontrivial exercise.

Additionally, the worldwide quantum workforce is presently ill-prepared to address the needs of the marketplace today or in the near future. The quantum workforce lacks individuals who are properly educated in the necessary physics, engineering, and materials science capable of supporting quantum technologies. This has led to a reluctance toward market insertion and adoption (Entanglementtech, 2022).

Finally, a fissure has formed between laboratories performing breakthrough research, investment firms, and the corporate ecosystem that is retarding the growth of global quantum markets. This fissure is widened by barriers to effective communication and knowledge transfer, leading to mistrust among these key stakeholders.

The concepts and information communicated here are indeed challenging for the scientific layperson to grasp. Notwithstanding,

we have endeavored to provide a prospectus that includes historical, foundational physics, innovative materials science, and applications-oriented insights that will guide the reader in obtaining a deeper appreciation and knowledge of quantum science and technologies.

## Author contributions

VH: Conceptualization, Writing—original draft, Writing—review and editing. PA: Conceptualization, Writing—original draft, Writing—review and editing.

## Funding

The author(s) declare that no financial support was received for the research, authorship, and/or publication of this article.

## Conflict of interest

The authors declare that the research was conducted in the absence of any commercial or financial relationships that could be construed as a potential conflict of interest.

The author(s) declared that they were an editorial board member of Frontiers, at the time of submission. This had no impact on the peer review process and the final decision.

## Publisher's note

All claims expressed in this article are solely those of the authors and do not necessarily represent those of their affiliated organizations, or those of the publisher, the editors and the reviewers. Any product that may be evaluated in this article, or claim that may be made by its manufacturer, is not guaranteed or endorsed by the publisher.

## References

- Agarwal, K., Martin, I., Lukin, M. D., and Demler, E. (2013). Polaronic model of two-level systems in amorphous solids. *Phys. Rev. B* 87, 144201. doi:10.1103/physrevb.87.144201
- Akhmerov, A. R., Dahlhaus, J. P., Hassler, F., Wimmer, M., and Beenakker, C. W. J. (2011). Quantized conductance at the Majorana phase transition in a disordered superconducting wire. *Phys. Rev. Lett.* 106 (5), 057001. doi:10.1103/physrevlett.106.057001
- Akyol, M., Jiang, W., Yu, G., Fan, Y., Gunes, M., Ekicibil, A., et al. (2016). Effect of heavy metal layer thickness on spin-orbit torque and current-induced switching in Hf/CoFeB/MgO structures. *Appl. Phys. Lett.* 109 (2). doi:10.1063/1.4958295
- Albertsson, D. I., Zahedinejad, M., Åkerman, J., Rodriguez, S., and Rusu, A. (2019). Compact macrospin-based model of three-terminal spin-Hall nano oscillators. *IEEE Trans. Magn.* 55, 1–8. doi:10.1109/tmag.2019.2925781
- Alicea, J. (2010). Majorana fermions in a tunable semiconductor device. *Phys. Rev. B* 81 (12), 125318. doi:10.1103/physrevb.81.125318
- Amunts, K., Ebell, C., Muller, J., Telefont, M., Knoll, A., and Lippert, T. (2016). The human brain project: creating a european research infrastructure to decode the human brain. *Neuron* 92 (3), 574–581. doi:10.1016/j.neuron.2016.10.046
- Amy, M., Glaudell, A. N., and Ross, N. J. (2020). Number-theoretic characterizations of some restricted Clifford+ T circuits. *Quantum* 4, 252. doi:10.22331/q-2020-04-06-252
- Anderson, B. P., and Kasevich, M. A. (1998). Macroscopic quantum interference from atomic tunnel arrays. *Science* 282 (5394), 1686–1689. doi:10.1126/science.282.5394.1686
- Ando, K., and Saitoh, E. (2010). Inverse spin-Hall effect in palladium at room temperature. *J. Appl. Phys.* 108 (11). doi:10.1063/1.3517131
- Antaios (2023). Antaios. Available at: <https://antaios.fr/-SOT-MRAM-#:~:text=SOT%20is%20based%20on%20spin,via%20the%20spin%20orbit%20interaction> (Accessed September 1, 22).
- Anton, S. M., Müller, C., Birenbaum, J. S., O'Kelley, S. R., Fefferman, A. D., Golubev, D. S., et al. (2012). Pure dephasing in flux qubits due to flux noise with spectral density scaling as  $1/f^\alpha$ . *Phys. Rev. B* 85 (22), 224505. doi:10.1103/physrevb.85.224505
- Apolloni, B., Carvalho, M. C., and De Falco, D. (1989). Quantum stochastic optimization. *Stoc. Proc. Appl.* 33 (2), 233–244. doi:10.1016/0304-4149(89)90040-9

- Apolloni, B., Cesa-Bianchi, N., and De Falco, D. (1988). "A numerical implementation of quantum annealing," in *Stochastic processes, physics and geometry, proceedings of the ascona-locarno conference*.
- Arnon, S., and Kedar, D. (2009). Non-line-of-sight underwater optical wireless communication network. *J. Opt. Soc. Am. A* 26, 530. doi:10.1364/josaa.26.000530
- Ariyoshi, S., Matsuo, H., Otani, C., Sato, H., Shimizu, H. M., and Kawase, K. (2005). "Characterization of an STJ-based direct detector of submillimeter waves," in *IEEE Transactions on Applied Superconductivity*, Vol. 15 (2), 920–923. doi:10.1109/TASC.2005.850119
- Arovas, D., Schrieffer, J. R., and Wilczek, F. (1984). Fractional statistics and the quantum Hall effect. *Phys. Rev. Lett.* 53, 722–723. doi:10.1103/physrevlett.53.722
- Asmussen, S. R. (2003). "Markov Chains." *Applied Probability and Queues. Stochastic Modelling and Applied Probability* 51, 3–8. doi:10.1007/0-387-21525-5\_1
- Aspect, A., Dalibard, J., and Roger, G. (1982). Experimental test of Bell's inequalities using time-varying analyzers. *Phys. Rev. Lett.* 49 (25), 1804–1807. doi:10.1103/physrevlett.49.1804
- Aspelmeyer, M., Bohm, H. R., Gyatso, T., Jennewein, T., Kaltenbaek, R., Lindenthal, M., et al. (2003). Long-distance free-space distribution of quantum entanglement. *Science* 301, 621–623. doi:10.1126/science.1085593
- Aumentado, J., Keller, M. W., Martinis, J. M., and Devoret, M. H. (2004). Nonequilibrium quasiparticles and 2e periodicity in single-Cooper-pair transistors. *Phys. Rev. Lett.* 92, 066802. doi:10.1103/physrevlett.92.066802
- Awad, A. A., Dürrenfeld, P., Houshang, A., Dvornik, M., Iacocca, E., Dumas, R. K., et al. (2017). Long-range mutual synchronization of spin Hall nano-oscillators. *Nat. Phys.* 13, 292–299. doi:10.1038/nphys3927
- Awschalom, D. D., and Flatte, M. E. (2007). Challenges for semiconductor spintronics. *Nat. Phys.* 3, 153–159. doi:10.1038/nphys551
- Baart, T. A., Shafiei, M., Fujita, T., Reichl, C., Wegscheider, W., and Vandersypen, L. M. K. (2016). Single-spin CCD. *Nat. Nanotechnol.* 11 (4), 330–334. doi:10.1038/nnano.2015.291
- Bader, K., Dengler, D., Lenz, S., Endeward, B., Jiang, S.-D., Neugebauer, P., et al. (2014). Room temperature quantum coherence in a potential molecular qubit. *Nat. Commun.* 5, 5304. doi:10.1038/ncomms6304
- Balantekin, A. B., and Takigawa, N. (1998). Quantum tunneling in nuclear fusion. *Rev. Mod. Phys.* 70 (1), 77–100. doi:10.1103/revmodphys.70.77
- Balasubramanian, G., Chan, I. Y., Kolesov, R., Al-Hmoud, M., Tisler, J., Shin, C., et al. (2008). Nanoscale imaging magnetometry with diamond spins under ambient conditions. *Nature* 455, 648–651. doi:10.1038/nature07278
- Balasubramanian, G., Neumann, P., Twitche, D., Markham, M., Kolesov, R., Mizuochi, N., et al. (2009). Ultralong spin coherence time in isotopically engineered diamond. *Nat. Mat.* 8, 383–387. doi:10.1038/nmat2420
- Ball, P. (2020). Physicists in China challenge Google's quantum advantage. *Nature* 588 (7838), 380. Bibcode:2020Natur.588.380B. doi:10.1038/d41586-020-03434-7
- Ballance, C. J., Harty, T. P., Linke, N. M., Sepiol, M. A., and Lucas, D. M. (2016). High-fidelity quantum logic gates using trapped-ion hyperfine qubits. *Phys. Rev. Lett.* 117, 060504. doi:10.1103/physrevlett.117.060504
- Bao, X. H., Xu, X. F., Li, C. M., Yuan, Z. S., Lu, C. Y., and Pan, J. W. (2012). Quantum teleportation between remote atomically ensemble quantum memories. *Proc. Natl. Acad. Sci. U. S. A.* 109, 20347–20351. doi:10.1073/pnas.1207329109
- Baranov, P. G., Bundakova, A. P., Soltamov, A. A., Orlinskii, S. B., Borovykh, I. V., Zondervan, R., et al. (2011). Silicon vacancy in SiC as a promising quantum system for single-defect and single-photon spectroscopy. *Phys. Rev. B* 83, 125203. doi:10.1103/physrevb.83.125203
- Baranov, P. G., Il'in, I. V., Mokhov, E. N., Muzafarova, M. V., Orlinskii, S. B., and Schmidt, J. (2005). EPR identification of the triplet ground state and photoinduced population inversion for a Si-C divacancy in silicon carbide. *JETP Lett.* 82, 441–443. doi:10.1134/1.2142873
- Barenco, A., Bennett, C. H., Cleve, R., DiVincenzo, D. P., Margolus, N., Shor, P., et al. (1995). Elementary gates for quantum computation. *Am. Phys. Soc. (APS)* 52 (5), 3457–3467. doi:10.1103/physreva.52.3457
- Barends, R., Kelly, J., Megrant, A., Sank, D., Jeffrey, E., Chen, Y., et al. (2013). Coherent Josephson qubit suitable for scalable quantum integrated circuits. *Phys. Rev. Lett.* 111 (8), 080502. doi:10.1103/physrevlett.111.080502
- Barends, R., Kelly, J., Megrant, A., Veitia, A., Sank, D., Jeffrey, E., et al. (2014a). Superconducting quantum circuits at the surface code threshold for fault tolerance. *Nature* 508, 500–503. doi:10.1038/nature13171
- Barends, R., Kelly, J., Megrant, A., Veitia, A., Sank, D., Jeffrey, E., et al. (2014b). Superconducting quantum circuits at the surface code threshold for fault tolerance. *Nature* 508, 500–503. doi:10.1038/nature13171
- Barrett, M. D., Chiaverini, J., Schaetz, T., Britton, J., Itano, W. M., Jost, J. D., et al. (2004). Deterministic quantum teleportation of atomic qubits. *Nature* 429, 737–739. doi:10.1038/nature02608
- Bars, I., and Terning, J. (2018) *Extra dimensions in space and time*. Springer, 27.
- Barthel, C., Reilly, D. J., Marcus, C. M., Hanson, M. P., and Gossard, A. C. (2009). Rapid single-shot measurement of a singlet–triplet qubit. *Phys. Rev. Lett.* 103, 160503. doi:10.1103/PhysRevLett.103.160503
- Bauer, G. E., Saitoh, E., and Van Wees, B. J. (2012). Spin caloritronics. *Nat. Mater.* 11 (5), 391–399. doi:10.1038/nmat3301
- Baumgratz, T., Cramer, M., and Plenio, M. B. (2014). Quantifying coherence. *Phys. Rev. Lett.* 113 (14), 140401. doi:10.1103/physrevlett.113.140401
- Beduz, C., Carravetta, M., Chen, J. Y. C., Concistrè, M., Denning, M., Frunzi, M., et al. (2012). Quantum rotation of ortho and para-water encapsulated in a fullerene cage. *Proc. Natl. Acad. Sci.* 109 (32), 12894–12898. doi:10.1073/pnas.1210790109
- Bell, J. S. (1964). On the einstein podolsky rosen paradox. *Phys. Phys. Fiz.* 1 (3), 195–200. doi:10.1103/physicsphysiquefizika.1.195
- Bell, J. S. (1987). *Speakable and unspeakable in quantum mechanics*. Cambridge University Press, 65.
- Bell, M. T., Paramanandam, J., Ioffe, L. B., and Gershenson, M. E. (2014a). Protected Josephson rhombus chains. *Phys. Rev. Lett.* 112 (16), 167001. doi:10.1103/physrevlett.112.167001
- Bell, M. T., Paramanandam, J., Ioffe, L. B., and Gershenson, M. E. (2014b). Protected Josephson rhombus chains. *Phys. Rev. Lett.* 112 (16), 167001. doi:10.1103/physrevlett.112.167001
- Bell, R. P. (1959). The tunnel effect correction for parabolic potential barriers. *Trans. Faraday Soc.* 55, 1–4. doi:10.1039/tf9595500001
- Bell, R. P. (1980). *The tunnel effect in chemistry*. London: Chapman & Hall. (Ronald.
- Benioff, P. (1980). The computer as a physical system: a microscopic quantum mechanical Hamiltonian model of computers as represented by Turing machines. *J. Stat. Phys.* 22, 563–591. doi:10.1007/bf01011339
- Benioff, P. (1982). Quantum mechanical hamiltonian models of turing machines. *J. Stat. Phys.* 29 (3), 515–546. doi:10.1007/BF01342185
- Benjamin, B. V., Gao, P., McQuinn, E., Choudhary, S., Chandrasekaran, A. R., Bussat, J. M., et al. (2014). Neurogrid: a mixed-analog-digital multichip system for large-scale neural simulations. *Proc. IEEE* 102 (5), 699–716. doi:10.1109/jproc.2014.2313565
- Bennett, C. H. (1973). Logical reversibility of computation. *IBM J. Res. Dev.* 17 (6), 525–532. doi:10.1147/rd.176.0525
- Bennett, C. H., and Brassard, G. (1984). in *Proceedings of IEEE international conference on computer, systems & signal processing* (IEEE), 175–179.
- Bennett, C. H., Brassard, G., Crépeau, C., Jozsa, R., Peres, A., and Wootters, W. K. (1993). Teleporting an unknown quantum state via dual classical and Einstein-Podolsky-Rosen channels. *Phys. Rev. Lett.* 70 (13), 1895–1899. doi:10.1103/physrevlett.70.1895
- Berger, L. (1996). Emission of spin waves by a magnetic multilayer traversed by a current. *Phys. Rev. B* 54 (13), 9353–9358. doi:10.1103/physrevb.54.9353
- Bermeister, A., Keith, D., and Culcer, D. (2014). Charge noise, spin-orbit coupling, and dephasing of single-spin qubits. *Appl. Phys. Lett.* 105, 192102. doi:10.1063/1.4901162
- Berrios, E., Gruebele, M., Shyshlov, D., Wang, L., and Babikov, D. (2012). High fidelity quantum gates with vibrational qubits. *J. Phys. Chem. A* 116 (46), 11347–11354. doi:10.1021/jp3055729
- Bez, R., Fantini, P., and Pirovano, A. (2019). "Historical review of semiconductor memories," in *Woodhead Publishing Series in Electronic and Optical Materials, Semiconductor Memories and Systems*. Editors A. Redaelli, and F. Pellizzer (Woodhead Publishing), 1–26.
- Bialczak, R. C., Ansmann, M., Hofheinz, M., Lucero, E., Neeley, M., O'Connell, A. D., et al. (2010). Quantum process tomography of a universal entangling gate implemented with Josephson phase qubits. *Nat. Phys.* 6, 409–413. doi:10.1038/nphys1639
- Biedenharn, L., Lieb, E., Simon, B., and Wilczek, F. (1990). The ancestry of the anyon. *Phys. Today* 43 (8), 90–91. doi:10.1063/1.2810672
- Binnig, G., and Rohrer, H. (1986). Scanning tunneling microscopy. *IBM J. Res. Dev.* 30 (4), 355–369. doi:10.1016/0039-6028(83)90716-1
- Blume-Kohout, R., Gamble, J. K., Nielsen, E., Rudinger, K., Mizrahi, J., Fortier, K., et al. (2017). Demonstration of qubit operations below a rigorous fault tolerance threshold with gate set tomography. *Nat. Commun.* 8, 14485. doi:10.1038/ncomms14485
- Boahen, K., Gao, P., McQuinn, E., Choudhary, S., Chandrasekaran, A. R., Bussat, J. M., et al. (2014). Neurogrid: a mixed-analog-digital multichip system for large-scale neural simulations. *Proc. IEEE* 102 (5), 699–716. doi:10.1109/jproc.2014.2313565
- Bohm, D., and Aharonov, Y. (1957). Discussion of experimental proof for the paradox of einstein, rosen, and podolsky. *Phys. Rev.* 108 (4), 1070–1076. doi:10.1103/physrev.108.1070

- Bohr, N. (1913a). I. On the constitution of atoms and molecules. *Phil. Mag.* 26, 1–25. doi:10.1080/14786441308634955
- Bohr, N. (1913b). On the constitution of atoms and molecules. Part II: systems containing only a single nucleus. *Phil. Mag.* 26 (153), 476–502. doi:10.1080/14786441308634993
- Bohr, N. (1913c). On the constitution of atoms and molecules. Part III: systems containing several nuclei. *Phil. Mag.* 26 (155), 857–875. doi:10.1080/14786441308635031
- Bommer, J. D. S., Zhang, H., Gül, Ö., Nijholt, B., Wimmer, M., Rybakov, F. N., et al. (2019). Spin-orbit protection of induced superconductivity in Majorana nanowires. *Phys. Rev. Lett.* 122, 187702. doi:10.1103/PhysRevLett.122.187702
- Bonn, D. (2020). *The physics of ice skating*. Available at: <https://www.nature.com/articles/d41586-019-03833-5>.
- Boschi, D., Branca, S., De Martini, F., Hardy, L., and Popescu, S. (1998). Experimental realization of teleporting an unknown pure quantum state via dual classical and einstein-podolsky-rosen channels. *Phys. Rev. Lett.* 80, 1121–1125. doi:10.1103/physrevlett.80.1121
- Bouchard, F., England, D., Bustard, P. J., Heshami, K., and Sussman, B. (2022). Quantum communication with ultrafast time-bin qubits. *PRX Quantum* 3 (1), 010332. doi:10.1103/prxquantum.3.010332
- Bouchard, F., Fickler, R., Boyd, R. W., and Karimi, E. (2017). High-dimensional quantum cloning and applications to quantum hacking. *Sci. Adv.* 3 (2), e1601915. doi:10.1126/sciadv.1601915
- Bouchard, F., Sit, A., Hufnagel, F., Abbas, A., Zhang, Y., Heshami, K., et al. (2018). Quantum cryptography with twisted photons through an outdoor underwater channel. *Opt. Express* 26 (17), 22563–22573. doi:10.1364/oe.26.022563
- Bouchiat, V., Vion, D., Joyez, P., Esteve, D., and Devoret, M. H. (1998). Quantum coherence with a single Cooper pair. *Phys. Scr.* 1998 (T76), 165. doi:10.1238/physica.topical.076a00165
- Bouland, A., and Aaronson, S. (2014). Generation of universal linear optics by any beam splitter. *Phys. Rev. A* 89 (6), 062316. doi:10.1103/physreva.89.062316
- Bouland, A., Mančinska, L., and Zhang, X. (2016). *Complexity classification of two-qubit commuting Hamiltonians*. arXiv preprint arXiv:1602.04145.
- Bouwmeester, D., Pan, J. W., Mattle, K., Eibl, M., Weinfurter, H., and Zeilinger, A. (1997a). Experimental quantum teleportation. *Nature* 390, 575–579. doi:10.1038/37539
- Bouwmeester, D., Pan, J. W., Mattle, K., Eibl, M., Weinfurter, H., and Zeilinger, A. (1997b). Experimental quantum teleportation. *Nature* 390 (6660), 575–579. doi:10.1038/37539
- Bouwmeester, D., Pan, J. W., Mattle, K., Eibl, M., Weinfurter, H., and Zeilinger, A. (1997c). Experimental quantum teleportation. *Nature* 390, 575–579. doi:10.1038/37539
- Bouwmeester, D., Pan, J. W., Mattle, K., Eibl, M., Weinfurter, H., and Zeilinger, A. (1997d). Experimental quantum teleportation. *Nature* 390, 575–579. doi:10.1038/37539
- Bowen, W. P., Treps, N., Buchler, B. C., Schnabel, R., Ralph, T. C., Bacher, H. A., et al. (2003). Experimental investigation of continuous-variable quantum teleportation. *Phys. Rev. A* 67, 032302. doi:10.1103/physreva.67.032302
- Braginsky, V. B., and Khalili, F. Y. (1996). Quantum nondemolition measurements: the route from toys to tools. *Rev. Mod. Phys.* 68 (1), 1–11. doi:10.1103/revmodphys.68.1
- Bravyi, S. B., and Kitaev, A. Y. (1998). *Quantum codes on a lattice with boundary*. Preprint at arXiv:quant-ph/9811052v1.
- Brendel, J., Gisin, N., Tittel, W., and Zbinden, H. (1999). Pulsed energy-time entangled twin-photon source for quantum communication. *Phys. Rev. Lett.* 82 (12), 2594–2597. doi:10.1103/physrevlett.82.2594
- Briegleb, H. J., Dür, W., Cirac, J. I., and Zoller, P. (1998). Quantum repeaters: the role of imperfect local operations in quantum communication. *Phys. Rev. Lett.* 81 (26), 5932–5935. doi:10.1103/physrevlett.81.5932
- Brogie, L. D. (1924). XXXV. A tentative theory of light quanta. *Lond. Edinb. Dublin Philosophical Mag. J. Sci.* 47 (278), 446–458. doi:10.1080/14786442408634378
- Brooks, P., Kitaev, A., and Preskill, J. (2013a). Protected gates for superconducting qubits. *Phys. Rev. A* 87 (5), 052306. doi:10.1103/physreva.87.052306
- Brooks, P., Kitaev, A., and Preskill, J. (2013b). Protected gates for superconducting qubits. *Phys. Rev. A* 87 (5), 052306. doi:10.1103/physreva.87.052306
- Brooks, M. (2024). *Quantum computing is taking on its biggest challenge: noise*. MIT Technology Review.
- Broome, M. A., Watson, T., Keith, D., Gorman, S., House, M., Keizer, J., et al. (2017a). High-fidelity single-shot singlet-triplet readout of precision-placed donors in silicon. *Phys. Rev. Lett.* 119, 046802. doi:10.1103/physrevlett.119.046802
- Broome, M. A., Watson, T., Keith, D., Gorman, S., House, M., Keizer, J., et al. (2017b). High-fidelity single-shot singlet-triplet readout of precision-placed donors in silicon. *Phys. Rev. Lett.* 119, 046802. doi:10.1103/physrevlett.119.046802
- Brown, J. (2000). *The quest for the quantum computer*. New York: Simon and Schuster.
- Bruzewicz, C. D., Chiaverini, J., McConnell, R., and Sage, J. M. (2019). Trapped-ion quantum computing: progress and challenges. *Appl. Phys. Rev.* 6 (2), 021314. doi:10.1063/1.5088164
- Bussi eres, F., Clausen, C., Tiranov, A., Korzh, B., Verma, V. B., Nam, S. W., et al. (2014a). Quantum teleportation from a telecom-wavelength photon to a solid-state quantum memory. *Nat. Phot.* 8, 775–778. doi:10.1038/nphoton.2014.215
- Bussi eres, F., Clausen, C., Tiranov, A., Korzh, B., Verma, V. B., Nam, S. W., et al. (2014b). Quantum teleportation from a telecom-wavelength photon to a solid-state quantum memory. *Nat. Photonics* 8 (10), 775–778. doi:10.1038/nphoton.2014.215
- Büttiker, M. (1987). Zero-current persistent potential drop across small-capacitance Josephson junctions. *Phys. Rev. B* 36 (7), 3548–3555. doi:10.1103/physrevb.36.3548
- Bylander, J., Gustavsson, S., Yan, F., Yoshihara, F., Harrabi, K., Fitch, G., et al. (2011). Noise spectroscopy through dynamical decoupling with a superconducting flux qubit. *Nat. Phys.* 7 (7), 565–570. doi:10.1038/nphys1994
- Cai, K., Yang, M., Ju, H., Wang, S., Ji, Y., Li, B., et al. (2017). Electric field control of deterministic current-induced magnetization switching in a hybrid ferromagnetic/ferroelectric structure. *Nat. Mater.* 16 (7), 712–716. doi:10.1038/nmat4886
- Callus, E., and Kok, P. (2021). Cumulative generation of maximal entanglement between spectrally distinct qubits using squeezed light. *Phys. Rev. A* 104 (5), 052407. doi:10.1103/physreva.104.052407
- Campagne-Ibarcq, P., Eickbusch, A., Touzard, S., Zalys-Geller, E., Frattini, N. E., Sivak, V. V., et al. (2020). Quantum error correction of a qubit encoded in grid states of an oscillator. *Nature* 584 (7821), 368–372. doi:10.1038/s41586-020-2603-3
- Canale, L., Comtet, J., Nigu es, A., Cohen, C., Clanet, C., Siria, A., et al. (2019). Nanorheology of interfacial water during ice gliding. *Phys. Rev. X* 9 (4), 041025. doi:10.1103/physrevx.9.041025
- Cao, H. J., and Song, H. S. (2007). Teleportation of a single qubit state via unique W state. *Int. J. Theor. Phys.* 46, 1636–1642. doi:10.1007/s10773-006-9301-2
- Cao, Y., Rushforth, A., Sheng, Y., Zheng, H., and Wang, K. (2019). Tuning a binary ferromagnet into a multistate synapse with spin-orbit-torque-induced plasticity. *Adv. Funct. Mater.* 29 (25), 1808104. doi:10.1002/adfm.201808104
- Cao, Y., Xing, G., Lin, H., Zhang, N., Zheng, H., and Wang, K. (2020). Prospect of spin-orbitronic devices and their applications. *IScience* 23 (10), 101614. doi:10.1016/j.isci.2020.101614
- Castelvecchi, D. (2017). Quantum computers ready to leap out of the lab in 2017. *Nature* 541 (7635), 9–10. doi:10.1038/541009a
- Catelan, G., Nigg, S. E., Girvin, S. M., Schoelkopf, R. J., and Glazman, L. I. (2012). Decoherence of superconducting qubits caused by quasiparticle tunneling. *Phys. Rev. B* 86 (18), 184514. doi:10.1103/physrevb.86.184514
- Catelan, G., Schoelkopf, R. J., Devoret, M. H., and Glazman, L. I. (2011). Relaxation and frequency shifts induced by quasiparticles in superconducting qubits. *Phys. Rev. B* 84 (6), 064517. doi:10.1103/physrevb.84.064517
- Chakravartula, V., Samiappan, D., Kumar, R., and Manjari, A. P. (2020). Implementation of quantum teleportation of photons across an air–water interface. *Opt. Quantum Electron.* 52, 1–10. doi:10.1007/s11082-020-02449-8
- Chatterjee, A., Stevenson, P., De Franceschi, S., Morello, A., de Leon, N. P., and Kuemmeth, F. (2021). Semiconductor qubits in practice. *Nat. Rev. Phys.* 3 (3), 157–177. doi:10.1038/s42254-021-00283-9
- Chen, J., Li, D., Liu, M., and Yang, Y. (2020). Bidirectional quantum teleportation by using a four-qubit GHZ state and two bell states. *IEEE Access* 8, 28925–28933. doi:10.1109/access.2020.2971973
- Chen, Y. A., Chen, S., Yuan, Z. S., Zhao, B., Chuu, C. S., Schmiedmayer, J., et al. (2008). Memory-builit quantum teleportation with photonic and atomic qubits. *Nat. Phys.* 4, 103–107. doi:10.1038/nphys832
- Chiesa, A., Macaluso, E., Petiziol, F., Wimberger, S., Santini, P., and Carretta, S. (2020). Molecular nanomagnets as qubits with embedded quantum-error correction. *J. Phys. Chem. Lett.* 11 (20), 8610–8615. doi:10.1021/acs.jpclett.0c02213
- Childs, A. M., Leung, D., Mančinska, L., and Ozols, M. (2010). *Characterization of universal two-qubit Hamiltonians*. arXiv preprint arXiv:1004.1645.
- Choi, J. G., Park, J., Kang, M. G., Kim, D., Rieh, J. S., Lee, K. J., et al. (2022). Voltage-driven gigahertz frequency tuning of spin Hall nano-oscillators. *Nat. Commun.* 13, 3783. doi:10.1038/s41467-022-31493-z
- Choudhury, B. S., and Dhara, A. (2016). A bidirectional teleportation protocol for arbitrary two-qubit state under the supervision of a third party. *Int. J. Theor. Phys.* 55, 2275–2285. doi:10.1007/s10773-015-2865-y
- Chow, J. M., DiCarlo, L., Gambetta, J. M., Motzoi, F., Frunzio, L., Girvin, S. M., et al. (2010). Optimized driving of superconducting artificial atoms for improved single-qubit gates. *Phys. Rev. A* 82 (4), 040305. doi:10.1103/physreva.82.040305



- Chow, J. M., Gambetta, J. M., Córcoles, A. D., Merkel, S. T., Smolin, J. A., Rigetti, C., et al. (2012). Universal quantum gate set approaching fault-tolerant thresholds with superconducting qubits. *Phys. Rev. Lett.* 109, 060501. doi:10.1103/PhysRevLett.109.060501
- Chow, J. M., Gambetta, J. M., Cross, A. W., Merkel, S. T., Rigetti, C., and Steffen, M. (2013). Microwave-activated conditional-phase gate for superconducting qubits. *New J. Phys.* 15, 115012. doi:10.1088/1367-2630/15/11/115012
- Chow, J. M., Gambetta, J. M., Magesan, E., Abraham, D. W., Cross, A. W., Johnson, B. R., et al. (2014). Implementing a strand of a scalable fault-tolerant quantum computing fabric. *Nat. Commun.* 5, 4015. doi:10.1038/ncomms5015
- Chow, J. M., Srinivasan, S. J., Magesan, E., Córcoles, A. D., Abraham, D. W., Gambetta, J. M., et al. (2015). Characterizing a four-qubit planar lattice for arbitrary error detection. *Quantum Inf. Comput.* XIII 9500, 315–323. doi:10.1117/12.2192740
- Christensen, B. G., Wilen, C. D., Opremcak, A., Nelson, J., Schlenker, F., Zimonick, C. H., et al. (2019). Anomalous charge noise in superconducting qubits. *Phys. Rev. B* 100, 140503. doi:10.1103/physrevb.100.140503
- Chuang, I. L., Gershenfeld, N., and Kubinec, M. (1998a). Experimental implementation of fast quantum searching. *Phys. Rev. Lett.* 80 (15), 3408–3411. doi:10.1103/physrevlett.80.3408
- Chuang, I. L., Gershenfeld, N., and Kubinec, M. (1998b). Experimental implementation of fast quantum searching. *Phys. Rev. Lett. Am. Phys. Soc.* 80 (15), 3408–3411. doi:10.1103/physrevlett.80.3408
- Chuang, I. L., and Yamamoto, Y. (1995). Simple quantum computer. *Phys. Rev. A* 52 (5), 3489–3496. doi:10.1103/physreva.52.3489
- Clausen, C., Usmani, I., Bussi eres, F., Sangouard, N., Afzelius, M., de Riedmatten, H., et al. (2011). Quantum storage of photonic entanglement in a crystal. *Nature* 469, 508–511. doi:10.1038/nature09662
- Commins, E. D. (2012). Electron spin and its history. *Annu. Rev. Nucl. Part. Sci.* 62, 133–157. doi:10.1146/annurev-nucl-102711-094908
- Cong, L., Wei, Z., Hua-bo, L., and Si-meng, W. (2017). Bidirectional quantum teleportation controlled by single-qutrit state. *Acta Phot. Sin.* 46 (5), 0527002.
- Conover, E. (2020). The new light-based quantum computer Jiuzhang has achieved quantum supremacy. *Sci. News*. Retrieved 2020-12-19. doi:10.1126/science.abe8770
- Constantin, M., and Yu, C. C. (2007). Microscopic model of critical current noise in Josephson junctions. *Phys. Rev. Lett.* 99, 207001. doi:10.1103/physrevlett.99.207001
- Coppersmith, D. (1994). *An approximate Fourier transform useful in quantum factoring*. Technical Report RC19642, IBM. arXiv:quant-ph/0201067.
- Cory, D. G., Fahmy, A. F., and Havel, T. F. (1996). “Nuclear magnetic resonance spectroscopy: an experimentally accessible paradigm for quantum computing” in *Proceedings of the Fourth Workshop on Physics and Computation*. Editors T. Toffoli, B. Biafore, and J. Leao (New England Complex Systems Institute), 87–91.
- Cory, D. G., Fahmy, A. F., and Havel, T. F. (1997). Ensemble quantum computing by NMR spectroscopy. *Proceedings of the National Academy of Sciences* 94 (5), 1634–1639. doi:10.1073/pnas.94.5.1634
- Cross, A. W., and Gambetta, J. M. (2015). Optimized pulse shapes for a resonator-induced phase gate. *Phys. Rev. A* 91, 032325. doi:10.1103/physreva.91.032325
- CT (2022a). Quantum hardware noise and advanced control. Available at: <https://www.ct.imm.cnr.it/?q=articles/quantum-hardware-noise-and-advanced-control>.
- CT (2022b). Quantum hardware noise and advanced control. Available at: <https://www.ct.imm.cnr.it/?q=articles/quantum-hardware-noise-and-advanced-control>.
- Cuff, T. M. (1993). *THE STM (scanning tunneling microscope) the forgotten contribution of Robert Francis Earhart to the discovery of quantum tunneling*.
- Danon, J., Chatterjee, A., Gyenis, A., and Kuemmeth, F. (2021). Protected solid-state qubits. *Appl. Phys. Lett.* 119 (26), 260502. doi:10.1063/5.0073945
- Das, N., Paul, G., and Majumdar, R. (2021). Quantum secure direct communication with mutual authentication using a single basis. *Int. J. Theor. Phys.* 60, 4044–4065. doi:10.1007/s10773-021-04952-4
- Davey, R. (2023). *How is China investing in quantum technology?* Available at: <https://www.a3oquantum.com/Article.aspx?ArticleID=435> (Accessed July 19, 2024).
- DBpedia (2023). *Bohr model*. Available at: [https://dbpedia.org/page/Bohr\\_model](https://dbpedia.org/page/Bohr_model) (Accessed March 1, 2023).
- Degen, C. L., Reinhard, F., and Cappellaro, P. (2017). Quantum sensing. *Rev. Mod. Phys.* 89 (3), 035002. doi:10.1103/revmodphys.89.035002
- De Graaf, S. E., Faoro, L., Burnett, J., Adamyan, A. A., Ya Tzalenchuk, A., Kubatkin, S. E., et al. (2018). Suppression of low-frequency charge noise in superconducting resonators by surface spin desorption. *Nat. Commun.* 9 (1), 1143. doi:10.1038/s41467-018-03577-2
- Demidov, V. E., Urazhdin, S., Ulrichs, H., Tiberkevich, V., Slavin, A., Baithar, D., et al. (2022). Magnetic nano-oscillator driven by pure spin current. *Nat. Mat.* 11 (2012), 1028–1031. doi:10.1038/nmat3459
- Demidov, V. E., Urazhdin, S., Zholud, A., Sadovnikov, A. V., and Demokritov, S. O. (2014). Nanoconstriction-based spin-Hall nano-oscillator. *Appl. Phys. Lett.* 105, 172410. doi:10.1063/1.4901027
- Dennis, E., Kitaev, A., Landahl, A., and Preskill, J. (2002). Topological quantum memory. *J. Math. Phys.* 43, 4452–4505. doi:10.1063/1.1499754
- de Riedmatten, H., Marcikic, I., Tittel, W., Zbinden, H., Collins, D., and Gisin, N. (2004). Long distance quantum teleportation in a quantum relay configuration. *Phys. Rev. Lett.* 92, 047904. doi:10.1103/physrevlett.92.047904
- Deutsch, D. (1985). Quantum theory, the Church-Turing principle and the universal quantum computer. *Proc. R. Soc. A* 400 (1818), 97–117. doi:10.1098/rspa.1985.0070
- Deutsch, D., and Jozsa, R. (1992). Rapid solution of problems by quantum computation. *Proc. R. Soc. Lond. Ser. A Math. Phys. Sci.* 439 (1907), 553–558. doi:10.1098/rspa.1992.0167
- Devoret, M. H., Wallraff, A., and Martinis, J. M. (2004). *Superconducting qubits: a short review*.
- Dewes, A., Ong, F. R., Schmitt, V., Lauro, R., Boulant, N., Bertet, P., et al. (2012). Characterization of a two-transmon processor with individual single-shot qubit readout. *Phys. Rev. Lett.* 108, 057002. doi:10.1103/PhysRevLett.108.057002
- DiCarlo, L., Chow, J. M., Gambetta, J. M., Bishop, L. S., Johnson, B. R., Schuster, D. I., et al. (2009). Demonstration of two-qubit algorithms with a superconducting quantum processor. *Nature* 460, 240–244. doi:10.1038/nature08121
- Didier, N., Sete, E. A., Combes, J., and da Silva, M. P. (2019a). AC flux sweet spots in parametrically modulated superconducting qubits. *Phys. Rev. Appl.* 12 (5), 054015. doi:10.1103/physrevapplied.12.054015
- Didier, N., Sete, E. A., Combes, J., and da Silva, M. P. (2019b). AC flux sweet spots in parametrically modulated superconducting qubits. *Phys. Rev. Appl.* 12 (5), 054015. doi:10.1103/physrevapplied.12.054015
- Didier, N., Sete, E. A., Combes, J., and da Silva, M. P. (2019c). AC flux sweet spots in parametrically modulated superconducting qubits. *Phys. Rev. Appl.* 12 (5), 054015. doi:10.1103/physrevapplied.12.054015
- Digital Strategy (2022a). *Digital strategy*. Available at: <https://digital-strategy.ec.europa.eu/en/policies/european-quantum-communication-infrastructure-euroqci>.
- Digital Strategy (2022b). *Digital strategy*. Available at: <https://digital-strategy.ec.europa.eu/en/policies/quantum>.
- Dirac, P. A. M. (1926). On the theory of quantum mechanics. *Proc. R. Soc. Lond. Ser. A, Contain. Pap. a Math. Phys. Character* 112 (762), 661–677. doi:10.1098/rspa.1926.0133
- Dirac, P. A. M. (1927). The quantum theory of the emission and absorption of radiation. *Proc. R. Soc. Lond. Ser. A, Contain. Pap. a Math. Phys. Character* 114 (767), 243–265. doi:10.1098/rspa.1927.0039
- DiVincenzo, D. (1995a). A two-bit gates are universal for quantum computation. *Phys. Rev. A* 51 (2), 1015–1022. doi:10.1103/PhysRevA.51.1015
- DiVincenzo, D. (1995b). Quantum computation. *Science* 270 (5234).
- DiVincenzo, D. P. (2000). The physical implementation of quantum computation. *Fortschritte der Physik Prog. Phys.* 48 (9), 771–783. doi:10.1002/1521-3978(200009)48:9<771::aid-prop771>3.0.co;2-e
- DiVincenzo, D. P. (2009). Fault-tolerant architectures for superconducting qubits. *Phys. Scr.* 2009 (T137), 014020. doi:10.1088/0031-8949/2009/t137/014020
- Dong, J., and Teng, J. F. (2008). Controlled teleportation of an arbitrary n-qudit state using nonmaximally entangled GHZ states. *Eur. Phys. J. D* 49, 129–134. doi:10.1140/epjd/e2008-00141-0
- Donohue, J. M., Agnew, M., Lavoie, J., and Resch, K. J. (2013). Coherent ultrafast measurement of time-bin encoded photons. *Phys. Rev. Lett.* 111 (15), 153602. doi:10.1103/physrevlett.111.153602
- Douçot, B., and Ioffe, L. B. (2012). Physical implementation of protected qubits. *Rep. Prog. Phys.* 75 (7), 072001. doi:10.1088/0034-4885/75/7/072001
- Douçot, B., and Vidal, J. (2002). Pairing of Cooper pairs in a fully frustrated Josephson-junction chain. *Phys. Rev. Lett.* 88 (22), 227005. doi:10.1103/physrevlett.88.227005
- Dr eau, A., Spinicelli, P., Maze, J. R., Roch, J. F., and Jacques, V. (2013). Single-shot readout of multiple nuclear spin qubits in diamond under ambient conditions. *Phys. Rev. Lett.* 110 (6), 060502. doi:10.1103/physrevlett.110.060502
- Duan, Y. J., Zha, X. W., Sun, X. M., and Xia, J. F. (2014a). Bidirectional quantum-controlled teleportation via a maximally seven-qubit entangled state. *Int. J. Theor. Phys.* 53, 2697–2707. doi:10.1007/s10773-014-2065-1
- Duan, Z., Smith, A., Yang, L., Youngblood, B., Lindner, J., Demidov, V. E., et al. (2014b). Nanowire spin torque oscillator driven by spin orbit torques. *Nat. Commun.* 5, 5616. doi:10.1038/ncomms6616
- Dumont, R. S., Rivlin, T., and Pollak, E. (2020). The relativistic tunneling flight time may be superluminal, but it does not imply superluminal signaling. *New J. Phys.* 22 (9), 093060. doi:10.1088/1367-2630/abb515

- Dürrenfeld, P., Awad, A. A., Houshang, A., Dumas, R. K., and Åkerman, J. (2017). A 20 nm spin Hall nano-oscillator. *Nanoscale* 9, 1285–1291. doi:10.1039/c6nr07903b
- Dutt, M. G., Childress, L., Jiang, L., Togan, E., Maze, J., Jelezko, F., et al. (2007). Quantum register based on individual electronic and nuclear spin qubits in diamond. *Science* 316 (5829), 1312–1316. doi:10.1126/science.1139831
- D-Wave Initiates Open Quantum Software Environment (2022a). *D-wave systems*. Archived from the original on 8 march 2021. Retrieved 24 Dec 2022.
- D-Wave Initiates Open Quantum Software Environment (2022b). *D-wave systems*. Archived from the original on 8 march 2022.
- Dwavesys (2022). Dwavesys. Available at: [https://docs.dwavesys.com/docs/latest/c\\_gs\\_2.html#eigenspectrum](https://docs.dwavesys.com/docs/latest/c_gs_2.html#eigenspectrum) (Accessed December 23, 22).
- Dynes, J. F., Takesue, H., Yuan, Z. L., Sharpe, A. W., Harada, K., Honjo, T., et al. (2009). Efficient entanglement distribution over 200 kilometers. *Opt. Express* 17, 11440–11449. doi:10.1364/oe.17.011440
- Egan, L., Debroy, D. M., Noel, C., Risinger, A., Zhu, D., Biswas, D., et al. (2020). Fault-tolerant operation of a quantum error-correction code. arXiv preprint arXiv:2009.11482.
- Ehrenfest, P. (1911). Welche Züge der Lichtquantenhypothese spielen in der Theorie der Wärmestrahlung eine wesentliche Rolle? [In which features of the light quantum hypothesis does thermal radiation play an essential role?]. *Ann. Phys.* 341 (11), 91–118. doi:10.1002/andp.19113411106
- Einstein, A. (1905a). Über einen die Erzeugung und Verwandlung des Lichtes betreffenden heuristischen Gesichtspunkt" (On a Heuristic Point of View about the Creation and Conversion of Light). *Ann. Phys.* 17 (6), 132–148. doi:10.1515/9783112596609
- Einstein, A. (1905b). Über die von der molekularkinetischen Theorie der Wärme geforderte Bewegung von in ruhenden Flüssigkeiten suspendierten Teilchen" (Investigations on the theory of Brownian Movement). *Ann. Phys.* 17 (4), 549–560.
- Einstein, A. (1905c). Zur elektrodynamik bewegter körper" (on the electrodynamics of moving bodies). *Ann. Phys.* 17 (10), 891–921. doi:10.1007/978-3-662-48039-7\_4
- Einstein, A. (1905d). Does the inertia of a body depend upon its energy-content. *Ann. Phys.* 18 (13), 639–641. doi:10.1002/andp.19053231314
- Einstein, A. (1905e). Die Grundlage der allgemeinen Relativitätstheorie (The basis of the general theory of relativity). *Ann. Phys.* 49, 769. doi:10.1007/978-3-662-48039-7\_12
- Einstein, A. (1905f). Zur elektrodynamik bewegter körper. *Ann. Phys.* 17 (10), 890–921. doi:10.1002/andp.19053221004
- Einstein, A., Podolsky, B., and Rosen, N. (1935). Can quantum-mechanical description of physical reality be considered complete? (PDF). *Phys. Rev.* 47 (10), 777–780. doi:10.1103/PhysRev.47.777
- Eisaman, M. D., Fan, J., Migdall, A., and Polyakov, S. V. (2011). Invited review article: single-photon sources and detectors. *Rev. Sci. Instrum.* 82, 071101. doi:10.1063/1.3610677
- Ekert, A. K., Huttner, B., Palma, G. M., and Peres, A. (1994). Eavesdropping on quantum-cryptographical systems. *Phys. Rev. A* 50 (2), 1047–1056. doi:10.1103/physreva.50.1047
- Eng, K., Ladd, T. D., Smith, A., Borselli, M. G., Kiselev, A. A., Fong, B. H., et al. (2015). Isotopically enhanced triple-quantum-dot qubit. *Sci. Adv.* 1, e1500214. doi:10.1126/sciadv.1500214
- Entanglementtech (2022). *Entanglementtech*. Available at: <https://entanglementtech.com/>.
- Epstein, J. M., Cross, A. W., Magesan, E., and Gambetta, J. M. (2014). Investigating the limits of randomized benchmarking protocols. *Phys. Rev. A* 89, 062321. doi:10.1103/physreva.89.062321
- Epstein, R. J., Mendoza, F. M., Kato, Y. K., and Awschalom, D. D. (2005). Anisotropic interactions of a single spin and dark-spin spectroscopy in diamond. *Nat. Phys.* 1 (2), 94–98. doi:10.1038/nphys141
- Escalera-Moreno, L., Baldoví, J. J., Gaita-Arino, A., and Coronado, E. (2018). Spin states, vibrations and spin relaxation in molecular nanomagnets and spin qubits: a critical perspective. *Chem. Sci.* 9 (13), 3265–3275. doi:10.1039/c7sc05464e
- Esposito, P., and Pedram, P. (2014). Quantum teleportation through noisy channels with multi-qubit GHZ states. *Quantum Inf. Process.* 13 (8), 1789–1811. doi:10.1007/s11128-014-0766-2
- Essential (2022). The 3 essential types of quantum computing-and their applications. Available at: <http://brainstormingbox.org/the-3-essential-types-of-quantum-computing-and-their-applications/> (Accessed December 23, 2022).
- Estimates (2022). *Estimates made from*. Available at: <https://www.researchnester.com/reports/quantum-computing-market/4910>.
- Everspin (2012). *Everspin ships first ST-MRAM memory with 500X performance of flash*. Computerworld (Accessed February 5, 2023).
- Everspin (2019). *Everspin enters pilot production phase for the world's First 28 nm 1 Gb STT-MRAM component* | Everspin. Available at: [www.everspin.com](http://www.everspin.com) (Accessed June 25, 2019).
- Fan, X., Celik, H., Wu, J., Ni, C., Lee, K. J., Lorenz, V. O., et al. (2014). Quantifying interface and bulk contributions to spin-orbit torque in magnetic bilayers. *Nat. Commun.* 5 (1), 3042. doi:10.1038/ncomms4042
- Fan, X., Wu, J., Chen, Y., Jerry, M. J., Zhang, H., and Xiao, J. Q. (2013). Observation of the nonlocal spin-orbital effective field. *Nat. Commun.* 4 (1), 1799. doi:10.1038/ncomms2709
- Fan, Y., Kou, X., Upadhyaya, P., Shao, Q., Pan, L., Lang, M., et al. (2016). Electric-field control of spin-orbit torque in a magnetically doped topological insulator. *Nat. Nanotechnol.* 11 (4), 352–359. doi:10.1038/nano.2015.294
- Faoro, L., Bergli, J., Altshuler, B. L., and Galperin, Y. M. (2005). Models of environment and T1 relaxation in Josephson charge qubits. *Phys. Rev. Lett.* 95, 046805. doi:10.1038/srep237868
- Faoro, L., and Ioffe, L. B. (2007). Microscopic origin of critical current fluctuations in large, small, and ultra-small area Josephson junctions. *Phys. Rev. B* 75, 132505. doi:10.1103/physrevb.75.132505
- Farhi, E., Goldstone, J., Gutmann, S., and Sipser, M. (2000). *Quantum computation by adiabatic evolution*. arXiv:quant-ph/0001106v1.
- Farquhar, E., and Hasler, P. (2006). "A field programmable neural array," in *IEEE international symposium on circuits and systems*, 4114–4117. doi:10.1109/ISCAS.2006.1693534
- Fattal, D., Diamanti, E., Inoue, K., and Yamamoto, Y. (2004). Quantum teleportation with a quantum dot single photon source. *Phys. Rev. Lett.* 92, 037904. doi:10.1103/physrevlett.92.037904
- Fedrizzi, A., Ursin, R., Herbst, T., Nespoli, M., Prevedel, R., Scheidl, T., et al. (2009). High-fidelity transmission of entanglement over a high-loss free-space channel. *Nat. Phys.* 5, 389–392. doi:10.1038/nphys1255
- Fell, J., and Axmacher, N. (2011). The role of phase synchronization in memory processes. *Nat. Rev. Neurosci.* 12, 105–118. doi:10.1038/nrn2979
- Feynman, R. (1982). Simulating physics with computers. *Int. J. Theor. Phys.* 21 (6/7), 467–488. doi:10.1007/BF02650179
- Feynman, R. P. (1986). Quantum mechanical computers. *Found. Phys.* 16 (6), 507–531. doi:10.1007/bf01886518
- Field, B., and Simula, T. (2018). Introduction to topological quantum computation with non-Abelian anyons. *Quantum Sci. Technol.* 3, 045004.
- Fink, D. G. (1975). *Electronic engineers handbook* (New York, NY: McGraw Hill).
- Fink, J. M. (2010). *Quantum nonlinearities in strong coupling circuit QED (Ph.D.)*. Zürich, Switzerland: ETH Zurich.
- First Quantum Satellite Successfully Launched (2016) Archived from the original on 18 march 2018. Austrian Academy of Sciences.
- Fortnow, L. (2003). One complexity theorist's view of quantum computing. *Theor. Comput. Sci.* 292 (3), 597–610. doi:10.1016/S0304-3975(01)00377-2
- Fortunebusinessinsights (2022). Fortunebusinessinsights. Available at: <https://www.fortunebusinessinsights.com/quantum-computing-market-104855>.
- Fowler, A. G., Mariantoni, M., Martinis, J. M., and Cleland, A. N. (2012a). Surface codes: towards practical large-scale quantum computation. *Phys. Rev. A* 86, 032324. doi:10.1103/physreva.86.032324
- Fowler, A. G., Stephens, A. M., and Groszkowski, P. (2009). High-threshold universal quantum computation on the surface code. *Phys. Rev. A* 80 (5), 052312. doi:10.1103/physreva.80.052312
- Fowler, A. G., Whiteside, A. C., and Hollenberg, L. C. (2012b). Towards practical classical processing for the surface code: timing analysis. *Phys. Rev. A* 86 (4), 042313. doi:10.1103/physreva.86.042313
- Fowler, R. H., and Nordheim, Dr. L. (1928). Electron emission in intense electric fields" (PDF). *Proc. R. Soc. A* 119 (781), 173–181. doi:10.1098/rspa.1928.0091
- Fredkin, E., and Toffoli, T. (1982). Conservative logic. *Int. J. Theor. Phys.* 21 (3–4), 219–253. doi:10.1007/BF01857727
- Freedman, S. J., and Clauser, J. F. (1972). Experimental test of local hidden-variable theories. *Phys. Rev. Lett.* 28 (14), 938–941. doi:10.1103/physrevlett.28.938
- Friis, N., Marty, O., Maier, C., Hempel, C., Holzäpfel, M., Jurcevic, P., et al. (2018). Observation of entangled states of a fully controlled 20-qubit system. *Phys. Rev. X* 8 (2), 021012. doi:10.1103/physrevx.8.021012
- Fukami, S., Zhang, C., DuttaGupta, S., Kurenkov, A., and Ohno, H. (2016). Magnetization switching by spin-orbit torque in an antiferromagnet-ferromagnet bilayer system. *Nat. Mater.* 15 (5), 535–541. doi:10.1038/nmat4566
- Fulara, H., Zahedinejad, M., Khymyn, R., Awad, A., Muralidhar, S., Dvornik, M., et al. (2019). Spin-orbit torque-driven propagating spin waves. *Sci. Adv.* 5, eaax8467. doi:10.1126/sciadv.aax8467



- Fulara, H., Zahedinejad, M., Khymyn, R., Dvornik, M., Fukami, S., Kanai, S., et al. (2020a). Giant voltage-controlled modulation of spin Hall nano-oscillator damping. *Nat. Commun.* 11, 4006. doi:10.1038/s41467-020-17833-x
- Fulara, H., Zahedinejad, M., Khymyn, R., Dvornik, M., Fukami, S., Kanai, S., et al. (2020b). Giant voltage-controlled modulation of spin Hall nano-oscillator damping. *Nat. Commun.* 11, 4006. doi:10.1038/s41467-020-17833-x
- Furusawa, A., Sørensen, J. L., Braunstein, S. L., Fuchs, C. A., Kimble, H. J., and Polzik, E. S. (1998). Unconditional quantum teleportation. *Science* 282, 706–709. doi:10.1126/science.282.5389.706
- Gali, A. (2011). Time-dependent density functional study on the excitation spectrum of point defects in semiconductors. *Phys. Status Solidi B* 248, 1337–1346. doi:10.1002/psb.201046254
- Gambetta, J. M., Chow, J. M., and Steffen, M. (2017). Building logical qubits in a superconducting quantum computing system. *Springer Sci. Bus. Media LLC* 3 (1), 2. doi:10.1038/s41534-016-0004-0
- Gamow, G. (1928). Zur quantentheorie des atomkernes. *Z. für Phys.* 51 (3–4), 204–212. doi:10.1007/bf01343196
- Gao, W. B., Fallahi, P., Togan, E., Delteil, A., Chin, Y., Miguel-Sanchez, J., et al. (2013). Quantum teleportation from a propagating photon to a solidstate spin qubit. *Nat. Commun.* 4, 2744. doi:10.1038/ncomms3744
- Geerlings, K. L. (2013). *Improving coherence of superconducting qubits and resonators*. Yale University.
- Gershenfeld, N. A., and Chuang, I. L. (1997). Bulk spin-resonance quantum computation. *Science* 275 (5298), 350–356. doi:10.1126/science.275.5298.350
- Gershenfeld, N. A., and Chuang, I. L. (1998). Quantum computing with molecules. *Sci. Am.* 278 (6), 66–71. doi:10.1038/scientificamerican0698-66
- Gertler, J. M., Baker, B., Li, J., Shirol, S., Koch, J., and Wang, C. (2021). Protecting a bosonic qubit with autonomous quantum error correction. *Nature* 590 (7845), 243–248. doi:10.1038/s41586-021-03257-0
- Giacomini, S., Sciarrino, F., Lombardi, E., and De Martini, F. (2002). Active teleportation of a quantum bit. *Phys. Rev. A* 66, 030302. doi:10.1103/physreva.66.030302
- Giovannetti, V., Lloyd, S., and Maccone, L. (2011). Advances in quantum metrology. *Nat. photonics* 5 (4), 222–229. doi:10.1038/nphoton.2011.35
- Gisin, N., Ribordy, G., Tittel, W., and Zbinden, H. (2002). Quantum cryptography. *Rev. Mod. Phys.* 74 (1), 145–195. doi:10.1103/revmodphys.74.145
- Gladchenko, S., Olaya, D., Dupont-Ferrier, E., Douçot, B., Ioffe, L. B., and Gershenson, M. E. (2009). Superconducting nanocircuits for topologically protected qubits. *Nat. Phys.* 5 (1), 48–53. doi:10.1038/nphys1151
- Globe News Wire (2023). *Globe news wire*. Available at: <https://www.globeewire.com/news-release/2022/10/10/2531311/0/en/Global-Magneto-Resistive-RAM-MRAM-Market-to-Reach-7-2-Billion-by-2027.html2/7/23>.
- Gobby, C., Yuan, A., and Shields, A. J. (2004). Quantum key distribution over 122 km of standard telecom fiber. *Appl. Phys. Lett.* 84 (19), 3762–3764. doi:10.1063/1.1738173
- Gollub, C., Troppmann, U., and de Vivie-Riedle, R. (2006). The role of anharmonicity and coupling in quantum computing based on vibrational qubits. *New J. Phys.* 8 (4), 48. doi:10.1088/1367-2630/8/4/048
- Golubov, A. A., Kupriyanov, M. Y., and Il'ichev, E. (2004). The current-phase relation in Josephson junctions. *Rev. Mod. Phys.* 76, 411–469. doi:10.1103/revmodphys.76.411
- Google (2022). *Google*. Available at: [https://www.google.com/search?q=quantum+cryptography+market+size&rlz=1C5CHFA\\_enUS943US965&oq=quantum+qencryption+market&aqs=chrome.2.69i57j0i22i3012j0i39014.16316j0j7&sourceid=chrome&ie=UTF-8](https://www.google.com/search?q=quantum+cryptography+market+size&rlz=1C5CHFA_enUS943US965&oq=quantum+qencryption+market&aqs=chrome.2.69i57j0i22i3012j0i39014.16316j0j7&sourceid=chrome&ie=UTF-8).
- Gottesman, D. (1998a). Theory of fault-tolerant quantum computation. *Phys. Rev. A* 57 (1), 127–137. doi:10.1103/physreva.57.127
- Gottesman, D. (1998b). *The Heisenberg representation of quantum computers*. arXiv:quant-ph/9807006v1.
- Gottesman, D. (2010). An introduction to quantum error correction and fault-tolerant quantum computation. In *Quantum information science and its contributions to mathematics. Proc. Symposia Appl. Math.* 68, 13–58.
- Gottesman, D., and Chuang, I. L. (1999). Demonstrating the viability of universal quantum computation using teleportation and single-qubit operations. *Nature* 402 (6760), 390–393. doi:10.1038/46503
- Green, T. J., Sastrawan, J., Uys, H., and Biercuk, M. J. (2013). Arbitrary quantum control of qubits in the presence of universal noise. *New J. Phys.* 15, 095004. doi:10.1088/1367-2630/15/9/095004
- Green, T. J., Uys, H., and Biercuk, M. J. (2012). High-order noise filtering in nontrivial quantum logic gates. *Phys. Rev. Lett.* 109, 020501. doi:10.1103/physrevlett.109.020501
- Greenberger, D. M., Horne, M. A., Shimony, A., and Zeilinger, A. (1990). Bell's theorem without inequalities. *Am. J. Phys.* 58 (12), 1131–1143. doi:10.1119/1.16243
- GREYB (2022). *Quantum computing market research*. Available at: <https://www.greyb.com/blog/quantum-computing-market-research/>.
- Grier, D., and Schaeffer, L. (2022). The classification of Clifford gates over qubits. *Quantum* 6, 734. doi:10.22331/q-2022-06-13-734
- Grimm, A., Frattini, N. E., Puri, S., Mundhada, S. O., Touzard, S., Mirrahimi, M., et al. (2020). Stabilization and operation of a Kerr-cat qubit. *Nature* 584 (7820), 205–209. doi:10.1038/s41586-020-2587-z
- Grover, L. K. (1996). “A fast quantum mechanical algorithm for database search,” in *Proceedings of the twenty-eighth annual ACM symposium on theory of computing. STOC '96* (Philadelphia, Pennsylvania, USA: Association for Computing Machinery), 212–219. arXiv:quant-ph/9605043. doi:10.1145/237814.237866
- Grover, L. K. (1996). in *Proceedings of the twenty-eighth annual ACM symposium on theory of computing* (New York: ACM), 212–219.
- Gulde, S., Riebe, M., Lancaster, G. P. T., Becher, C., Eschner, J., Häffner, H., et al. (2003). Implementation of the Deutsch-Jozsa algorithm on an ion-trap quantum computer. *Nature* 421 (6918), 48–50. doi:10.1038/nature01336
- Gündoğan, M., Ledingham, P. M., Kutluer, K., Mazzera, M., and De Riedmatten, H. (2015). Solid-state spin-wave quantum memory for time-bin qubits. *Phys. Rev. Lett.* 114 (23), 2380501. doi:10.1103/physrevlett.114.230501
- Gurney, R. W., and Condon, E. U. (1928). Wave mechanics and radioactive Disintegration. *Nature* 122 (3073), 439. doi:10.1038/122439a0
- Gustavsson, S., Yan, F., Catelani, G., Bylander, J., Kamal, A., Birenbaum, J., et al. (2016). Suppressing relaxation in superconducting qubits by quasiparticle pumping. *Science* 354, 1573–1577. doi:10.1126/science.aah5844
- Gyenis, A., Di Paolo, A., Koch, J., Blais, A., Houck, A. A., and Schuster, D. I. (2021). Moving beyond the transmon: noise-protected superconducting quantum circuits. *PRX Quantum* 2 (3), 030101. doi:10.1103/prxquantum.2.030101
- Hadfield, R. H. (2009). Single-photon detectors for optical quantum information applications. *Nat. Phot.* 3, 696–705. doi:10.1038/nphoton.2009.230
- Hales, L., and Hallgren, S. (2000). “An improved quantum Fourier transform algorithm and applications,” in *Proceedings 41st annual symposium on foundations of computer science*, 515–525. doi:10.1109/SFCS.2000.892139
- Hamilton, C. A., Kautz, R. L., Steiner, R. L., and Lloyd, F. L. (1985). A practical Josephson voltage standard at 1 V. *IEEE Electron Device Lett.* 6 (12), 623–625. doi:10.1109/edl.1985.26253
- Hanson, R., Kouwenhoven, L. P., Petta, J. R., Tarucha, S., and Vandersypen, L. M. (2007). Spins in few-electron quantum dots. *Rev. Mod. Phys.* 79 (4), 1217–1265. doi:10.1103/revmodphys.79.1217
- Harris, R., Johansson, J., Berkley, A. J., Johnson, M. W., Lanting, T., Han, S., et al. (2010a). Experimental demonstration of a robust and scalable flux qubit. *Phys. Rev. B* 81 (13), 134510. doi:10.1103/PhysRevB.81.134510
- Harris, R., Johansson, J., Berkley, A. J., Johnson, M. W., Lanting, T., Han, S., et al. (2010b). Experimental demonstration of a robust and scalable flux qubit. *Phys. Rev. B* 81 (13), 134510. doi:10.1103/PhysRevB.81.134510
- Harrow, A. W., Hassidim, A., and Lloyd, S. (2008). Quantum algorithm for linear systems of equations. *Phys. Rev. Lett.* 103 (15), 150502. arXiv:0811.3171. doi:10.1103/physrevlett.103.150502
- Harrow, A. W., and Montanaro, A. (2017). Quantum computational supremacy. *Nature* 549 (7671), 203–209. doi:10.1038/nature23458
- Harvey, A. H. (2017). “Properties of ice and supercooled water,” in *CRC handbook of chemistry and physics*. Editors W. M. Haynes, D. R. Lide, and T. J. Bruno 97th ed. (Boca Raton, FL: CRC Press).
- Harvey-Collard, P., Jacobson, N. T., Rudolph, M., Dominguez, J., Ten Eyck, G. A., Wendt, J. R., et al. (2017). Coherent coupling between a quantum dot and a donor in silicon. *Nat. Commun.* 8, 1029. doi:10.1038/s41467-017-01113-2
- Hassanpour, S., and Houshmand, M. (2016). Bidirectional teleportation of a pure EPR state by using GHZ states. *Quantum Inf. Process.* 15 (2), 905–912. doi:10.1007/s11128-015-1096-8
- Haxel, O., Jensen, J. H. D., and Suess, H. E. (1949). On the “magic numbers” in nuclear structure. *Phys. Rev.* 75 (11), 1766. doi:10.1103/physrev.75.1766.2
- He, Y., Gorman, S. K., Keith, D., Kranz, L., Keizer, J. G., and Simmons, M. Y. (2019). A two-qubit gate between phosphorus donor electrons in silicon. *Nature* 571, 371–375. doi:10.1038/s41586-019-1381-2
- Heisenberg, W. (1925). Über quantentheoretische Umdeutung kinematischer und mechanischer Beziehungen. *Z. für Phys.* 33, 879–893. doi:10.1007/bf01328377
- Hell, M., Leijnse, M., and Flensberg, K. (2017). Two-dimensional platform for networks of Majorana bound states. *Phys. Rev. Lett.* 118 (10), 107701. doi:10.1103/physrevlett.118.107701

- Hennighausen, Z., and Kar, S. (2021). Twistronics: a turning point in 2D quantum materials. *Electron. Struct.* 3 (1), 014004. doi:10.1088/2516-1075/abd957
- Henriques, F., Valenti, F., Charpentier, T., Lagoin, M., Gouriou, C., Martínez, M., et al. (2019). Phonon traps reduce the quasiparticle density in superconducting circuits. *Appl. Phys. Lett.* 115, 212601. doi:10.1063/1.5124967
- Hensen, B., Wei Huang, W., Yang, C. H., Wai Chan, K., Yoneda, J., Tantau, T., et al. (2020). A silicon quantum-dot-coupled nuclear spin qubit. *Nat. Nanotechnol.* 15, 13–17. doi:10.1038/s41565-019-0587-7
- Hirsch, J. E. (1999). Spin Hall effect. *Phys. Rev. Lett.* 83, 1834–1837. doi:10.1103/physrevlett.83.1834
- Holder, A. M., Osborn, K. D., Lobb, C. J., and Musgrave, C. B. (2013). Bulk and surface tunneling hydrogen defects in alumina. *Phys. Rev. Lett.* 111, 065901. doi:10.1103/physrevlett.111.065901
- Hong, W. Q. (2016). Asymmetric bidirectional controlled teleportation by using a seven-qubit entangled state. *Int. J. Theor. Phys.* 55, 384–387. doi:10.1007/s10773-015-2671-6
- Honjo, T., Nam, S. W., Takesue, H., Zhang, Q., Kamada, H., Nishida, Y., et al. (2008). Long-distance entanglement-based quantum key distribution over optical fiber. *Opt. Express* 16 (23), 19118–19126. doi:10.1364/oe.16.019118
- Horsman, C., Fowler, A., Devitt, S., and Meter, R. V. (2012). Surface code quantum computing by lattice surgery. *New J. Phys.* 14, 123011. doi:10.1088/1367-2630/14/12/123011
- Houck, A. A., Koch, J., Devoret, M. H., Girvin, S. M., and Schoelkopf, R. J. (2009). Life after charge noise: recent results with transmon qubits. *Quantum Inf. Process.* 8 (2–3), 105–115. doi:10.1007/s11128-009-0100-6
- Houck, A. A., Schreier, J. A., Johnson, B. R., Chow, J. M., Koch, J., Gambetta, J. M., et al. (2008). Controlling the spontaneous emission of a superconducting transmon qubit. *Phys. Rev. Lett.* 101 (8), 080502. doi:10.1103/physrevlett.101.080502
- HPC (2022). *HPC wire*. Available at: <https://www.hpcwire.com/off-the-wire/nec-develops-unit-cell-key-to-scaling-fully-connected-quantum-annealing-architecture/>.
- Hsieh, W. T., Bell, M., Lu, W. S., Zhang, W., Kamenov, P., Kalashnikov, K., et al. (2019). Symmetry protected qubits through fluxon pairing. *APS March Meet. Abstr.* 2019, A29–A005.
- Hsueh, Y. L., Büch, H., Tan, Y., Wang, Y., Hollenberg, L. C., Klimeck, G., et al. (2014). Spin-lattice relaxation times of single donors and donor clusters in silicon. *Phys. Rev. Lett.* 113 (24), 246406. doi:10.1103/physrevlett.113.246406
- Hu, C. (2022). IBM's biggest quantum chip yet could help solve the trickiest math problems. *Pop. Sci.*
- Hu, X., Liu, Y., and Nori, F. (2012). Strong coupling of a spin qubit to a superconducting stripline cavity. *Phys. Rev. B* 86, 035314. doi:10.1103/physrevb.86.035314
- Huang, P., and Hu, X. (2014). Electron spin relaxation due to charge noise. *Phys. Rev. B* 89, 195302. doi:10.1103/physrevb.89.195302
- Huang, W., Yang, C. H., Chan, K. W., Tantau, T., Hensen, B., Leon, R. C. C., et al. (2019). Fidelity benchmarks for two-qubit gates in silicon. *Nature* 569, 532–536. doi:10.1038/s41586-019-1197-0
- Huang, Z., Mundada, P. S., Gyenis, A., Schuster, D. I., Houck, A. A., and Koch, J. (2021). Engineering dynamical sweet spots to protect qubits from 1/f noise. *Phys. Rev. Appl.* 15 (3), 034065. doi:10.1103/physrevapplied.15.034065
- Huelga, S. F., Plenio, M. B., and Vaccaro, J. A. (2002). Remote control of restricted sets of operations: teleportation of angles. *Phys. Rev. A* 65 (4), 042316. doi:10.1103/physreva.65.042316
- Humphreys, P. C., Metcalf, B. J., Spring, J. B., Moore, M., Jin, X. M., Barbieri, M., et al. (2013). Linear optical quantum computing in a single spatial mode. *Phys. Rev. Lett.* 111 (15), 150501.
- Hund, F. (1927). Zur deutung der molekelspektren. i. *Z. für Phys.* 40 (10), 742–764. doi:10.1007/bf01400234
- Huo, M., Qin, J., Cheng, J., Yan, Z., Qin, Z., Su, X., et al. (2018). Deterministic quantum teleportation through fiber channels. *Sci. Adv.* 4 (10), eaas9401. doi:10.1126/sciadv.aas9401
- IBM (2016). *IBM makes quantum computing available on IBM Cloud*. Available at: [www-03.ibm.com](http://www-03.ibm.com) (Accessed May 4, 2016).
- Iedema, M. J., Dresser, M. J., Doering, D. L., Rowland, J. B., Hess, W. P., Tsekouras, A. A., et al. (1998). Ferroelectricity in water ice. *J. Phys. Chem. B* 102 (46), 9203–9214. doi:10.1021/jp982549e
- Igata, K., and Yamamoto, Y. (1988). “Quantum mechanical computers with single atom and photon fields,” in *International Conference on Quantum Electronics*. Editors H. Inaba, T. Yajima, and T. Ikegami (Optica Publishing Group), Tu14.
- IMEC (2023). IMEC enters the race to unleash quantum computing with silicon qubits. Available at: [www.imec-int.com](http://www.imec-int.com) (Accessed March 10, 2023).
- Indico (2022). *Indico*. Available at: [https://indico.fnal.gov/event/44309/contributions/191634/attachments/132006/162964/AMatos\\_De choreneMechs.pdf](https://indico.fnal.gov/event/44309/contributions/191634/attachments/132006/162964/AMatos_De choreneMechs.pdf) (Accessed June 1, 2022).
- Innovationcloud (2022). *Innovationcloud*. Available at: <https://innovationcloud.com/blog/what-is-quantum-technology-and-how-it-will-impact-our-future.html>.
- Intel Invests US\$50 Million to Advance Quantum Computing (2022). *Intel newsroom*. Intel Newsroom.
- Ioffe, L. B., and Feigel'man, M. V. (2002). Possible realization of an ideal quantum computer in Josephson junction array. *Phys. Rev. B* 66 (22), 224503. doi:10.1103/physrevb.66.224503
- Ioffe, L. B., Feigel'man, M. V., Ioselevich, A., Ivanov, D., Troyer, M., and Blatter, G. (2002). Topologically protected quantum bits using Josephson junction arrays. *Nature* 415 (6871), 503–506. doi:10.1038/415503a
- Iogansen, L. V. (1964). The possibility of resonance transmission of electrons in crystals through a system of barriers. *Sov. Phys. JETP* 18 (1), 146–150.
- Ion Trap Quantum Computing (2023). *Ion trap quantum computing*. Available at: <https://www.physics.ox.ac.uk/research/group/ion-trap-quantum-computing> (Accessed April 2, 2023).
- Iyengar, S. S., Kumar, K. J., and Mastriani, M. (2020). *Bidirectional teleportation for underwater quantum communications*. arXiv preprint arXiv:2009.04241.
- Jackson, J. D. (1987). The impact of special relativity on theoretical physics. *Phys. Today* 40 (5), 34–42. doi:10.1063/1.881108
- Jafferis, D., Zlokapa, A., Lykken, J. D., Kolchmeyer, D. K., Davis, S. I., Lauk, N., et al. (2022). Traversable wormhole dynamics on a quantum processor. *Nature* 612 (7938), 51–55. doi:10.1038/s41586-022-05424-3
- Jahnke, K. D., Naydenov, B., Teraji, T., Koizumi, S., Umeda, T., Isoya, J., et al. (2012). *Long coherence time of spin qubits in  $^{12}\text{C}$  enriched polycrystalline CVD diamond*. arXiv preprint arXiv:1206.4260.
- Jain, B. K. (2009). *Digital electronics - a modern approach by B K jain*.
- Jain, S. (2014). *Fundamentals of physical geology*. New Delhi, India: Springer India.
- Jaklevic, R. C., Lambe, J., Silver, A. H., and Mercereau, J. E. (1964). Quantum interference effects in Josephson tunneling. *Phys. Rev. Lett.* 12 (7), 159–160. doi:10.1103/physrevlett.12.159
- Jakobi, I., Momenzadeh, S. A., De Oliveira, F. F., Michl, J., Ziem, F., Schreck, M., et al. (2016). Efficient creation of dipolar coupled nitrogen-vacancy spin qubits in diamond. *J. Phys. Conf. Ser.* 752 (1), 012001. doi:10.1088/1742-6596/752/1/012001
- Jamali, M., Lee, J. S., Jeong, J. S., Mahfouzi, F., Lv, Y., Zhao, Z., et al. (2015). Giant spin pumping and inverse spin Hall effect in the presence of surface and bulk spin-orbit coupling of topological insulator Bi<sub>2</sub>Se<sub>3</sub>. *Nano Lett.* 15 (10), 7126–7132. doi:10.1021/acs.nanolett.5b03274
- Jelesko, F., Gaebel, T., Popa, I., Gruber, A., and Wrachtrup, J. (2004). Observation of coherent oscillations in a single electron spin. *Phys. Rev. Lett.* 92, 076401. doi:10.1103/physrevlett.92.076401
- Jin, X. M., Ren, J. G., Yang, B., Yi, Z. H., Zhou, F., Xu, X. F., et al. (2010). Experimental freespace quantum teleportation. *Nat. Phot.* 4, 376–381. doi:10.1038/nphoton.2010.87
- Jones, C., Fogarty, M. A., Morello, A., Gyure, M. F., Dzurak, A. S., and Ladd, T. D. (2018). Logical qubit in a linear array of semiconductor quantum dots. *Phys. Rev. X* 8, 021058. doi:10.1103/physrevx.8.021058
- Kalashnikov, K., Hsieh, W. T., Zhang, W., Lu, W. S., Kamenov, P., Di Paolo, A., et al. (2020). Bifluxon: fluxon-parity-protected superconducting qubit. *PRX Quantum* 1 (1), 010307. doi:10.1103/prxquantum.1.010307
- Kan, M. (2019). *Google claims quantum computing achievement, IBM says not so fast*. PCMag.
- Kane, B. E. (1998). A silicon-based nuclear spin quantum computer. *nature* 393 (6681), 133–137. doi:10.1038/30156
- Karlsson, A., and Bourennane, M. (1998). Quantum teleportation using three-particle entanglement. *Phys. Rev. A* 58, 4394–4400. doi:10.1103/physreva.58.4394
- Khaetskii, A. V., and Nazarov, Y. V. (2001). Spin-flip transitions between Zeeman sublevels in semiconductor quantum dots. *Phys. Rev. B* 64, 125316. doi:10.1103/PhysRevB.64.125316
- Kim, J. P., Kim, T., Wuyang, H., Rao, H. M., Kangho, L., Zhu, X., et al. (2011). “San diego, CA, USA,” in *A 45nm 1Mb embedded STT-MRAM with design techniques to minimize read-disturbance*. 2011 Symposium on VLSI circuits (VLSIC). *ieeexplore.ieee.org*. Qualcomm Inc. Archived from the original on 1 July 2017. Retrieved 2/5/2023.
- Kim, Y. H., Kulik, S. P., and Shih, Y. (2001). Quantum teleportation of a polarization state with a complete bell-state measurement. *Phys. Rev. Lett.* 86, 1370–1373. doi:10.1103/physrevlett.86.1370
- Kimble, H. J. (2008). The quantum internet. *Nature* 453, 1023–1030. doi:10.1038/nature07127

- Kiselev, S. I., Sankey, J. C., Krivorotov, I. N., Emley, N. C., Schoelkopf, R. J., Buhrman, R. A., et al. (2003). Microwave oscillations of a nanomagnet driven by a spin-polarized current. *nature* 425 (6956), 380–383. doi:10.1038/nature01967
- Kitaev, A. Y. (2003). Fault-tolerant quantum computation by anyons. *Ann. Phys.* 303 (1), 2–30. doi:10.1016/s0003-4916(02)00018-0
- Kitaev, A. (1997). Fault-tolerant quantum computation by anyons. *Ann. Phys.* 303 (1), 2–30. doi:10.1016/s0003-4916(02)00018-0
- Kjaergaard, M., Schwartz, M. E., Braumüller, J., Krantz, P., Wang, J. I. J., Gustavsson, S., et al. (2020). Superconducting qubits: current state of play. *Annu. Rev. Condens. Matter Phys.* 11, 369–395. doi:10.1146/annurev-conmatphys-031119-050605
- Klots, A. R., and Ioffe, L. B. (2021). Set of holonomic and protected gates on topological qubits for a realistic quantum computer. *Phys. Rev. B* 104 (14), 144502. doi:10.1103/physrevb.104.144502
- Knill, E., Laflamme, R., Martinez, R., and Tseng, C. H. (2000). An algorithmic benchmark for quantum information processing. *Nature* 404, 368–370. doi:10.1038/35006012
- Knill, E., Laflamme, R., and Milburn, G. J. (2001). A scheme for efficient quantum computation with linear optics. *Nature* 409 (6816), 46–52. doi:10.1038/35051009
- Kobayashi, T., Salfi, J., Chua, C., Van Der Heijden, J., House, M. G., Culcer, D., et al. (2021). Engineering long spin coherence times of spin-orbit qubits in silicon. *Nat. Mater.* 20 (1), 38–42. doi:10.1038/s41563-020-0743-3
- Koch, J., Yu, T. M., Gambetta, J., Houck, A. A., Schuster, D. I., Majer, J., et al. (2007). Charge-insensitive qubit design derived from the Cooper pair box. *Phys. Rev. A* 76 (4), 042319. doi:10.1103/physreva.76.042319
- Kocher, C., and Commins, E. (1967). Polarization correlation of photons emitted in an atomic cascade. *Phys. Rev. Lett. - Phys. Rev. Lett.* 18, 575–577. doi:10.1103/PhysRevLett.18.575
- Koehl, W. F., Buckley, B. B., Heremans, F. J., Calusine, G., and Awschalom, D. D. (2011). Room temperature coherent control of defect spin qubits in silicon carbide. *Nature* 479 (7371), 84–87. doi:10.1038/nature10562
- Korzh, B., Walenta, N., Lunghi, T., Gisin, N., and Zbinden, H. (2014). Free-running InGaAs single photon detector with 1 dark count per second at 10% efficiency. *Appl. Phys. Lett.* 104, 081108. doi:10.1063/1.4866582
- Krantz, P., Kjaergaard, M., Yan, F., Orlando, T. P., Gustavsson, S., and Oliver, W. D. (2019). A quantum engineers guide to superconducting qubits. *Appl. Phys. Rev.* 6, 021318. doi:10.1063/1.5089550
- Krauter, H., Salart, D., Muschik, C. A., Petersen, J. M., Shen, H., Fernholz, T., et al. (2013). Deterministic quantum teleportation between distant atomic objects. *Nat. Phys.* 9, 400–404. doi:10.1038/nphys2631
- Kringhøj, A., Casparis, L., Hell, M., Larsen, T. W., Kuemmeth, F., Leijnse, M., et al. (2018). Anharmonicity of a superconducting qubit with a few-mode Josephson junction. *Phys. Rev. B* 97 (6), 060508. doi:10.1103/physrevb.97.060508
- Krizakova, V., Perumkunnil, M., Couet, S., Gambardella, P., and Garello, K. (2022). Spin-orbit torque switching of magnetic tunnel junctions for memory applications. *J. Magnetism Magnetic Mater.* 562, 169692. doi:10.1016/j.jmmm.2022.169692
- Krogstrup, P., Ziino, N. L. B., Chang, W., Albrecht, S. M., Madsen, M. H., Johnson, E., et al. (2015). Epitaxy of semiconductor–superconductor nanowires. *Nat. Mater.* 14 (4), 400–406. doi:10.1038/nmat4176
- Kruglyak, V. V., Demokritov, S. O., and Grundler, D. (2010). Magnonics. *J. Phys. D Appl. Phys.* 43 (26), 264001. doi:10.1088/0022-3727/43/26/264001
- Kuate Defo, R., Nguyen, H., Ku, M. J., and Rhone, T. D. (2021). Methods to accelerate high-throughput screening of atomic qubit candidates in van der Waals materials. *J. Appl. Phys.* 129 (22), 225105. doi:10.1063/5.0048833
- Kuhlmann, A. V., Houel, J., Ludwig, A., Greuter, L., Reuter, D., Wieck, A. D., et al. (2013). Charge noise and spin noise in a semiconductor quantum device. *Nat. Phys.* 9, 570–575. doi:10.1038/nphys2688
- Kumar, P., Sendelbach, S., Beck, M., Freeland, J., Wang, Z., Wang, H., et al. (2016). Origin and reduction of 1/f magnetic flux noise in superconducting devices. *Phys. Rev. Appl.* 6, 041001. doi:10.1103/physrevapplied.6.041001
- Kurenkov, A., DuttaGupta, S., Zhang, C., Borders, W. A., Fukami, S., and Ohno, H. (2017). “Spin-orbit torque memristor, operated by pulsed currents,” in *JSAP annual meetings extended abstracts the 64th JSAP spring meeting 2018* (The Japan: Society of Applied Physics), 2150.
- Kurtsiefer, C., Zarda, P., Halder, M., Weinfurter, H., Gorman, P. M., Tapster, P. R., et al. (2002). Quantum cryptography: a step towards global key distribution. *Nature* 419, 450. doi:10.1038/419450a
- Kuzmanović, M., Dvir, T., Leboeuf, D., Ilić, S., Haim, M., Möckli, D., et al. (2022). Tunneling spectroscopy of few-monolayer NbSe<sub>2</sub> in high magnetic fields: triplet superconductivity and Ising protection. *Phys. Rev. B* 106 (18), 184514. doi:10.1103/physrevb.106.184514
- Kwiat, P. G., Berglund, A. J., Altepeter, J. B., and White, A. G. (2000). Experimental verification of decoherence-free subspaces. *Science* 290 (5491), 498–501. doi:10.1126/science.290.5491.498
- Ladd, T. D., Jelezko, F., Laflamme, R., Nakamura, Y., Monroe, C., and O’Brien, J. L. (2010). Quantum computers. *Nature* 464, 45–53. doi:10.1038/nature08812
- Lambert, H. N. J., Rueda, A., Sedlmeir, F., and Schwefel, H. G. (2020a). Quantum information technologies: coherent conversion between microwave and optical photons—an overview of physical implementations (adv. Quantum technol. 1/2020). *Adv. Quantum Technol.* 3, 1900077. doi:10.1002/quote.202070011
- Lambert, N. J., Rueda, A., Sedlmeir, F., and Schwefel, H. G. (2020b). Coherent conversion between microwave and optical photons—an overview of physical implementations. *Adv. Quantum Technol.* 3 (1), 1900077. doi:10.1002/quote.201900077
- Landry, O., van Houwelingen, J. A. W., Beveratos, A., Zbinden, H., and Gisin, N. (2007). Quantum teleportation over the Swisscom telecommunication network. *J. Opt. Soc. Am. B* 24, 398–403. doi:10.1364/josab.24.000398
- Lawler, G. F. (2006). *Introduction to stochastic processes*. 2nd ed. New York: Chapman & Hall/CRC Press. doi:10.1201/9781315273600
- Lawrie, W. I. L., Rimbach-Russ, M., Riggelen, F. V., Hendrickx, N. W., Snoo, S. D., Sammak, A., et al. (2023). Simultaneous single-qubit driving of semiconductor spin qubits at the fault-tolerant threshold. *Nat. Commun.* 14 (1), 3617
- Lawrie, W. I. L., Russ, M., van Riggelen, F., Hendrickx, N. W., de Snoo, S. L., Sammak, A., et al. (2021). *Simultaneous driving of semiconductor spin qubits at the fault-tolerant threshold*. arXiv preprint arXiv:2109.07837.
- Lee, H. Y., Chen, P. S., Wu, T. Y., Chen, Y. S., Wang, C. C., Tzeng, P. J., et al. (2008). “Low power and high-speed bipolar switching with a thin reactive Ti buffer layer in robust HfO<sub>2</sub> based RRAM,” in *2008 IEEE international electron devices meeting*, 1–4.
- Lee, N., Benichi, H., Takeno, Y., Takeda, S., Webb, J., Huntington, E., et al. (2011). Teleportation of nonclassical wave packets of light. *Science* 332, 330–333. doi:10.1126/science.1201034
- Lee, T. H. (2003) *The design of CMOS radio-frequency integrated circuits (PDF)*. Cambridge University Press.
- Leek, P. J., Filipp, S., Maurer, P., Baur, M., Bianchetti, R., Fink, J. M., et al. (2009). Using sideband transitions for two-qubit operations in superconducting circuits. *Phys. Rev. B* 79, 180511. doi:10.1103/physrevb.79.180511
- Letzter, R. (2020). China claims fastest quantum computer in the world. *Lives Sci.* 11.
- Levenson-Falk, E. M., Kos, F., Vijay, R., Glazman, L., and Siddiqi, I. (2014). Single-quasiparticle trapping in aluminum nanobridge Josephson junctions. *Phys. Rev. Lett.* 112, 047002. doi:10.1103/physrevlett.112.047002
- Levy, J. (2002). Universal quantum computation with spin-1/2 pairs and Heisenberg exchange. *Phys. Rev. Lett.* 89 (14), 147902. doi:10.1103/physrevlett.89.147902
- Li, R., Petit, L., Franke, D. P., Dehollain, J. P., Helsen, J., Steudtner, M., et al. (2018). A crossbar network for silicon quantum dot qubits. *Sci. Adv.* 4, eaar3960. doi:10.1126/sciadv.aar3960
- Li, Y., Edmonds, K. W., Liu, X., Zheng, H., and Wang, K. (2019). Manipulation of magnetization by spin-orbit torque. *Adv. Quantum Technol.* 2 (1–2), 1800052. doi:10.1002/quote.201800052
- Li, Y. H., and Jin, X. M. (2016). Bidirectional controlled teleportation by using nine-qubit entangled state in noisy environments. *Quantum Inf. Process.* 15 (2), 929–945. doi:10.1007/s11128-015-1194-7
- Li, Y. H., Li, X. L., Nie, L. P., and Sang, M. H. (2016). Quantum teleportation of three and four-qubit state using multi-qubit cluster states. *Int. J. Theor. Phys.* 55, 1820–1823. doi:10.1007/s10773-015-2821-x
- Li, Y. H., Li, X. L., Sang, M. H., Nie, Y. Y., and Wang, Z. S. (2013). Bidirectional controlled quantum teleportation and secure direct communication using five-qubit entangled state. *Quantum Inf. Process.* 12, 3835–3844. doi:10.1007/s11128-013-0638-1
- Lidar, D. A., Chuang, I. L., and Whaley, K. B. (1998). Decoherence-free subspaces for quantum computation. *Phys. Rev. Lett.* 81 (12), 2594–2597. doi:10.1103/physrevlett.81.2594
- Likharev, K. K., and Semenov, V. K. (1991). RSFQ logic/memory family: a new Josephson-junction technology for sub-terahertz-clock-frequency digital systems. *IEEE Trans. Appl. Supercond.* 1 (1), 3–28. doi:10.1109/77.80745
- Lilienfeld, J. E. (1930). Method and apparatus for controlling electric current. *U. S. Pat. no. 1 745, 175*.
- Lim, C. C. W., Curty, M., Walenta, N., Xu, F., and Zbinden, H. (2014). Concise security bounds for practical decoy-state quantum key distribution. *Phys. Rev. A* 89, 022307. doi:10.1103/physreva.89.022307
- Lin, W., Pollard, S. D., Guo, R., Yoong, H. Y., Chen, S., Wang, H., et al. (2018). Tuning of current-induced effective magnetic field through Rashba effect engineering in hybrid multiferroic structures. *NPG Asia Mater.* 10 (8), 740–748. doi:10.1038/s41427-018-0069-7



- Liu, L., Lee, O. J., Gudmundsen, T. J., Ralph, D. C., and Buhrman, R. A. (2012a). Current-induced switching of perpendicularly magnetized layers using spin torque from the spin Hall effect. *Phys. Rev. Lett.* 109 (9), 096602. doi:10.1103/physrevlett.109.096602
- Liu, L., Pai, C. F., Li, Y., Tseng, H. W., Ralph, D. C., and Buhrman, R. A. (2012b). Spin-torque switching with the giant spin Hall effect of tantalum. *Science* 336 (6081), 555–558. doi:10.1126/science.1218197
- Liu, L., Pai, C. F., Ralph, D. C., and Buhrman, R. A. (2012c). Magnetic oscillations driven by the spin Hall effect in 3-terminal magnetic tunnel junction devices. *Phys. Rev. Lett.* 109, 186602. doi:10.1103/physrevlett.109.186602
- Liu, R. H., Chen, L., Urazhdin, S., and Du, Y. W. (2017). Controlling the spectral characteristics of a spin-current auto-oscillator with an electric field. *Phys. Rev. Appl.* 8, 021001. doi:10.1103/physrevapplied.8.021001
- Liu, R. H., Lim, W. L., and Urazhdin, S. (2013). Spectral characteristics of the microwave emission by the spin Hall nano-oscillator. *Phys. Rev. Lett.* 110, 147601. doi:10.1103/physrevlett.110.147601
- Liu, X., and Hersam, M. C. (2019). 2D materials for quantum information science. *Nat. Rev. Mater.* 4, 669–684. doi:10.1038/s41578-019-0136-x
- Liu, X. H., Edmonds, K. W., Zhou, Z. P., and Wang, K. Y. (2020). Tuning interfacial spins in antiferromagnetic–ferromagnetic–heavy-metal heterostructures via spin-orbit torque. *Phys. Rev. Appl.* 13 (1), 014059. doi:10.1103/physrevapplied.13.014059
- Liu, Z. M., and Zhou, L. (2014). Quantum teleportation of a three-qubit state using a five-qubit cluster state. *Int. J. Theor. Phys.* 53, 4079–4082. doi:10.1007/s10773-014-2158-x
- Lloyd, S. (1993). A potentially realizable quantum computer. *Science*. 261 (5128), 1569–1571. doi:10.1126/science.261.5128.1569
- Lo, H.-K., Curty, M., and Tamaki, K. (2014). Secure quantum key distribution. *Nat. Phot.* 8, 595–604. doi:10.1038/nphoton.2014.149
- Locatelli, N., Cros, V., and Grollier, J. (2022). Spin-torque building blocks. *Nat. Mat.* 13 (2014), 11–20. doi:10.1038/nmat3823
- Lombardi, E., Sciarrino, F., Popescu, S., and De Martini, F. (2002). Teleportation of a vacuum one-photon qubit. *Phys. Rev. Lett.* 88, 070402. doi:10.1103/physrevlett.88.070402
- Loss, D., and DiVincenzo, D. P. (1998). Quantum computation with quantum dots. *Phys. Rev. A* 57 (1), 120–126. doi:10.1103/physreva.57.120
- Lund, A. P., and Ralph, T. C. (2002). Nondeterministic gates for photonic single-rail quantum logic. *Phys. Rev. A* 66 (3), 032307. doi:10.1103/physreva.66.032307
- Lutchyn, R. M., Sau, J. D., and Sarma, S. D. (2010). Majorana fermions and a topological phase transition in semiconductor-superconductor heterostructures. *Phys. Rev. Lett.* 105 (7), 077001. doi:10.1103/physrevlett.105.077001
- Lvovsky, A. I., Sanders, B. C., and Tittel, W. (2009). Optical quantum memory. *Nat. Photonics* 3 (12), 706–714. doi:10.1038/nphoton.2009.231
- Ma, X.-S., Herbst, T., Scheidl, T., Wang, D., Kropatschek, S., Naylor, W., et al. (2012). Quantum teleportation over 143 kilometres using active feed-forward. *Nature* 489, 269–273. doi:10.1038/nature11472
- Maan, A. K., Jayadevi, D. A., and James, A. P. (2016). A survey of memristive threshold logic circuits. *IEEE Trans. Neural Netw. Learn. Syst.* 28 (9), 1734–1746. doi:10.1109/TNNLS.2016.2547842
- Macrae, N. (1992). “John von Neumann: The Scientific Genius Who Pioneered the Modern Computer, Game Theory,” in *Nuclear deterrence, and much more* (Pantheon Press).
- Mądzik, M. T., Asaad, S., Youssry, A., Joecker, B., Rudinger, K. M., Nielsen, E., et al. (2022). Precision tomography of a three-qubit donor quantum processor in silicon. *Nature* 601, 348–353. doi:10.1038/s41586-021-04292-7
- Mądzik, M. T., Laucht, A., Hudson, F. E., Jakob, A. M., Johnson, B. C., Jamieson, D. N., et al. (2021). Conditional quantum operation of two exchange-coupled single-donor spin qubits in a MOS-compatible silicon device. *Nat. Commun.* 12, 181. doi:10.1038/s41467-020-20424-5
- Maeda, F. (1937). *Mathematical foundations of quantum mechanics. Journal of science of the Hiroshima university, series A (mathematics, physics, chemistry)*, 191–213.
- Majer, J., Chow, J. M., Gambetta, J. M., Koch, J., Johnson, B. R., Schriefer, J. A., et al. (2007). Coupling superconducting qubits via a cavity bus. *Nat. Lond.* 449, 443–447. doi:10.1038/nature06184
- Makhlin, Y., Schoen, G., and Shnirman, A. (2001). Quantum state engineering with Josephson-junction devices. *Rev. Mod. Phys.* 73 (2), 357–400. doi:10.1103/revmodphys.73.357
- Makino, K., Hashimoto, Y., Yoshikawa, J. I., Ohdan, H., Toyama, T., van Loock, P., et al. (2016). Synchronization of optical photons for quantum information processing. *Sci. Adv.* 2 (5), e1501772. doi:10.1126/sciadv.1501772
- Malia, B. K., Wu, Y., Martínez-Rincón, J., and Kasevich, M. A. (2022). Distributed quantum sensing with mode-entangled spin-squeezed atomic states. *Nature* 612 (7941), 661–665. doi:10.1038/s41586-022-05363-z
- Man, Z. X., Xia, Y. J., and An, N. B. (2007). Quantum teleportation of an unknown N-Qubit W-Like state. *JETP Lett.* 85, 662–666. doi:10.1134/s0021364007120168
- Manchon, A., Koo, H. C., Nitta, J., Frolov, S. M., and Duine, R. A. (2015). New perspectives for Rashba spin-orbit coupling. *Nat. Mater.* 14 (9), 871–882. doi:10.1038/nmat4360
- Mansuripur, M. (2015). Origin of the spin-orbit interaction. *Phys. Scr.* 90, 085501. doi:10.1088/0031-8949/90/8/085501
- Manucharyan, V. E., Koch, J., Glazman, L. I., and Devoret, M. H. (2009). Fluxonium: single cooper-pair circuit free of charge offsets. *Science* 326 (5949), 113–116. doi:10.1126/science.1175552
- Marcikic, I., de Riedmatten, H., Tittel, W., Zbinden, H., and Gisin, N. (2003). Longdistance teleportation of qubits at telecommunication wavelengths. *Nature* 421, 509–513. doi:10.1038/nature01376
- Marín-Suárez, M., Peltonen, J. T., and Pekola, J. P. (2020). Active quasiparticle suppression in a non-equilibrium superconductor. *Nano Lett.* 20, 5065–5071. doi:10.1021/acs.nanolett.0c1264
- Martinis, J. M. (2009). Superconducting phase qubits. *Quantum inf. Process.* 8 (2), 81–103. doi:10.1007/s11128-009-0105-1
- Martinis, J. M. (2021). Saving superconducting quantum processors from decay and correlated errors generated by gamma and cosmic rays. *npj Quantum Inf.* 7, 90. doi:10.1038/s41534-021-00431-0
- Martinis, J. M., Cooper, K. B., McDermott, R., Steffen, M., Ansmann, M., Osborn, K. D., et al. (2005). Decoherence in Josephson qubits from dielectric loss. *Phys. Rev. Lett.* 95, 210503. doi:10.1103/physrevlett.95.210503
- Martinis, J. M., Devoret, M. H., and Clarke, J. (1985). Energy-level quantization in the zero-voltage state of a current-biased Josephson junction. *Phys. Rev. Lett.* 55, 1543–1546. doi:10.1103/physrevlett.55.1543
- Martinis, J. M., Devoret, M. H., and Clarke, J. (2020). Quantum Josephson junction circuits and the dawn of artificial atoms. *Nat. Phys.* 16, 234–237. doi:10.1038/s41567-020-0829-5
- Mastriani, M., Iyengar, S. S., and Kumar, L. (2021). Satellite quantum communication protocol regardless of the weather. *Opt. Quantum Electron.* 53 (4), 181. doi:10.1007/s11082-021-02829-8
- Maunz, P. L. W. (2016). High optical access trap 2.0. *Sandia Natl. Lab. Rep. No. SAND2016-0796R*. doi:10.2172/1237003
- Mayer, M. G. (1949). On closed shells in nuclei. II. *Phys. Rev.* 75 (12), 1969. doi:10.2172/4410667
- Maze, J. R., Stanwix, P. L., Hodges, J. S., Hong, S., Taylor, J. M., Cappellaro, P., et al. (2008). Nanoscale magnetic sensing with an individual electronic spin in diamond. *Nature* 455, 644–647. doi:10.1038/nature07279
- McArdle, S., Endo, S., Aspuru-Guzik, A., Benjamin, S. C., and Yuan, X. (2020). Quantum computational chemistry. *Rev. Mod. Phys.* 92, 015003. doi:10.1103/revmodphys.92.015003
- McDermott, R. (2009). Materials origins of decoherence in superconducting qubits. *IEEE Trans. Appl. Supercond.* 19 (1), 2–13. doi:10.1109/tasc.2008.2012255
- Menicucci, N. C., and Caves, C. M. (2002). Local realistic model for the dynamics of bulk-ensemble NMR information processing. *Phys. Rev. Lett.* 88 (16), 167901. doi:10.1103/PhysRevLett.88.167901
- Merkel, C., and Kudithipudi, D. (2014). “Neuromemristive extreme learning machines for pattern classification,” in *2014 IEEE computer society annual symposium on VLSCI (IEEE)*, 77–82.
- Mermin, N. D. (1993). Hidden variables and the two theorems of John Bell. *Rev. Mod. Phys.* 65 (3), 803–815. arXiv:1802.10119. Bibcode:1993RvMP.65.803
- Merzbacher, E. (2002). The early history of quantum tunneling. *Phys. Today* 55 (8), 44–49. doi:10.1063/1.1510281
- Metcalfe, B. J., Spring, J. B., Humphreys, P. C., Thomas-Peter, N., Barbieri, M., Kolthammer, W. S., et al. (2014). Quantum teleportation on a photonic chip. *Nat. Phot.* 8, 770–774. doi:10.1038/nphoton.2014.217
- Metcalfe, M., Boaknin, E., Manucharyan, V., Vijay, R., Siddiqi, I., Rigetti, C., et al. (2007). Measuring the decoherence of a qubit with the cavity bifurcation amplifier. *Phys. Rev. B* 76 (17), 174516. doi:10.1103/physrevb.76.174516
- Mi, X., Ippoliti, M., Quintana, C., Greene, A., Chen, Z., Gross, J., et al. (2022). Time-crystalline eigenstate order on a quantum processor. *Nature* 601 (7894), 531–536. doi:10.1038/s41586-021-04257-w
- Microsoft (2022). News microsoft. Available at <https://news.microsoft.com/source/features/innovation/azure-quantum-majorana-topological>





- Pais, A. (1979). Einstein and the quantum theory. *Rev. Mod. Phys.* 51 (4), 863–914. doi:10.1103/RevModPhys.51.863
- Paladino, E., Faoro, L., Falci, G., and Fazio, R. (2002). Decoherence and 1/f noise in Josephson qubits. *Phys. Rev. Lett.* 88 (22), 228304. doi:10.1103/physrevlett.88.228304
- Paladino, E., Galperin, Y., Falci, G., and Altshuler, B. (2014). 1/f noise: implications for solid-state quantum information. *Rev. Mod. Phys.* 86, 361–418. doi:10.1103/revmodphys.86.361
- Pan, J. W., Bouwmeester, D., Weinfurter, H., and Zeilinger, A. (1998). Experimental entanglement swapping: entangling photons that never interacted. *Phys. Rev. Lett.* 80 (18), 3891–3894. doi:10.1103/physrevlett.80.3891
- Pan, J. W., Chen, Z. B., Lu, C. Y., Weinfurter, H., Zeilinger, A., and Żukowski, M. (2012). Multiphoton entanglement and interferometry. *Rev. Mod. Phys.* 84 (2), 777–838. doi:10.1103/revmodphys.84.777
- Patel, R. B., Ho, J., Ferreyrol, F., Ralph, T. C., and Pryde, G. J. (2016). A quantum Fredkin gate. *Sci. Adv.* 2 (3), e1501531. doi:10.1126/sciadv.1501531
- Paul, W. (1990). Electromagnetic traps for charged and neutral particles. *Rev. Mod. Phys.* 62 (3), 531–540. doi:10.1103/revmodphys.62.531
- Peng, C.-Z., Yang, T., Bao, X. H., Zhang, J., Jin, X. M., Feng, F. Y., et al. (2005). Experimental free-space distribution of entangled photon pairs over 13 km: towards satellite-based global quantum communication. *Phys. Rev. Lett.* 94, 150501. doi:10.1103/physrevlett.94.150501
- Peres, A. (1985). Reversible logic and quantum computers. *Phys. Rev. A* 32 (6), 3266–3276. doi:10.1103/physreva.32.3266
- Pérez-Delgado, C. A., and Kok, P. (2011). Quantum computers: definition and implementations. *Phys. Rev. A* 83 (1), 012303. doi:10.1103/PhysRevA.83.012303
- Peruzzo, A., McClean, J., Shadbolt, P., Yung, M. H., Zhou, X. Q., Love, P. J., et al. (2014). A variational eigenvalue solver on a photonic quantum processor. *Nat. Commun.* 5, 4213. doi:10.1038/ncomms5213
- Petit, L., Eenink, H. G. J., Russ, M., Lawrie, W. I. L., Hendrickx, N. W., Philips, S. G. J., et al. (2020). Universal quantum logic in hot silicon qubits. *Nature* 580, 355–359. doi:10.1038/s41586-020-2170-7
- Pfaff, W., Hensen, B. J., Bernien, H., van Dam, S. B., Blok, M. S., Taminiau, T. H., et al. (2014). Unconditional quantum teleportation between distant solidstate quantum bits. *Science* 345, 532–535. doi:10.1126/science.1253512
- Phillips, W. A. (1987). Two-level states in glasses. *Rep. Prog. Phys.* 50, 1657–1708. doi:10.1088/0034-4885/50/12/003
- PhysOrg.com Miranda Marquít (2007). *First use of Deutsch's Algorithm in a cluster state quantum computer.*
- Pickett, M. D., Medeiros-Ribeiro, G., and Williams, R. S. (2012). A scalable neuristor built with Mott memristors. *Nat. Mater.* 12 (2), 114–117. doi:10.1038/nmat3510
- Pirandola, S., Andersen, U. L., Banchi, L., Berta, M., Bunandar, D., Colbeck, R., et al. (2020). Advances in quantum cryptography. *Adv. Opt. Photonics* 12 (4), 1012–1236. doi:10.1364/aop.361502
- Pirandola, S., Eisert, J., Weedbrook, C., Furusawa, A., and Braunstein, S. L. (2015a). Advances in quantum teleportation. *Nat. Phot.* 9, 641–652. doi:10.1038/nphoton.2015.154
- Place, A. P. M., Rodgers, L. V. H., Mundada, P., Smitham, B. M., Fitzpatrick, M., Leng, Z., et al. (2021). New material platform for superconducting transmon qubits with coherence times exceeding 0.3 milliseconds. *Nat. Commun.* 12 (1), 1779. doi:10.1038/s41467-021-22030-5
- Poletto, S., Gambetta, J. M., Merkel, S. T., Smolin, J. A., Chow, J. M., Córcoles, A. D., et al. (2012). Entanglement of two superconducting qubits in a waveguide cavity via monochromatic two-photon excitation. *Phys. Rev. Lett.* 109, 240505. doi:10.1103/PhysRevLett.109.240505
- Politi, A., Matthews, J. C., and O'Brien, J. L. (2009). Shor's quantum factoring algorithm on a photonic chip. *Science* 325 (5945), 1221. arXiv:0911.1242. doi:10.1126/science.1173731
- Pollak, E. (2017a). Transition path time distribution, tunneling times, friction, and uncertainty. *Phys. Rev. Lett.* 118 (7), 070401. doi:10.1103/physrevlett.118.070401
- Pollak, E. (2017b). Quantum tunneling: the longer the path, the less time it takes. *J. Phys. Chem. Lett.* 8 (2), 352–356. doi:10.1021/acs.jpclett.6b02692
- Poon, C.-S., and Zhou, K. (2011). Neuromorphic silicon neurons and large-scale neural networks: challenges and opportunities. *Front. Neurosci.* 5, 108. doi:10.3389/fnins.2011.00108
- Powell, A., Jenny, J., Muller, S., McD. Hobgood, H., Tsvetkov, V., Lenoard, R., et al. (2006). Growth of sic substrates. *Syst.* 16, 751–777. doi:10.1142/s0129156406004016
- Prenat, G., Jabeur, K., Di Pendina, G., Boule, O., and Gaudin, G. (2015). Beyond STT-MRAM, spin orbit torque RAM SOT-MRAM for high speed and high reliability applications. *Spintronics-based Computing*, 145–157.
- Pufall, M. R., Rippard, W. H., Csaba, G., Nikonov, D. E., Bourianoff, G. I., and Porod, W. (2015). Physical implementation of coherently coupled oscillator networks. *IEEE J. Explor. Solid-State Comput. Devices Circuits* 1, 76–84. doi:10.1109/jxcdc.2015.2468070
- Puliylil, S., Banik, M., and Alimuddin, M. (2022). Thermodynamic signatures of genuinely multipartite entanglement. *Phys. Rev. Lett.* 129 (7), 070601. doi:10.1103/physrevlett.129.070601
- Puri, S., Boutin, S., and Blais, A. (2017). Engineering the quantum states of light in a Kerr-nonlinear resonator by two-photon driving. *npj Quantum Inf.* 3 (1), 18. doi:10.1038/s41534-017-0019-1
- QCI (2022). We believe that quantum computing, and all of its power, should be made accessible to all businesses, not just an elite quantum workforce. Available at: <https://www.quantumcomputinginc.com/blog/quantum-annealing-gate/> (Accessed December 22, 2022).
- Quach, J. Q., McGhee, K. E., Ganzer, L., Rouse, D. M., Lovett, B. W., Gauger, E. M., et al. (2022). Superabsorption in an organic microcavity: toward a quantum battery. *Sci. Adv.* 8 (2), eabk3160. doi:10.1126/sciadv.abk3160
- Quantum Computing (2022). *Quantum computing.* Available at: <https://quantumcomputing.com/whurley/china-goes-big-with-92-acre-10-billion-quantum-research-center>.
- Quantum Technology Market Size (2022a). *Growth to reach CAGR 30.2 % by 2028 provided by: market research store.*
- Quantum Technology Market Size (2022b). *Quantum technology market size & growth to reach CAGR 30.2 % by 2028 provided by: market research store* (Accessed December 30, 2022).
- Quantumzeitgeist (2022). *David deutsch the father of quantum computing but who is he.* Available at: <https://www.economist.com/technology-quarterly/2017/03/09/david-deutsch-father-of-quantum-computing> (Accessed December 5, 2022).
- Raussendorf, R., and Briegel, H. J. (2001). A one-way quantum computer. *Phys. Rev. Lett.* 86 (22), 5188–5191. doi:10.1103/physrevlett.86.5188
- Raussendorf, R., and Harrington, J. (2007). Fault-tolerant quantum computation with high threshold in two dimensions. *Phys. Rev. Lett.* 98, 190504. doi:10.1103/physrevlett.98.190504
- Raussendorf, R., Harrington, J., and Goyal, K. (2007a). Topological fault-tolerance in cluster state quantum computation. *New J. Phys.* 9 (6), 199. doi:10.1088/1367-2630/9/6/199
- Ray, P., Chakrabarti, B. K., and Chakrabarti, A. (1989). Sherrington-Kirkpatrick model in a transverse field: absence of replica symmetry breaking due to quantum fluctuations. *Phys. Rev. B* 39 (16), 11828–11832. doi:10.1103/PhysRevB.39.11828
- Razavy, M. (2003). Quantum theory of tunneling. *World Sci.* 4–462. doi:10.1142/9789812564887
- Reed, M. D., Maune, B., Andrews, R., Borselli, M., Eng, K., Jura, M., et al. (2016). Reduced sensitivity to charge noise in semiconductor spin qubits via symmetric operation. *Phys. Rev. Lett.* 116, 110402. doi:10.1103/physrevlett.116.110402
- Ren, J. G., Xu, P., Yong, H. L., Zhang, L., Liao, S. K., Yin, J., et al. (2017). Ground-to-satellite quantum teleportation. *Nature* 549, 70–73. doi:10.1038/nature23675
- Riebe, M., Chwalla, M., Benhelm, J., Häffner, H., Hänsel, W., Roos, C. F., et al. (2007). Quantum teleportation with atoms: quantum process tomography. *New J. Phys.* 9, 211. doi:10.1088/1367-2630/9/7/211
- Riebe, M., Häffner, H., Roos, C. F., Hänsel, W., Benhelm, J., Lancaster, G. P. T., et al. (2004). Deterministic quantum teleportation with atoms. *Nature* 429, 734–737. doi:10.1038/nature02570
- Rigetti, C., Gambetta, J. M., Poletto, S., Plourde, B. L. T., Chow, J. M., Córcoles, A. D., et al. (2012). Superconducting qubit in a waveguide cavity with a coherence time approaching 0.1 ms. *Am. Phys. Soc. (APS)* 86 (10), 100506. doi:10.1103/physrevb.86.100506
- Rigetti Launches Quantum Cloud Services (2018). *Announces \$1Million challenge.* HPCwire. Retrieved 2022-09-31.
- Rigolin, G. (2005). Quantum teleportation of an arbitrary two-qubit state and its relation to multipartite entanglement. *Phys. Rev. A* 71 (3), 032303. doi:10.1103/physreva.71.032303
- Risté, D., Bultink, C. C., Tiggelman, M. J., Schouten, R. N., Lehnert, K. W., and DiCarlo, L. (2013). Millisecond charge-parity fluctuations and induced decoherence in a superconducting transmon qubit. *Nat. Commun.* 4 (1), 1913. doi:10.1038/ncomms2936
- Riwar, R.-P., and Catelani, G. (2019). Efficient quasiparticle traps with low dissipation through gap engineering. *Phys. Rev. B* 100, 144514. doi:10.1103/physrevb.100.144514
- Riwar, R.-P., Hosseinkhani, A., Burkhart, L. D., Gao, Y. Y., Schoelkopf, R. J., Glazman, L. I., et al. (2016). Normal-metal quasiparticle traps for superconducting qubits. *Phys. Rev. B* 94, 104516. doi:10.1103/physrevb.94.104516

- Rong, X., Geng, J., Shi, F., Liu, Y., Xu, K., Ma, W., et al. (2015). Experimental fault-tolerant universal quantum gates with solid-state spins under ambient conditions. *Nat. Commun.* 6, 8748. doi:10.1038/ncomms9748
- Rostem, K., de Visser, P. J., and Wollack, E. J. (2018). Enhanced quasiparticle lifetime in a superconductor by selective blocking of recombination phonons with a phononic crystal. *Phys. Rev. B* 98, 014522. doi:10.1103/physrevb.98.014522
- Ruiz, A. D. L. F. (2014). Quantum annealing. *arXiv preprint arXiv:1404.2465*. doi:10.48550/arXiv.1404.2465
- Ruskov, R., and Tahan, C. (2012). Coherent phonons as a new element of quantum computing and devices. *J. Phys. Conf. Ser.* 398 (1), 012011. doi:10.1088/1742-6596/398/1/012011
- Ryan, C. A., Johnson, B. R., Ristè, D., Donovan, B., and Ohki, T. A. (2017). Hardware for dynamic quantum computing. *Rev. Sci. Instrum.* 88 (10), 104703. doi:10.1063/1.5006525
- Sadeghi Zadeh, M. S., Houshmand, M., and Aghababa, H. (2017). Bidirectional teleportation of a two-qubit state by using eight-qubit entangled state as a quantum channel. *Int. J. Theor. Phys.* 56, 2101–2112. doi:10.1007/s10773-017-3353-3
- Saglmyurek, E., Sinclair, N., Jin, J., Slater, J. A., Oblak, D., Bussières, F., et al. (2011). Broadband waveguide quantum memory for entangled photons. *Nature* 469, 512–515. doi:10.1038/nature09719
- Sainadh, U. S., Sang, R. T., and Litvinyuk, I. V. (2020). Attoclock and the quest for tunnelling time in strong-field physics. *J. Phys. Photonics* 2 (4), 042002. doi:10.1088/2515-7647/aba009
- Saleh, B. E. A., and Teich, M. C. (1991). *Fundamentals of photonics Ch.22*. Wiley.
- Sanders, Y. R., Wallman, J. J., and Sanders, B. C. (2015). Bounding quantum gate error rate based on reported average fidelity. *New J. Phys.* 18, 012002. doi:10.1088/1367-2630/18/1/012002
- Sang, M. H. (2016). Bidirectional quantum teleportation by using five-qubit cluster state. *Int. J. Theor. Phys.* 55, 1333–1335. doi:10.1007/s10773-015-2774-0
- Sangouard, N., Simon, C., de Riedmatten, H., and Gisin, N. (2011). Quantum repeaters based on atomic ensembles and linear optics. *Rev. Mod. Phys.* 83, 33–80. doi:10.1103/revmodphys.83.33
- Sato, H., Honjo, H., Watanabe, T., Niwa, M., Koike, H., Miura, S., et al. (2018a). “14ns write speed 128Mb density Embedded STT-MRAM with endurance>1010 and 10yrs retention@85C using novel low damage MTJ integration process,” in *IEEE international electron devices meeting (IEDM), San Francisco, CA, USA, 2018, 27IEEE international electron devices meeting (IEDM), San Francisco, CA, USA, 2018 (IEEE)*, 2.1–27.2.4. doi:10.1109/IEDM.2018.8614606
- Sato, M., Takahashi, Y., and Fujimoto, S. (2009). Non-Abelian topological order in s-wave superfluids of ultracold fermionic atoms. *Phys. Rev. Lett.* 103 (2), 020401. doi:10.1103/physrevlett.103.020401
- Satzinger, K. J., Liu, Y., Smith, A., Knapp, C., Newman, M., Jones, C., et al. (2021). Realizing topologically ordered states on a quantum processor. *Science* 374 (6572), 1237–1241. doi:10.1126/science.abi8378
- Sau, J. D., Lutchyn, R. M., Tewari, S., and Sarma, S. D. (2010). Generic new platform for topological quantum computation using semiconductor heterostructures. *Phys. Rev. Lett.* 104 (4), 040502. doi:10.1103/physrevlett.104.040502
- Scarani, V., and Renner, R. (2008). Quantum cryptography with finite resources: unconditional security bound for discrete-variable protocols with one-way postprocessing. *Phys. Rev. Lett.* 100, 200501. doi:10.1103/physrevlett.100.200501
- Schaibley, J. R., Yu, H., Clark, G., Rivera, P., Ross, J. S., Seyler, K. L., et al. (2016). Valleytronics in 2D materials. *Nat. Rev. Mater.* 1 (11), 1–15. doi:10.1038/natrevmats.2016.55
- Schindler, P., Nigg, D., Monz, T., Barreiro, J. T., Martinez, E., Wang, S. X., et al. (2013). A quantum information processor with trapped ions. *New J. Phys.* 15 (12), 123012. doi:10.1088/1367-2630/15/12/123012
- Scholarpedia (2022). *Scholarpedia*. Available at: [http://www.scholarpedia.org/article/1/f\\_noise](http://www.scholarpedia.org/article/1/f_noise).
- Schreier, J. A., Houck, A. A., Koch, J., Schuster, D. I., Johnson, B. R., Chow, J. M., et al. (2008). Suppressing charge noise decoherence in superconducting charge qubits. *Phys. Rev. B* 77 (18), 180502. doi:10.1103/physrevb.77.180502
- Schrödinger, E. (1926). Quantisierung als eigenwertproblem. *Ann. Phys.* 384 (4), 361–376. doi:10.1002/andp.19263840404
- Schrödinger, E. (1935). Discussion of probability relations between separated systems. *Proc. Camb. Philosophical Soc.* 31, 555–563. doi:10.1017/s0305004100013554
- Schumacher, B. (1995). Quantum coding. *Phys. Rev. A* 51 (4), 2738–2747. doi:10.1103/physreva.51.2738
- Schwegler, E., Sharma, M., Gygi, F., and Galli, G. (2008). Melting of ice under pressure. *Proc. Natl. Acad. Sci.* 105 (39), 14779–14783. doi:10.1073/pnas.0808137105
- SCI (2023). 33525 *stj detectors*. Available at: <https://sci.esa.int/web/sci-fmi/-/33525-stj-detectors> (Accessed March 20, 23).
- Science Daily (2006). *12-qubits reached in quantum information quest*.
- Science the Wire (2022). *Science the wire*. Available at: <https://science.thewire.in/the-sciences/quantum-entanglement-applications-qkd/>.
- Scitechdaily (2022). Scientists strengthen spin-orbit qubits in milestone critical for scale up of quantum computers. Available at: <https://scitechdaily.com/scientists-strengthen-spin-orbit-qubits-in-milestone-critical-for-scale-up-of-quantum-computers/>.
- SCL (2022). Schrödinger's cat, Einstein's dice and the chandelier: a novice's guide to quantum computers. Available at: <https://www.scl.org/articles/10503-schr-dingers-cat-einsteins-dice-and-the-chandelier-a-novice-s-guide-to-quantum-computers> (Accessed December 28, 22).
- Sengupta, A., Panda, P., Wijesinghe, P., Kim, Y., and Roy, K. (2016). Magnetic tunnel junction mimics stochastic cortical spiking neurons. *Sci. Rep.* 6, 30039. doi:10.1038/srep30039
- Session 8-4 (2023). *32-Mb 2T1R SPRAM with localized bi-directional write driver and '1'/'0' dual-array equalized reference cell*. vlisymposium.org. Archived from the original on 5 Feb 2023.
- Shahmoon, E., Levit, S., and Ozeri, R. (2009). *Qubit coherent control with squeezed light fields*. arXiv preprint arXiv:0901.2824.
- Shao, Q., Yu, G., Lan, Y. W., Shi, Y., Li, M. Y., Zheng, C., et al. (2016). Strong Rashba-Edelstein effect-induced spin-orbit torques in monolayer transition metal dichalcogenide/ferromagnet bilayers. *Nano Lett.* 16 (12), 7514–7520. doi:10.1021/acs.nanolett.6b03300
- Sharad, M., Augustine, C., Panagopoulos, G., and Roy, K. (2012). *Proposal for neuromorphic hardware using spin devices*. arXiv:1206.3227.
- Sherson, J. F., Krauter, H., Olsson, R. K., Julsgaard, B., Hammerer, K., Cirac, I., et al. (2006). Quantum teleportation between light and matter. *Nature* 443, 557–560. doi:10.1038/nature05136
- Shi, J., Lopez-Dominguez, V., Garesci, F., Wang, C., Almasi, H., Grayson, M., et al. (2020). Electrical manipulation of the magnetic order in antiferromagnetic PtMn pillars. *Nat. Electron.* 3 (2), 92–98. doi:10.1038/s41928-020-0367-2
- Shor, P. W. (1994). “Algorithms for quantum computation: discrete logarithms and factoring,” in *Proceedings 35th annual symposium on foundations of computer science*. IEEE Comput. Soc. Press, 124–134. doi:10.1109/sfcs.1994.365700
- Shor, P. W. (1997). Polynomial-time algorithms for prime factorization and discrete logarithms on a quantum computer. *SIAM J. Comput.* 26, 1484–1509. doi:10.1137/s0097539795293172
- Shrivastava, K. N. (1983). Theory of spin–lattice relaxation. *Phys. Stat. Solidi B* 117, 437–458. doi:10.1002/psb.2221170202
- Siddiqi, I. (2021). Engineering high-coherence superconducting qubits. *Nat. Rev. Mater.* 6, 875–891. doi:10.1038/s41578-021-00370-4
- Siddiqi, A. U., and Wilde, M. M. (2022). *The SWAP imposter: bidirectional quantum teleportation and its performance*. arXiv preprint arXiv:2210.10882.
- Sillanpää, M. A., Park, J. I., and Simmonds, R. W. (2007). Coherent quantum state storage and transfer between two phase qubits via a resonant cavity. *Nat. Lond.* 449, 438–442. doi:10.1038/nature06124
- Simmonds, R. W., Lang, K. M., Hite, D. A., Nam, S., Pappas, D. P., and Martinis, J. M. (2004). Decoherence in Josephson phase qubits from junction resonators. *Phys. Rev. Lett.* 93 (7), 077003. doi:10.1103/physrevlett.93.077003
- Simon, D. R. (1997). On the power of quantum computation. *SIAM J. Comput.* 26 (5), 1474–1483. doi:10.1137/S0097539796298637
- Sinova, J., Valenzuela, S. O., Wunderlich, J., Back, C. H., and Jungwirth, T. (2015). Spin Hall effects. *Rev. Mod. Phys.* 87, 1213–1260. doi:10.1103/revmodphys.87.1213
- Sipser, M. (1997). *Introduction to the theory of computation*. Boston: PWS Pub. Co.
- Sisodia, M., and Pathak, A. (2018). Comment on “quantum teleportation of eight-qubit state via six-qubit cluster state”. *Int. J. Theor. Phys.* 57, 2213–2217. doi:10.1007/s10773-018-3746-y
- Sitharama Iyengar, S., Latish Kumar, K. J., and Mastriani, M. (2020). *Bidirectional teleportation for underwater quantum communications*. arXiv e-prints, arXiv:2009.
- Slavin, A., and Tiberkevich, V. (2009). Nonlinear auto-oscillator theory of microwave generation by spin-polarized current. *IEEE Trans. Magn.* 45, 1875–1918. doi:10.1109/tmag.2008.2009935
- Slonczewski, J. C. (1996). Current-driven excitation of magnetic multilayers. *J. Magnetism Magnetic Mater.* 159 (1–2), L1–L7. doi:10.1016/0304-8853(96)00062-5
- Smart, S. E., Hu, Z., Kais, S., and Mazziotti, D. A. (2022). Relaxation of stationary states on a quantum computer yields a unique spectroscopic fingerprint of the computer's noise. *Commun. Phys.* 5 (1), 28. doi:10.1038/s42005-022-00803-8

- Smith, W. C., Kou, A., Xiao, X., Vool, U., and Devoret, M. H. (2020). Superconducting circuit protected by two-Cooper-pair tunneling. *npj Quantum Inf.* 6 (1), 8. doi:10.1038/s41534-019-0231-2
- Soare, A., Ball, H., Hayes, D., Sastrawan, J., Jarratt, M. C., McLoughlin, J. J., et al. (2014). Experimental noise filtering by quantum control. *Nat. Phys.* 10, 825–829. doi:10.1038/nphys3115
- Son, N. T., Carlsson, P., ul Hassan, J., Janzén, E., Umeda, T., Isoya, J., et al. (2006). Divacancy in 4H-SiC. *Phys. Rev. Lett.* 96, 055501. doi:10.1103/physrevlett.96.055501
- Son, N. T., Zolnai, Z., and Janzen, E. (2022). Silicon vacancy related TV2a center in 4H-SiC. *Phys. Rev. B* 68, 205211. doi:10.1103/physrevb.68.205211
- Spagnolo, M., Morris, J., Piacentini, S., Antesberger, M., Massa, F., Crespi, A., et al. (2022). Experimental photonic quantum memristor. *Nat. Photonics* 16 (4), 318–323. doi:10.1038/s41566-022-00973-5
- Spavieri, G., and Mansuripur, M. (2015). Origin of the spin-orbit interaction. *Phys. Scr.* 90 (8), 085501. doi:10.1088/0031-8949/90/8/085501
- Spierings, D. C., and Steinberg, A. M. (2020). Measuring the time tunneling particles spend in the barrier. *Opt. Opto-Atomic, Entanglement-Enhanced Precis. Metrology II* 11296, 45–52. doi:10.1117/12.2552583
- Spierings, D. C., and Steinberg, A. M. (2021). *Tunneling takes less time when it's less probable*. arXiv preprint arXiv:2101.12309.
- Srinatha, N., Omkar, S., Srikanth, R., Banerjee, S., and Pathak, A. (2014). The quantum cryptographic switch. *Quantum inf. Process.* 13, 59–70. doi:10.1007/s11128-012-0487-3
- Stanescu, T. D. (2016). *Introduction to topological quantum matter & quantum computation*. CRC Press.
- Stano, P., and Loss, D. (2022). Review of performance metrics of spin qubits in gated semiconducting nanostructures. *Nat. Rev. Phys.* 4, 672–688. doi:10.1038/s42254-022-00484-w
- Steffen, L., Salathe, Y., Opliger, M., Kurpiers, P., Baur, M., Lang, C., et al. (2013). Deterministic quantum teleportation with feedforward in a solid-state system. *Nature* 500, 319–322. doi:10.1038/nature12422
- Steffen, M. (2011). Superconducting qubits are getting serious. *Physics* 4, 103. doi:10.1103/physics.4.103
- Strogatz, S. (2004). *Sync: the emerging science of spontaneous order*.
- Su, X., Tian, C., Deng, X., Li, Q., Xie, C., and Peng, K. (2016). Quantum entanglement swapping between two multipartite entangled states. *Phys. Rev. Lett.* 117 (24), 240503. doi:10.1103/physrevlett.117.240503
- Sun, Q.-C., Mao, Y. L., Chen, S. J., Zhang, W., Jiang, Y. F., Zhang, Y. B., et al. (2016). Quantum teleportation with independent sources and prior entanglement distribution over a network. *Nat. Phot.* 10, 671–675. doi:10.1038/nphoton.2016.179
- Sung, Y., Ding, L., Braumüller, J., Vepsäläinen, A., Kannan, B., Kjaergaard, M., et al. (2021). Realization of high-fidelity cz and z z-free iswap gates with a tunable coupler. *Phys. Rev. X* 11 (2), 021058. doi:10.1103/physrevx.11.021058
- Liu, M. (2024). *Synopsys: eMRAM for low-power SoCs in advanced process nodes*. Available at: <https://www.synopsys.com/designware-ip/technical-bulletin/emram-low-power-advanced-nodes.html> (Accessed July 24, 2024).
- Takahashi, S., Hanson, R., van Tol, J., Sherwin, M. S., and Awschalom, D. D. (2008). Quenching spin decoherence in diamond through spin bath polarization. *Phys. Rev. Lett.* 101, 047601. doi:10.1103/physrevlett.101.047601
- Takahashi, S., Tupitsyn, I. S., van Tol, J., Beedle, C. C., Hendrickson, D. N., and Stamp, P. C. E. (2011). Decoherence in crystals of quantum molecular magnets. *Nature* 476, 76–79. doi:10.1038/nature10314
- Takeda, S., Mizuta, T., Fuwa, M., van Loock, P., and Furusawa, A. (2013). Deterministic quantum teleportation of photonic quantum bits by a hybrid technique. *Nature* 500, 315–318. doi:10.1038/nature12366
- Takei, N., Aoki, T., Koike, S., Yoshino, K. i., Wakui, K., Yonezawa, H., et al. (2005b). Experimental demonstration of quantum teleportation of a squeezed state. *Phys. Rev. A* 72, 042304. doi:10.1103/physreva.72.042304
- Takei, N., Yonezawa, H., Aoki, T., and Furusawa, A. (2005a). High-fidelity teleportation beyond the no-cloning limit and entanglement swapping for continuous variables. *Phys. Rev. Lett.* 94, 220502. doi:10.1103/physrevlett.94.220502
- Takei, S., Fregoso, B. M., Hui, H. Y., Lobos, A. M., and Sarma, S. D. (2013). Soft superconducting gap in semiconductor Majorana nanowires. *Phys. Rev. Lett.* 110 (18), 186803. doi:10.1103/physrevlett.110.186803
- Takemura, R., Kawahara, T., Miura, K., Yamamoto, H., Hayakawa, J., Matsuzaki, N., et al. (2009). “32-mb 2t1r spram with localized bi-directional write driver and 1’/0’ dual-array equalized reference cell,” in *2009 symposium on VLSI circuits (IEEE)*, 84–85.
- Takesue, H., Dyer, S. D., Stevens, M. J., Verma, V., Mirin, R. P., and Nam, S. W. (2015). Quantum teleportation over 100 km of fiber using highly efficient superconducting nanowire single-photon detectors. *Optica* 2 (10), 832–835. doi:10.1364/optica.2.000832
- Takesue, H., Nam, S. W., Zhang, Q., Hadfield, R. H., Honjo, T., Tamaki, K., et al. (2007). Quantum key distribution over a 40-dB channel loss using superconducting single-photon detectors. *Nat. photonics* 1 (6), 343–348. doi:10.1038/nphoton.2007.75
- Tame, M. S., Prevedel, R., Paternostro, M., Böhi, P., Kim, M. S., and Zeilinger, A. (2007). Experimental realization of Deutsch’s algorithm in a one-way quantum computer. *Phys. Rev. Lett.* 98 (14), 140501. doi:10.1103/physrevlett.98.140501
- Tarantino, S., Da Lio, B., Cozzolino, D., and Bacco, D. (2020). Feasibility study of quantum communications in aquatic scenarios. *Optik* 216, 164639. doi:10.1016/j.ijleo.2020.164639
- Tarequzzaman, M., Böhnert, T., Decker, M., Costa, J. D., Borme, J., Lacoste, B., et al. (2019). Spin torque nano-oscillator driven by combined spin injection from tunneling and spin Hall current. *Commun. Phys.* 2, 20. doi:10.1038/s42005-019-0119-7
- Taupin, M., Khaymovich, I. M., Meschke, M., Mel’nikov, A. S., and Pekola, J. P. (2016). Tunable quasiparticle trapping in Meissner and vortex states of mesoscopic superconductors. *Nat. Commun.* 7, 10977. doi:10.1038/ncomms10977
- Taylor, J. (2004). *Modern physics for scientists and engineers*. Prentice Hall, 479.
- Team, I. Q. (2020). *ibmq\_armonk v1.1.5*. Available at: <https://quantum-computing.ibm.com>.
- Techinasia (2022). Techinasia. Available at: <https://www.techinasia.com/alibaba-15bn-damo> (Accessed December 30, 22).
- Toffoli, T. (1980). “An adapted and condensed version: Toffoli, Tommaso (1980),” in *Reversible computing (PDF)*. *Automata, languages and programming, seventh colloquium*. Editors J. W. de Bakker, and J. van Leeuwen (Noordwijkerhout, Netherlands: Springer Verlag), 632–644. doi:10.1007/3-540-10003-2\_104
- Techtarget (2022). *Techtarget*. Available at: <https://www.techtarget.com/searchenterpriseai/definition/neuromorphic-computing>.
- Thomas, L. H. (1926). *The motion of the spinning electron Nature*, 117–514.
- Thomas, L. H. (1927). *I. The kinematics of an electron with an axis. Mag* 3, 1–22. doi:10.1080/14786440108564170
- Tiangong-2 takes China one step closer to space station (2018). *chinaspacereport*. Archived from the original.
- Tinkham, M. (2004). *Introduction to superconductivity*. 2nd edn. Dover.
- Tokura, Y., Van der Wiel, W. G., Obata, T., and Tarucha, S. (2006). Coherent single electron spin control in a slanting Zeeman field. *Phys. Rev. Lett.* 96, 047202. doi:10.1103/physrevlett.96.047202
- Tomamichel, M., Lim, C. C. W., Gisin, N., and Renner, R. (2012). Tight finite-key analysis for quantum cryptography. *Nat. Commun.* 3, 634. doi:10.1038/ncomms1631
- Tomshardware (2022). *Tomshardware*. Available at: <https://www.tomshardware.com/news/intel-demonstrates-stt-mram-for-14-cache#~:text=Intel%20researchers%20have%20demonstrated%202MB,step%20forward%20for%20the%20technology> (Accessed September 1, 2023).
- Topological Quantum Computer (2023). *Topological quantum computer*. Available at: [https://en.wikipedia.org/wiki/Topological\\_quantum\\_computer](https://en.wikipedia.org/wiki/Topological_quantum_computer) (Accessed April 22, 23).
- Tougaw, P. D., and Lent, C. S. (1994). Logical devices implemented using quantum cellular automata. *J. Appl. Phys.* 75 (3), 1818–1825. doi:10.1063/1.356375
- Trauzettel, B., Bulaev, D., Loss, D., and Burkard, G. (2007). Spin qubits in graphene quantum dots. *Nat. Phys.* 3, 192–196. doi:10.1038/nphys544
- Trebst, S., Troyer, M., Wang, Z., and Ludwig, A. W. (2008). A short introduction to Fibonacci anyon models. *Prog. Theor. Phys. Suppl.* 176, 384–407. doi:10.1143/ptps.176.384
- Trif, M., Golovach, V. N., and Loss, D. (2008). Spin dynamics in InAs nanowire quantum dots coupled to a transmission line. *Phys. Rev. B* 77, 045434. doi:10.1103/physrevb.77.045434
- Trixler, F. (2013). Quantum tunnelling to the origin and evolution of life. *Curr. Org. Chem.* 17 (16), 1758–1770. doi:10.2174/13852728113179990083
- Troppmann, U., Tesch, C. M., and de Vivie-Riedle, R. (2003). Preparation and addressability of molecular vibrational qubit states in the presence of anharmonic resonance. *Chem. Phys. Lett.* 378 (3–4), 273–280. doi:10.1016/s0009-2614(03)01266-1
- Tsunegi, S., Taniguchi, T., Miwa, S., Nakajima, K., Yakushiji, K., Fukushima, A., et al. (2018). Evaluation of memory capacity of spin torque oscillator for recurrent neural networks. *Jpn. J. Appl. Phys.* 57, 120307. doi:10.7567/jjap.57.120307
- Tucker, J. (1979). Quantum limited detection in tunnel junction mixers. *IEEE J. Quantum Electron.* 15 (11), 1234–1258. doi:10.1109/jqe.1979.1069931
- Tyryshkin, A. M., Tojo, S., Morton, J. J., Riemann, H., Abrosimov, N. V., Becker, P., et al. (2012). Electron spin coherence exceeding seconds in high-purity silicon. *Nat. Mater.* 11 (2), 143–147. doi:10.1038/nmat3182
- Uhlenbeck, G., and Goudsmit, S. (1926). Spinning electrons and the structure of spectra. *Nature* 117, 264–265. doi:10.1038/117264a0



- Ursin, R., Jennewein, T., Aspelmeyer, M., Kaltenbaek, R., Lindenthal, M., Walther, P., et al. (2004). Quantum teleportation across the danube. *Nature* 430, 849. doi:10.1038/430849a
- Ursin, R., Tiefenbacher, F., Schmitt-Manderbach, T., Weier, H., Scheidl, T., Lindenthal, M., et al. (2007). Entanglement-based quantum communication over 144 km. *Nat. Phys.* 3, 481–486. doi:10.1038/nphys629
- Van Duzer, T., and Turner, C. W. (1981). *Principles of superconductive devices and circuits*. 2nd edn. Prentice Hall.
- Valenzuela, S. O., and Tinkham, M. (2006). Direct electronic measurement of the spin Hall effect. *Nature* 442 (7099), 176–179. doi:10.1038/nature04937
- Valery, J. A., Chowdhury, S., Jones, G., and Didier, N. (2022). Dynamical sweet spot engineering via two-tone flux modulation of superconducting qubits. *PRX Quantum* 3 (2), 020337. doi:10.1103/prxquantum.3.020337
- Valivarthi, R., Davis, S. I., Peña, C., Xie, S., Lauk, N., Narváez, L., et al. (2020). Teleportation systems toward a quantum internet. *PRX Quantum* 1 (2), 020317. doi:10.1103/prxquantum.1.020317
- Valivarthi, R., Puigibert, M. G., Zhou, Q., Aguilar, G. H., Verma, V. B., Marsili, F., et al. (2016). Quantum teleportation across a metropolitan fibre network. *Nat. Phot.* 10, 676–680. doi:10.1038/nphoton.2016.180
- van Der Heijden, J., Kobayashi, T., House, M. G., Salfi, J., Barraud, S., Laviéville, R., et al. (2018). Readout and control of the spin-orbit states of two coupled acceptor atoms in a silicon transistor. *Sci. Adv.* 4 (12), eaat9199. doi:10.1126/sciadv.aat9199
- Van der Heijden, J., Salfi, J., Mol, J. A., Verduijn, J., Tettamanzi, G. C., Hamilton, A. R., et al. (2014). Probing the spin states of a single acceptor atom. *Nano Lett.* 14 (3), 1492–1496. doi:10.1021/nl4047015
- Vandersypen, L., Steffen, M., Breyta, G., Yannoni, C. S., Sherwood, M. H., and Chuang, I. L. (2001). Experimental realization of Shor's quantum factoring algorithm using nuclear magnetic resonance. *Nature* 414, 883–887. doi:10.1038/414883a
- Vandersypen, L. M., Steffen, M., Breyta, G., Yannoni, C. S., Cleve, R., and Chuang, I. L. (2000). Experimental realization of an order-finding algorithm with an NMR quantum computer. *Phys. Rev. Lett.* 85 (25), 5452–5455. doi:10.1103/physrevlett.85.5452
- Vandersypen, L. M. K., Bluhm, H., Clarke, J. S., Dzurak, A. S., Ishihara, R., Morello, A., et al. (2017). Interfacing spin qubits in quantum dots and donors—hot, dense and coherent. *npj Quantum Inf.* 3, 34. doi:10.1038/s41534-017-0038-y
- Van Harlingen, D. J., Plourde, B. L. T., Robertson, T. L., Reichardt, P. A., and Clarke, J. (2004). *Decoherence in flux qubits due to 1/f noise in Josephson junctions*. Boston, MA: Springer US, 171–184.
- Varley, J. B., Janotti, A., and Van de Walle, C. G. (2016). Defects in AlN as candidates for solid-state qubits. *Phys. Rev. B* 93 (16), 161201. doi:10.1103/physrevb.93.161201
- Veldhorst, M., Hwang, J. C. C., Yang, C. H., Leenstra, A. W., de Ronde, B., Dehollain, J. P., et al. (2014). An addressable quantum dot qubit with fault-tolerant control-fidelity. *Nat. Nanotech.* 9, 981–985. doi:10.1038/nnano.2014.216
- Veldhorst, M., Yang, C. H., Hwang, J. C. C., Huang, W., Dehollain, J. P., Muhonen, J. T., et al. (2015). A two-qubit logic gate in silicon. *Nature* 526, 410–414. doi:10.1038/nature15263
- Verma, V. (2020). Bidirectional quantum teleportation by using two GHZ-states as the quantum channel. *IEEE Commun. Lett.* 25 (3), 936–939. doi:10.1109/lcomm.2020.3036587
- Vool, U., and Devoret, M. (2017). Introduction to quantum electromagnetic circuits. *Int. J. Circuit Theory Appl.* 45 (7), 897–934. doi:10.1002/cta.2359
- Wadley, P., Howells, B., Železný, J., Andrews, C., Hills, V., Campion, R. P., et al. (2016). Electrical switching of an antiferromagnet. *Science* 351 (6273), 587–590. doi:10.1126/science.aab1031
- Waldrop, M. M. (2013). Neuroelectronics: smart connections. *Nature* 503 (7474), 22–24. doi:10.1038/503022a
- Wall, M. (2016). *China Launches pioneering 'hack-proof' quantum-communications satellite*. Space.com. Purch.
- Wang, C., Gao, Y. Y., Pop, I. M., Vool, U., Axline, C., Brecht, T., et al. (2014). Measurement and control of quasiparticle dynamics in a superconducting qubit. *Nat. Commun.* 5, 5836. doi:10.1038/ncomms6836
- Wang, C., Li, X., Xu, H., Li, Z., Wang, J., Yang, Z., et al. (2022a). Towards practical quantum computers: transmon qubit with a lifetime approaching 0.5 milliseconds. *npj Quantum Inf.* 8, 3. doi:10.1038/s41534-021-00510-2
- Wang, D. S., Fowler, A. G., and Hollenberg, L. C. (2011). Surface code quantum computing with error rates over 1%. *Phys. Rev. A* 83 (2), 020302. doi:10.1103/physreva.83.020302
- Wang, J. I., Yamoah, M. A., Li, Q., Karamlou, A. H., Dinh, T., Kannan, B., et al. (2022b). Hexagonal boron nitride as a low-loss dielectric for superconducting quantum circuits and qubits. *Nat. Mater.* 21 (4), 398–403. doi:10.1038/s41563-021-01187-w
- Wang, X. L., Cai, X. D., Su, Z. E., Chen, M. C., Wu, D., Li, L., et al. (2015). Quantum teleportation of multiple degrees of freedom of a single photon. *Nature* 518, 516–519. doi:10.1038/nature14246
- Warner, M., Din, S., Tupitsyn, I. S., Morley, G. W., Stoneham, A. M., Gardener, J. A., et al. (2013). Potential for spin-based information processing in a thin-film molecular semiconductor. *Nature* 503, 504–508. doi:10.1038/nature12597
- Watson, T. F., Weber, B., House, M. G., Büch, H., and Simmons, M. Y. (2015). High-fidelity rapid initialization and read-out of an electron spin via the single donor D-charge state. *Phys. Rev. Lett.* 115 (16), 166806. doi:10.1103/physrevlett.115.166806
- Watson, T. F., Weber, B., Hsueh, Y. L., Hollenberg, L. C., Rahman, R., and Simmons, M. Y. (2017). Atomically engineered electron spin lifetimes of 30 s in silicon. *Sci. Adv.* 3 (3), e1602811. doi:10.1126/sciadv.1602811
- Weber, B., Hsueh, Y. L., Watson, T. F., Li, R., Hamilton, A. R., Hollenberg, L. C. L., et al. (2018). Spin-orbit coupling in silicon for electrons bound to donors. *npj Quantum Inf.* 4, 61. doi:10.1038/s41534-018-0111-1
- Weber, J. R., Koehl, W. F., Varley, J. B., Janotti, A., Buckley, B. B., Van de Walle, C. G., et al. (2010). Quantum computing with defects. *Proc. Natl. Acad. Sci. U. S. A.* 107, 8513–8518. doi:10.1073/pnas.1003052107
- Wedge, C. J., Timco, G. A., Spielberg, E. T., George, R. E., Tuna, F., Rigby, S., et al. (2012). Chemical engineering of molecular qubits. *Phys. Rev. Lett.* 108, 107204. doi:10.1103/physrevlett.108.107204
- Weinstein, Y. S., Pravia, M. A., Fortunato, E. M., Lloyd, S., and Cory, D. G. (2001). Implementation of the quantum Fourier transform. *Phys. Rev. Lett.* 86, 1889–1891. doi:10.1103/physrevlett.86.1889
- Wen, X. G. (1991). Non-Abelian statistics in the fractional quantum Hall states. *Phys. Rev. Lett.* 66 (6), 802. doi:10.1103/PhysRevLett.66.802
- Wendin, G., and Shumeiko, V. S. (2007). Quantum bits with Josephson junctions (review article). *Low Temp. Phys.* 33, 724–744. doi:10.1063/1.2780165
- Werner, R. F. (2001). All teleportation and dense coding schemes. *J. Phys. A Math. Gen.* 34 (35), 7081–7094. doi:10.1088/0305-4470/34/35/332
- Wiegardt, K., Pohl, K., Jibril, I., and Huttner, G. (1984). Hydrolysis products of the monomeric amine complex (C<sub>6</sub>H<sub>15</sub>N<sub>3</sub>)FeCl<sub>3</sub>: the structure of the octameric iron(III) cation of [(C<sub>6</sub>H<sub>15</sub>N<sub>3</sub>)<sub>6</sub>Fe<sub>8</sub>(μ<sub>3</sub>-O)<sub>2</sub>(μ<sub>2</sub>-OH)<sub>12</sub>]Br<sub>7</sub> · 8H<sub>2</sub>O. *Angew. Chem. Int. Edn Engl.* 23, 77–78. doi:10.1002/anie.198400771
- Wien, W. (1897). XXX. On the division of energy in the emission-spectrum of a black body. *Series* 43 (262), 214–220. doi:10.1080/14786449708620983
- Wikipedia (2022). Adiabatic quantum computation. Available at: [https://en.wikipedia.org/wiki/Adiabatic\\_quantum\\_computation](https://en.wikipedia.org/wiki/Adiabatic_quantum_computation) (Accessed December 28, 22).
- Wikipedia (2022b). Ice. Available at: [https://en.wikipedia.org/wiki/Ice#cite\\_ref-Physics\\_of\\_Ice\\_6-0](https://en.wikipedia.org/wiki/Ice#cite_ref-Physics_of_Ice_6-0) (Accessed December 31, 2022).
- Wikipedia (2022c). List of quantum processors. Available at: [https://en.wikipedia.org/wiki/List\\_of\\_quantum\\_processors#cite\\_note-IonQ32-22](https://en.wikipedia.org/wiki/List_of_quantum_processors#cite_note-IonQ32-22) (Accessed December 29, 22).
- Wikipedia (2022d). Max Planck. Available at: [https://en.wikipedia.org/wiki/Max\\_Planck](https://en.wikipedia.org/wiki/Max_Planck) (Accessed February 12, 2022).
- Wikipedia (2022e). Principle of locality. Available at: [https://en.wikipedia.org/wiki/Principle\\_of\\_locality](https://en.wikipedia.org/wiki/Principle_of_locality) (Accessed December 5, 2022).
- Wikipedia (2022f). Quadratic unconstrained binary optimization. Available at: [https://en.wikipedia.org/wiki/Quadratic\\_unconstrained\\_binary\\_optimization](https://en.wikipedia.org/wiki/Quadratic_unconstrained_binary_optimization) (Accessed December 23, 2022).
- Wikipedia (2022g). Quantum superposition. Available at: [https://en.wikipedia.org/wiki/Quantum\\_superposition](https://en.wikipedia.org/wiki/Quantum_superposition) (Accessed December 30, 22).
- Wikipedia (2022h). Flux qubit. Available at: [https://en.wikipedia.org/wiki/Flux\\_qubit](https://en.wikipedia.org/wiki/Flux_qubit).
- Wikipedia (2022i). Neuromorphic engineering. Available at: [https://en.wikipedia.org/wiki/Neuromorphic\\_engineering#cite\\_note-Maan\\_1%E2%80%936](https://en.wikipedia.org/wiki/Neuromorphic_engineering#cite_note-Maan_1%E2%80%936).
- Wikipedia (2022j). Orbit interaction. Available at: [https://en.wikipedia.org/wiki/Spin%E2%80%93orbit\\_interaction](https://en.wikipedia.org/wiki/Spin%E2%80%93orbit_interaction) (Accessed June 22, 2023).
- Wikipedia (2022k). Quantum tunnelling. Available at: [https://en.wikipedia.org/wiki/Quantum\\_tunnelling](https://en.wikipedia.org/wiki/Quantum_tunnelling) (Accessed January 16, 23).
- Wikipedia (2022l). Spin transfer torque. Available at: [https://en.wikipedia.org/wiki/Spin-transfer\\_torque](https://en.wikipedia.org/wiki/Spin-transfer_torque) (Accessed July 1, 23).
- Wikipedia (2022m). Superconducting quantum computing. Available at: [https://en.wikipedia.org/wiki/Superconducting\\_quantum\\_computing](https://en.wikipedia.org/wiki/Superconducting_quantum_computing).
- Wikipedia (2022n). Topological quantum computer. Available at: [https://en.wikipedia.org/wiki/Topological\\_quantum\\_computer](https://en.wikipedia.org/wiki/Topological_quantum_computer).
- Wikipedia (2022o). Transmon. Available at: [https://en.wikipedia.org/wiki/Transmon#cite\\_note-4](https://en.wikipedia.org/wiki/Transmon#cite_note-4).
- Wikipedia (2022p). Anyon. Available at: [https://en.wikipedia.org/wiki/Anyon#cite\\_note-24](https://en.wikipedia.org/wiki/Anyon#cite_note-24).
- Wikipedia, Romeira, B., and Figueiredo, J. (2023). Quantum tunnelling. Available at: [https://en.wikipedia.org/wiki/Quantum\\_tunnelling](https://en.wikipedia.org/wiki/Quantum_tunnelling) (Accessed January 16, 23).
- Wikipedia (2023). Turing machine. Available at: [https://en.wikipedia.org/wiki/Turing\\_machine](https://en.wikipedia.org/wiki/Turing_machine) (Accessed May 7, 23).

- Wilczek, F. (2006). From electronics to anyonics. *Phys. World* 19, 22–23. doi:10.1088/2058-7058/19/1/31
- Willett, R. L., Nayak, C., Shtengel, K., Pfeiffer, L. N., and West, K. W. (2013). Magnetic-field-tuned aharonov-bohm oscillations and evidence for non-abelian anyons at  $\nu = 5/2$ . *Phys. Rev. Lett.* 111 (18), 186401. doi:10.1103/physrevlett.111.186401
- Williams, C. P., and Clearwater, S. H. (1998). *Explorations in quantum computing*. Santa Clara: Telos.
- Wolchover, N. (2021). Eternal change for No energy: a time crystal finally made real. *Quanta Mag.*
- Wood, B. D., Stimpson, G. A., March, J. E., Lekhai, Y. N. D., Stephen, C. J., Green, B. L., et al. (2022). Long spin coherence times of nitrogen vacancy centers in milled nanodiamonds. *Phys. Rev. B* 105 (20), 205401. doi:10.1103/physrevb.105.205401
- Wu, Y., Bao, W.-Su, Cao, S., and Jian-Wei, P. (2021). Qubits meet materials science. *Nat. Rev. Mater* 6, 869. doi:10.1038/s41578-021-00378-w
- Wu, Y., Bao, W.-Su, Cao, S., and Pan, J.-W. (2021a). Qubits meet materials science. *Nat. Rev. Mater* 6, 869. doi:10.1038/s41578-021-00378-w
- Xia, X. X., Sun, Q. C., Zhang, Q., and Pan, J. W. (2017). Long distance quantum teleportation. *Quantum Sci. Technol.* 3 (1), 014012. doi:10.1088/2058-9565/aa9baf
- Xu, J. S., Yung, M. H., Xu, X. Y., Tang, J. S., Li, C. F., and Guo, G. C. (2016). Robust bidirectional links for photonic quantum networks. *Sci. Adv.* 2 (1), e1500672. doi:10.1126/sciadv.1500672
- Xu, Q., Zheng, G., Wang, Y. X., Zoller, P., Clerk, A. A., and Jiang, L. (2022). *Autonomous quantum error correction and fault-tolerant quantum computation with squeezed cat qubits*. arXiv preprint arXiv:2210.13406.
- Yan, A. (2013). Bidirectional controlled teleportation via six-qubit cluster state. *Int. J. Theor. Phys.* 52, 3870–3873. doi:10.1007/s10773-013-1694-0
- Yan, F., Gustavsson, S., Kamal, A., Birenbaum, J., Sears, A. P., Hover, D., et al. (2016b). The flux qubit revisited to enhance coherence and reproducibility. *Nat. Commun.* 7, 12964. doi:10.1038/ncomms12964
- Yan, F., Krantz, P., Sung, Y., Kjaergaard, M., Campbell, D. L., Orlando, T. P., et al. (2018). Tunable coupling scheme for implementing high-fidelity two-qubit gates. *Phys. Rev. Appl.* 10 (5), 054062. doi:10.1103/physrevapplied.10.054062
- Yan, Y., Wan, C., Zhou, X., Shi, G., Cui, B., Han, J., et al. (2016a). Strong electrical manipulation of spin-orbit torque in ferromagnetic heterostructures. *Adv. Electron. Mater.* 2 (10), 1600219. doi:10.1002/aelm.201600219
- Yan, Z., Yun, J. J., Sui, W. B., Xi, L., Xie, Z. T., Cao, J. W., et al. (2021). Current switching of interface antiferromagnet in ferromagnet/antiferromagnet heterostructure. *Appl. Phys. Lett.* 118 (3), 032402. doi:10.1063/5.0039074
- Yang, C. H., Leon, R. C. C., Hwang, J. C. C., Saraiva, A., Tantt, T., Huang, W., et al. (2020). Operation of a silicon quantum processor unit cell above one kelvin. *Nature* 580, 350–354. doi:10.1038/s41586-020-2171-6
- Yang, G., Lian, B. W., Nie, M., and Jin, J. (2017). Bidirectional multi-qubit quantum teleportation in noisy channel aided with weak measurement. *Chin. Phys. B* 26 (4), 040305. doi:10.1088/1674-1056/26/4/040305
- Yang, Y. Q., Zha, X. W., and Yu, Y. (2016). Asymmetric bidirectional controlled teleportation via seven-qubit cluster state. *Int. J. Theor. Phys.* 55, 4197–4204. doi:10.1007/s10773-016-3044-5
- Yanofsky, N. S., and Mannucci, M. (2013). *Quantum computing for computer scientists*. Cambridge University Press.
- Yao, X., Klyukin, K., Lu, W., Onen, M., Ryu, S., Kim, D., et al. (2020). Protonic solid-state electrochemical synapse for physical neural networks. *Nat. Commun.* 11 (1), 3134. doi:10.1038/s41467-020-16866-6
- Yin, J., Cao, Y., Yong, H. L., Ren, J. G., Liang, H., Liao, S. K., et al. (2013). Lower bound on the speed of nonlocal correlations without locality and measurement choice loopholes. *Phys. Rev. Lett.* 110 (26), 260407. doi:10.1103/physrevlett.110.260407
- Yin, J., Ren, J. G., Lu, H., Cao, Y., Yong, H. L., Wu, Y. P., et al. (2012). Quantum teleportation and entanglement distribution over 100kilometre freespace channels. *Nature* 488, 185–188. doi:10.1038/nature11332
- Yogendra, K., Fan, D., Jung, B., and Roy, K. (2016). Magnetic pattern recognition using injection-locked spin-torque nano-oscillators. *IEEE Trans. Electron Devices* 63, 1674–1680. doi:10.1109/te.2016.2523423
- Yoneda, J., Huang, W., Feng, M., Yang, C. H., Chan, K. W., Tantt, T., et al. (2021). Coherent spin qubit transport in silicon. *Nat. Commun.* 12, 4114. doi:10.1038/s41467-021-24371-7
- Yoneda, J., Takeda, K., Otsuka, T., Nakajima, T., Delbecq, M. R., Allison, G., et al. (2018). A quantum-dot spin qubit with coherence limited by charge noise and fidelity higher than 99.9%. *Nat. Nanotech* 13, 102–106. doi:10.1038/s41565-017-0014-x
- Yonezawa, H., Braunstein, S. L., and Furusawa, A. (2007). Experimental demonstration of quantum teleportation of broadband squeezing. *Phys. Rev. Lett.* 99, 110503. doi:10.1103/physrevlett.99.110503
- You, J. Q., Hu, X., Ashhab, S., and Nori, F. (2007). Low-decoherence flux qubit. *Phys. Rev. B* 75, 140515. doi:10.1103/physrevb.75.140515
- You, J. Q., and Nori, F. (2007). Superconducting circuits and quantum information. *Phys. Today* 58 (11), 42–47. arXiv:quant-ph/0601121. doi:10.1063/1.2155757
- Yuan, W. (2015). Quantum teleportation of an arbitrary three-qubit state using GHZ-like states. *Int. J. Theor. Phys.* 54, 851–855. doi:10.1007/s10773-014-2279-2
- Yuan, Z.-S., Chen, Y. A., Zhao, B., Chen, S., Schmiedmayer, J., and Pan, J. W. (2008). Experimental demonstration of a BDCZ quantum repeater node. *Nature* 454, 1098–1101. doi:10.1038/nature07241
- Yukawa, M., Benichi, H., and Furusawa, A. (2008). Highfidelity continuousvariable quantum teleportation toward multistep quantum operations. *Phys. Rev. A* 77, 022314. doi:10.1103/physreva.77.022314
- Yun, J., Bai, Q., Yan, Z., Chang, M., Mao, J., Zuo, Y., et al. (2020). Tailoring multilevel-stable remanence states in exchange-biased system through spin-orbit torque. *Adv. Funct. Mat.* 30, 1909092. doi:10.1002/adfm.201909092
- Zadrozny, J. M., Niklas, J., Poluektov, O. G., and Freedman, D. E. (2015). Millisecond coherence time in a tunable molecular electronic spin qubit. *ACS central Sci.* 1 (9), 488–492. doi:10.1021/acscentsci.5b00338
- Zahedinejad, M., Awad, A. A., Muralidhar, S., Khymyn, R., Fulara, H., Mazraati, H., et al. (2020). Two-dimensional mutually synchronized spin Hall nano-oscillator arrays for neuromorphic computing. *Nat. Nanotechnol.* 15, 47–52. doi:10.1038/s41565-019-0593-9
- Zahedinejad, M., Fulara, H., Khymyn, R., Houshang, A., Dvornik, M., Fukami, S., et al. (2022). Memristive control of mutual spin Hall nano-oscillator synchronization for neuromorphic computing. *Nat. Mat.* 21, 81–87. doi:10.1038/s41563-021-01153-6
- Zajac, D. M., Hazard, T. M., Mi, X., Nielsen, E., and Petta, J. R. (2016). Scalable gate architecture for a one-dimensional array of semiconductor spin qubits. *Phys. Rev. Appl.* 6, 054013. doi:10.1103/physrevapplied.6.054013
- Zakrzewski, J. (2012). Viewpoint: crystals of Time physics.aps.org. *APS Phys. Archived Orig. 2 Febr.*, 2017. doi:10.1103/Physics.5.1116
- Zeng, Z., Finocchio, G., and Jiang, H. (2013). Spin transfer nano-oscillators. *Nanoscale* 5 (6), 2219–2231. doi:10.1039/c2nr33407k
- Zetterling, C. M. (2002). *Process technology for silicon carbide devices* (Institution of Electrical Engineers).
- Zhang, B., Liu, X. T., Wang, J., and Tang, C. J. (2016). Quantum teleportation of an arbitrary N-qubit state via GHZ-like states. *Int. J. Theor. Phys.* 55, 1601–1611. doi:10.1007/s10773-015-2798-5
- Zhang, L., Zhou, J., Li, H., Shen, L., and Feng, Y. P. (2021). Recent progress and challenges in magnetic tunnel junctions with 2D materials for spintronic applications. *Appl. Phys. Rev.* 8 (2), 021308. doi:10.1063/5.0032538
- Zhang, Q., Takesue, H., Nam, S. W., Langrock, C., Xie, X., Baek, B., et al. (2008). Distribution of time-energy entanglement over 100 km fiber using superconducting single photon detectors. *Opt. Express* 16, 5776–5781. doi:10.1364/oe.16.005776
- Zhang, T. C., Goh, K. W., Chou, C. W., Lodahl, P., and Kimble, H. J. (2003). Quantum teleportation of light beams. *Phys. Rev. A* 67, 033802. doi:10.1103/physreva.67.033802
- Zhou, R. G., Li, X., Qian, C., and Ian, H. (2020). Quantum bidirectional teleportation  $2 \leftrightarrow 2$  or  $2 \leftrightarrow 3$  Qubit teleportation protocol via 6-Qubit entangled state. *Int. J. Theor. Phys.* 59, 166–172. doi:10.1007/s10773-019-04306-1
- Zhou, R. G., Xu, R., and Lan, H. (2019). Bidirectional quantum teleportation by using six-qubit cluster state. *Ieee Access* 7, 44269–44275. doi:10.1109/access.2019.2901960
- Zhou, R.-G., Zhang, Y. N., Xu, R., Qian, C., and Hou, I. (2019c). Asymmetric bidirectional controlled teleportation by using nine-qubit entangled state in noisy environment. *Ieee Access* 7, 75247–75264. doi:10.1109/access.2019.2920094
- Zhou, Y., and Ramanathan, S. (2015). Mott memory and neuromorphic devices. *Proc. IEEE* 103 (8), 1289–1310. doi:10.1109/JPROC.2015.2431914
- Zmuidzinas, J., and Richards, P. L. (2004). Superconducting detectors and mixers for millimeter and submillimeter astrophysics. *Proc. IEEE* 92 (10), 1597–1616. doi:10.1109/jproc.2004.833670
- Zuo, X., Liu, Y., Zhang, W., and Zhang, Z. (2009). Simpler criterion on W state for perfect quantum state splitting and quantum teleportation. *Sci. China Ser. G Phys. Mech. Astronomy* 52 (12), 1906–1912. doi:10.1007/s11433-009-0305-9
- Žutić, I., Fabian, J., and Sarma, S. D. (2004). Spintronics: fundamentals and applications. *Rev. Mod. Phys.* 76 (2), 323–410. doi:10.1103/revmodphys.76.323
- Zwerver, A. M. J., Krähenmann, T., Watson, T. F., Lampert, L., George, H. C., Pillarisetty, R., et al. (2022). Qubits made by advanced semiconductor manufacturing. *Nat. Electron* 5, 184–190. doi:10.1038/s41928-022-00727-9